FE-2033-19(Vol.1)
Distribution Category UC-90c

HOT LOW BTU PRODUCER GAS DESULFURIZATION IN FIXED BED OF IRON OXIDE-FLY ASH

FINAL REPORT

DILIP K. JOSHI
ERNEST L. LEUENBERGER

UNDER CONTRACT NO. E(49-18)2033 AND EX-76-C-01-2033

PREPARED FOR THE
ENERGY RESEARCH AND DEVELOPMENT ADMINISTRATION

AIR PRODUCTS AND CHEMICALS, INC.
HOUDRY TECHNICAL CENTER
P. O. BOX 427
MARCUS HOOK, PENNSYLVANIA 19061

Blank Page

TABLE OF CONTENTS

PAGE

APPENDICES

LIST OF TABLES

LIST OF TABLES
(CONTINUED)

LIST OF TABLES
(CONTINUED)

LIST OF FIGURES

LIST OF FIGURES
(CONTINUED)

LIST OF FIGURES
(CONTINUED)

LIST OF FIGURES
(CONTINUED)

LIST OF FIGURES
(CONTINUED)

LIST OF FIGURES
(CONTINUED)

FINAL REPORT

1.0 ABSTRACT

This work was undertaken to support the Morgantown Energy Research Center on their development of a process for desulfurizing hot, low BTU producer gas with iron oxide sorbents. Specific objectives of APCI support were sorbent development and definition of scale-up criteria for commercial design.

Several experimental sorbents were prepared using commercially available raw materials and were tested for capacity for hydrogen sulfide removal from the producer gas. Effects of iron oxide source, iron oxide content, sorbent support and binder on sorbent performance were investigated. Changes in the properties like porosity, crushing strength, surface area, attrition resistance, x-ray diffraction patterns, DTA, density, of the sorbents after undergoing a single absorption and regeneration cycle were evaluated.

Effects of process variables like GHSV, superficial velocity, temperature, H_2S concentration in producer gas, pellet diameter, iron oxide content and pressure on the absorption dynamics were experimentally determined. Several mathematical models to describe the isothermal sorption of H_2S were developed. They include the shrinking core model, film resistance model, kinetically limited reaction rate model and a semi-empirical model obtained by slightly modifying a fundamental model. All the models were evaluated using experimental data. The semi-empirical model was able to predict the shapes of breakthrough curves and sorbent performance at 10% breakthrough for H_2S.

Several schemes to regenerate sulfided sorbents yielding a high concentration of sulfur dioxide without exceeding 1500°F were considered. A short experimental program was completed to study effect of process variables on regeneration dynamics using air-steam. Heat effects for the highly exothermic regeneration were incorporated in the isothermal sorption models and were tested with experimental data. The adiabatic kinetically controlled model was best able to correlate the regeneration data.

A cyclic process simulation model for combined absorption and regeneration was programmed. This program has the option of using any of the

developed models to scale up the laboratory scale experimental data for large scale operation for the condition that no decline in sorption capacity occurs.

Normally regeneration produces a sulfur-dioxide containing gas. However, during the course of the experimental work it was found that at some conditions, 20 to 30% of the total sulfur in the effluents was in the form of elemental sulfur. It is recommended that the possibility of producing elemental sulfur on regeneration be explored further.

2.0 SUMMARY

2.1 General

The work described herein was carried out to support the efforts of the Morgantown Energy Research Center in their effort to develop a process for desulfurizing hot low BTU producer gas with iron oxide absorbents. The process consists of sorbing hydrogen sulfide in fixed beds at about 1200°F followed by regeneration of spent absorbent with oxygen containing gas at temperatures between 1000 and 1500°F. It was a goal of the process to produce a regeneration effluent containing high SO_2 concentration to sulfur and to limit the maximum temperature of the bed during regeneration to below 1500°F - in order not to overheat the absorbent. Conversion of sulfur dioxide, so produced, to sulfur was beyond the scope of this project although an interesting lead was uncovered during the course of the work as described below.

The results obtained under this contract were 1) development of improved absorbents, 2) development and confirmation of a mathematical model of the absorption process to aid scale-up, and 3) development and confirmation of a math model for the regeneration step for the same purpose. These three areas of work are summarized below along with potentially important finding of a possible way to produce elemental sulfur directly on regeneration.

2.2 Sorbent Development

Many sorbents were prepared. Of these several are recommended for commercial application although not all were tested on regeneration in this project.

Several of the better ones are:

For all sorption pressure ranges

1. 42% Iron Oxide on Fly Ash
2. 42% Iron Oxide in Silica

For sorption pressures around 400 psi

3. 63% Iron Oxide on Fly Ash

Sorbent 1 proved to be regenerable in the single regeneration method used to explore variable effects in the process.

The 42% iron oxide sorbents have a sorption capacity of about 18 gms S per 100 gms fresh absorbent.

Sorbents were made as extrudates in 1/8 and 1/4 inch diameter sizes. Methocel was needed and used as an extrusion aid. Kaolin and bentonite were investigated as binders and bentonite is the preferred material. A variety of iron oxide source materials were investigated. Best of them were iron oxides obtained from the armco or U.S. Steel companies.

At higher sorbent iron oxide content, 63%, the absorption capacity was pressure sensitive being 132 gms S per 1000 c.c. sorbent at 20 psi and 320 gms at 400 psi. At the higher pressure, capacity increased directly with iron oxide content.

Crush strengths attained in the fresh absorbents was typically about 2.7 pounds per millimeter of length, or higher.

Most process studies were done with 42% iron oxide in fly-ash absorbent. This absorbent, as made, underwent changes during process exposure through a single sorption and regeneration cycle. Crush strength and attrition resistance increased while pore volume and surface area decreased. The differential thermal analysis (DTA) shows regenerated sorbent is different from fresh sorbent. However, determining the nature and significance of the differences was beyond the scope of this work. On completion of regeneration with a steam-air mixture a small amount of residual sulfur resides in the sorbent. It does not appear by X-ray analysis to be iron sulfate and its nature is not known. The iron oxide-fly ash sorbent mainly used in the process work was α - Fe_2O_3 in both fresh and once regenerated absorbent.

In two tests, fresh 42% iron oxide-fly ash absorbent disintegrated in a hydrogen sulfide free reducing gas at around 900°F and it is therefore recommended that the above mentioned sorbents be used at temperatures above 900°F. Operating procedures to avoid exposing absorbents to these conditions may be required.

2.3 Absorption

Typically, at 1200°F and 1800 GHSV (based on gas volume at STP), about 70% of the fresh sorbent capacity was utilized before the hydrogen sulfide concentration in the effluents reached 10% on the inlet concentration.

Effects of process variables on the dynamic sorption performance were studied over the ranges listed below

Temperature	600°F to 1400°F
Pressure	20 psig to 400 psig
GHSV (gas at STP)	1300 to 3600
Superficial velocity	0.05 ft/sec to 2.33 ft/sec
Feed gas hydrogen sulfide concentration by volume	.6% to 1.2%
Sorbent pellet diameter	1/8 inch to 1/4 inch
Sorbent added iron oxide content	8 to 63 wt%

Three fundamental mathematical models describing the process of isothermal sorption were developed. They are: shrinking core model, kinetic model and film transfer model. These models were tested using the process variables data. The criteria for model selection were, ability to predict the shape of the breakthrough curves and ability to predict sorption efficiency at 10% breakthrough. None of the fundamental models and their combinations satisfied both the criteria. A semi-empirical model was found to satisfy both the criteria reasonably well. The relationship between sorption efficiency and fractional breakthrough predicted by this semi-empirical model is

$$\tau = 1 + (A_1\ NA_b{}^{F} + A_2\ NA_b{}^{K})\ \ln\left(\frac{F}{(1-F)^2}\right)$$

All these sorption models are programmed. The mathematical model may be adapted to convert new laboratory derived information (with new sorbents or new conditions) into new commercial scale data.

2.4 Regeneration

Once sulfided absorbents were regenerated using a feed containing 85% steam and 15% air. Typically 85% of the sorbed sulfur was removed after regeneration. A short experimental program was carried out to study the effect of following process variables.

Temperature	1000°F and 1200°F
Pressure	20 psig and 150 psig
GHSV (gas at STP)	700, 1300 and 6500
Superficial velocity	.17 ft/sec and .33 ft/sec
Feed air concentration mole pct.	15 and 20
Sorbent pellet diameter	1/4 inch and 1/8 inch
Added iron oxide in fresh sorbent	21% and 42%

Regeneration breakthrough curves for oxygen were much steeper than the hydrogen sulfide breakthrough curves in absorption. Exotherms of about 300°F were observed.

The isothermal sorption models were adapted for regeneration with air-steam mixture by incorporating the large adiabatic heat effect accompanying regeneration. The three fundamental models (shrinking core, kinetic and film transfer) were tested using the criteria described in the absorption section. The kinetic model was found to be the most satisfactory. The relationship between efficiency and fractional breakthrough predicted by the kinetic model is

$$\tau = 1 + A\ N^{K}A_{b}$$

A cyclic process simulation model combining absorption and regeneration was developed and programmed to generate output for both absorption step and regeneration step. Experimental evaluation of the durability of sorbent through multiple cycle processing was beyond the scope of this project and was not done.

2.5 Sulfur Formed During Regeneration

Unexpectedly large quantities of elemental sulfur were produced in the steam-air regeneration studies. Detailed investigation of the phenomena was not within the scope of the present work. However analyses indicated that, at low regeneration rates, about 20 to 30% of the sulfur in the effluents was elemental sulfur, the remainder being in the form of sulfur dioxide, with very small quantities of sulfur trioxide. The observation is significant in that if sulfur can be generated rapidly and directly, the need for "add on" facilities to convert sulfur dioxide into sulfur is eliminated. It is recommended that the method for producing elemental sulfur on regeneration be investigated further.

3.0 INTRODUCTION

The Air Products and Chemicals, Inc. Research, Development, and Engineering program is aimed at assisting ERDA in developing their hot producer gas desulfurization process. A cyclic fixed-bed technique using an iron oxide-fly ash absorbent at producer gas temperature and pressure is the ultimate objective. The process is being developed by ERDA at the Morgantown Energy Research Center.

The chemical reactions that are believed to occur during desulfurization and regeneration are summarized in Table 3.1. During desulfurization, hydrogen sulfide in the hot producer gas reacts with the iron oxide sorbent to form an iron sulfide. This reaction is mildly exothermic, resulting in a moderate adiabatic gas temperature rise of 20°F for each percent of H_2S in the producer gas. If heat transfer between gas and solid is inadequate, the solid adiabatic temperature rise of 100°F per 10% sorbent iron oxide could lead to localized hot spots in the solid pellets. Once the sorbent is sulfided, regeneration is accomplished by oxidizing the iron sulfide to iron oxide. Like most oxidations, this regeneration is highly exothermic. The resulting adiabatic temperature rises could be extensive enough under certain conditions to destroy both the physical integrity and the chemical activity of the sorbent. The heat release problem is compounded by the oxidation of any carbon dust or coke deposited in the bed during sulfur absorption. In regeneration, as in desulfurization, local solid hot spots can develop in cases of poor heat transfer between solid and gas phases.

The APCI support program is designed to accomplish the following general objectives:

1. To develop a suitable fixed bed absorbent from readily available inexpensive raw materials.
2. To gain an understanding of the fundamentals of the desulfurization and regeneration processes as they occur in a lab scale reactor (the ERDA pressure unit).
3. To use this understanding of the process fundamentals to define scale-up criteria for the design of a commercial size system.

The original APCI project was divided into eight separate tasks. Scope of the original contract was revised after mutual consultations between ERDA and APCI. A comparison of the original and revised scope is given below.

TABLE 3.1
ERDA PRODUCER GAS DESULFURIZATION WITH IRON OXIDE: REACTION SCHEME

ABSORPTION

$3H_2S + Fe_2O_3 \longrightarrow 2FeS_{1.5} + 3H_2O$

ΔH = -21.85 KCAL/G-MOLE, Fe_2O_3

GAS ADIABATIC TEMPERATURE RISE = $20^{o}F/1\%\ H_2S$

SOLID ADIABATIC TEMPERATURE RISE = $100^{o}F/10\%\ Fe_2O_3$

REGENERATION

$2FeS_{1.5} + 4.5O_2 \longrightarrow Fe_2O_3 + 3SO_2$

ΔH = -350.1 KCAL/G-MOLE, Fe_2O_3

GAS ADIABATIC TEMPERATURE RISE = $195^{o}F/1\%\ O_2$

SOLID ADIABATIC TEMPERATURE RISE = $1575^{o}F/10\%\ Fe_2O_3$

COKE BURNING

$C + O_2 \longrightarrow CO_2$

ΔH = -94.1 KCAL/G-MOLE, C OR O_2

GAS ADIABATIC TEMPERATURE RISE = $235^{o}F/1\%\ O_2$

SOLID ADIABATIC TEMPERATURE RISE = $565^{o}F$/1% COKE

Task No.	Original Contract	Revised Contract
I	Development and Optimization of Absorbent Characteristics	Unchanged
II	Isothermal Sorption Model Development and Experimental Confirmation	Unchanged
III	Adiabatic Sorption Model Development	Unchanged
IV	Reactor Design Evaluation	Omitted
V	Process Optimization for Commercial Design	Omitted
VI	Coking Study	Regeneration Study
VII	Coking Effects Modeling	Regeneration Modeling
VIII	Provide Consulting Services as Needed	Unchanged

This report describes all work done on the above tasks during the project.

Specific objectives of sorbent development (Task I) were to:

1. Identify practical sources of Fe_2O_3.
2. Prepare sorbents using different sources and levels of Fe_2O_3 and evaluate H_2S sorption dynamics.
3. Evaluate other sources of fly ash by physical properties and sorption capacities and dynamics.
4. Evaluate bentonite and kaolin as binders by physical properties and sorption capacities and dynamics.

Full identification of a practical and optimum performance sorbent and knowledge of its sorption dynamics is the product of this phase.

Specific objectives of model development and confirmation (Task II) are to:

1. Derive dimensionless scale-up parameters from fundamental principles. These parameters, which we call sorption numbers, are functions of producer gas H_2S concentration, sorbent H_2S capacity, bed geometry and properties, sorbent properties, and bed operating conditions.

2. Conduct an experimental program to confirm that sorption dynamics uniquely correlates with the scale-up parameter(s) predicted by one of the models investigated. Pressure, temperature, velocity, bed geometry, sorbent particle size, and sorbent composition effects on sorption dynamics are to be correlated.

The product of this phase is the identification of process scale-up criteria for isothermal sorption of H_2S on iron oxide/fly ash sorbent. Seecific objectives of Task III (adiabatic sorption model development) were to add heat balance to all evaluated sorption models and develop a cyclic model combining absorption and regeneration.

Specific objectives of regeneration study (Task VI) are to:

1. Compare alternate regeneration schemes.
2. Complete a core experimental program for air-steam regeneration.

Specific objective for regeneration modeling was to select a model developed in Task III that would best explain the effect of process variables on regeneration efficiency observed in Task VI.

Section 4 of this report describes the chemical analysis and physical properties of the experimental absorbents. Section 5 describes the dynamic test procedure for absorption and results of the iron oxide source and process variables studies. Section 6 briefly describes development of isothermal sorption models and compares the experimentally observed absorption dynamics with model predictions. Section 7 describes the alternate regeneration schemes. Section 8 describes the brief air-steam regeneration experimental program, changes in sorbent properties as a result of absorption and regeneration and elemental sulfur formation during regeneration. Section 9 describes the adiabatic regeneration models and compares experimentally observed regeneration dynamics with model predictions. The Appendices include description of the pilot unit, data for sorption and regeneration experiments, derivations for the mathematical models and listing of a computer program for the process simulation model for combined absorption-regeneration cycle.

4.0 PREPARATION OF EXPERIMENTAL SORBENTS

4.1 Physical Properties of Experimental Sorbents

Table 4.1 is a listing of each sorbent prepared and tested this year, the APCI codes for the sorbent and test run, the physical properties of the sorbent, and the test operating conditions. The last column of Table 4.1 is an indication of the sorbent performance which will be defined in Section 5.2 of this report. In short, Table 4.1 provides a summary of all experimental work done this year using the lab scale ERDA pressure unit.

As indicated in Table 4.2, a total of 20 distinct sorbent preparations were tested this year. These preparations varied in:

1. Source of Iron Oxide: 7 commercial sources were evaluated.
2. Sorbent Iron Oxide Content: Preparations varied from 8 to 63 percent added iron oxide on fly ash. All preparations used U.S. Steel iron oxide source.
3. Support Material: Both iron oxide on fly ash and iron oxide on silica were tested.
4. Type of Binder: Both bentonite and kaolin were used as sorbent binder.
5. Sorbent Particle Size: 1/4 inch diameter pellets and 1/8 inch diameter pellets were extruded.

Details of the method of sorbent preparation and its effect on sorbent properties are given in a separate APCI report prepared under this current ERDA contract entitled "Final Report on Preparation and Properties of H_2S Absorbents", FE-2033-14, UC-90-C, 21 July 1976, by R. J. Jenkins. The various sorbent heat treatments described in the report were used to hold the sorbent porosity and sorbent crushing strength within a given range for all sorbents tested. Data presented in the sorbent preparation report demonstrate that heat treatment has a large effect on sorbent crushing strength but very little effect on porosity. As a result, it proved impossible to prepare high porosity sorbent containing more than 50% added iron oxide on fly ash. Most sorbents prepared had a porosity between 16 and 20 weight percent as measured by water absorption. In contrast, 50.4% Fe_2O_3 on fly ash (812X1-1X5) could not be prepared with a porosity greater than 12.4% and 63% Fe_2O_3 on fly ash (813X1-1X4) has a maximum porosity of 11.6%. These low porosities may explain the peculiar behavior of high iron oxide sorbents at 20 psig described in Section 5.3.1.

TABLE 4.1
DYNAMIC SORPTION RUNS FOR ERDA SORBENT
DEVELOPMENT AND MODEL CONFIRMATION TASKS (TASKS I AND II)

	Sorbent Description									Operating Conditions									
Run Number	Sorbent Code	% Added Iron Oxide	Iron Oxide Source	Sorbent Support	Sorbent Binder	Porosity (% H_2O Absorption)	Crushing Strength (lb. per mm)	Bulk Density (Kg/L)	Particle Density (Kg/L)	Volume of Bed (cm^3)	Run Pressure (psig)	Bed Temp. (^oF)	Wet Gas GHSV	% H_2S in Feed Gas	10% Breakthrough Sorption Efficiency	Porosity Volume Percent of Fresh Sorbent	Weight % S in Sulfided Sorbent	Time for Perfect Operation Hours	Porosity Vol.% of Sulfided Sorbent
1700SG	705X10-1X5	21.0	J&L Steel	Fly Ash	Bentonite	19.3	6.00	1.010	1.870	500	20	1200	1800	0.6	0.57	35.5	11.07	5.59	29.62
** 1701SG	705X10-1X5	21.0	J&L Steel	Fly Ash	Bentonite	19.3	6.00	1.010	1.870	500	20	1200	1800	0.6	-	35.5	11.00	6.24	33.62
1702SG	705X10-1X5	21.0	J&L Steel	" "	"	19.3	6.00	1.010	1.870	500	20	1200	1800	0.6	-	35.5	10.90	7.51	32.51
1703SG	705X10-1X5	21.0	J&L Steel	" "	"	19.3	6.00	1.010	1.870	500	20	1200	1800	0.6	0.81	35.5	11.20	4.42	31.97
** 1704SG	705X9-2X1	21.0	U.S. Steel	" "	"	16.10	5.43	1.184	1.947	500	20	1200	1800	0.6	-	32.0	10.80	10.50	30.19
1705SG	705X9-2X1	21.0	U.S. Steel	" "	"	16.10	5.43	1.184	1.947	500	20	1200	1800	0.6	0.58	32.0	10.63	9.58	30.08
1706SG	705X9-2X1	21.0	U.S. Steel	" "	"	16.10	5.43	1.184	1.947	500	20	1200	1800	0.6	0.77	32.0	10.70	8.55	29.70
1707SG	705X11-1X5	21.0	Armco Steel	" "	"	17.4	6.46	1.115	1.957	500	20	1200	5200	0.6	0.55	33.8	14.20	3.19	32.70
1708SG	705X8-5X1	21.0	Fischer Sci.	" "	"	17.9	4.17	1.152	1.900	500	20	1200	6700	0.6	0.36	34.4	13.20	3.03	34.20
1709SG	705X15-1X2	21.0	Republic BOF	" "	"	19.8	4.40	1.067	1.769	500	20	1200	6900	0.6	0.25	35.2	9.43	2.29	31.90
1710SG	705X15-1X2	21.0	Republic BOF	" "	"	19.8	4.40	1.067	1.769	500	20	1200	6900	0.6	0.36	35.2	8.00	1.65	36.31
1711SG	705X15-1X2	21.0	Republic BOF	" "	"	19.8	4.40	1.067	1.769	500	20	1400	6800	0.6	0.20	35.2	8.40	1.83	35.14
1712SG	705X13-1X2	21.0	Youngstown	" "	"	18.8	3.6	1.113	1.861	500	20	1200	6900	0.6	0.53	35.3	10.40	2.27	31.20
1713SG	705X14-1X2	21.0	Republic OH	" "	"	16.4	3.5	1.153	1.904	500	20	1200	1800	0.6	0.50	30.8	9.70	6.61	29.72
1714SG	705X10-1X1	21.0	J&L Steel	" "	"	20.4	3.72	1.031	1.798	500	20	1200	1700	0.6	0.49	36.7	10.70	7.33	34.49
1715SG	705X11-1X5	21.0	Armco Steel	" "	"	17.4	6.46	1.115	1.954	500	20	1200	1700	0.6	0.70	33.8	13.20	10.57	33.62
1716SG	705X14-1X2	21.0	Republic OH	" "	"	16.4	3.5	1.181	1.904	500	20	1400	1800	0.6	0.71	30.8	10.10	7.47	29.67
1717SG	705X13-1X2	21.0	Youngstown	" "	"	18.8	3.6	1.113	1.861	500	20	1200	1700	0.6	0.65	35.3	9.50	8.32	31.64
1718SG	705X9-2X1	21.0	U.S. Steel	" "	"	16.1	5.43	1.184	1.947	500	20	1200	1700	0.6	0.59	31.6	10.50	8.96	28.63
1719SG	705X15-1X2	21.0	Republic BOF	" "	"	19.8	4.40	1.067	1.769	400	20	1200	1700	0.6	0.42	35.2	8.13	5.91	34.92
1720SG	803X1-1X2	25.2	U.S. Steel	" "	"	18.6	6.33	1.045	1.861	500	20	1200	1800	0.6	0.63	34.3	11.20	9.48	32.47
1721SG	802X1-1X3	16.8	U.S. Steel	" "	"	18.0	7.47	1.079	1.798	500	20	1200	1700	0.6	0.61	32.7	8.26	6.32	31.26
1722SG	801X1-1X3	12.6	U.S. Steel	" "	"	19.7	4.58	1.012	1.717	500	20	1200	1800	0.6	0.62	33.8	7.01	5.99	33.53
1723SG	800X1-1X2	8.4	U.S. Steel	" "	"	20.7	4.67	0.990	1.687	500	20	1200	1800	0.6	0.48	34.9	5.72	4.31	34.67
1724SG	705X12-1X3*	21.0	U.S. Steel	" "	"	17.6	6.43	1.136	1.850	500	20	1200	1800	0.6	0.63	32.7	10.00	9.38	30.30
1725SG	801X2-1X2*	12.6	U.S. Steel	" "	"	17.7	4.67	1.135	1.781	500	20	1200	1800	0.6	0.70	31.6	6.73	6.28	31.00
1726SG	705X9-2X4	21.0	U.S. Steel	" "	"	16.13	7.70	1.166	1.964	500	20	1200	1800	0.6	0.63	31.8	9.35	5.66	30.10
1727SG	705X9-2X4	21.0	U.S. Steel	" "	"	16.13	7.70	1.166	1.964	500	20	1200	1800	0.6	0.59	31.8	9.92	9.71	27.80
1728SG	705X9-2X4	21.0	U.S. Steel	" "	"	16.13	7.70	1.166	1.964	500	20	1400	1800	0.6	0.58	31.8	8.99	8.20	30.98
1729SG	705X9-2X4	21.0	U.S. Steel	" "	"	16.13	7.70	1.166	1.964	500	20	1200	4100	0.6	0.47	31.8	10.30	3.47	30.13
1730SG	801X2-1X4*	12.6	U.S. Steel	" "	"	18.18	5.05	1.108	1.771	500	20	1200	1800	0.6	0.83	32.3	7.27	5.90	31.40
1731SG	705X9-2X4	21.0	U.S. Steel	" "	"	16.13	7.70	1.166	1.964	500	150	1200	1700	0.6	0.69	31.8	11.40	8.64	26.63
1732SG	705X9-2X4	21.0	U.S. Steel	" ""	"	16.13	7.70	1.166	1.964	500	150	1400	1800	0.6	0.67	31.8	8.17	5.93	28.80
1733SG	705X12-1X3*	21.0	U.S. Steel	" "	"	17.57	6.00	1.136	1.850	500	150	1200	1800	0.6	0.82	32.7	11.00	7.87	33.60
1734SG	801X1-1X5	12.6	U.S. Steel	" "	"	19.89	7.70	1.043	1.702	1000	20	1200	1800	0.6	0.75	34.0	7.23	5.72	33.60
1735SG	705X9-2X4	21.0	U.S. Steel	" "	"	16.13	7.70	1.166	1.964	500	20	1200	3500	0.6	0.48	31.8	10.60	4.27	28.90
1736SG	803X1-1X4	25.2	U.S. Steel	" "	"	19.34	4.40	1.101	1.836	500	20	600	1800	0.6	0.0	35.6	7.23	5.60	32.90

TABLE 4.1
DYNAMIC SORPTION RUNS FOR ERDA SORBENT DEVELOPMENT AND MODEL CONFIRMATION TASKS (TASKS I AND II)

(CONTINUED)

	Sorbent Description									Operating Conditions									
Run Number	Sorbent Code	% Added Iron Oxide	Iron Oxide Source	Sorbent Support	Sorbent Binder	Porosity (% H_2O Absorption)	Crushing Strength (lb. per mm)	Bulk Density (Kg/L)	Particle Density (Kg/L)	Volume of Bed (cm^3)	Run Pressure (psig)	Bed Temp. (^oF)	Wet Gas GHSV	% H_2S in Feed Gas	10% Breakthrough Sorption Efficiency	Porosity Volume Percent of Fresh Sorbent	Weight % S in Sulfided Sorbent	Time for Perfect Operation Hours	Porosity Vol.% of Sulfided Sorbent
**1737SG	803X1-1X4	25.2	U.S. Steel	Fly Ash	Bentonite	19.34	4.40	1.101	1.836	500	20	900	-	-	-	-	-	-	-
1738SG	705X9-3X4	21.0	U.S. Steel	" "	"	15.30	8.50	1.146	1.946	1000	20	1200	1700	0.6	0.66	29.8	10.30	6.59	27.52
1739SG	705X9-3X7	21.0	U.S. Steel	" "	"	15.40	8.10	1.148	1.954	1000	20	1200	3400	0.6	0.51	29.9	9.50	3.54	28.39
1740SG	705X9-3X4	21.0	U.S. Steel	" "	"	15.25	8.45	1.146	1.946	500	20	1200	3500	0.6	0.41	29.7	9.50	3.70	27.51
1741SG	705X9-3X6	21.0	U.S. Steel	" "	"	15.10	9.85	1.143	1.967	1000	20	1200	1800	1.2	0.60	29.7	10.20	3.45	27.86
1742SG	705X9-3X6	21.0	U.S. Steel	" "	"	15.10	9.85	1.143	1.967	500	150	1200	1800	0.6	0.70	29.7	10.60	10.29	33.38
1743SG	705X12-1X5*	21.0	U.S. Steel	" "	"	17.75	2.54	1.138	1.854	500	150	1200	1800	0.6	0.92	33.0	10.60	10.91	30.91
1744SG	Alum. Balls	-	-	-	-	-	-	-	-	1320	150	1100	600	0.6	-	-	-	-	-
1745SG	Alum. Balls	-	-	-	-	-	-	-	-	1390	20	1100	600	0.6	-	-	-	-	-
1746SG	812X1-1X5	50.4	U.S. Steel	Fly Ash	Bentonite	12.40	4.67	1.458	2.432	500	20	1200	1800	0.6	0.51	30.3	21.40	20.97	26.46
1747SG	813X1-1X4	63.0	U.S. Steel	" "	"	11.58	5.40	1.622	2.679	500	20	1200	1800	0.6	0.32	31.1	26.40	33.05	28.85
1748SG	814X1-1X7	42.0	U.S. Steel	" "	"	15.96	2.67	1.298	2.138	500	20	1200	1800	0.6	0.77	34.2	18.10	16.86	28.83
**1749SG	803X1-1X4	25.2	U.S. Steel	" "	"	19.34	4.43	1.101	1.836	500	20	1200	1800	0.6	-	35.6	9.09	6.64	34.60
1750SG	705X9-3X1	21.0	U.S. Steel	" "	"	14.60	9.33	1.157	1.976	1400	20	1200	1300	0.6	0.76	28.8	10.10	12.41	27.53
1751SG	705X12-1X5*	21.0	U.S. Steel	" "	"	17.75	2.54	1.138	1.854	500	20	1200	1800	0.6 +	0.87	33.0	10.80	12.23	30.90
1752SG	814X4-2X6	42.0	U.S. Steel	Silica	Kaolin	17.70	5.54	1.264	2.120	500	20	1200	1800	0.6	0.68	37.6	14.00	17.19	35.60
1753SG	814X2-2X6	42.0	U.S. Steel	Fly Ash	Kaolin	16.90	4.08	1.204	2.100	500	20	1200	1800	0.6	0.75	35.6	17.70	19.53	32.30
1754SG	814X3-1X6	42.0	U.S. Steel	Silica	Bentonite	17.50	6.38	1.246	2.127	500	20	1200	1800	0.6	0.72	37.3	15.00	17.58	35.50
1755SG	705X16-1X6	21.0	U.S. Steel	Silica	Bentonite	18.10	4.13	1.152	1.876	500	20	1200	1800	0.6	0.78	34.0	8.06	7.14	33.08
1756SG	814X1-1X7	42.0	U.S. Steel	Fly Ash	Bentonite	15.96	2.67	1.298	2.138	500	20	1200	1800	0.6	0.71	34.2	17.60	18.08	31.41
1757SG	814X1-1X7	42.0	U.S. Steel	" "	"	15.96	2.67	1.298	2.138	250	20	1200	3500	0.6	0.46	34.2	17.60	8.56	30.61
1758SG	705X9-2X1	21.0	U.S. Steel	" "	"	16.10	5.43	1.184	1.947	500	20	900	1700	0.6	0.42	31.6	10.00	9.76	28.70
1759SG	812X1-1X5	50.4	U.S. Steel	" "	"	12.40	4.67	1.458	2.432	500	20	1250	1800	1.2	0.39	30.2	20.00	13.22	28.10
1760SG	705X12-1X5*	21.0	U.S. Steel	" "	"	17.75	2.54	1.138	1.854	500	400	1200	1800	0.6	0.88	33.0	10.90	10.75	31.50
1761SG	705X9-3X7	21.0	U.S. Steel	" "	"	15.36	8.11	1.148	1.954	500	400	1200	1800	0.6	0.80	30.00	11.10	10.96	27.60
1762SG	814X1-1X12	42.0	U.S. Steel	" "	"	15.34	3.35	1.316	2.190	500	400	1200	1800	0.6	0.76	33.70	18.80	18.47	31.40
1763SG	813X1-1X4	63.0	U.S. Steel	" "	"	11.58	5.40	1.622	2.674	500	400	1200	1800	0.6	0.72	31.15	26.80	43.08	27.62
1764SG	814X1-1X12	42.0	U.S. Steel	" "	"	15.34	3.35	1.316	2.190	500	400	1400	1700	0.6	0.69	33.70	17.70	17.22	30.24
1765SG	814X1-1X12	42.0	U.S. Steel	" "	"	15.34	3.35	1.316	2.190	500	150	1200	1700	0.6	0.76	-	-	-	-
1766SG	814X3-3X2	42.0	U.S. Steel	Silica	"	16.93	5.05	1.276	2.150	500	400	1200	1800	0.6	0.79	36.5	15.70	15.64	32.86
1767SG	814X1-1X12	42.0	U.S. Steel	Fly Ash	"	15.34	3.35	1.316	2.190	500	150	1200	3500	0.6	0.65	33.7	18.90	8.58	31.60
1768SG	813X1-1X9	63.0	U.S. Steel	" "	"	11.56	5.46	1.597	2.690	500	400	1200	1800	0.6	0.74	31.18	29.80	34.81	27.20

Key: * Sorbent with 1/8 pellet diameter (all others 1/4 inch pellet diameter).
** Run was not completed.
+ No water in feed gas.

TABLE 4.2

CHEMICAL COMPOSITION OF IRON OXIDE SOURCES AND FORT MARTIN FLY ASH

	← Iron Oxide Sources →							Fort Martin Fly Ash
Composition	Fischer Sci	U.S. Steel	J&L	Armco	Youngstown	Republic OH	Republic BOF	
Fe_2O_3	100.0	79.8	61.6	72.8	64.3	80.5	69.5	18.7
Sulphur		0.7	1.9	0.0	1.2	0.4	0.2	NA
Al_2O_3		0.7	0.6	0.6	0.8	0.5	0.7	24.4
ZnO		0.1	10.8	3.6	15.2	0.1	0.2	NA
CaO		0.4	0.6	0.2	1.0	0.9	11.1	NA
MgO		0.3	0.4	0.2	0.5	0.8	1.5	1.0
Na_2O		0.7	0.9	0.2	1.1	0.4	0.6	0.6
PbO		0.1	2.2	0.7	1.4	0.03	0.1	0.1
CuO		0.1	0.2	0.1	0.1	0.03	0.1	0.02
MnO		0.4	0.5	0.5	0.7	0.6	0.8	NA
Flourine		0.1	0.1	0.2	0.1	0.1	0.8	NA
TiO_2		NA	NA	NA	NA	NA	NA	0.4
K_2O		NA	NA	NA	NA	NA	NA	0.04
SiO_2 & Unknowns		16.4	20.4	20.9	15.6	14.3	14.3	54.7

NA = Not analyzed

All Analyses determined at Houdry Technical Center

The use of silica as a support in place of fly ash seemed to increase sorbent porosity. The effect was not pronounced. For example, APCI Code 814X4-2X6 is 42% iron oxide on silica and has a porosity of 17.7%; sorbent 814X2-2X6 is 42% iron oxide on fly ash and has a 16.9% porosity.

The crushing strength of sorbents prepared for testing varies from 2.6 to 9.9 pounds of force per millimeter of pellet length. As mentioned in the "Final Report" by R. J. Jenkins, the sorbents with high crushing strength were exposed to "severe" heat treatments. No significant effect of sorbent hardness on sorption dynamics was noted from the experimental tests summarized in Table 4.1.

Sorbent bulk densities range from 1.0 kg/l for 8.4% added iron oxide on fly ash to 1.6 kg/l for 63% added iron oxide on silica fly ash. Density changes are largely a function of added iron oxide content of the sorbent.

4.2 Chemical Analysis of Experimental Sorbents

Table 4.2 lists this Laboratory's analysis of the seven iron oxide sources and the fly ash used to prepare the experimental sorbents in Table 4.1. In some cases the analysis in Table 4.2 differs significantly from the suppliers typical analysis in Table 4.3. Major impurities in the iron oxide are ZnO in the Youngstown, J&L, and ARMCO sources and CaO in the Republic BOF source. The J&L, Youngstown, and U.S. Steel sources contain more than 0.5 percent sulfur. All sources except Fischer Scientific contain significant levels of unknowns despite the fact that analysis was done for all impurities listed in the suppliers typical analysis.

The fly ash was found to consist mainly of SiO_2, Al_2O_3 and Fe_2O_3 as also reported in Bureau of Mines Report of Investigations 7947. The iron oxide in the fly ash could not be analyzed by X-ray fluorescence since it was bound in a matrix with SiO_2 and Al_2O_3. For this reason, fly ash iron oxide is assumed to contribute fewer sulfur sorption sites than the added iron oxide in the finished sorbent pellets.

The chemical analysis of the seven nominally 25 percent iron oxide experimental sorbents using different iron oxide sources is given in Table 4.4. Each of these sorbents was prepared so that the added iron oxide calculated from the suppliers typical analyses was 25 percent. Added iron oxide as calculated from the analysis of Table 4.2 varies from 15 to 25 percent. Major impurities analyzed in the finished sorbents are the Al_2O_3 and SiO_2 contained in the fly ash. Amounts of ZnO and CaO impurities are consistent with the iron oxide source chemical analysis.

TABLE 4.3

PHYSICAL AND CHEMICAL PROPERTIES OF APCI PREPARED 25% IRON OXIDE ON FLY ASH ABSORBENTS

CALCINED PELLET APCI CODE NO.	705X8-5X4	705X9-1X9	705X10-1X4	705X11-1X4
FLY ASH SOURCE	← BUREAU OF MINES, MORGANTOWN →			
IRON OXIDE SOURCE	FISHER SCIENTIFIC	U.S. STEEL HOMESTEAD, PA.	J & L STEEL PITTSBURGH, PA.	ARMCO STEEL MIDDLETOWN, OHIO
	LABORATORY GRADE	← ELECTROSTATIC PRECIPITATE →		OPEN HEARTH SLUDGE
COMPOSITION OF IRON OXIDE POWDER, WT. % (TYPICAL, AS REPORTED BY SUPPLIERS)				
TOTAL IRON				
AS Fe	69.9	63.5	61.1	51.2
AS Fe_2O_3	100.0	90.8	87.4	73.2
SULFUR		1.0	1.6	0.7
ZINC OXIDE		0.2	5.7	21.0
LEAD OXIDE		NR	1.4	0.6
SODIUM OXIDE		NR	NR	1.2
FLUORINE		NR	NR	1.2
CA, MN, CU, MG OXIDES		2.4	NR	2.8
AL, SI OXIDES		1.2	NR	0.8
PHYSICAL PROPERTIES OF CALCINED PELLETS				
BULK DENSITY, Kg/L	1.152	1.151	1.075	1.115
PELLET DENSITY, Kg/L	1.996	1.942	1.905	1.979
TRUE DENSITY, Kg/L	2.912	2.935	2.882	3.025
PORE VOLUME, cc/g	0.157	0.174	0.177	0.174
SURFACE AREA, M^2/g	<5	<5	<5	<5
CRUSHING STRENGTH, Lb/mm	7.4	5.6	5.2	6.5

TABLE 4.4

CHEMICAL COMPOSITION OF SORBENT PELLETS

APCI Pellet Code No.	705x8-5x2	705x9-2x1	705x10-1x4	705x11-1x4	705x13-1x2	705x14-1x2	705x15-1x2
Iron Oxide Source	Fischer Scientific	U.S. Steel	J&L Steel	Armco	Youngstown	Republic Open Hearth	Republic BOF
Fly Ash Source	← Fort Martin Fly Ash Supplied by Bureau of Mines, Morgantown →						
Chemical Composition of Sorbent Pellets							
Added Fe_2O_3 (from iron oxide source)	25.0	20.3	15.5	20.9	20.4	20.9	18.9
Total Fe_2O_3	37.2	32.3	30.3	37.2	31.4	33.0	30.3
Sulfur	0.2	0.1	0.2	0.2	0.2	0.2	0.2
Al_2O_3	17.0	18.4	16.4	16.2	16.1	16.4	15.5
ZnO	0.02	0.1	2.6	1.1	4.3	0.1	0.1
CaO	0.2	0.1	0.2	0.2	0.2	0.2	1.1
MgO	0.9	0.9	0.9	0.8	0.9	1.0	1.2
Na_2O	0.6	0.7	0.7	0.6	0.8	0.6	0.7
PbO	0.0	0.02	0.6	0.2	0.4	0.0	0.04
CuO	0.01	0.04	0.1	0.04	0.1	0.02	0.04
MnO	0.04	0.1	0.1	0.2	0.2	0.2	0.2
Flourine	0.01	0.1	0.2	0.01	0.01	0.02	0.1
SiO_2 & Unknowns	43.8	47.2	47.9	43.2	45.5	48.3	50.5

5.0 DYNAMIC TESTS OF EXPERIMENTAL SORBENTS

5.1 Dynamic Test Procedure

The unit used for dynamic testing of experimental sorbents was originally described in the Final Report for OCR Contract No. E(49-18)-1510, Pages 5.1 to 5.15. The pertinent sections of that final report are included in Appendix A . This unit, herein referred to as the ERDA pressure unit, was designed to operate at 150 psig and 1600°F. Since generation of electricity from producer gas using a combined power cycle is expected to be more economical at higher pressures, the unit was modified for operation at 400 psig. Dynamic tests at 400 psig used a modified flow scheme described in Appendix A.2.

A total of 68 dynamic sorptions were conducted in the ERDA pressure unit. Each dynamic test was conducted by the following method.

1. Each test was a sorption of hydrogen sulfide on fresh experimental sorbent. Regenerations and sorptions on regenerated sorbents were not carried out.

2. The tar and particulate free simulated low BTU producer gas feed to the ERDA pressure unit had the following nominal volumetric composition:

N_2	48.6%
CO	20.5%
H_2	14.9%
CO_2	6.5%
CH_4	1.9%
H_2S	0.6%
H_2O	7.0%

3. The hydrogen sulfide content of the off-gas from the ERDA pressure unit was analyzed at 5-minute intervals by an automatic online GC unit. The test run was concluded after the concentration of the off-gas equalled the feed gas hydrogen sulfide concentration for at least 2 hours.

4. Sorbent capacities were determined by analysis of the spent experimental sorbents for total sulfur. An X-ray fluorescence technique was used for this analysis.

5.2 Analysis of Sorption Dynamics Data

Each dynamic test run conducted was analyzed in terms of a sorption efficiency. This efficiency is explained by the following definitions:

Percent Breakthrough - The H_2S concentration in the sorber effluent gas expressed as a percentage of the H_2S concentration in the feed gas. The percent breakthrough for a sorber bed varies with onstream time.

Perfect Sorption - A sorber is operating perfectly if the effluent gas contains no H_2S until the bed is saturated with sulfur.

Perfect Sorption Time - The time at which H_2S would break through a perfectly operating sorber. This time is the minimum time in which H_2S-laden feed gas could saturate a sorbent bed with sulfur. Perfect sorption time is also defined as the sorber ultimate sulfur capacity divided by the sulfur flow rate in the feed gas. Every sorber has a perfect sorption time for a given sulfur feed rate.

Ultimate Sulfur Capacity - The sorbent sulfur capacity in weight sulfur per volume of sorber bed at 100% bed sulfur breakthrough. Ultimate sulfur capacity is the maximum amount of sulfur the sorbent can hold at the given temperature and pressure.

Dimensionless Onstream Time - The ratio of sorber onstream time to perfect sorption time.

Dimensionless Breakthrough Time - Dimensionless onstream time when arbitrary but set H_2S concentrations appear in the effluent.

Sorption Efficiency - The ratio of sorber onstream time for actual operation to sorber onstream time for perfect sorption. The sorption efficiency has the same definition and value as the dimensionless breakthrough time. However, sorption efficiency is not completely defined unless the percent breakthrough is given. In this report, sorption efficiency at 10% breakthrough is implied when the percent breakthrough is not specified.

Sorbent Performance - Sorbent performance at a set of sorption conditions is completely specified by a plot of percent breakthrough versus dimensionless time (or sorption efficiency). This report uses sorption efficiency at 10% breakthrough as a concise measurement of sorbent performance. Sorption efficiency for perfect sorption is equal to one. Perfect sorption is the best possible sorbent performance.

Available Sulfur Capacity - As indicated by the definitions above, sorber onstream time is the product of perfect sorption time and sorption efficiency. Since perfect sorption time is proportional to the ultimate (or 100% breakthrough) sorbent sulfur capacity, onstream time is proportional to the product of sorption efficiency and ultimate sulfur capacity. This product is the available sulfur capacity. It represents the weight of sulfur per unit volume of bed that can be processed prior to 10% breakthrough.

Optimum Sorbent - The optimum sorbent for a given set of operating conditions is herein defined as the sorbent with the longest onstream time prior to 10% breakthrough. This statement is equivalent to saying that the optimum sorbent has the largest available sulfur capacity. This optimum sorbent is an economic optimum if:

1. The purchase cost of all sorbents are the same.
2. The durability of all sorbents are the same.
3. The sorption efficiency is an average efficiency for the sorbent life cycle.

Since experimental work at APCI has used freshly prepared sorbents to determine sorption efficiencies, and since durability of sorbents has not been determined, sorbents referred to as optimum within this report are not necessarily optimum with respect to purchase and operating costs.

The raw data for the sorption dynamics test runs and the resultant percent breakthrough versus efficiency data are presented in Appendix B. Table 5.1 outlines the method used to calculate sorbent performance curves (percent breakthrough versus dimensionless time) in this Appendix. The calculation depends solely on the percent breakthrough versus time information collected experimentally using an online gas chromatograph and a clock. Uncertainty introduced from measurements

TABLE 5.1

CALCULATION OF DIMENSIONLESS TIME FROM SORPTION DYNAMICS INFORMATION

II.1 DEFINITION OF DIMENSIONLESS TIME (SORPTION EFFICIENCY):

$$\tau = \frac{C_{H_2S^\circ}\ \mathrm{GHSV}\ t}{M_o}$$

II.2 SORBENT BED CAPACITY (M_o) AS CALCULATED FROM SORPTION DYNAMICS INFORMATION:

$$M_o = \mathrm{GHSV}\ C_{H_2S^\circ} \int_{t\,=\,0}^{t\,=\,\text{Bed Saturation Time}} (1 - F)dt$$

II.3 BY SUBSTITUTING THE SORBENT BED CAPACITY CALCULATED IN II.2 INTO THE DEFINITION OF DIMENSIONLESS TIME, A DIMENSIONLESS TIME WHICH IS INDEPENDENT OF GHSV AND $C_{H_2S}^\circ$ MEASUREMENT IS OBTAINED:

$$\tau = \frac{t}{\displaystyle\int_{t\,=\,0}^{t\,=\,\text{Bed Saturation Time}} (1 - F)dt}$$

II.4 NOMENCLATURE:

C_{H_2S} = Bed Effluent H_2S Concentration (Moles/SCF)

$C_{H_2S^\circ}$ = Bed Feed H_2S Concentration (Moles/SCF)

F = Dimensionless Effluent Concentration ($C_{H_2S}/C_{H_2S^\circ}$)

GHSV = Bed Gas Hourly Space Rate (SCFH/Ft.^{3} Bed)

M_o = Bed Capacity (Moles/Ft.^{3} of Bed)

t = Real Time (Hours)

τ = Dimensionless Time (Chemical Efficiency) using these devices is small. Clocks can be read to within one minute for a total run time exceeding 10 hours; the online GC has held calibration (less than 1% change in GC analysis of standard calibration gas) for periods of 30 hours. Since the data used to calculate sorbent performance is precise, sorbent performance uncertainty is minimized. Figure 5.1 is an indication of the reproducibility of sorbent performance curves using the method of Table 5.1 to calculate dimensionless time.

Ultimate sulfur capacity is measured by analysis of the sulfided experimental sorbents by X-ray flourescence. Precision of the analysis of samples from the same test run is ± 0.1% wt. Capacities measured using samples of duplicate sorbent preparations sulfided in duplicate runs can vary as much as ± 2%.

Reproducibility of available sulfur capacity depends on the reproducibility of sorption efficiency and ultimate sulfur capacity.

5.3 Selection of a Sorbent Iron Oxide Source

Four criteria were used in selecting the iron oxide sources suitable for commercial sorbent manufacture:

1. Source iron oxide content.
2. Source availability.
3. Ultimate sulfur capacity of sorbent made using the source.
4. Dynamic performance of sorbent made using the source.

On the basis of the first two criteria, six candidate iron oxide sources were chosen:

Iron Oxide Source	Source Fe_2O_3 Content (Weight Percent)
U.S. Steel	79.8
J&L Steel	61.6
Armco	72.8
Youngstown	64.3
Republic OH	80.5
Republic BOF	69.5

The iron oxide content listed for the six sources is calculated from the Houdry Technical Center analysis of source iron. All this iron may not be in the form of Fe_2O_3, as assumed in the above table.

FIGURE 5.1

DIMENSIONLESS BREAKTHROUGH CURVES FOR DUPLICATE RUNS

NOMINAL CONDITIONS: 1800 GHSV, 0.7 PERCENT H_2S IN FEED, 1200°F, 20 PSIG

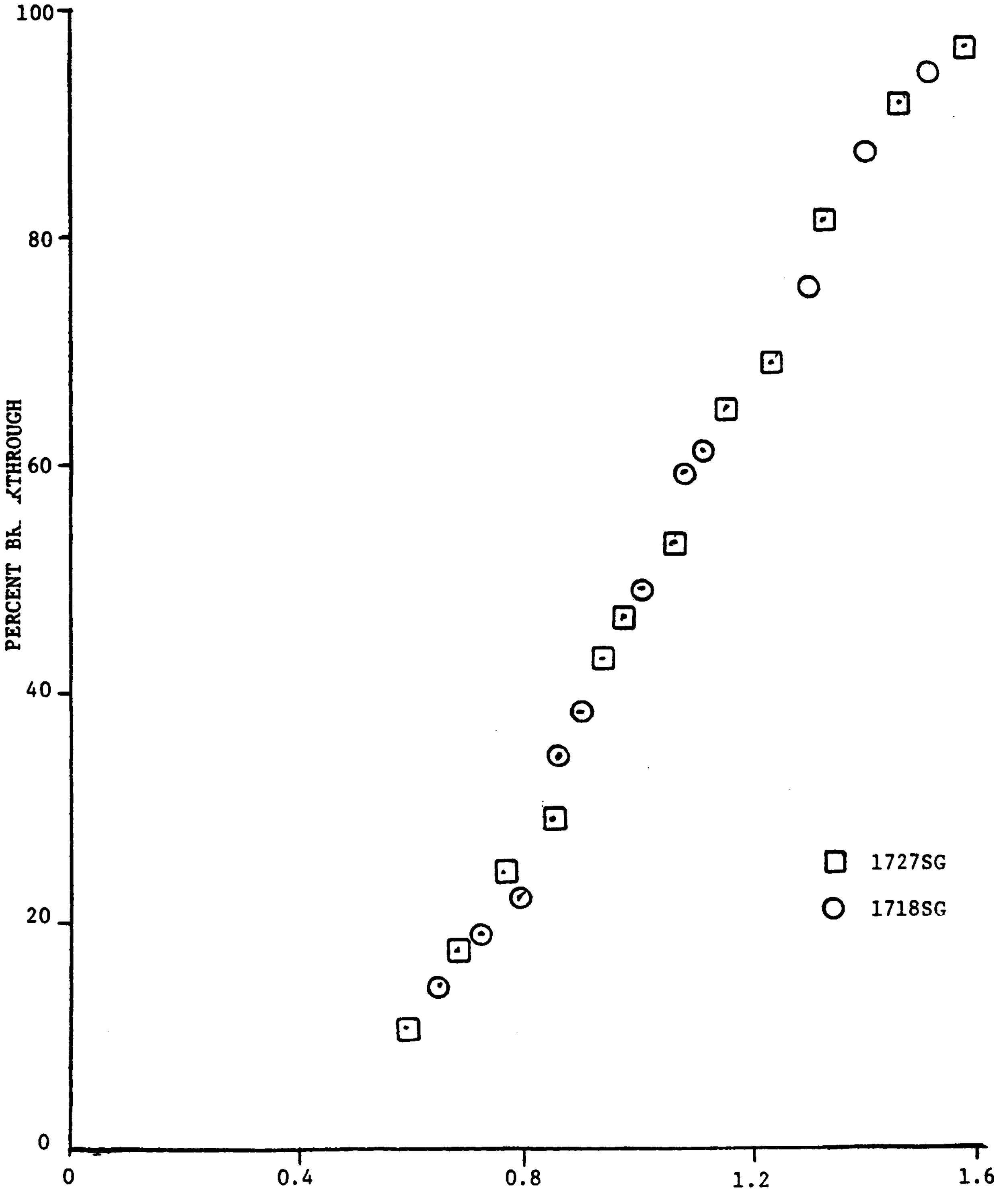

τ, DIMENSIONLESS TIME ON STREAM OR SORPTION EFFICIENCY

PCRD-1296
3-24-76
E.L.L.

5.3.1 Effect of Iron Oxide Source on Sorbent Ultimate Sulfur Capacity

Sorbents were prepared using approximately 25 weight percent of each of the six sources listed above and 75 weight percent Fort Martin fly ash. These sorbents were fully sulfided during dynamic tests and the sulfur content of the spent sorbent was analyzed by X-ray flourescence. Table 5.2 lists the capacity of each of the six sorbents in weight percent sulfur. Table 5.2 also lists the ultimate sulfur capacity per gram of added sorbent iron oxide and ultimate sulfur capacity per gram of added source. The capacity per gram of added iron oxide measures the activity of the source iron. This activity is probably a measure of the amount of the calculated iron oxide content (based on source iron content) that is actually iron oxide. The capacity per gram of source is a measure of the weight of sulfur that potentially can be removed for each gram of source purchased. The capacity per gram of source is assumed to be proportional to the percentage of chemically active iron oxide in the source material. Table 5.2 indicates that Armco, J&L Steel, and U.S. Steel iron oxide sources contain the larger amounts of active iron oxide on the basis of sulfur capacity.

It is stated in Bureau of Mines Investigation 7947, Page 9, that fly ash alone has a 2.5 weight percent sulfur capacity. Since all sorbents tested have approximately the same fly ash content, subtracting the fly ash capacity from the total sorbent capacity to give the true sulfur capacity of the iron oxide source does not effect the ranking of source active iron oxide content given alone.

5.3.2 Effect of Iron Oxide Source on Sorbent Performance

Typical performance curves for sorbents prepared using different iron oxide sources on fly ash are presented in Figure 5.2. The figure indicates that the sorbents using the two Republic Steel sources and the sorbent using J&L source define a single performance curve with sorption efficiency between 0.45 and 0.50 at 10% breakthrough. Armco Steel iron oxide source on fly ash has the best performance curve, with efficiency of 0.70 at 10% breakthrough. U.S. Steel and Youngstown sources on fly ash define a more efficient breakthrough curve than the Republic sorbents but less efficient than Armco Steel sorbent.

5.3.3 Available Sulfur Capacity for Sorbents Using Different Iron Oxide Sources

Available sulfur capacity is defined in Section 5.2 as the product of sorbent ultimate sulfur capacity and sorption efficiency. Table 5.3 lists the available sulfur capacity for each of the six iron oxide sources selected for study. Ultimate sulfur capacities are computed for 26% added iron oxide source/74% fly ash sorbent using the

TABLE 5.2

SULFUR CAPACITY PER GRAM ADDED IRON OXIDE AND SULFUR CAPACITY PER GRAM IRON OXIDE SOURCE

Iron Oxide Source	Sorbent Code	Weight % Sulfur in Spent Pellets*	Weight of Spent Pellets Per Weight of Fresh Pellets	Weight % Iron Oxide Source in Fresh Pellets	Weight Fraction Iron Oxide in Source	Ultimate Capacity	
						Grams Sulfur Per Gram Added Iron Oxide	Grams Sulfur Per Gram of Added Source
U.S. Steel	705X9-2	10.2	1.062	25.5	.798	.532	.425
J&L Steel	705X10	11.0	1.022	24.9	.616	.733	.451
Armco Steel	705X11	13.7	1.017	28.7	.728	.667	.485
Youngstown	705X13	10.0	1.033	31.7	.643	.507	.326
Republic Open Hearth	705X14	9.9	1.026	26.0	.805	.485	.391
Republic BOF	705X15	8.5	1.025	27.3	.695	.459	.319

* These capacities are the average of the sulfur analyses of spent sorbents from two or more sorption runs.

FIGURE 5.2

EFFECT OF IRON OXIDE SOURCE ON SORBENT PERFORMANCE

CONSTANT PARAMETERS: 1800 GHSV, 1200°F, 20 psig,
0.6% H_2S in Feed, 0.6 fps superficial velocity

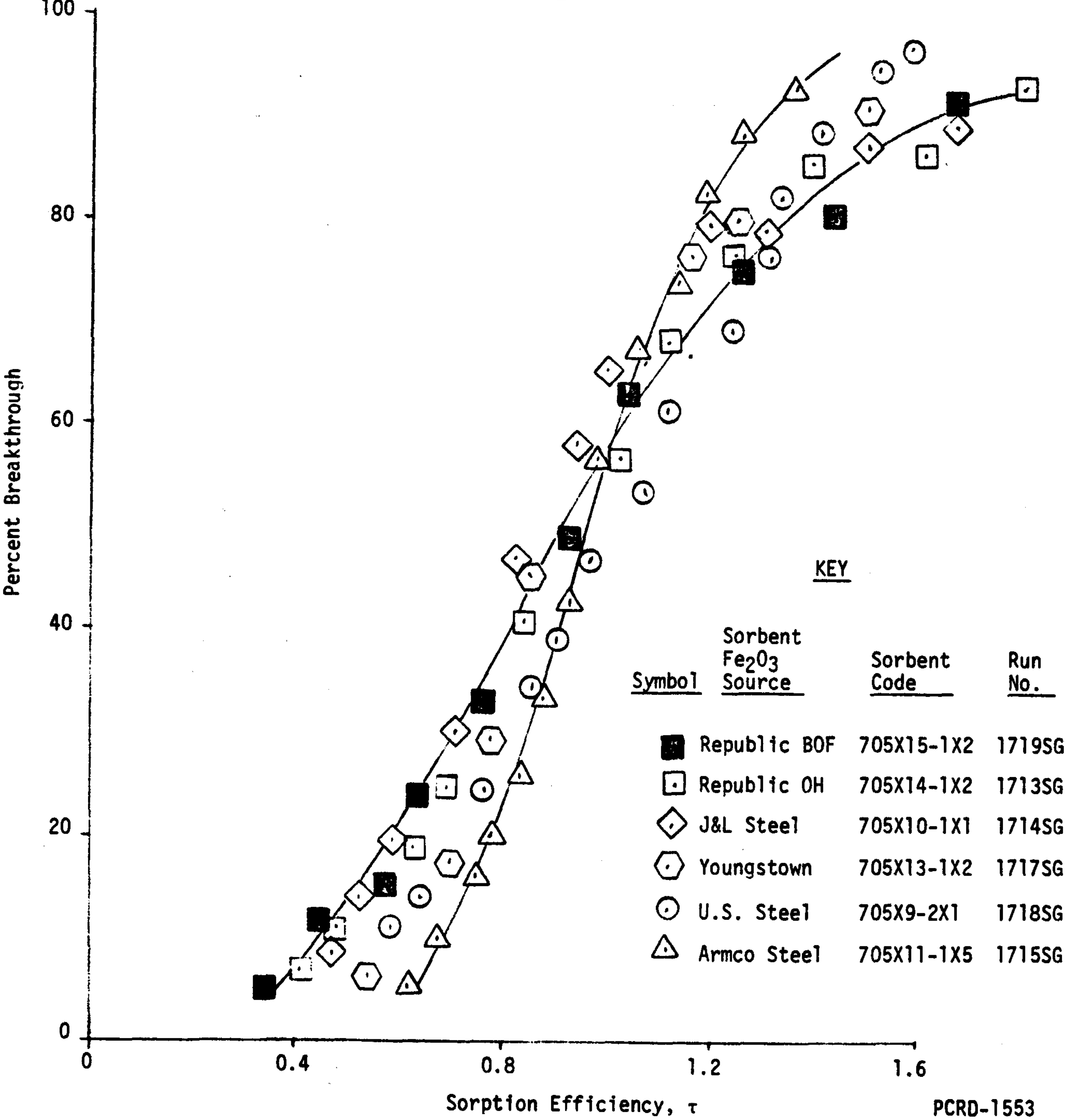

Symbol	Sorbent Fe_2O_3 Source	Sorbent Code	Run No.
■	Republic BOF	705X15-1X2	1719SG
☐	Republic OH	705X14-1X2	1713SG
◇	J&L Steel	705X10-1X1	1714SG
⬡	Youngstown	705X13-1X2	1717SG
⊙	U.S. Steel	705X9-2X1	1718SG
△	Armco Steel	705X11-1X5	1715SG

TABLE 5.3
AVAILABLE SULFUR CAPACITY FOR SIX DIFFERENT 26% ADDED IRON OXIDE SOURCE ON FLY ASH SORBENTS

Iron Oxide Source	Grams Sulfur Per Gram Added Iron Oxide Source	Fresh Sorbent Sulfur Capacity (gm Sulfur/gm Sorbent)	Sorbent Density (gm/l)	Sorbent Ultimate Sulfur Capacity (gm/l)	Sorption Efficiency at 10% Breakthrough	Number of Dynamic Tests Used to Obtain Efficiency	Available Sulfur Capacity (gm/l)
U.S. Steel	.425	.110	1184	130	0.60	4	78
J&L Steel	.451	.117	1010	118	0.53	2	63
Armco Steel	.485	.126	1115	140	0.70	1	98
Youngstown	.326	.085	1113	95	0.65	1	62
Republic Open Hearth	.391	.102	1153	118	0.50	1	59
Republic BOF	.319	.083	1067	89	0.42	1	37

source sulfur capacity of Table 5.2. Sorption efficiencies at 10% breakthrough were obtained from dynamic tests using the experimental sorbents listed in Table 5.2, which contain between 24 and 32 percent added iron oxide source. Test results for the efficiency of U.S. Steel and J&L Steel sources are based on more than one dynamic sorption; duplicate dynamic tests were not conducted for the other sorbents. The test conditions listed in Figure 5.2 were used to obtain the sorption efficiencies of Table 5.3.

The available sulfur capacities of Table 5.3 indicate that sorbents using Armco and U.S. Steel iron oxide sources should have longer onstream times than sorbent using an equal weight fraction of another iron oxide source. This conclusion is confirmed by time versus percent breakthrough plots, such as Figure 5.3. Of the two high available capacity sorbents, the sorbent using Armco Steel source appears to have an advantage over the sorbent using U.S. Steel source. The significant difference between the two sorbents is the higher efficiency of the Armco sorbent. However, the sorption efficiency for the Armco source on fly ash is based on only one dynamic test (1715SG), while the efficiency of U.S. Steel source on fly ash is based on five duplicate tests (1705SG, 1706SG, 1718SG, 1726SG, and 1727SG). Four of the five test runs using U.S. Steel sorbent are in close agreement; the fifth run, 1706SG, has a significantly higher efficiency (0.77). The efficiency for U.S. Steel sorbent in Table 5.3 is based on the four runs which are in close agreement and should be considered highly reliable; the uncertainty of the efficiency for the Armco sorbent is greater. Thus, on the basis of available data, both U.S. Steel and Armco iron oxide sources must be considered as suitable sources for commercial sorbent. The above conclusion is based on the available sulfur capacity of freshly prepared sorbent. The results should not be applied to regenerated sorbents until verified by life cycle testing.

Earlier analyses of the effect of iron oxide source had shown both U.S. Steel and Armco iron oxide sources as nearly equivalent (Quarterly Report No. 2, Sections II A.3 and III F). At that time, only runs 1705SG and 1706SG were available for use in obtaining the sorption efficiency of U.S. Steel source on fly ash. On the basis of the data available at that time, U.S. Steel source was chosen for use in process variable testing. These dynamic test results are presented in Sections 5.4 and 5.5 of this report.

5.4 Effects of Design Variables on Performance of Sorbent Using U.S. Steel Iron Oxide at 20 psig

5.4.1 Effects of Velocity and GHSV on Sorbent Performance

For the purposes of engineering design, two different velocity effects have been determined in a program to define scale-up criteria: linear velocity effects and GHSV effects. When linear velocity

FIGURE 5.3

ABSORPTION DYNAMICS WITH DIFFERENT IRON OXIDE SERIES

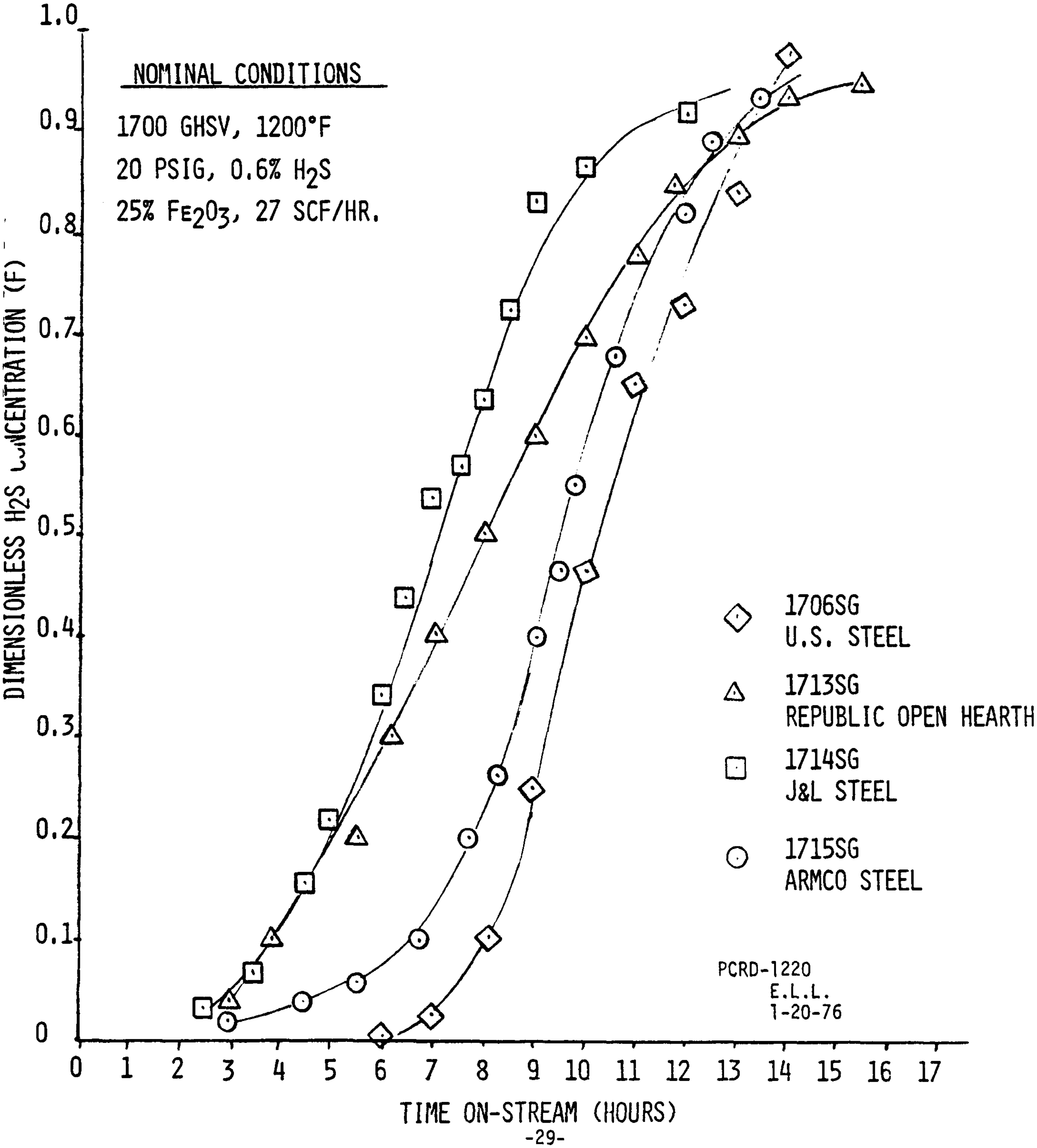

NOMINAL CONDITIONS

1700 GHSV, 1200°F
20 PSIG, 0.6% H_2S
25% Fe_2O_3, 27 SCF/HR.

PCRD-1220
E.L.L.
1-20-76

is specified for a given producer gas volumetric flow rate, the bed cross-sectional area is also fixed. Thus the effect of linear velocity on sorbent performance may also be considered an effect of bed geometry on performance. GHSV is defined as the volumetric flow rate of producer gas in units of sorber volumes per hour. Its reciprocal, space time, is easily related to the contact time of the process gas with the sorbent bed. If a practical range of operating GHSV's can be determined for a sorbent, then the volume of sorbent required for any producer gas flow rate can be quickly estimated. When designing a commercial sorber, the GHSV specification fixes the sorber size and the linear velocity specification fixes the sorber geometry.

The APCI velocity effects experimental program involved two steps:

(a) Determination of linear velocity effects at constant GHSV. These effects were expected to be small since the contact time between producer gas and sorbent was not varied during these studies.

(b) Determination of the effects of GHSV at constant linear velocity on sorption dynamics.

In order to determine the effect of linear velocity at 3600 GHSV, Run 1739SG was conducted using a one liter charge of sorbent and a producer gas rate of 120 standard cubic feet per hour. Then both the sorbent volume and the gas rate were cut in half for Run 1740SG. As a result, both runs were at 3600 GHSV, but Run 1739SG had a 2.3 fps velocity and Run 1740SG had a 1.2 fps linear velocity.

Figure 5.4 shows the performance curves for these two runs. The run at the higher velocity has a 0.51 efficiency at 10% breakthrough, while the lower velocity run has an efficiency of 0.41. Thus Figure 5.4 shows a significant linear velocity effect at constant GHSV. This result indicates that sorption efficiency can be improved by modifying the sorber geometry to increase linear velocity. Improvements in performance from increased velocity involve a trade-off with the increased bed pressure drop at higher velocities.

The linear velocity effects described above were also observed at 1800 GHSV. Run 1738SG at 1.2 fps had an efficiency of 0.66, while Run 1718SG at 0.6 fps had an efficiency of 0.58.

The effect of GHSV at constant linear velocity is demonstrated by Figure 5.5. Both Run 1738SG and Run 1740SG were conducted using 60 SCFH of producer gas and thus have the same linear velocity. Run

FIGURE 5.4

EFFECT OF LINEAR VELOCITY ON SORBENT PERFORMANCE AT 3600 GHSV

CONSTANT PARAMETERS: Sorbent Code 705X9-3X4, 21% Added Fe_2O_3 on Fly Ash, 1200°F, 20 psig, 0.6% H_2S in Producer Gas Feed

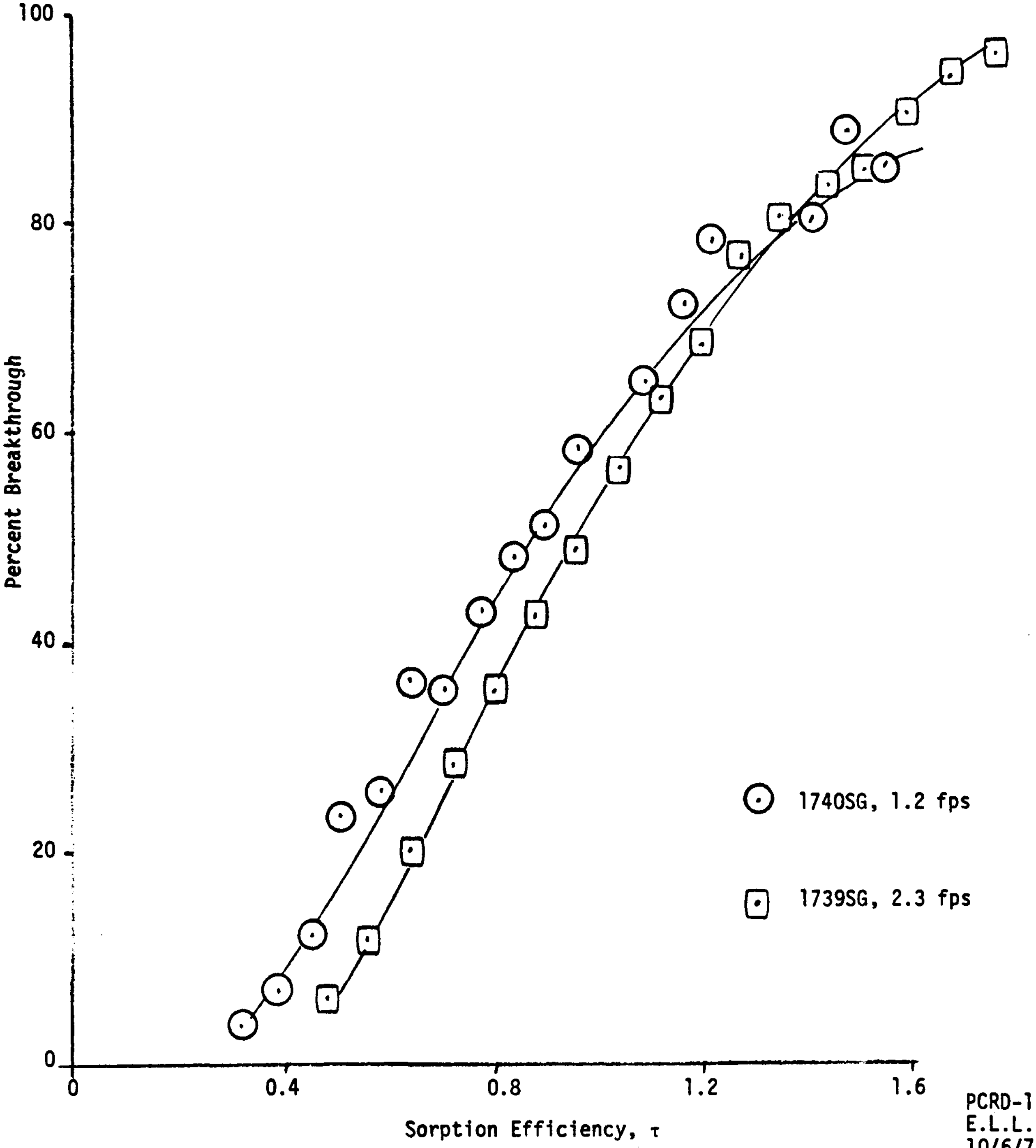

PCRD-1554
E.L.L.
10/6/76

FIGURE 5.5
EFFECT OF GHSV ON SORBENT PERFORMANCE AT 1.2 fps LINEAR VELOCITY

CONSTANT PARAMETERS: Sorbent Code 705X9-3X4, 21% Added Fe_2O_3 on
Fly Ash, 1200°F, 20 psig, 0.6% H_2S in Feed Gas

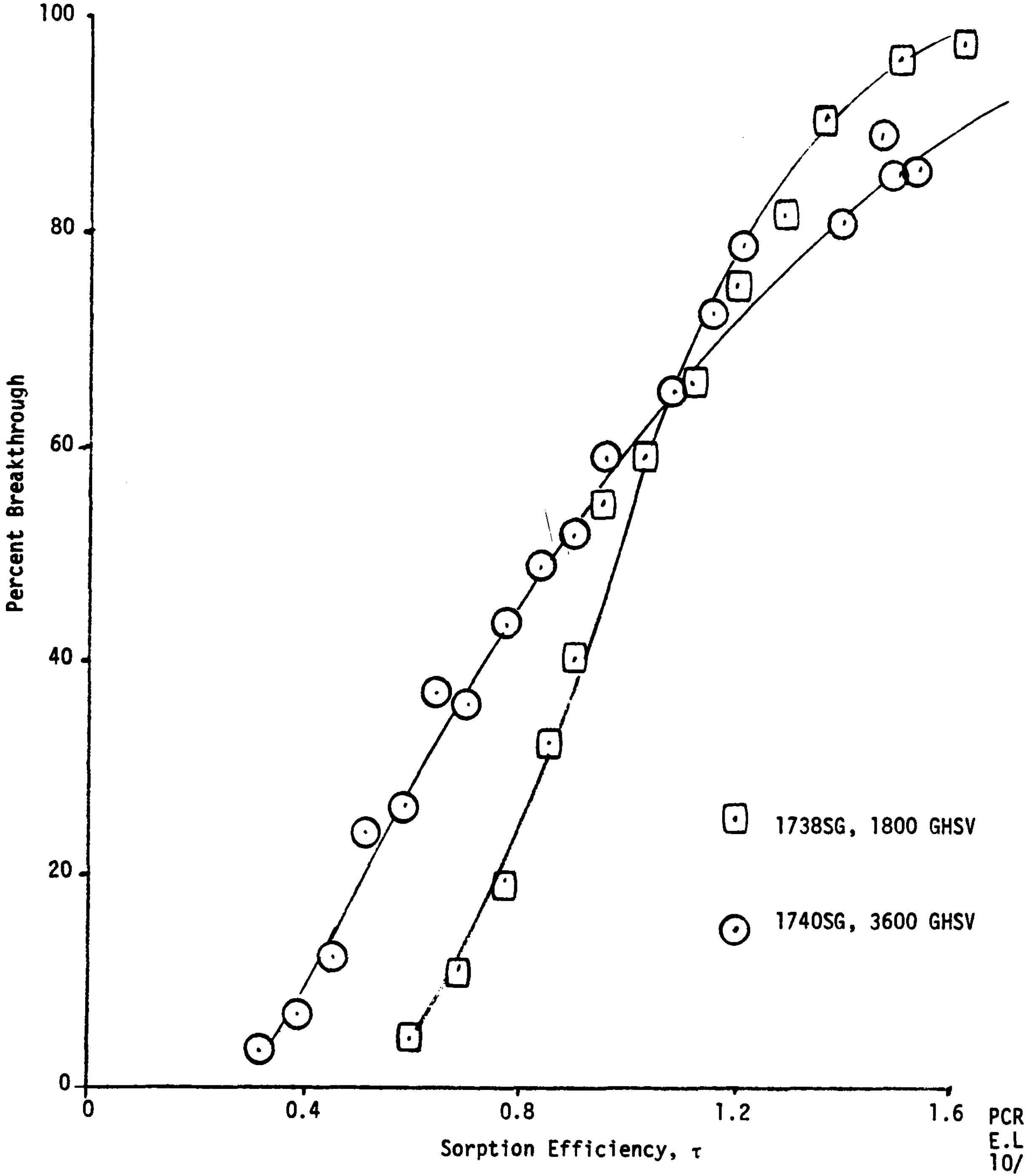

PCRD-1555
E.L.L.
10/6/76

1738SG had a one liter charge of sorbent while 1740SG had a half liter charge. Thus 1738SG has twice the contact time and half the GHSV of Run 1740SG. As expected, the run with the longer contact time exhibits a higher efficiency.

The velocity effects demonstrated by Figures 5.4 and 5.5 indicate two opposing trends in sorbent performance when producer gas throughout is increased:

(1) As the GHSV of a sorber is increased at constant linear velocity, sorption efficiency is significantly reduced.

(2) The above decrease in efficiency can be compensated by an increase in linear velocity.

As a result of these two velocity effects, GHSV can be increased without significantly reducing sorbent efficiency. For example, Run 1718SG has an efficiency of 0.58 at 0.6 fps and 1800 GHSV. If the GHSV is doubled, Run 1739SG illustrates that high efficiency can be maintained by quadrupling the linear velocity. This run has an efficiency of 0.51 at 1.2 fps and 3600 GHSV, which is not much lower than that of Run 1718SG.

The observed effect of GHSV at constant linear velocity on sorption dynamics is a "constant pattern" effect. Constant pattern GHSV effects have two distinguishing characteristics:

(1) The change in onstream time to a given breakthrough for a change in GHSV always equals the change in perfect sorption time.

(2) The volume of sorbent in the bed that is not fully saturated prior to breakthrough is the same at any GHSV. Perry's handbook (Chemical Engineers Handbook, Perry and Chilton, McGraw-Hill, 1973) refers to this property of constant pattern sorptions as the "length-of-unused-bed" approach to scale-up on pages beginning with 16-24.

The knowledge that a sorption process displays constant pattern GHSV effects enables a designer to predict the effect of a change in GHSV on sorber performance without the use of a model. For example, if the GHSV of a sorber is doubled and no other design variable (linear velocity, temperature, etc.) is changed, sorber onstream time will be reduced by one-half the perfect sorption time for the original sorber. If a designer wishes to size a sorber using the length-of-unused-bed scale-up technique for constant pattern sorption, he estimates the volume of the bed required to give the desired onstream time using perfect sorption and then adds an experimentally determined "unused" bed volume.

The existence of constant pattern sorption dynamics can be demonstrated from real time plots for two runs at different GHSV and constant linear velocity. Figure 5.6 is such a real time plot for Runs 1738SG and 1740SG, whose dimensionless time performance curves were earlier presented as Figure 5.5. It appears from the plot that if the two breakthrough curves were superimposed upon each other, they would form a single curve, or a "constant pattern". This constant pattern gives the type of dynamic behavior described above its name.

5.4.2 Temperature Effects on Sorbent Performance

Sorption dynamics test runs were conducted at four levels of temperature: 600°F, 900°F, 1200°F, and 1400°F. All tests were made with sorbent prepared with 21 to 25% added iron oxide, U.S. Steel iron oxide source, 1/4 inch diameter sorbent size, and 1/2 liter of sorbent. Operating conditions were 1800 GHSV, 20 psig, and 0.6% H_2S in the sorber feed. Figure 5.7 shows the percent breakthrough versus sorption efficiency plots for test runs at 600°F, 900°F, 1200°F, and 1400°F. The figure shows that sorption efficiency rapidly improves between 600°F and 900°F. Little improvement is found between 900°F and 1200°F, and the sorption dynamics appear to be identical at 1200°F and at 1400°F.

The first two attempts to conduct a dynamic test at 900°F led to sintering of the sorbent. The sorbent bed was heated to 900°F with a flow of hot nitrogen. The bed was then exposed to a simulated producer gas of the following volumetric composition:

	Percent
Nitrogen	48
Carbon Monoxide	20
Hydrogen	15
Carbon Dioxide	6
Methane	2
Steam	9

This is the composition of a hydrogen sulfide-free feed gas. Sorbent beds are routinely exposed to this gas mixture prior to a test run for periods of up to five hours. The purpose of the above procedure is to

FIGURE 5.6

TWO DYNAMIC SORPTION RUNS AT DIFFERENT GHSV AND EQUAL LINEAR VELOCITY

CONSTANT PARAMETERS: 1200°F, 20 psig, 0.6% H_2S in Feed,
1.2 fps Superficial Velocity

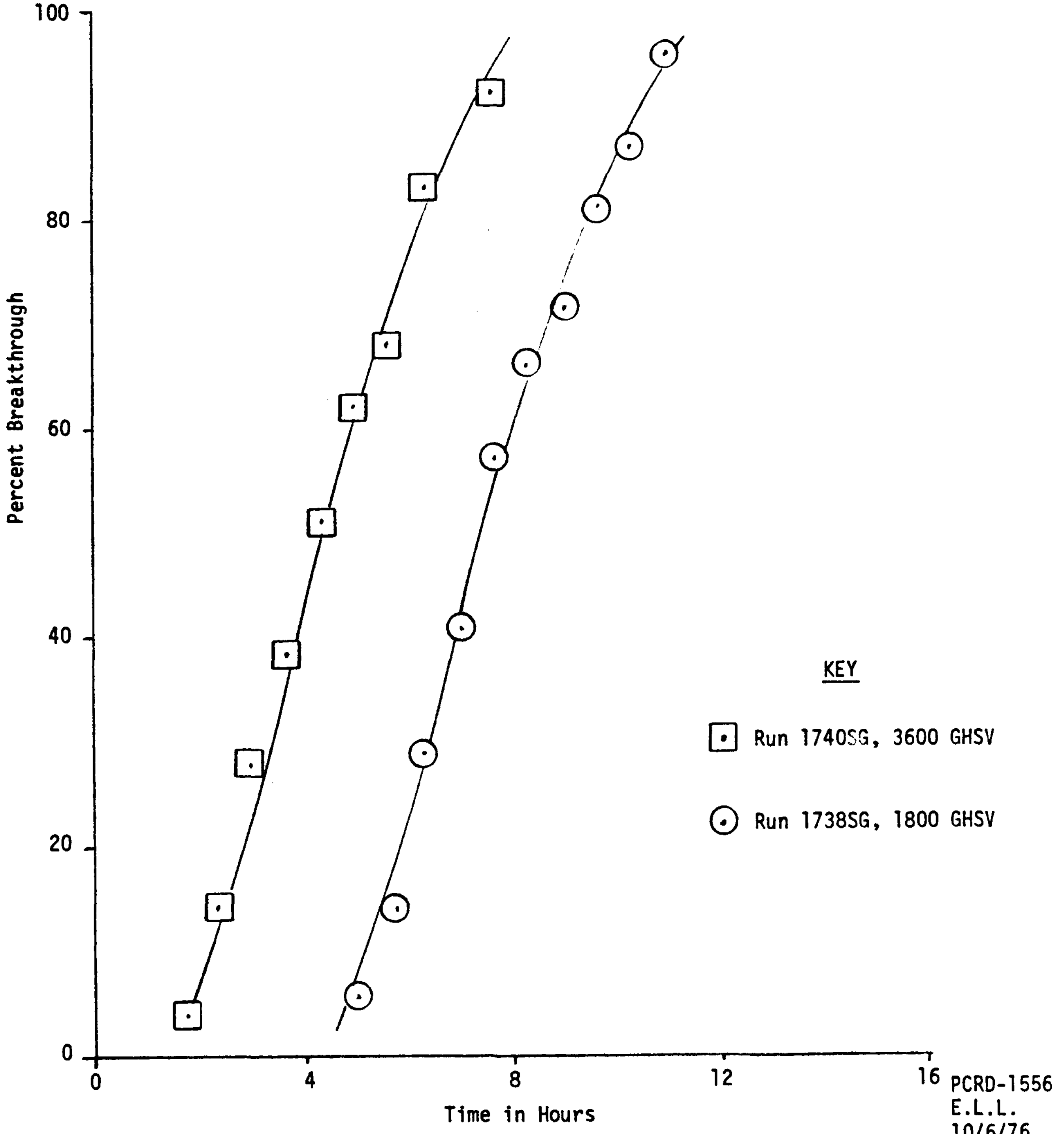

PCRD-1556
E.L.L.
10/6/76

FIGURE 5.7

TEMPERATURE EFFECTS ON SORBENT PERFORMANCE

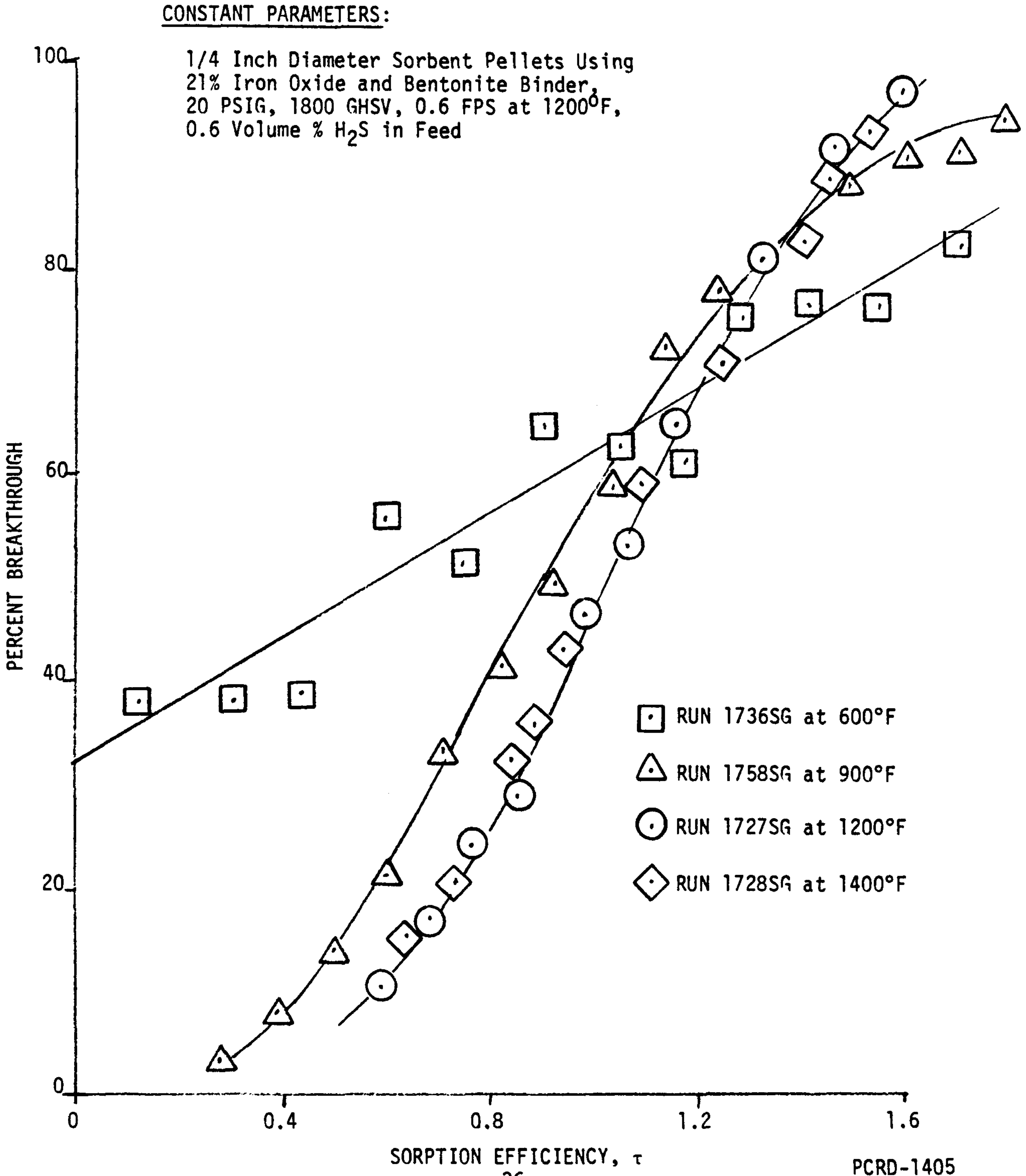

PCRD-1405
E.L.L.
6-4-76

provide time for bed temperature to equilibrate before starting the run by adding hydrogen sulfide to the feed. After the sorbent was exposed to a 900°F stream of the above sulfur-free feed for an hour, a bed pressure drop of 80 psi and a bed temperature rise of 100°F were observed. The sorbent discharged from the bed at this time was found to have disintegrated into a powder.

Run 1758SG, the third attempt to conduct a dynamic test at 900°F, used a modified startup procedure. The bed of sorbent was again brought to 900°F using hot nitrogen. The run was then started and the bed was immediately exposed to producer gas containing hydrogen sulfide. Thus bed exposure to H_2S-free producer gas was minimized.

On discharge, the sorbent pellets in the inlet section of the bed were observed to be intact. The pellets at the outlet section of the bed, which had been exposed to gas that had been desulfurized by the inlet section of the bed, were sintered. These observations confirm the assumption that exposure to H_2S-free producer gas leads to sorbent disintegration at 900°F. The sorbent deterioration observed at 900°F is unusual, since pellets discharged from runs at 600°F, 1200°F, and 1400°F were intact.

5.4.3 Effect of Producer Gas Hydrogen Sulfide Concentration on Sorbent Performance

Runs 1738SG and 1741SG differ only in the hydrogen sulfide concentration of the producer gas. Figure 5.8 presents the dynamic performance curves for these two runs. Sorbent performance appears to be better at lower levels of producer gas hydrogen sulfide. However, the effect is small and may not be statistically significant.

5.4.4 Effect of Sorbent Pellet Diameter on Performance at 20 psig

Of the 54 experimental sorptions conducted at 20 psig, three used 1/8 inch diameter sorbent pellets. For each of these three runs, a corresponding sorption was conducted using 1/4 inch diameter sorbent pellets. Performance curves for some of these runs were presented in Figure 4, Monthly Report No. 8. The following excerpt from Table 4.1 allows a concise comparison of the effect of pellet size on sorption efficiency at 10% breakthrough for runs conducted at 20 psig.

Runs Using 1/8 Inch Pellet		Corresponding Runs Using 1/4 Inch Pellets	
Run Number	Sorption Efficiency	Run Number	Sorption Efficiency
1724SG	0.63	1727SG	0.59
1725SG	0.70	1722SG	0.62
1730SG	0.83	1734SG	0.75

FIGURE 5.8

EFFECT OF PRODUCER GAS HYDROGEN SULFIDE CONCENTRATION ON SORBENT PERFORMANCE

CONSTANT PARAMETERS: 1200°F, 20 PSIG, 1800 GHSV,
60 SCFH OF PRODUCER GAS,
SORBENT: 21% ADDED Fe_2O_3
U.S. STEEL IRON OXIDE SOURCE
1/4 INCH DIAMETER PELLETS

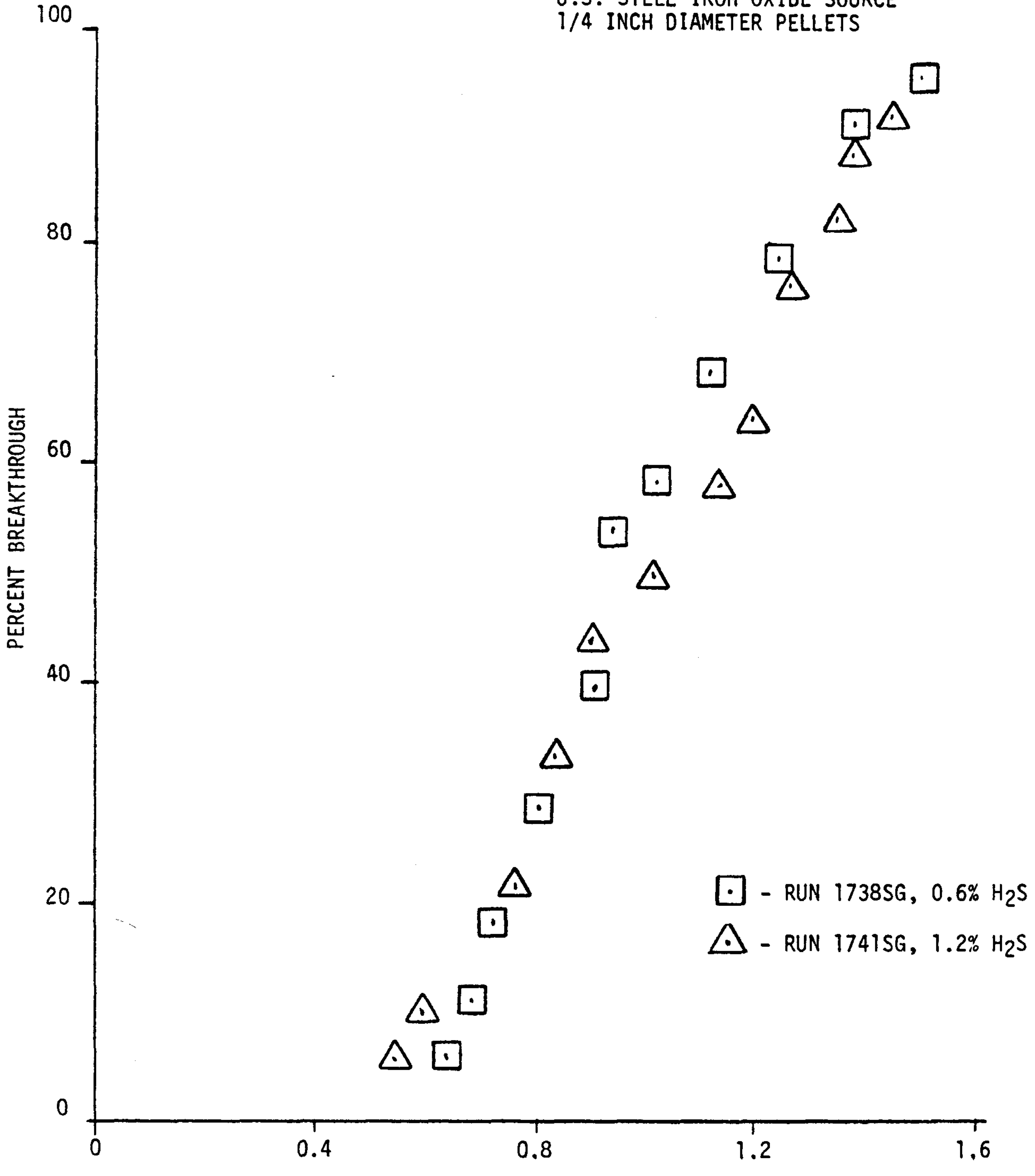

PCRD-1389
E.L.L.
5-17-76

Comparison of the effect of sorbent pellet diameter on efficiency indicates that the smaller diameter pellets have between 5 and 10 percent higher efficiency than the larger diameter pellets at 20 psig. Further information on the operating conditions for the runs listed above may be found in Table 4.1.

5.4.5 Effects of Binder and Support Material on Sorbent Performance

Four different types of sorbent preparations were tested at 20 psig to determine the effect of binder and support on dynamic performance:

(1) Iron oxide/fly ash using bentonite binder.

(2) Iron oxide/fly ash using kaolin binder.

(3) Iron oxide/silica using bentonite binder.

(4) Iron oxide/silica using kaolin binder.

The physical properties of these sorbents are given in Table 4.1. U.S. Steel iron oxide source was used in all preparations. The fly ash used was supplied by ERDA-MERC; the silica was supplied by Illinois Mineral. Figure 5.9 presents the sorbent performance curves typical of the above preparations using 42% added iron oxide. Since all four sorbents define the same performance curve with little data scatter, it can be concluded that the type of binding material or support material doesn't affect sorption dynamics at the 42% iron oxide level.

Figure 5.10 compares the dynamic performance at 20 psig of iron oxide/silica sorbent using bentonite binder for 21 and 42% added iron oxide levels. Again the data describe a single curve with little scatter, indicating that this change in iron oxide content does not affect performance.

Dynamic performance at 20 psig of iron oxide/fly ash sorbent for 8%, 42% and 63% added iron oxide levels is reported in Section III B of Quarterly Report No. 3. The results indicate that for iron oxide/fly ash sorbents, the efficiency at 10% breakthrough was significantly influenced by weight percent iron oxide (.48 at 8% iron oxide versus .77 at 42% iron oxide). If sorption efficiency at 21% iron oxide on fly ash is interpolated from these values, one may see that at 21% iron oxide content, the iron oxide/silica sorbent may have higher sorption efficiency than the iron oxide/fly ash sorbent.

FIGURE 5.9

EFFECT OF SUPPORT AND BINDER ON SORPTION EFFICIENCY

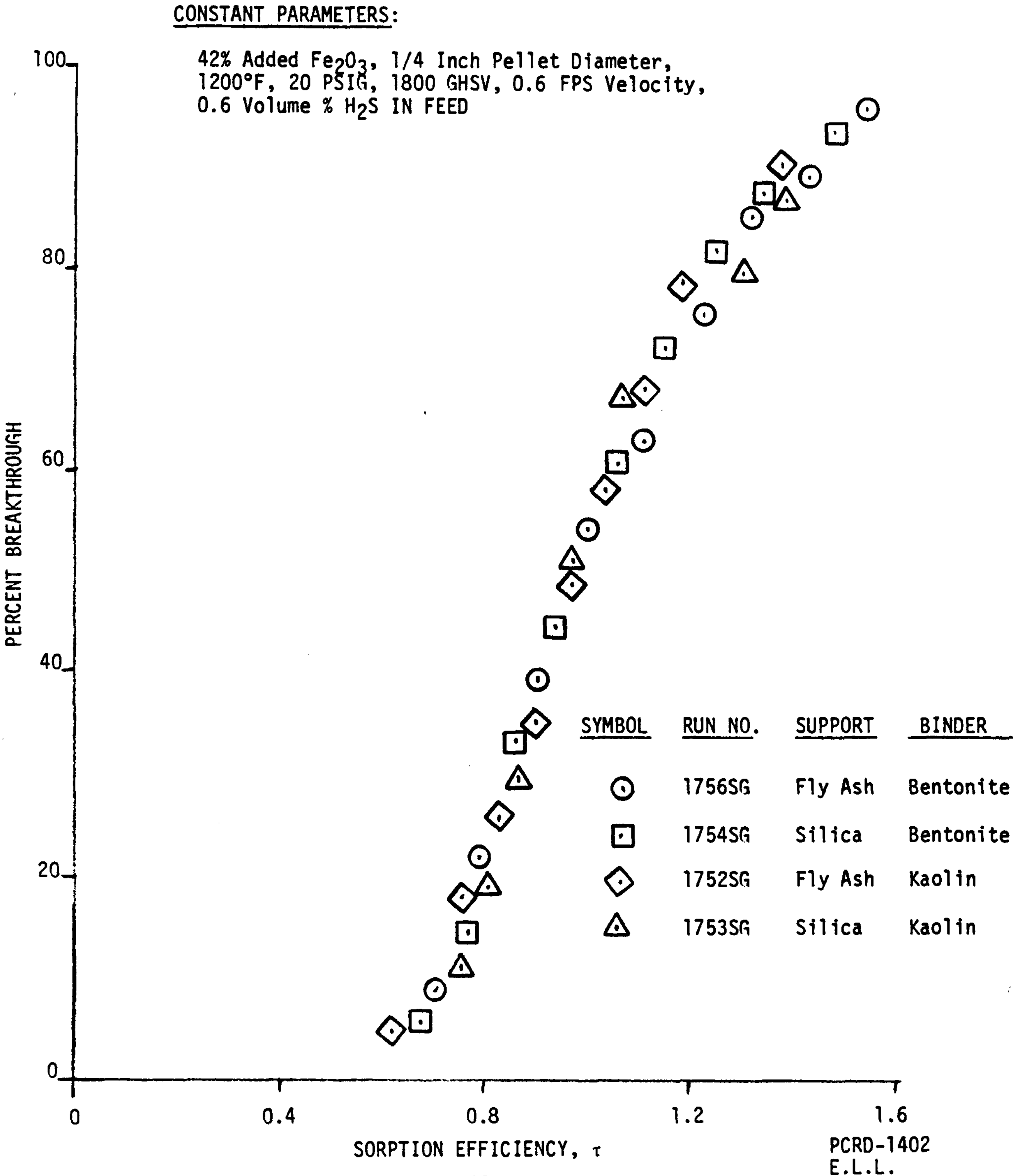

PCRD-1402
E.L.L.
6-4-76

FIGURE 5.10

EFFECT OF ADDED Fe_2O_3 ON PERFORMANCE OF SORBENT USING SILICA SUPPORT

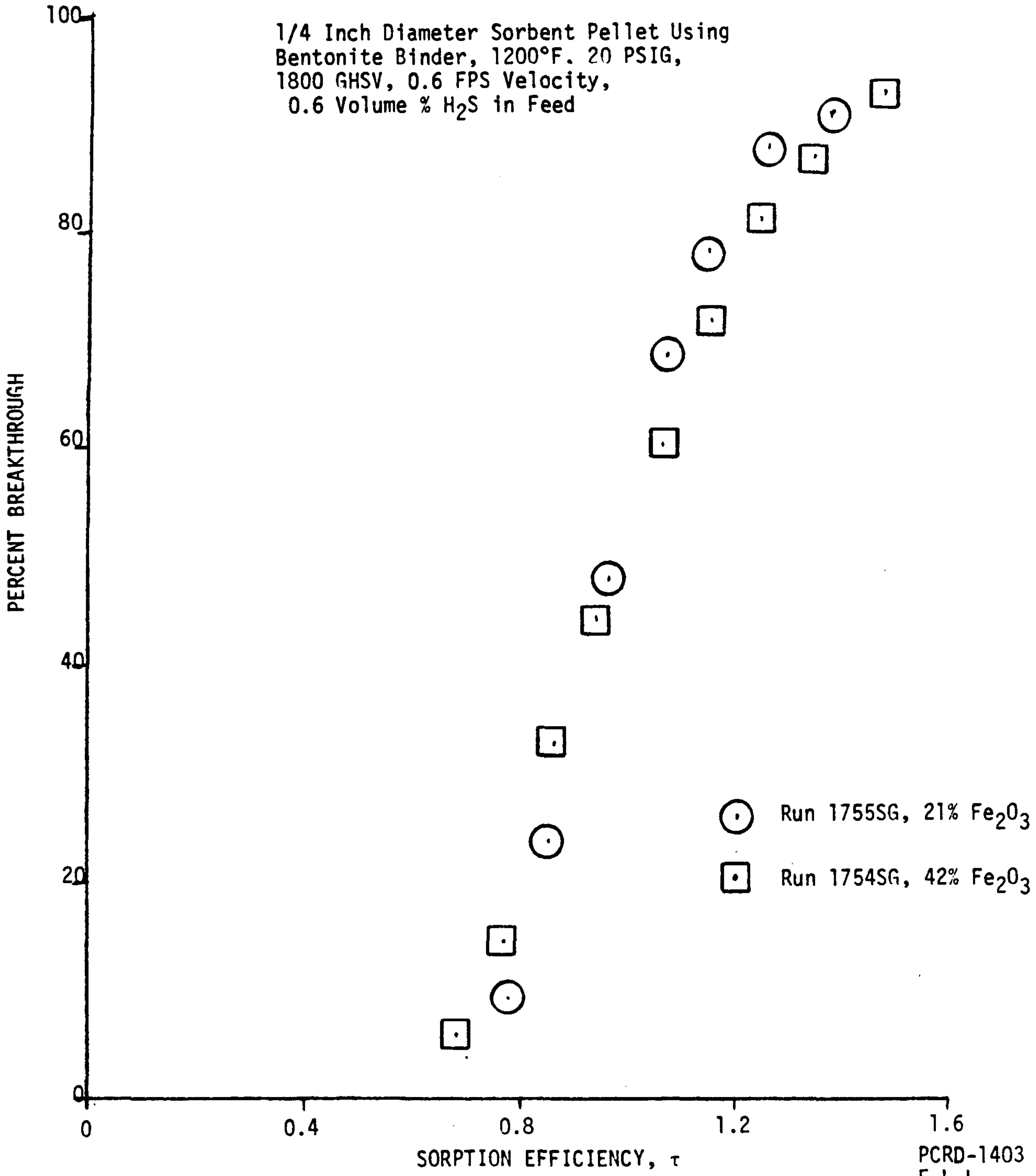

CONSTANT PARAMETERS:

1/4 Inch Diameter Sorbent Pellet Using
Bentonite Binder, 1200°F. 20 PSIG,
1800 GHSV, 0.6 FPS Velocity,
0.6 Volume % H_2S in Feed

PCRD-1403
E.L.L.
6-4-76

5.4.6 Effect of Sorbent Iron Oxide Content on Sorbent Performance

Figure 5.11 indicates the effect of sorbent iron oxide content on sorbent performance. Run 1748SG, using a sorbent prepared with 42 weight percent added iron oxide, performs the best of those sorbents tested. The performance curve for this sorbent most nearly approximates a vertical line at sorption efficiency of one, which would be perfect sorption. The performance curves of sorbents prepared with less than 42% added iron oxide have the same shape as the curve for the 42% sorbent, but sorbent performance is poorer (i.e., sorption efficiencies at each percent breakthrough are farther from unity than the efficiencies of Run 1748SG). Performance curves for sorbents prepared with more than 42% added iron oxide also indicate a decrease in performance when compared to Run 1748SG; however, these curves for high iron oxide levels are different in shape than those for lower levels of iron oxide. For example, the curve for 63% iron oxide sorbent has at least two points of inflection, while the curve for the 42% iron oxide sorbent has only one point of inflection. This change in curve shape probably indicates a change in the controlling mechanism for sulfur sorption. Both changes may be caused by the low porosity of sorbents with more than 42% added iron oxide (see Table 4.1 of this report).

5.5 Ultimate Sulfur Capacity and Optimum Iron Oxide Content at 20 psig

As explained by the definitions in Section 5.2, the product of the ultimate sulfur capacity and the sorption efficiency is proportional to the amount of producer gas a given sorber can process to a given breakthrough. This section presents the experimental ultimate sulfur capacities as a function of sorbent composition. This information and the efficiency information presented above in Section 5.4.6, allows the determination of the optimum iron oxide content of U.S. Steel iron oxide source on fly ash sorbent at 20 psig.

5.5.1 Effects of Sorbent Composition on Ultimate Sulfur Capacity

Figure 5.12 is a plot of weight percent sulfur in sulfided sorbent versus the sorbent added iron oxide content for pellets with both silica and fly ash support. Both silica and fly ash supported sorbents can be correlated by straight lines with the same slope. This constant slope of 0.37 grams sulfur per gram of iron oxide indicates the added iron oxide is converted to a sulfide with the empirical formula $FeS_{0.9}$. Figure 5.12 indicates that silica supported sorbent with no added iron oxide has zero sulfur capacity, while fly ash supported sorbent with no added iron oxide has 2 weight percent sulfur capacity. Thus the sulfur capacity of the fly ash estimated using Figure 5.12 is 2 weight

FIGURE 5.11

EFFECT OF IRON OXIDE CONTENT ON SORPTION EFFICIENCY

AT 20 PSIG

CONSTANT PARAMETERS: 1800 GHSV, 1200°F,
0.6% H_2S IN FEED,
U.S. STEEL Fe_2O_3 SOURCE

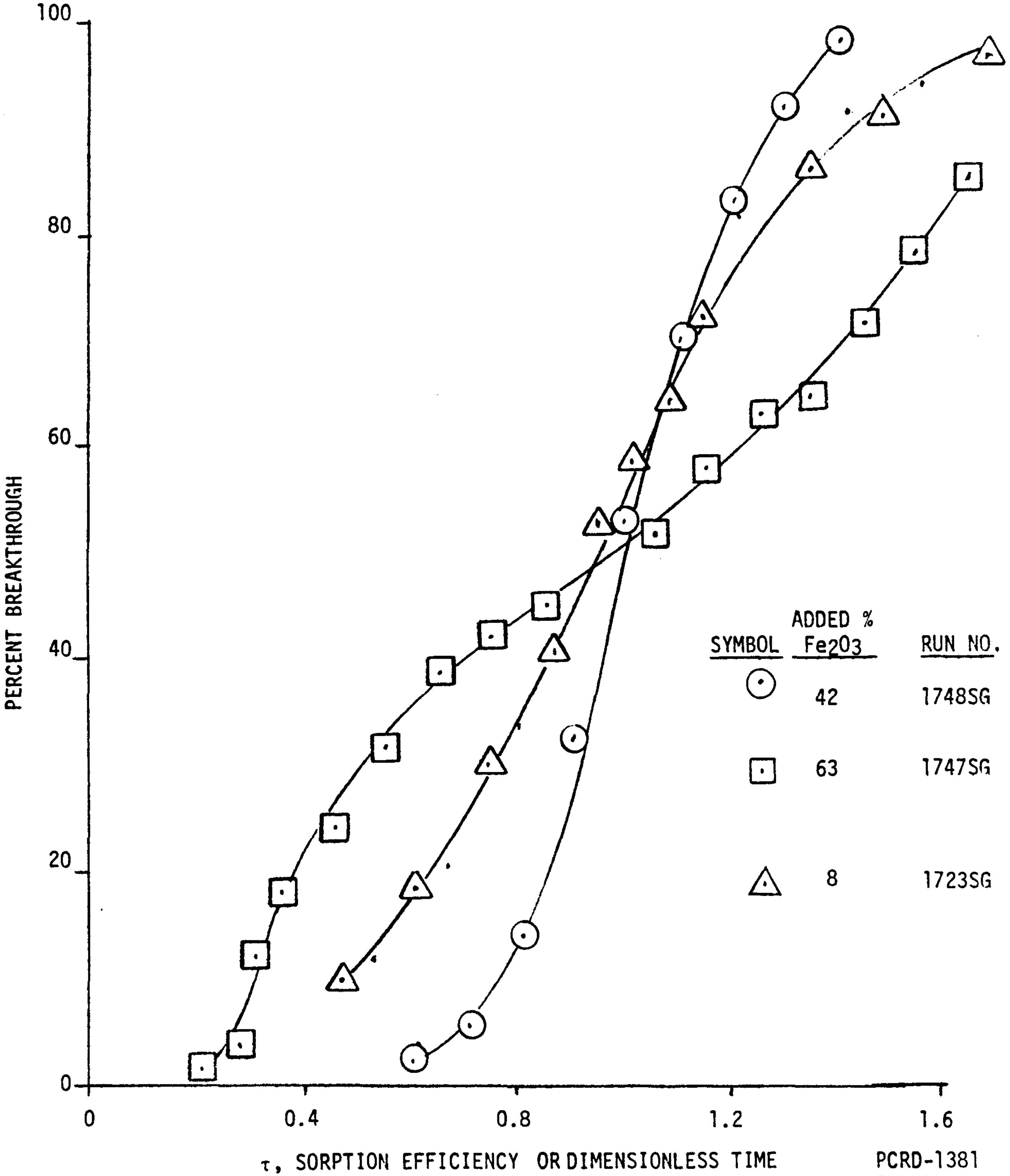

PCRD-1381
E.L.L.
5-17-76

FIGURE 5.12

EFFECT OF ADDED IRON OXIDE ON ULTIMATE SULFUR CAPACITY FOR SORBENTS WITH FLY ASH AND WITH SILICA SUPPORTS

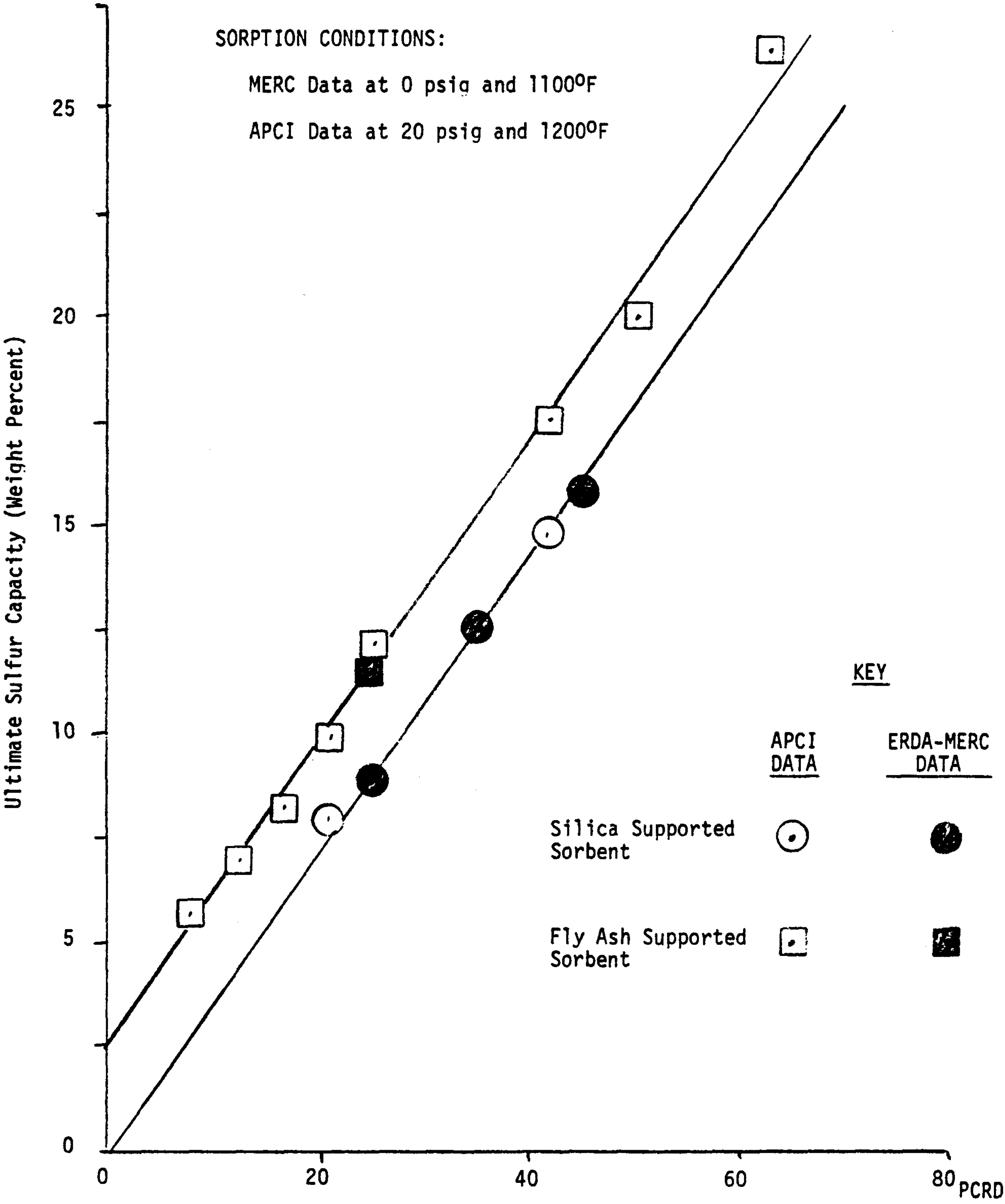

PCRD-1557
E.L.L.
10/6/76

percent, which is in agreement with the reported capacity of 2.5 weight percent at 1000°F in Bureau of Mines Report of Investigations 7947, Page 9. The only difference in sulfur capacity between silica and fly ash supported sorbents is the sulfur capacity of the fly ash.

The unshaded data points of Figure 5.12 were obtained at APCI Houdry Technical Center by X-ray fluorescence of sulfided sorbent. These sorbents were sulfided at 20 psig and 1200°F. The shaded data points were obtained at ERDA's Morgantown Energy Research Center by sulfur mass balance. MERC sulfur sorption runs were at 0 psig and 1100°F. The MERC data has not been previously published. All data points fit the curves of Figure 5.12 in spite of the differences in sorption conditions. In general, APCI sorption runs indicated the ultimate sulfur capacity increases with pressure and temperature. However, these temperature and pressure effects were not significant between 20 psig and 400 psig pressure, nor were they significant between 900°F and 1400°F. Only at 600°F was sulfur capacity significantly different than the predictions of Figure 5.12.

5.5.2 Optimum Iron Oxide Content at 20 psig

The effect of iron oxide content on ultimate sulfur capacity of fly ash supported sorbents (Figure 5.12) and the effect of iron oxide content on performance of fly ash supported sorbents at 20 psig (Figure 5.11) are combined in Figure 5.13 to determine the effect of added iron oxide on available sulfur capacity. The plot clearly shows that 42% added iron oxide on fly ash has the largest available sulfur capacity at 20 psig. The decrease in available capacity for sorbents with iron oxide contents greater than 42% is caused solely by the sharp decrease in efficiency at 50.4 and 63% added iron oxide contents noted in Section 5.4.6. Section 5.6 will demonstrate that this effect of iron oxide content on efficiency at high iron oxide contents is much less pronounced at higher pressures and the change in sorption efficiency will be shown to affect the optimum iron oxide content.

5.6 Effects of Pressure on Performance of Sorbents Using U.S. Steel Iron Oxide Source

Feasible commercial operating pressures for hot stage producer gas include pressures up to 400 psig. Since generation of electricity from producer gas using a combined power cycle is expected to be more economical at higher pressures, experimental desulfurization programs at 400 psig and at 150 psig were conducted. The following five sorbents were tested at both 20 psig and 400 psig to determine the effects of sorption pressure on their performance:

(1) 63% Fe_2O_3 on fly ash, 1/4 inch diameter pellets.

(2) 42% Fe_2O_3 on fly ash, 1/4 inch diameter pellets.

(3) 42% Fe_2O_3 on silica, 1/4 inch diameter pellets.

FIGURE 5.13

AVAILABLE SULFUR CAPACITY VERSUS SORBENT IRON OXIDE CONTENT AT 20 PSIG

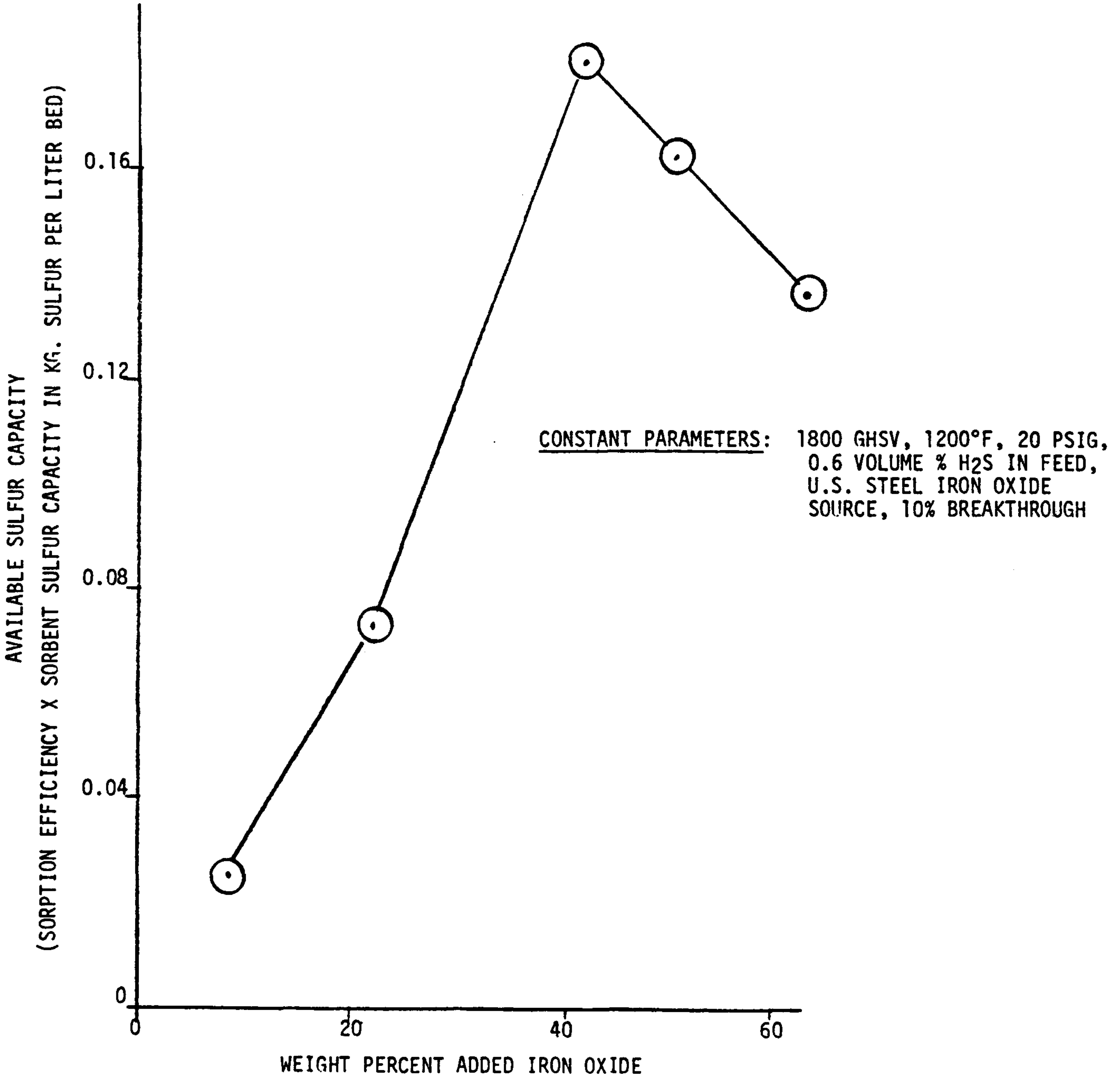

CONSTANT PARAMETERS: 1800 GHSV, 1200°F, 20 PSIG, 0.6 VOLUME % H_2S IN FEED, U.S. STEEL IRON OXIDE SOURCE, 10% BREAKTHROUGH

PCRD-1383
E.L.L.
5-17-76

FIGURE 5.14
EFFECT OF PRESSURE ON PERFORMANCE OF 63% IRON OXIDE/FLY ASH SORBENT

CONSTANT PARAMETERS:

1/4 Inch Diameter Sorbent Pellets,
1200°F, 1800 GHSV, 0.6% H_2S in Feed

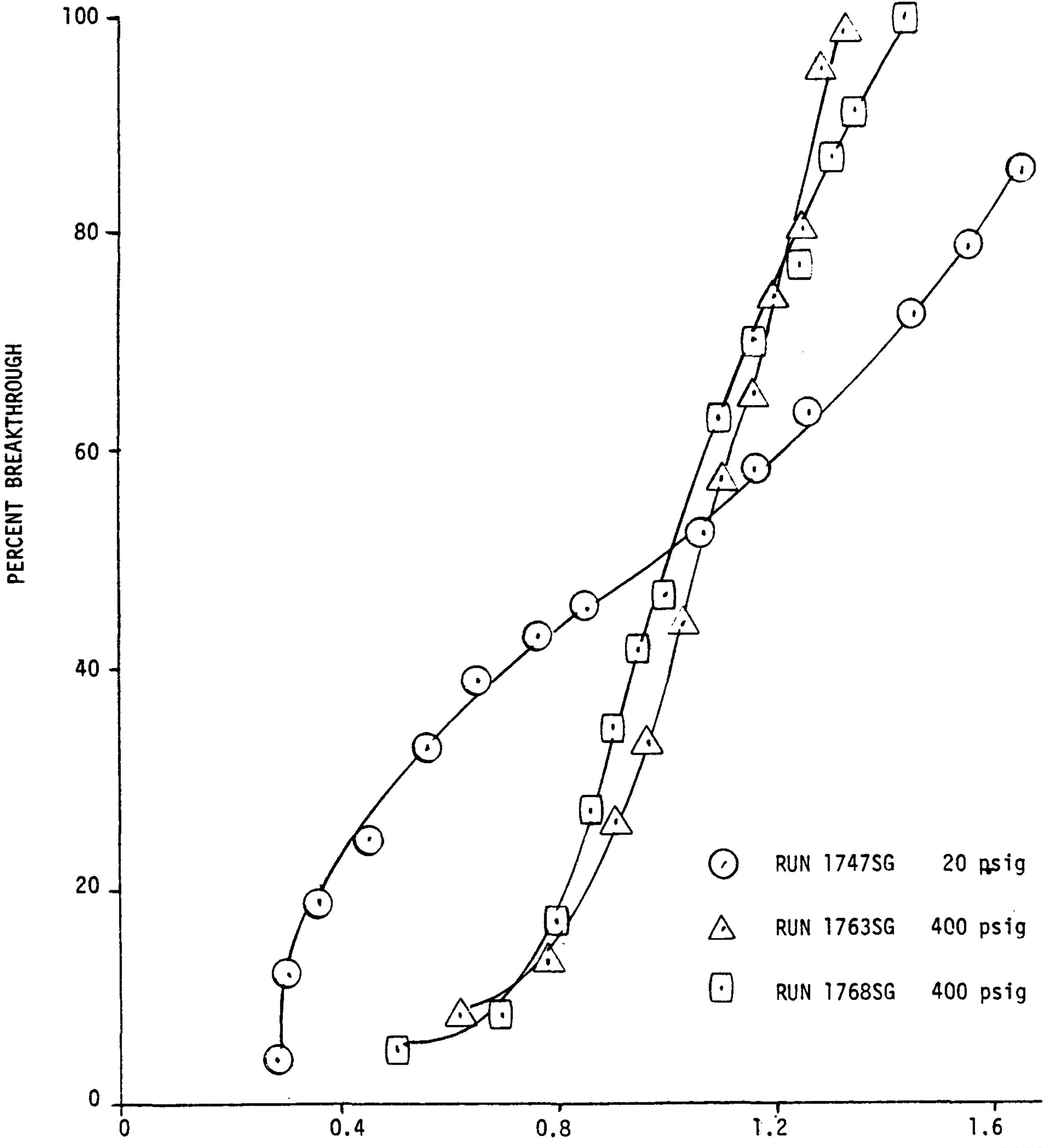

PCRD-1503
E.L.L.
8-10-76

(4) 21% Fe_2O_3 on fly ash, 1/4 inch diameter pellets.

(5) 21% Fe_2O_3 on fly ash, 1/8 inch diameter pellets.

The second, fourth, and fifth of the above sorbents were also tested at 150 psig to determine the curvature of sorption efficiency versus pressure plots. In general, efficiency was shown to increase nonlinearly with pressure.

Figures 5.14 through 5.17 demonstrate the effects of pressure on the performance of the five different experimental sorbents. Except for operating pressure and sorbent composition, all tests were conducted at identical operating conditions: 1800 GHSV, 1200°F, 0.6 percent H_2S feed concentration, and 0.6 fps superficial velocity corrected to 20 psig and 1200°F.

The sorbent with the lowest sorption efficiency at 20 psig was the 63% iron oxide on fly ash. Figure 5.14 shows that this efficiency at 10% breakthrough was increased from 0.32 at 20 psig to 0.72 at 400 psig. Doubling the sorption efficiency means that the sorbent can process twice as much producer gas prior to 10% breakthrough at 400 psig than at 20 psig. Note that the increased performance of the 63% added iron oxide sorbent at 400 psig has been confirmed by duplicate test runs.

The sorbent with the second lowest efficiency at 20 psig is the 21% iron oxide on fly ash with 1/4 inch diameter pellets. The effect of pressure on the performance of this sorbent is less pronounced than the least efficient sorbent. Figure 5.15 illustrates that as the pressure is increased from 20 to 150 and then to 400 psig, the sorption efficiency of the 21% iron oxide on fly ash increased from 0.58 to 0.70 and finally to 0.80.

Both the 42% iron oxide on silica and the 42% added iron oxide on fly ash have high efficiencies at 20 psig pressure. In fact, the 42% iron oxide on fly ash was indicated in Section III E of Quarterly Report No. 3 to be the optimum sorbent at 20 psig.

Figure 5.16 is a plot of the effect of pressure on the performance of these high efficiency sorbents. Both silica and fly ash supported sorbent have efficiency of 0.71 at 20 psig. At 400 psig, both sorbents have slightly increased efficiencies of 0.77. The performance curve from 42% iron oxide on fly ash at 150 psig lies between the high and low pressure dynamic data. Figure 5.16 illustrates the effects of two variables on the performance of 42% added iron oxide sorbents.

(1) There is no effect of support material on performance of the 42% Fe_2O_3 sorbent at either level of pressure.

(2) The effect of pressure on the efficiency of high performance 42% Fe O sorbent is small although it is statistically significant.

FIGURE 5.15

EFFECT OF PRESSURE ON PERFORMANCE OF 21% IRON OXIDE/FLY ASH SORBENT

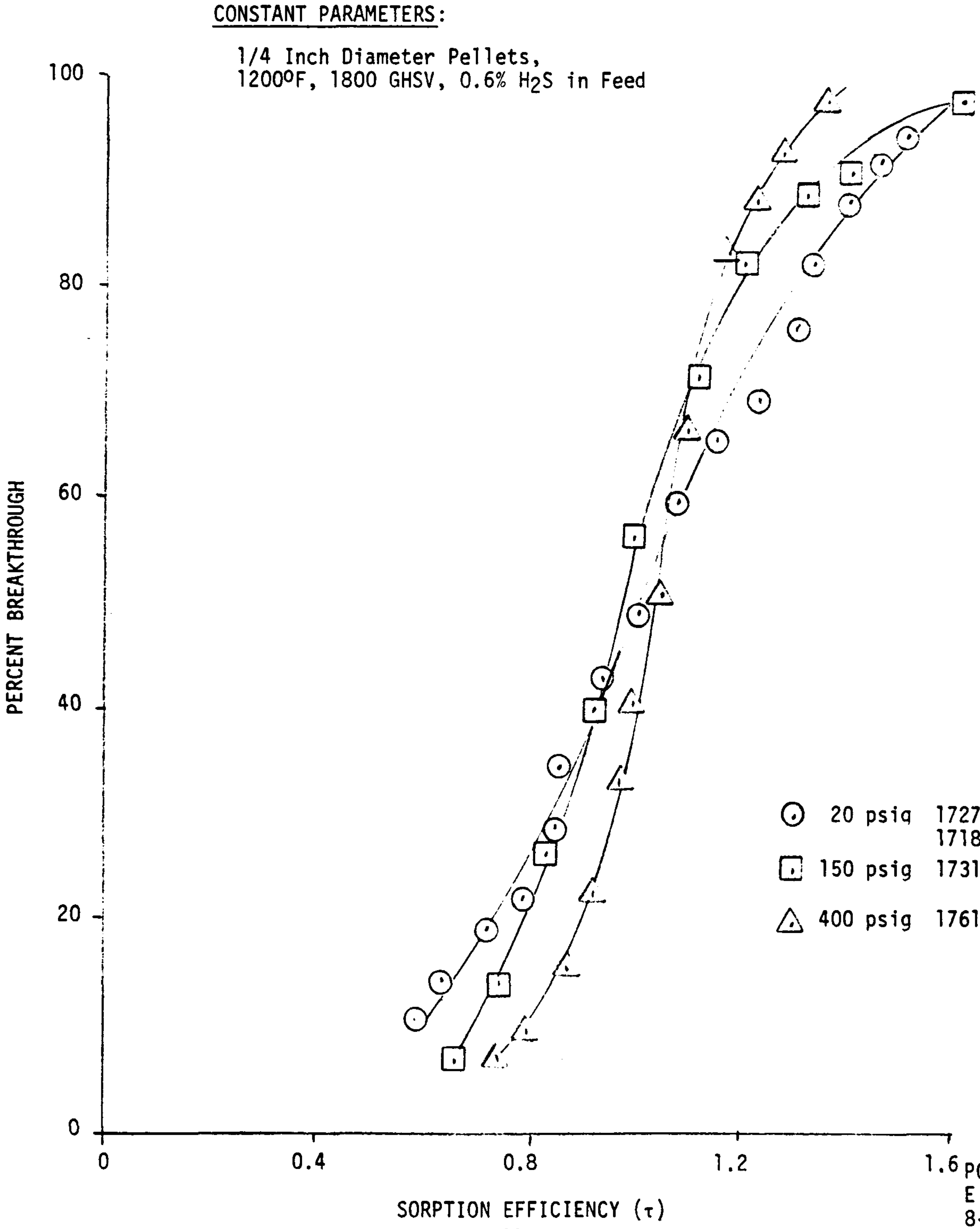

PCRD-1504
E.L.L.
8-10-76

FIGURE 5.16

EFFECT OF PRESSURE ON PERFORMANCE OF 42% IRON OXIDE ON FLY ASH AND 42% IRON OXIDE ON SILICA

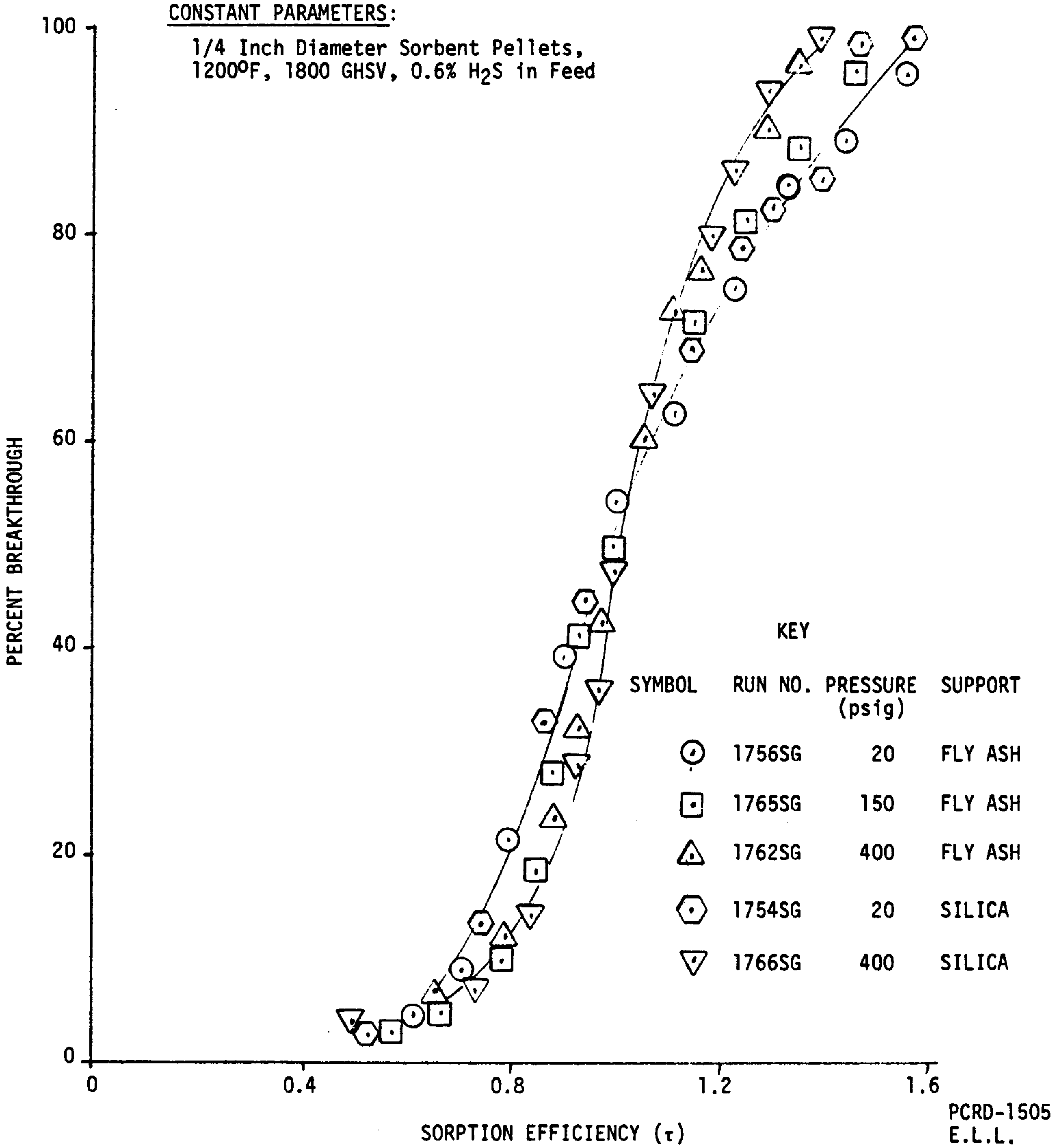

FIGURE 5.17
EFFECT OF PRESSURE ON SORPTION EFFICIENCY AT 10% BREAKTHROUGH

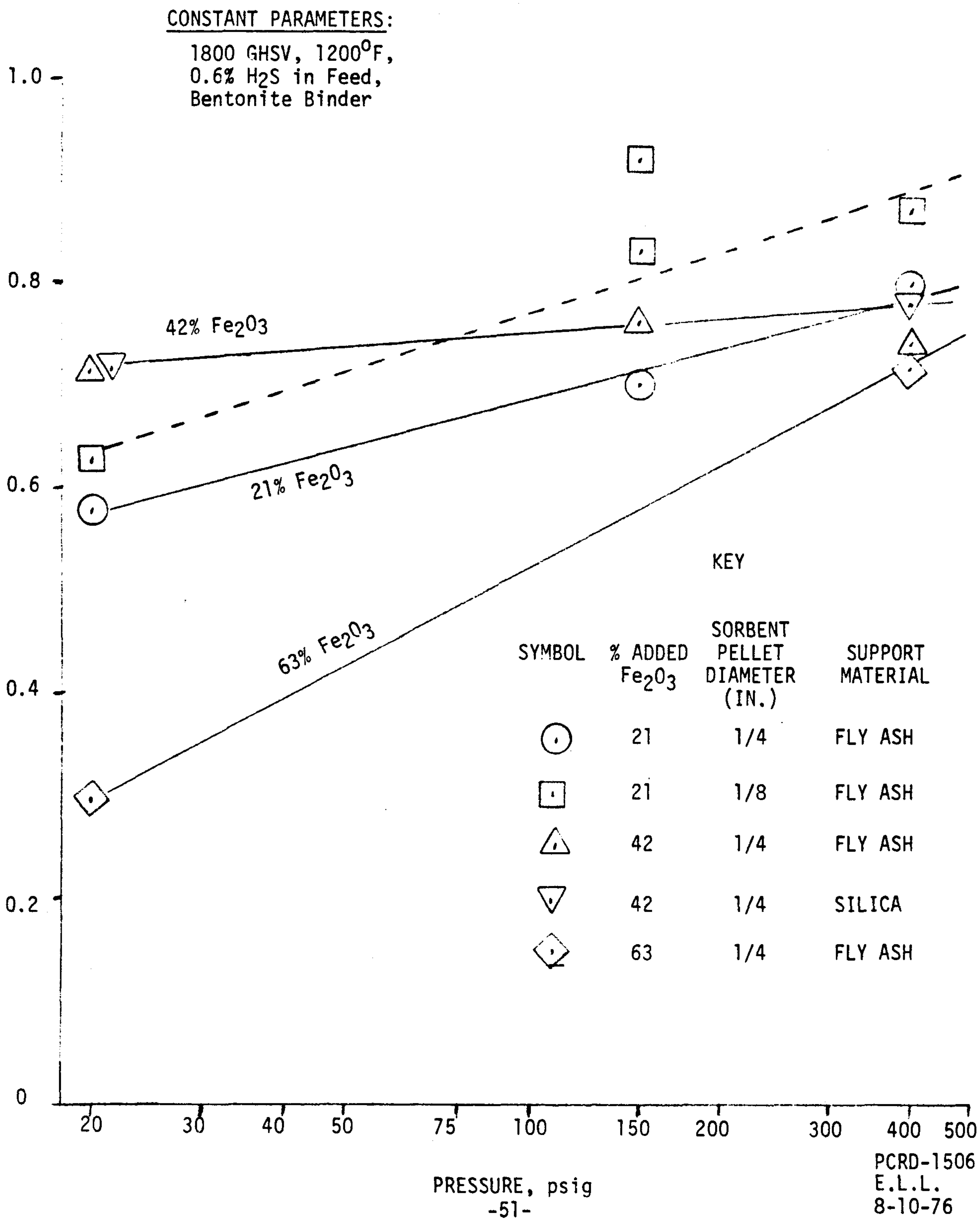

PCRD-1506
E.L.L.
8-10-76

From the performance curves presented in Figures 5.14, 5.15 and 5.16 it appears that an increase in operating pressure will have a considerably greater effect on a low performance sorbent than on a sorbent with high efficiency at lower pressure. Figure 5.17 further illustrates this. Sorption efficiencies at 10% breakthrough are plotted versus the log of operating pressure for each sorbent tested. Three of the four 1/4 inch diameter sorbent preparations tested can be correlated by straight line fit on Figure 5.17. The effect of pressure on sorbent performance is indicated by the slope of the line. The lower the sorbent efficiency at 20 psig, the steeper the slope of the correlation, and hence the greater the pressure effect.

The effect of pressure on 1/8 inch diameter, 21% Fe_2O_3 sorbent pellets may or may not be correlated by a straight line on Figure 5.17. Points plotted for this sorbent at 20 and 150 psig indicate larger effect of pressure in this range using the 1/8 inch pellets than would be expected from the behavior of 1/4 inch pellets using 21% Fe_2O_3. As a result, the effect of sorbent pellet diameter on efficiency is larger at 150 psig than at 20 psig. This size effect on sorbent performance is further demonstrated by Figure 5.18. The solid line represents the best performance curve that was experimentally determined using 1/4 inch diameter sorbent at 150 psig. The data used in constructing this line were presented in Figure 5.15. The data points plotted in Figure 5.18 represent duplicate runs at 150 psig using 1/8 inch diameter sorbent pellets. The figure illustrates that a 20 to 30% increase in sorption efficiency (at 10% breakthrough) can be obtained by reducing sorbent particle size at high pressure. This effect is two to three times as large as the effect observed at 20 psig (see Section 5.4.4). Moreover, one of the dynamic sorptions using 1/8 inch diameter sorbent pellets indicates a sorption efficiency of 0.92.

The performance curve for the 1/8 inch diameter, 21% iron oxide sorbent pellets does not change much between 150 psig and 400 psig, as illustrated by the sorption efficiencies at ten percent breakthrough plotted on Figure 5.17. Since the efficiency of 1/4 inch pellets continues to increase with pressure, particle size effects do not appear as significant at 400 psig as they do at 150 psig. Also, as a result of this large change in efficiency between 20 psig and 150 psig, as well as the small change in efficiency between 150 psig and 400 psig, the data for the 1/8 inch diameter pellets on Figure 5.16 cannot be fit by a straight line without considerable data scatter, as shown by the dashed line.

Two additional runs were conducted at pressures greater than 20 psig using 42% Fe_2O_3 on fly ash. The purpose of these additional runs was to verify the effects of temperature and velocity at high pressure. Sorbent performance for 1800 GHSV, 400 psig pressure and 1400°F was found to be the same as for the 1200°F run at 400 psig already discussed. Sorbent performance at 1200°F, 150 psig, and 3600 GHSV was found to correlate with the velocity effects discussed in Section 5.4.1.

FIGURE 5.18

EFFECT OF PELLET DIAMETER ON SORBENT PERFORMANCE AT 150 PSIG

CONSTANT PARAMETERS: 1800 GHSV, 1200°F, 150 PSIG,
0.6% H_2S IN FEED, 30 SCFH PRODUCER GAS,
SORBENT USING 21% ADDED Fe_2O_3 AND
U.S. STEEL IRON OXIDE SOURCE

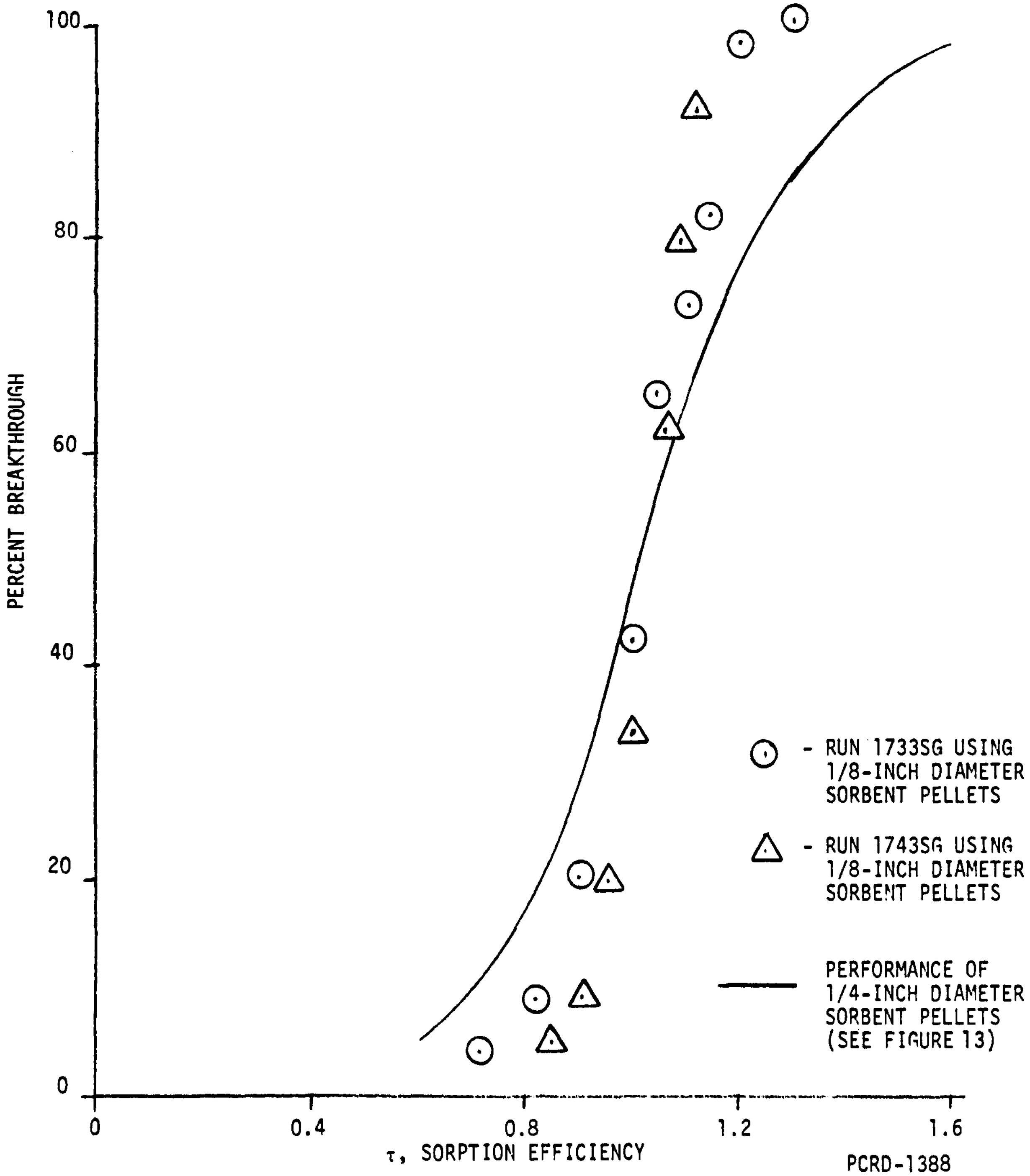

PCRD-1388
E.L.L.
5-17-76

5.7 Optimum Iron Oxide Content at 400 psig

The product of total bed sulfur capacity and sorption efficiency is a measure of the amount of producer gas the bed can process prior to 10% breakthrough. This quantity is referred to as the bed sulfur capacity available at 10% breakthrough, or available sulfur capacity. The optimum sorbent maximizes available sulfur capacity.

Sorption efficiencies at 10% breakthrough for 400 psig pressure are presented in Figures 5.14 through 5.16 for sorbents with 21, 42, and 63 percent added iron oxide. Total bed sulfur capacities at 20 psig were presented in Section 5.5.1. These total sulfur capacities do not vary significantly with sorption pressure between 20 psig and 400 psig. Figure 5.13 and the above information was used to prepare Figure 5.19, which shows two plots of available capacity versus sorbent iron oxide: one plot at 20 psig pressure and one at 400 psig. The major difference between the plots at the two pressures is the capacity at 63% iron oxide, which is doubled at 400 psig. The reason for the available capacity increase is the efficiency increase illustrated by Figure 5.14. It is apparent that doubling the available capacity at 63% iron oxide content has shifted the maximum available capacity from 0.17 Kg sulfur per liter of bed at 42% iron oxide and 20 psig to a value in excess of 0.32 Kg of sulfur per liter of bed at more than 63% iron oxide and 400 psig. In short, Figure 5.19 illustrates that the increase in performance of 63% iron oxide on fly ash sorbent at 400 psig has doubled the maximum experimentally measured available sulfur capacity. This means that a sorber operating at 400 psig could be designed to have the same onstream time as a 20 psig sorber but need be only half as large as the 20 psig sorber.

5.8 Conclusions Based on Experimental Work

Conclusions from the sorbent development work are summarized below:

(1) Armco Steel and U.S. Steel iron oxide sources are the most suitable commercial iron oxide sources of the limited number APCI has investigated. These two sources are superior in both ultimate and available sulfur capacity.

(2) At 20 psig, the optimum iron oxide content of iron oxide/fly ash sorbent is 42%. This optimum is caused by the poor efficiency of sorbents prepared with higher levels of iron oxide at this pressure.

FIGURE 5.19
AVAILABLE SULFUR CAPACITY VERSUS
SORBENT IRON OXIDE CONTENT

CONSTANT PARAMETERS:

1800 GHSV, 1200°F, 0.6% H_2S in Feed,
U.S. Steel Iron Oxide Source on Fly Ash
with Bentonite Binder, 10% Breakthrough

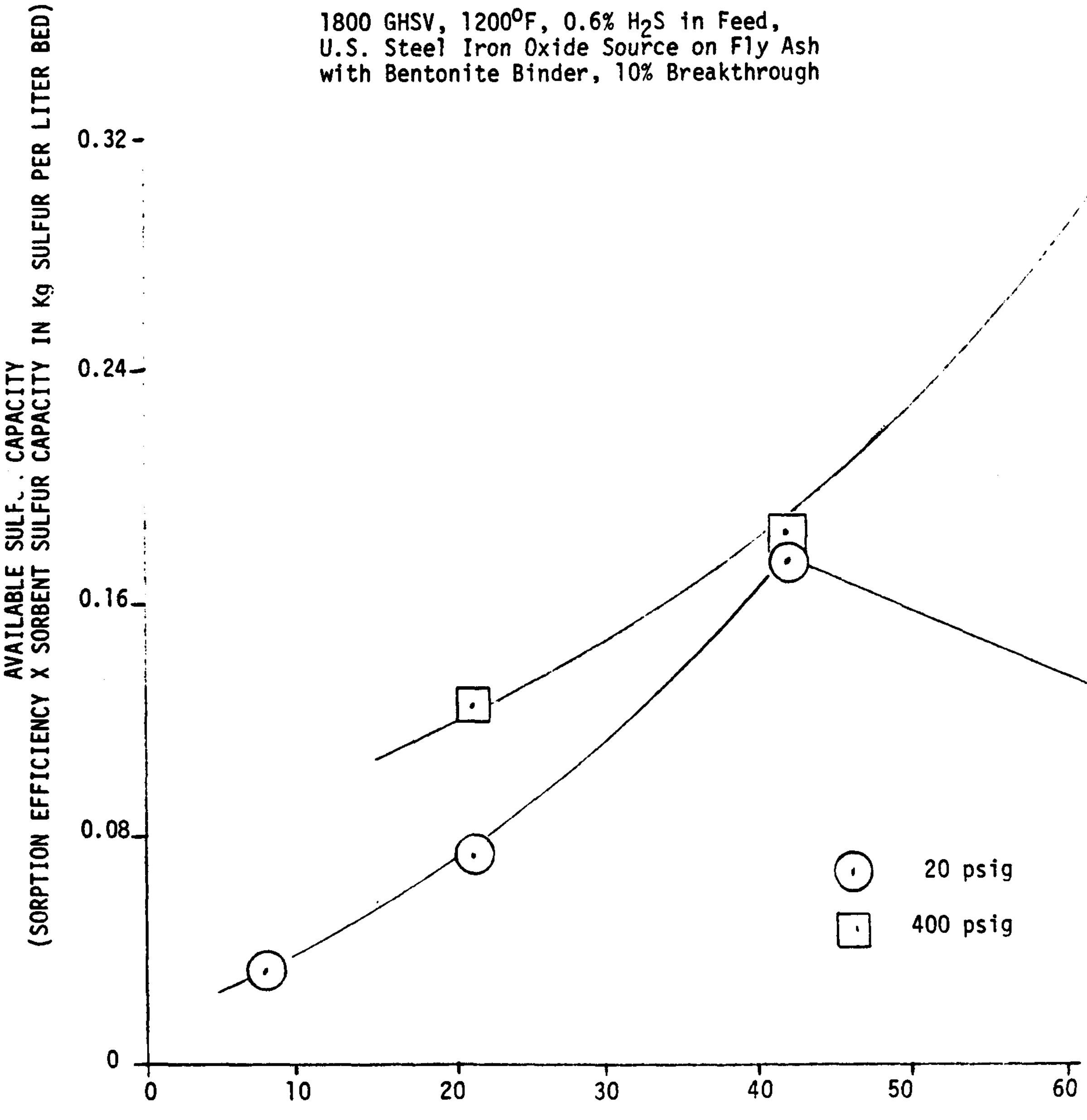

PCRD-1507
E.L.L.
8-10-76

(3) At 400 psig, the optimum iron oxide content of iron oxide/fly ash sorbent is greater than 60%. This increase in optimum content is caused by the increased efficiency of sorbents with high iron oxide content at 400 psig.

(4) No effect of the binder (bentonite or kaolin) on sorption dynamics was observed.

(5) The performance of iron oxide/silica sorbent is at least equal to the performance of iron oxide/fly ash sorbent.

(6) The sulfur capacity of iron oxide/silica sorbent is less than the capacity of iron oxide/fly ash due to fly ash sulfur capacity.

Except for experimental work conducted to investigate commercial iron oxide sources, all dynamic tests used sorbent prepared with U.S. Steel iron oxide source. Conclusions 2 through 6 should not be extended to sorbents using other iron oxide sources or ingredients or preparation methods without further testing.

The optimum iron oxide content described above is based on the available sulfur capacity of freshly prepared sorbent. The conclusions should not be applied to regenerated sorbents until verified by sorbent life cycle testing. The optimum iron oxide content based on available sulfur capacity is an economic optimum if sorbent cost and sorbent durability do not vary with sorbent iron oxide content.

The following conclusions result from APCI investigations into the effects of process variables on sorbent performance:

(1) Velocity effects indicate that sorbent performance improves as velocity is increased at constant GHSV. This improvement is limited by increased bed pressure drop at high velocities. Performance is decreased by increasing GHSV at constant velocity.

(2) Sorption efficiency increased most rapidly with temperature below 900°F. Only a small temperature effect was observed between 900°F and 1200°F, and no effect was observed above 1200°F. Sorption of low BTU producer gas at 900°F leads to excessive sorbent disintegration for the absorbent tested.

(3) Effects of H_2S feed concentration on efficiency are not significant in the range investigated (0.6 and 1.2% vol.).

(4) Sorbent pellet size does not greatly effect performance at low pressures. However, the performance of 1/8 inch diameter pellet increases more rapidly with pressure than does the performance of 1/4 inch diameter sorbents. As a result, using a smaller diameter pellet may increase sorption efficiency significantly at pressures above 100 psig.

(5) Sorption efficiency is always increased with pressure. The size of the effect appears more pronounced if sorbent performance is poor at the lower pressure.

6.0 CORRELATION OF SORPTION DYNAMICS DATA USING AN ISOTHERMAL MODEL

The performance curves presented in Section 5 illustrate the effects of process variables on sorption efficiency. This dynamic data can be correlated using an isothermal sorption model over the following range of operating conditions:

(a)	Temperature*	600°F to 1400°F
(b)	Pressure	20 psig to 400 psig
(c)	GHSV	1300 to 3600
(d)	Superficial Velocity	0.05 fps to 2.33 fps
(e)	Feed Gas H_2S Concentration	0.6 to 1.2 Mole Percent
(f)	Sorbent Pellet Diameter	1/8 Inch to 1/4 Inch
(g)	Sorbent Iron Oxide Content	8 to 42 Weight Percent Added Fe_2O_3 from U.S. Steel Iron Oxide Source

* Special start-up procedures are required around 900°. See Section 5.4.2.

The range of variables listed above indicates that the model correlates all the experimental results of Section 5 except the effects of iron oxide source and the performance of 63 percent added iron oxide on fly ash. No attempt was made to correlate the effect of iron oxide source because only a limited number of test runs used a source other than U.S. Steel iron oxide. Similarly, sorbent preparation method was not considered as a variable. The unusual performance curve for 63 percent added iron oxide on fly ash at 20 psig presented in Figure 5.10 could not be correlated.

The sorption dynamics model presented in this section is capable of predicting onstream times for desulfurization of producer gas within the range of operation conditions listed above. The model predicts sorption efficiency given the seven design variables: temperature, pressure, GHSV, superficial velocity, feed gas H_2S concentration, sorbent pellet diameter, and sorbent iron oxide content. Sorbent sulfur capacity must be known to convert sorption efficiency to onstream time in hours; this ultimate sulfur capacity can be determined from sorbent composition using Figure 5.11. Onstream time in hours is the product of sorption efficiency and the perfect sorption time, which was defined in terms of bed sulfur capacity in Section 5.2.

The dynamics model presented in this section may be used to determine the operating time of a commercial scale sorption vessel given the seven design variables and the sorbent sulfur capacity. However, the model should be experimentally verified if it is extended beyond the range of applicability given above.

6.1 Development of an Isothermal Sorption Model to Correlate Hot Stage Producer Gas Desulfurization Dynamics

The effects of process variables on sorption dynamics are determined by the mechanics of the hydrogen sulfide sorption process. Essentially, a sorption process consists of a series of steps. Each step occurs at a rate determined by the sorber design variables, and the slowest rate defines the rate of the overall process. For the purpose of model development, hydrogen sulfide sorption was considered to involve the following sequence of steps:

1. Transfer of hydrogen sulfide from the bulk of the producer gas to the surface of the sorbent pellet.
2. Knudsen diffusion of the hydrogen sulfide from the pellet surface to a sorption site within the pellet interior.
3. Chemical reaction of the hydrogen sulfide with iron oxide at the sorption site.

If the first step is the slowest step of the sorption mechanism, then the sorption is external diffusion controlled. If the second step controls, the sorption is limited by internal diffusion. If the third step is rate controlling, a kinetic model describes the dynamics. Three sorption models are derived in Appendix B: the internal diffusion controlled shrinking core model, the external diffusion controlled film model, and the rate of reaction controlled kinetic model. The film and kinetic models are derived simultaneously and can be considered as special cases of the resultant film-kinetic model.

Each sorption model is described by a function of design variables called a sorption number, which is a model parameter proportional to the reciprocal of the controlling rate. The sorption efficiency predicted for a given level of sulfur breakthrough always is decreased by increasing the value of the sorption number. The dependence of the sorption number on design variables is different for each model, as is the general shape of the dynamic performance curve. Table 6.1 summarizes the dependence of sorption numbers on design variables and the shape of the performance curve predicted by each of the three sorption models. The realtionships of Table 6.1 are determined from the differential equations derived in Appendix B. Nomenclature for Table 6.1 and the balance of this section appears in Table 6.2.

TABLE 6.1
A COMPARISON OF SORPTION DYNAMICS PREDICTED BY THREE ISOTHERMAL MODELS

MODEL	SORPTION NUMBER	TYPICAL PERFORMANCE CURVE
FILM MODEL	$C_1 \; \frac{\text{GHSV } a^{1.5} \; T^{.17}}{\sqrt{VP}}$	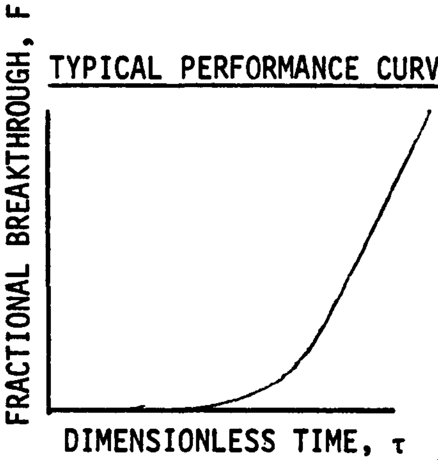
SHRINKING CORE MODEL	$C_o \; \frac{\text{GHSV } a^2 \sqrt{T}}{P}$	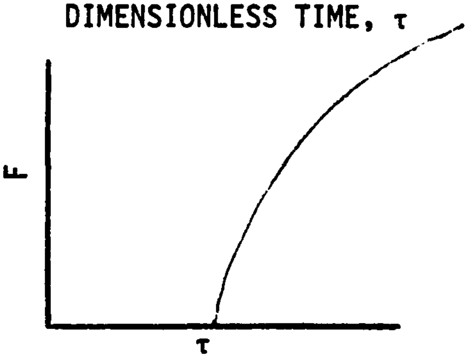
KINETIC MODEL	$C_2 \; \frac{\text{GHSV } T \; e^{\beta/T}}{PI_o}$	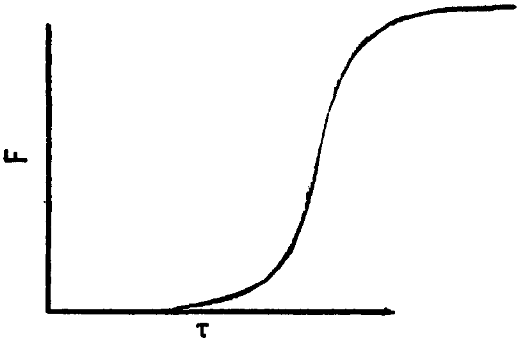

TABLE 6.2

NOMENCLATURE FOR ISOTHERMAL MODELS

1. DESIGN VARIABLES

a	Sorbent pellet radius (ft.).
GHSV	Gas hourly space velocity (hr.$^{-1}$).
I_0	Fresh sorbent iron oxide concentration (lb. moles/ft.^{3} solid).
P	Unit pressure (atm)
T	Dimensionless absolute temperature (temperature in °F/492°R).
V	Gas superficial velocity at run conditions (ft./hr.).

2. SORPTION NUMBERS

N_{Ab}^{σ}	Shrinking core sorption number.
N_{Ab}^{F}	Film sorption number.
N_{Ab}^{K}	Kinetic sorption number.

3. MODEL PARAMETERS

β	Activation energy divided by 978 BTU/lb. mole (dimensionless).
C_0	Reciprocal of effective Knudsen diffusivity for shrinking core sorption number (hr./ft.^{2}).
C_1	Proportionality constant for film sorption number (hr.$^{+\frac{1}{2}}$/ft.).
C_2	Reciprocal Arrhenius frequency for kinetic sorption number (hr. lb. mole/ft.^{3}).
F	Fractional sulfur breakthrough (sulfur breakthrough/feed sulfur concentration).
t	Sorber onstream time (hrs.).
t_p	Perfect sorption time (hrs.) (Defined as bed sulfur capacity divided by the feed rate of sulfur to the bed).
τ	Dimensionless time or sorption efficiency (t/t_p).

The successful sorption dynamics model must meet two levels of model confirmation criteria:

Level 1 - The model must be able to predict the shape of the experimentally observed breakthrough curves.

Level 2 - The model must predict the experimentally observed effects of design variables on sorption efficiency.

This section examines the three isothermal sorption models in terms of the two levels of model confirmation. In general, experimental performance curves most closely resemble those predicted by the kinetic model, although some runs at high space rate are better correlated by the shrinking core model. In no case does the film model satisfy Level 1 confirmation. The effect of design variables on sorption efficiency is not adequately predicted by any single sorption model. An empirical sorption model is formulated to correlate the experimental data and a fundamental basis for this model is postulated.

6.2 Level 1 Confirmation Plots for the Film, Shrinking Core, and Kinetic Isothermal Models

As suggested by Table 6.1, each sorption model is characterized by a typically shaped sorption performance curve. If the sorption is efficient (that is, if the sorption number is small enough) these typical breakthrough curves can be represented by simple constant pattern solutions to the model differential equations. Table 6.3 lists these constant pattern solutions for the three isothermal models. The film and kinetic constant pattern solutions are analytical solutions to the model sorption dynamics equations when the sorption numbers are less than 0.3. The equation given for the shrinking core constant pattern is a rough approximation for a complicated set of algebraic equations that describe the model solution when the sorption number is less than 6. If any of the constant pattern solutions predict dimensionless times of less than zero for a given fractional breakthrough, then the sorption efficiency for that given sulfur breakthrough is zero. The constant pattern solutions of Table 6.3 indicate the following criteria can be used for Level 1 model confirmation:

1. If a plot of $\ell n F$ versus τ linearizes the performance curve, then the film model passes Level 1 confirmation.
2. If a plot of $\ell n \left(\frac{F}{1 - F}\right)$ versus τ is linear, then the performance curve can be correlated by the kinetic model.

TABLE 6.3

CONSTANT PATTERN SOLUTIONS FOR LEVEL 1 CONFIRMATION

SORPTION MODEL	CONSTANT PATTERN SOLUTION	RANGE OF APPLICABILITY
FILM MODEL	$\tau = 1 + N_{Ab}{}^{F}\ (\ln F + 1)$	$0 \leqslant N_{Ab}{}^{F} < .3$ $e^{-N_{Ab}{}^{F-1}} \leqslant F \leqslant 1$
KINETIC MODEL	$\tau = 1 + N_{Ab}{}^{K}\ \ln\left(\frac{F}{1-F}\right)$	$0 \leqslant N_{Ab}{}^{K} < .3$ $e^{-N_{Ab}{}^{K-1}} \leqslant \frac{F}{1-F} < \infty$
SHRINKING CORE MODEL	$\tau = 1 - \frac{N_{Ab}{}^{\phi}}{15}\left(\ln\ (1 - F) + 1\right)$	$0 \leqslant N_{Ab}{}^{\phi} < 6.$ $0 \leqslant F \leqslant 1$

CONSTANT PATTERN SOLUTION FOR A MODEL USING ALL THREE ISOTHERMAL MECHANISMS

$$\tau = 1 + \left(N_{Ab}{}^{F} + N_{Ab}{}^{K}\right)\left(\ln F + 1\right) - \left(\frac{N_{Ab}}{15} + N_{Ab}{}^{K}\right)\left(\ln\ (1 - F) + 1\right)$$

$$0 \leqslant N_{Ab}{}^{F} + N_{Ab}{}^{K} + \frac{N_{Ab}{}^{\phi}}{15} < .3$$

FOR ALL F SUCH THAT $\tau \geqslant 0$

3. If a plot of $\ell n\ (1 - F)$ versus τ is linear, then the shrinking core model is the indicated sorption model.

For each linearized performance curve, the slope is proportional to the rate of sorption and inversely proportional to the sorption number.

If all three isothermal models are empirically combined, then the constant pattern solution at the bottom of Table 6.3 is obtained. This solution states that the sorption efficiency is a linear combination of ℓnF and $\ell n\ (1 - F)$. The film-kinetic constant pattern solution derived in Appendix B.2 is a special case of the empirical constant pattern solution of Table 6.3. The combined constant pattern can also be used for Level 1 model confirmation by determining the three sorption numbers in the constant pattern equation using a linear regression technique. The sorption would be film controlled if the ℓnF coefficient was largest, internal diffusion controlled if the $\ell n\ (1 - F)$ coefficient was largest, and kinetically controlled if the coefficients were equal for all breakthrough curves analyzed.

Figures 6.1, 6.2, and 6.3 represent linearized performance curves for each of the three isothermal sorption models. Each figure contains a curve for both Run 1756SG and Run 1757SG. The first figure, Figure 6.1, is a plot of ℓnF versus τ. If the two runs described straight lines on this plot, the film model would pass Level 1 confirmation. Figure 6.1 illustrates that the film model cannot describe these two typical performance curves, since neither curve is linearized. Figure 6.2 is a plot of

$$\ell n \frac{F}{1 - F} \text{ versus } \tau$$

for the two experimental runs. The plot linearizes the run at low GHSV but not the run at higher at GHSV. Thus, Figure 6.2 illustrates that the kinetic model can predict the shape of some experimental breakthrough curves, although it does not in all cases pass Level 1 confirmation. Figure 6.3 presents Level 1 confirmation for the shrinking core model using the two test runs. The run at high GHSV is nearly linearized on this plot. The low GHSV run is not linearized at low fractional breakthroughs, which is the region of the breakthrough curve that is most important for predicting sorber onstream time. Thus, the shrinking core model is most accurate in predicting breakthrough curves at high GHSV.

From the linearized performance curves presented in Figures 6.1, 6.2 and 6.3, it appears that the experimental data could best be represented by a combined mechanism sorption model. This model would generate breakthrough curves with characteristic shape intermediate to the kinetic and shrinking models. Such curves are generated by the empirical model of Table 6.3 when the shell model sorption number is much larger than the film model sorption number. This inequality implies that the shell sorption

FIGURE 6.1

CONFIRMATION FOR FILM SORPTION MODEL

RUN CONDITIONS: 1200°F, 20 psig, 0.6 fps superficial velocity, 1/4 inch diameter pellets, 42% added iron oxide

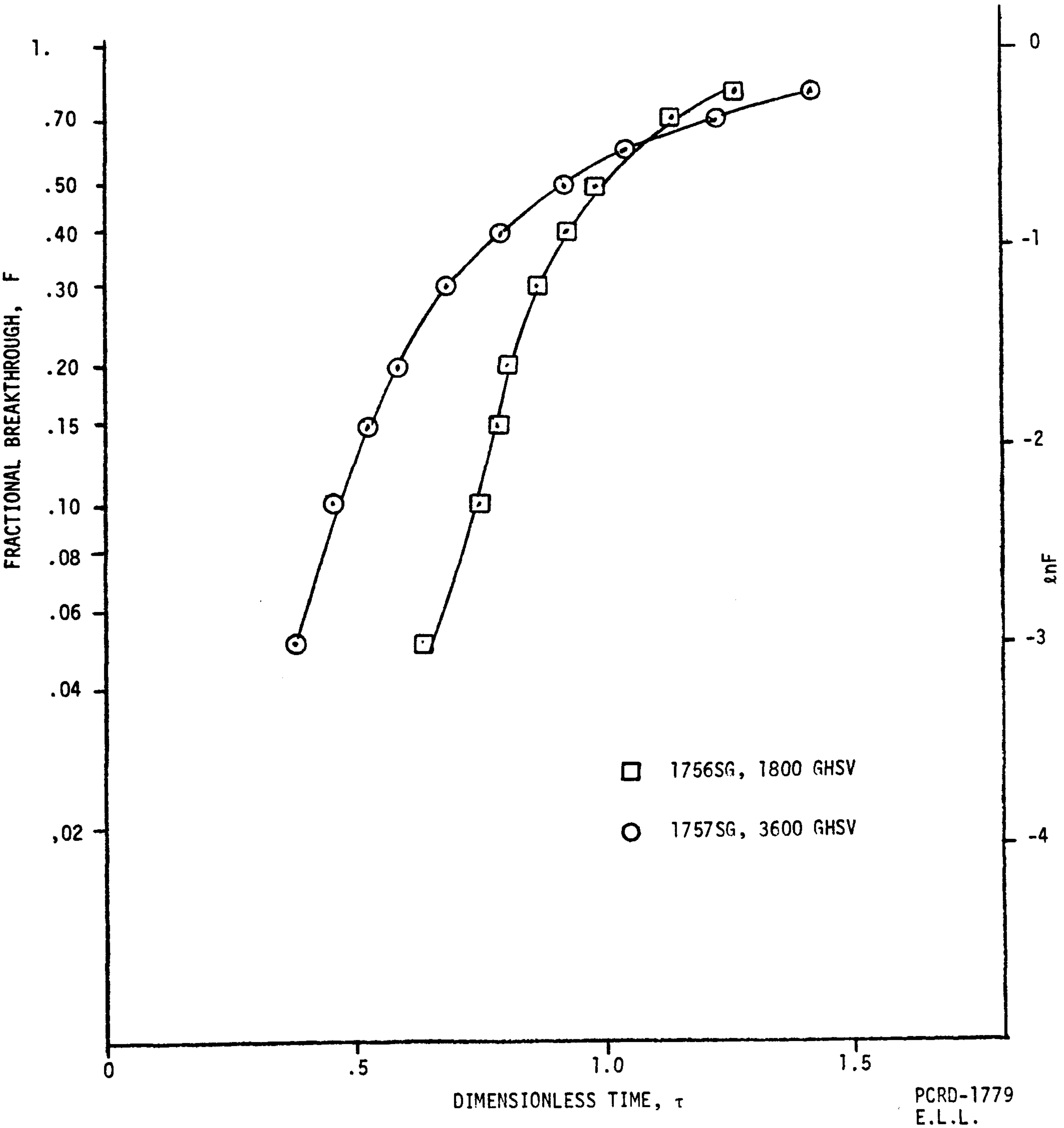

PCRD-1779
E.L.L.
5-9-77

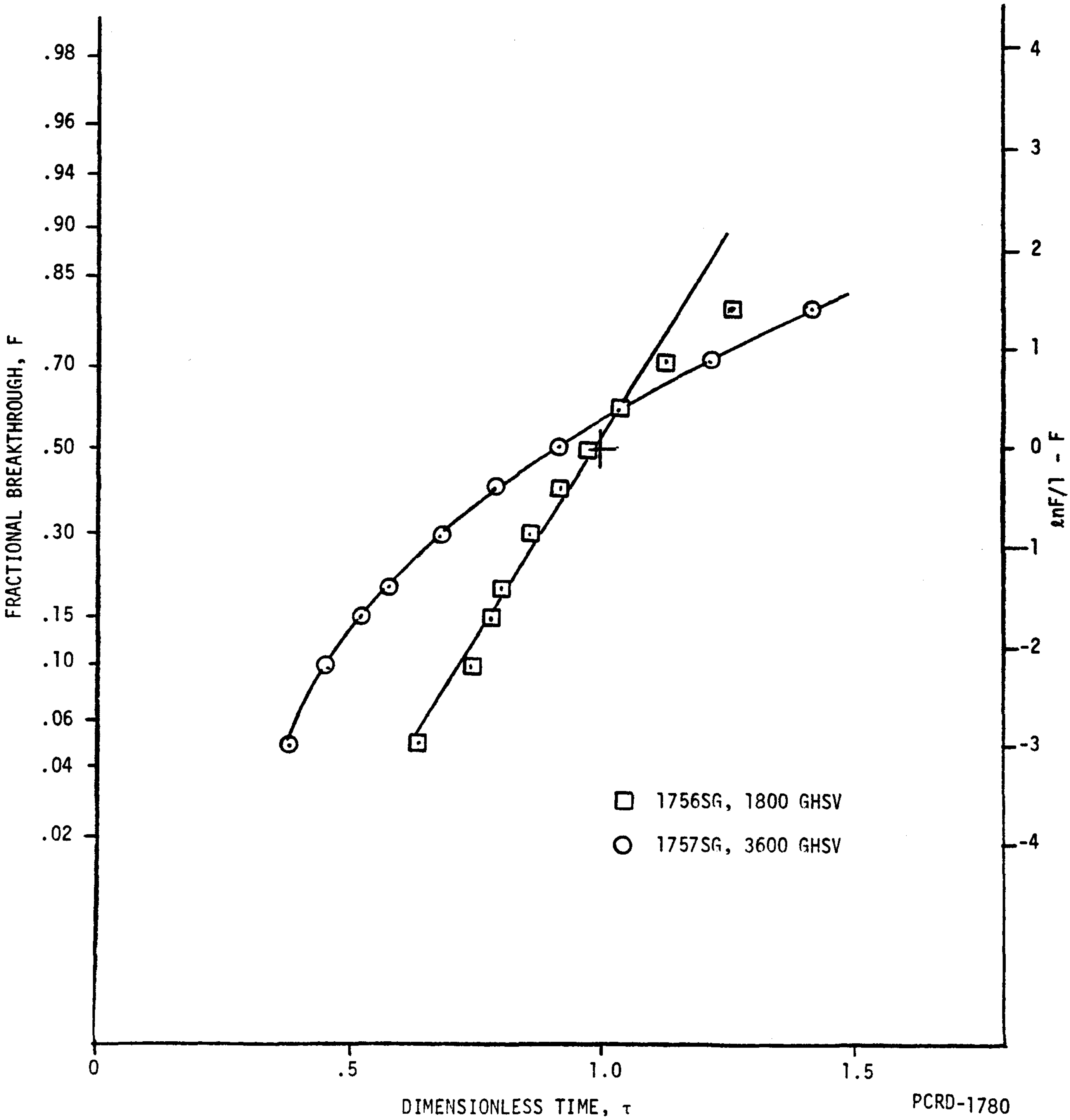

FIGURE 6.2

LEVEL 1 CONFIRMATION FOR KINETIC SORPTION MODEL

RUN CONDITIONS: 1200°F, 20 psig, 0.6 fps superficial velocity, 1/4 inch diameter pellets, 42% added iron oxide

PCRD-1780
E.L.L.
5-9-77

FIGURE 6.3

LEVEL 1 CONFIRMATION FOR SHRINKING CORE SORPTION MODEL

RUN CONDITIONS: 1200°F, 20 psig, 0.6 fps superficial velocity, 1/4 inch diameter pellets, 42% added iron oxide

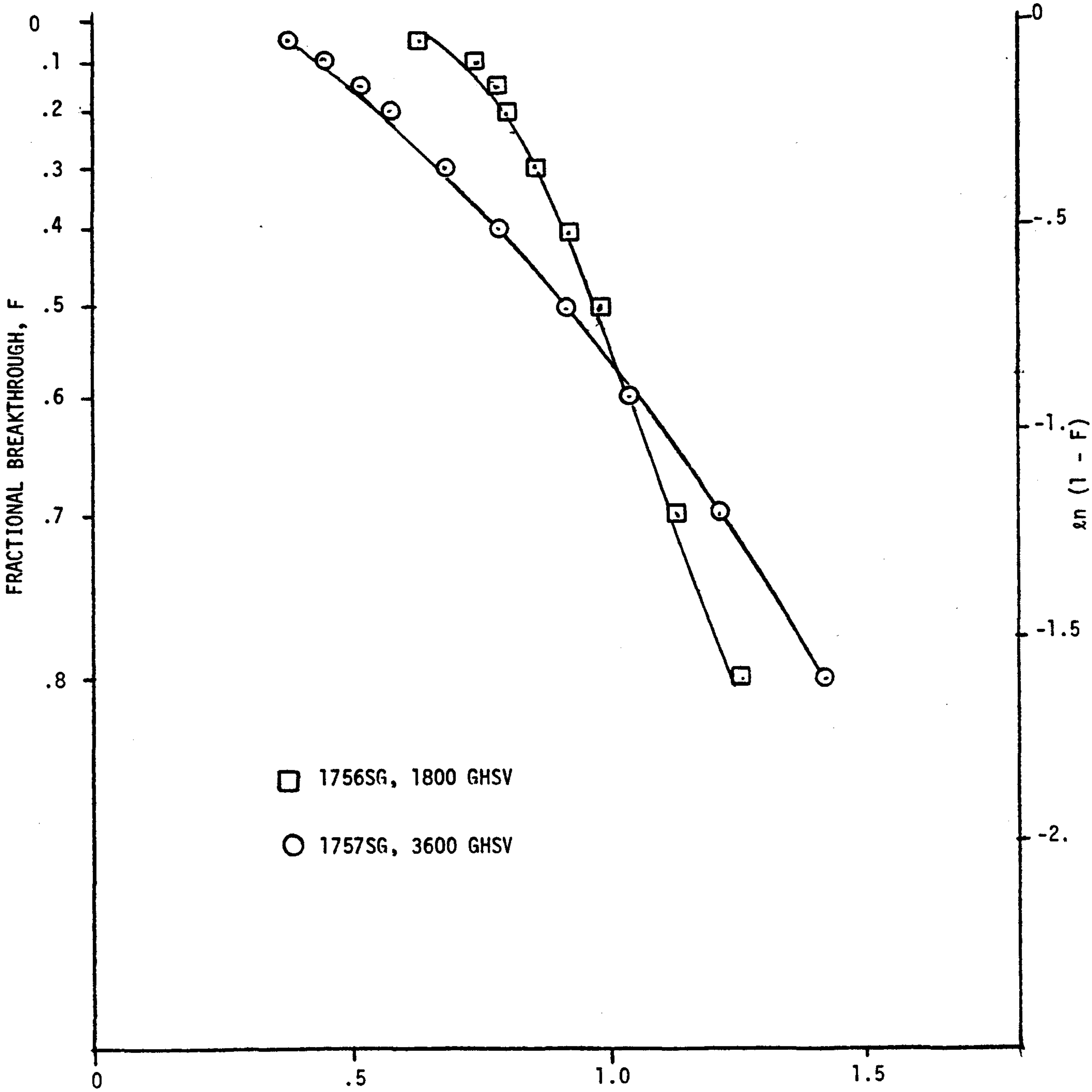

PCRD-1781
E.L.L.
5-9-77

number is significantly larger than zero and that internal diffusion is a rate controlling part of the sorption mechanism. Figure 6.4 is a linearized performance curve for a combined mechanism empirical model where the shell sorption number is proportional to the kinetic number plus twice the film number. If the film sorption number were zero, the model of Figure 6.4 would represent equal kinetic and Knudsen diffusion resistances. Figure 6.4 demonstrates that such a model can accurately represent the two experimental test runs. Indeed, any experimental run presented in Section 5 except the unusually shaped performance curve for 63% added iron oxide at 20 psig can be generated using a combined mechanism empirical model.

In conclusion, no single mechanism sorption model satisfies Level 1 confirmation for all experimental performance curves. Both shrinking core and kinetic models do satisfy Level 1 confirmation for some experimental data. A combined mechanism sorption model can satisfy the Level 1 criteria for all the experimental data if the film sorption number is much smaller than the shell diffusion number. Such a model generates performance curves similar to those of a combined internal diffusion - kinetic model with equal contribution from both mechanisms.

6.3 A Comparison of Predicted and Experimental Effects of Design Variables on Sorption Efficiency

The three isothermal sorption models each predict different effects of design variables on sorber onstream times. If the sorption is efficient enough so that constant pattern performance applies, then the change in onstream time can be predicted from the effect of design variables on sorption number. For all three models, constant pattern performance predicts that dimensionless time minus one is proportional to sorption number:

$$\tau - 1 = k N_{Ab} \qquad (6.1)$$

The proportionality constant, k, depends on the model and the value of the fractional breakthrough at time τ. Equation 6.1 can be used to compare model predictions and experimental changes in efficiency τ for constant pattern breakthrough using the following procedure:

Step 1 - The proportionality constant is determined for the model and level of breakthrough. If 10% breakthroughs are used, then k is determined from the base case efficiency at 10% breakthrough and the base case sorption number. The value of the sorption number and its dependence on design variables are determined by the model.

FIGURE 6.4

LEVEL 1 CONFIRMATION USING AN EMPIRICAL SORPTION MODEL

MODEL: $\tau = 1 + (A_1 N_{Ab}{}^{K} + A_2 N_{Ab}{}^{F}) \; \ln\left(\frac{F}{(1 - F)^2}\right)$

RUN CONDITIONS: 1200°F, 20 psig, 0.6 ft./sec.,
1/4 inch pellets, 42% added Fe_2O_3

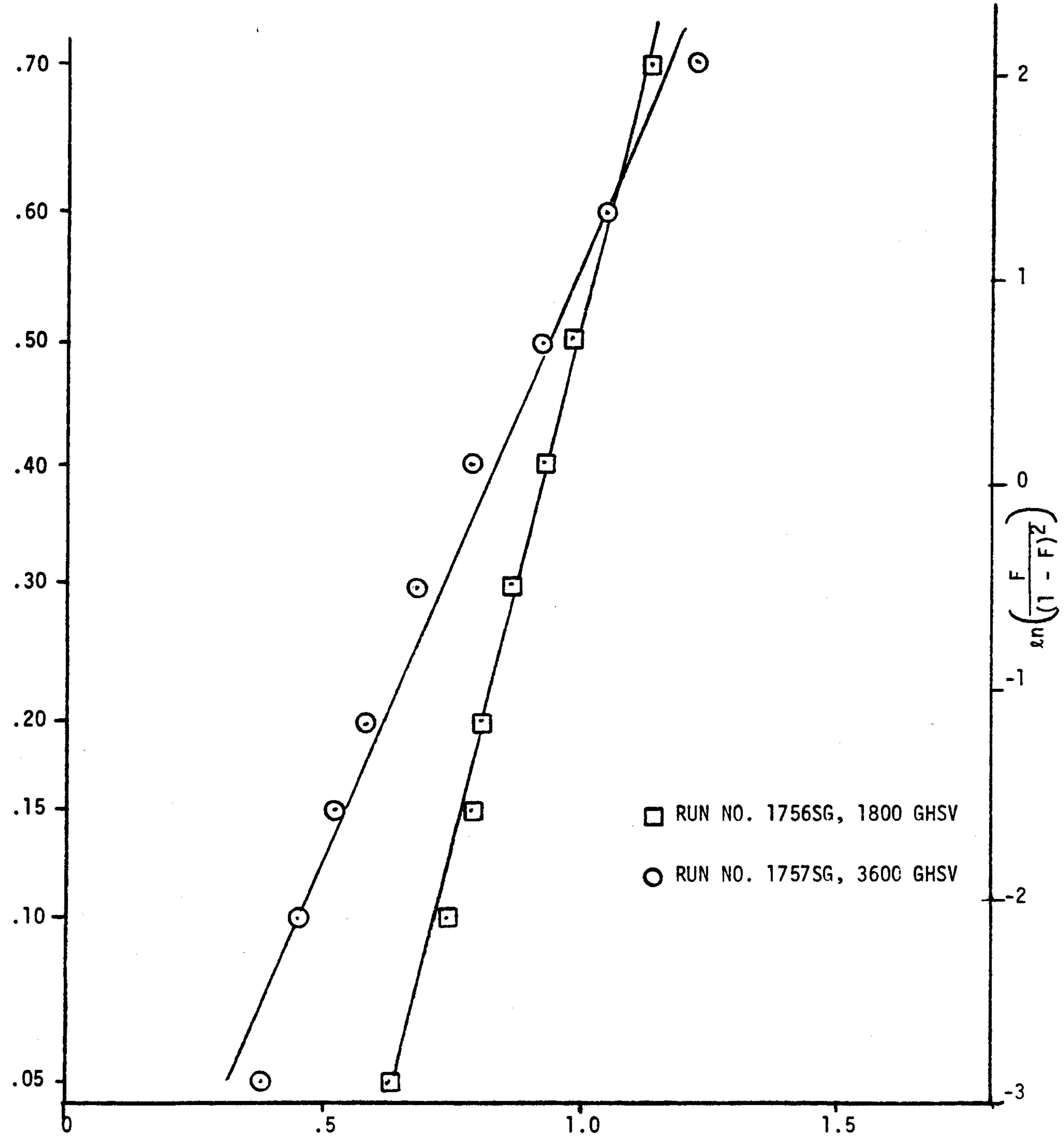

DIMENSIONLESS TIME, τ

PCRD-1782
D.K.J.
5-9-77

Step 2 - The value of k, the dependence of model sorption number on design variables, and Equation (6.1) are used to predict the experimental efficiencies at 10% breakthrough.

Step 3 - Predictions of Equation (6.1) are compared with experimental efficiencies to evaluate the accuracy of the sorption model.

If the experimental efficiencies agree with the model constant pattern predictions determined from Equation (6.1), then the model passes Level 2 confirmation criteria. Table 6.4 illustrates this procedure for each of the three isothermal models. The expressions for the constant pattern solutions were obtained using Run 1727SG as a base run. The sorption numbers used are functions of design variables iron oxide content, GHSV, velocity, pellet size, and unit pressure as described in Table 6.1. The temperature effects and empirical constants of the sorption numbers are combined in the proportionality constant, k. All efficiencies of Table 6.4 are at 10% sulfur breakthrough.

Table 6.4 also demonstrates that none of the single mechanism sorption models can predict all the experimentally observed effects of design variables. The kinetic model can account for the effect of iron oxide content, GHSV, and pellet size on efficiency, but it predicts no linear velocity effect. The kinetic model pressure effect is also much larger than the experimental observations. The film model predicts the linear velocity effect and the lack of a pressure effect for large diameter pellets with 42% iron oxide, but does not predict any effect of iron oxide content. Film model particle size effects are generally too large. The shrinking core model seems to combine the failings of the film and kinetic models.

If the combined mechanism model of Table 6.3 is used to predict the effects of design variables on efficiency, most experimental data at 10% sulfur breakthrough can be correlated. Since the shrinking core model correlation is superior to neither the film model nor the kinetic sorption model, it is not surprising that the shell diffusion number does not appear in the final correlation. Thus the correlation of Table 6.5 is a film-kinetic form of the combined mechanism model. The variable X, in the correlation is the dependence of the film number on design variables and the variable X_2 is the kinetic sorption number design variable dependence. The correlation accuracy was tested by evaluating the correlation coefficient of a plot of predicted versus experimental efficiency. If the model were perfect, this coefficient would be 1.00. The correlation coefficient for all runs listed in Table 6.5 is 0.85. If experimental and predicted efficiencies are compared on a run-by-run basis, the model

TABLE 6.4

OBSERVED EFFECTS OF EXPERIMENTAL VARIABLES ON SORPTION EFFICIENCY VERSUS EFFECTS OF PREDICTED BY SHRINKING CORE, KINETIC, AND FILM TRANSFER ISOTHERMAL SORPTION MODELS

Run Number	1727SG	1756SG	1756SG	1757SG	1727SG	1738SG	1727SG	1724SG	1756SG	1762SG	1724SG	1733SG
Variable Changed	Iron Oxide Content (Wp, wt.%)		GHSV		Superficial Velocity (3600 V, fps)		Pellet Diameter (24 a, inch)		Pressure (P, atm)		Pressure Effect for 1/8 Inch Pellet (P, atm)	
Level	21	42	1800	3600	0.6	1.2	1/4	1/8	2.4	28.2	2.4	11.2
Observed Efficiency (at 10% Breakthrough)	.58	.74	.74	.45	.58	.66	.58	.64	.74	.78	.64	.83
Predicted Efficiency												
A. Shrinking Core(1): $\tau = 1 + k\ N_{Ab}$	.58	.58	.58	.16	.58	.58	.58	.90	.58	.96	.90	.98
B. Kinetic (2): $\tau = 1 + k\ N_{Ab}^{K}$	.58	.79	.79	.58	.58	.58	.58	.58	.79	.98	.58	.91
C. Film Transfer(3): $\tau = 1 + k\ N_{Ab}^{F}$	.58	.58	.58	.16	.58	.70	.58	.85	.58	.58	.85	.85
Observed Change in Efficiency	+.16		-.29		+.08		+.06		+.04		+.19	
Predicted Change in Efficiency												
A. Shrinking Core	0		-.42		0		+.32		+.38		+.08	
B. Kinetic	+.21		-.21		0		0		+.19		+.33	
C. Film Transfer	0		-.42		+.12		+.27		0		0	

NOTES:

(1) $k\ N_{Ab} = -5.16\ \frac{a^2\ GHSV}{P}$

(2) $k\ N_{Ab}^{K} = -0.0118\ \frac{GHSV}{P\ W_p}$

(3) $k\ N_{Ab}^{F} = 0.00439\ \frac{a^{1.5}\ GHSV}{\sqrt{VP}}$

TABLE 6.5
FILM-KINETIC MODEL PREDICTIONS VERSUS EXPERIMENTAL EFFECTS OF SYSTEM VARIABLES ON SORPTION EFFICIENCY AT 10 PERCENT BREAKTHROUGH

SORPTION MODEL $\tau = 1 - 8.84\ X_1 - 5.01 \times 10^{-8}\ X_2$

CONSTANT PARAMETERS U.S. Steel Iron Oxide Source, Fly Ash Support, Bentonite Binder

NOTATION

F = Fractional Sulfur Breakthrough

τ = Sorption Efficiency

$$X_1 = \frac{\text{GHSV}\sqrt{a^3}\ T^{0.17}}{\sqrt{PV}} \qquad X_2 = \frac{T \exp(16/T) \cdot \text{GHSV}}{P I_0}$$

a = Sorbent Pellet Radius (ft.)

I_0 = Sorbent Iron Oxide Concentration (lb. moles/ft.^{3})

P = Pressure (atm.)

T = Absolute Temperature Divided by 492°F (dimensionless)

V = Superficial Linear Velocity at Run Conditions (ft. hr.$^{-1}$)

Run Number	GHSV	Linear Velocity (ft. hr.$^{-1}$)	Pressure (atm.)	Temperature (°F)	Pellet Radius (inches)	Weight % Iron Oxide	Lb. Moles Per Ft.^{3} Fe_2O_3	Experimental τ	Predicted τ
1718SG	1800	2100	2.4	1200	1/8	21.0	0.16	0.59	0.63
1720SG	1800	2100	2.4	1200	1/8	25.2	0.20	0.63	0.65
1721SG	1800	2100	2.4	1200	1/8	16.8	0.13	0.61	0.61
1722SG	1800	2100	2.4	1200	1/8	12.6	0.10	0.62	0.58
1723SG	1800	2100	2.4	1200	1/8	8.4	0.06	0.48	0.48
1724SG	1800	2100	2.4	1200	1/16	21.0	0.16	0.63	0.81
1725SG	1800	2100	2.4	1200	1/16	12.6	0.10	0.70	0.76
1727SG	1800	2100	2.4	1200	1/8	21.0	0.16	0.59	0.63

TABLE 6.5

FILM-KINETIC MODEL PREDICTIONS VERSUS EXPERIMENTAL EFFECTS OF SYSTEM VARIABLES ON SORPTION EFFICIENCY AT 10 PERCENT BREAKTHROUGH

(CONTINUED)

Run Number	GHSV	Linear Velocity (ft. hr.$^{-1}$)	Pressure (atm.)	Temperature (°F)	Pellet Radius (inches)	Weight % Iron Oxide	Lb. Moles Per Ft.^{3} Fe_2O_3	Experimental τ	Predicted τ
1728SG	1800	2350	2.4	1400	1/8	21.0	0.16	0.58	0.67
1729SG	3600	4200	2.4	1200	1/8	21.0	0.16	0.47	0.42
1730SG	1800	4200	2.4	1200	1/16	12.6	0.10	0.83	0.78
1731SG	1800	450	11.2	1200	1/8	21.0	0.16	0.69	0.70
1733SG	1800	450	11.2	1200	1/16	21.0	0.16	0.82	0.88
1734SG	1800	4200	2.4	1200	1/8	12.6	0.10	0.75	0.66
1736SG	1800	1350	2.4	600	1/8	21.0	0.16	0	0
1738SG	1800	4200	2.4	1200	1/8	21.0	0.16	0.66	0.71
1739SG	3600	8400	2.4	1200	1/8	21.0	0.16	0.51	0.54
1740SG	3600	4200	2.4	1200	1/8	21.0	0.16	0.41	0.42
1742SG	1800	450	11.2	1200	1/8	21.0	0.16	0.70	0.70
1743SG	1800	450	11.2	1200	1/16	21.0	0.16	0.92	0.88
1747SG	1800	2100	2.4	1200	1/8	63.0	0.69	0.31	0.70
1750SG	1300	4200	2.4	1200	1/8	21.0	0.16	0.76	0.79
1756SG	1800	2100	2.4	1200	1/8	42.0	0.37	0.71	0.68
1757SG	3600	2100	2.4	1200	1/8	42.0	0.37	0.46	0.37
1758SG	1800	1700	2.4	900	1/8	21.0	0.16	0.42	0.49
1760SG	1800	180	28.2	1200	1/16	21.0	0.16	0.87	0.90
1761SG	1800	180	28.2	1200	1/8	21.0	0.16	0.80	0.72
1762SG	1800	180	28.2	1200	1/8	42.0	0.37	0.74	0.72
1763SG	1800	180	28.2	1200	1/8	63.0	0.69	0.72	0.72
1764SG	1800	180	28.2	1400	1/8	42.0	0.37	0.75	0.73
1765SG	1800	450	11.2	1200	1/8	42.0	0.37	0.76	0.71
1767SG	3600	900	11.2	1200	1/8	42.0	0.37	0.64	0.59

MODEL CORRELATION COEFFICIENT $\rho = 0.850$

is found to be least accurate for low pressure sorptions using 63% iron oxide on fly ash. This sorbent performance curve had an unusual shape (see Figure 5.13). The correlation also tends to over-estimate the effect of particle size on efficiency at low pressure.

In general, the film-kinetic model will pass Level 2 model confirmation for sorption efficiencies at 10% breakthrough. However, the correlation does not pass Level 1 confirmation due to the relatively large film sorption number required by the correlation:

$$\tau = 1 + \left(N_{Ab}{}^{K} + N_{Ab}{}^{F}\right)\left(\ln F + 1\right) - N_{Ab}{}^{K}\left(\ln\,(1 - F) + 1\right) \qquad (6.2)$$

The Level 1 confirmation plots of Section 6.2 demonstrated that Equation (6.2) will not correctly predict the shape of the performance curves for some runs even if the film sorption number is zero (i.e., kinetic model). As the film number is increased, the shape of the performance curves become more and more like those of the film model, which does not correctly predict breakthrough curves for any of the 70 experimental runs conducted! Nevertheless, a large film number is required to pass Level 2 confirmation, as demonstrated by the failure of the kinetic model to predict observed sorption efficiencies.

An empirical model that satisfies both Level 1 and Level 2 confirmation can be developed by slightly modifying the expression for film-kinetic model as described below.

$$\tau = 1 + \left(A_1\, N_{Ab}{}^{F} + A_2\, N_{Ab}{}^{K}\right) \ln\left(\frac{F}{(1 - F)^2}\right)$$

This empirical equation satisfies Level 1 confirmation as shown in Figure 6.5 and Level 2 confirmation at 10% breakthrough with the same accuracy as Table 6.4.

7.0 REGENERATION PROCESS CONCEPT

7.1 Chemistry and Constraints

Sulfided sorbent can be regenerated by oxidizing the iron sulfide to iron oxide and sulfur dioxide:

$$FeS + 1.5O_2 \longrightarrow FeO + SO_2 \qquad \Delta H = -75 \text{ Kcal/gmole oxygen}$$

$$2FeS + 3.5O_2 \longrightarrow Fe_2O_3 + 2SO_2 \qquad \Delta H = -84 \text{ Kcal/gm mole } O_2$$

$$FeS_2 + 2.5O_2 \longrightarrow FeO + 2SO_2 \qquad \Delta H = -67 \text{ Kcal/gmole } O_2$$

$$2FeS_2 + 5.5O_2 \longrightarrow Fe_2O_3 + 4SO_4 \qquad \Delta H = -74 \text{ Kcal/gmole oxygen}$$

The above reactions proceed rapidly to completion at hot producer gas temperatures. The reactions are highly exothermic. If the sorbent were regenerated using a mixture of oxygen and nitrogen (for example, air), the gas adiabatic temperature rise would be 195°F for each 1 volume percent oxygen consumption. Using 100% air could cause a computed reactor temperature rise of 4100°F if all the oxygen was consumed. Since such a temperature rise would surely sinter the sorbent, any acceptable scheme for adiabatic regeneration based on oxygen must use a diluted air or oxygen stream as the regeneration gas. Normally, such schemes result in low SO_2 concentrations in the regeneration off-gas. Concentrating this off-gas sulfur content will reduce the size of the sulfur recovery plant and thus reduce overall costs. Therefore, the majority of adiabatic regeneration schemes reviewed consist of two steps: (1) a regeneration step where the bed temperature is kept below 1500°F to prevent sorbent deterioration, and (2) a means for increasing the SO_2 concentration.

The problem of removing the heat of regeneration can also be solved by providing internal bed cooling for the regeneration. Since internal cooling coils would be exposed to the highly corrosive alternating oxidizing and reducing atmospheres, this solution to the heat of regeneration problem will require the development of new materials for cooling coil manufacture. Because new technology will be required, this study does not consider internally cooled regenerators as an alternative to adiabatic regenerators.

7.2 Alternate Regeneration Schemes

Table 7.1 is a concise comparison of energy and heat exchange requirements for six adiabatic regeneration schemes. The schemes use either oxygen or air diluted with a recycle or other process stream as regeneration gas. The regeneration products contain at least 15% SO_2, except for the air/stack gas regeneration scheme which yields a 2% SO_2 stream. The other five schemes require recycling between 20 and 38 moles of material for each mole of SO_2 produced. Since about 167 moles of producer gas are processed per mole of sulfur sorbed, the volume of regeneration gas processed is only 12 to 22 percent of the volume of producer gas processed. Thus the capital costs of heating and cooling equipment required to use cold recycle streams is about 28 to 38 percent of the capital costs required for cooling and heating in presently available cold stage desulfurization schemes using the 0.6 exponential cost factor. Since hot streams may not be recyclable using present compressor technology, this capital cost must be considered and must be less than that of cold stage desulfurization for a regeneration scheme to be practical. Because the last scheme listed in Table 7.1 uses a hot SO_2 and nitrogen recycle, this scheme has been eliminated from further consideration. The first five regeneration schemes of Table 7.1 remain practical according to the criteria examined. Of the five schemes, the air/once-through stack gas scheme is least attractive due to the large volume of stack gas that must be circulated to produce hot regeneration gas and the low SO_2 content of the off-gas.

The air-steam regeneration is not in heat balance due to the loss of latent heat of condensation, but the pumping costs are very low as liquid water is pumped. Air feed/cold N_2 and SO_2 recycle are good in heat balance, but the pumping costs are high.

Of the four cold recycle streams of Table 7.1, the air/liquid water recycle requires the lowest recycle pumping costs. The compressor on the cold SO_2 and nitrogen gas recycle stream in the fourth scheme requires a minimum (or ideal) work equivalent to 0.7% of the heating value of the producer gas, while the liquid recycles of the first three schemes require little energy to operate their liquid recycle pumps. The two regeneration schemes that require pure oxygen are more expensive than the air/liquid water recycle due to the cost of the oxygen.

Figure 7.1 is a simplified flow sheet for the air-steam regeneration gas/liquid water recycle scheme of Table 7.1. Air at ambient temperature (100°F) is introduced into recycle steam at 1100°F to form the 1000°F air/steam regeneration gas. Inside the regeneration vessel (sorber) the oxygen is consumed by the iron sulfide bed to produce SO_2 and regenerated sorbent. The heat of regeneration raises the gas temperature to 1500°F. The hot product gas is then cooled to 300°F by

TABLE 7.1

COMPARISON OF REGENERATION SCHEMES

Oxygen Source	Recycle or Process Stream Used to Dilute Oxygen	Regeneration Product	Moles Recycle or Process Stream per Mole SO_2 Generated	Major Energy Costs in Percent of Producer Gas Heating Value*		Additional Heat Required to Maintain Heat Balance
				Heat Exchanged Between Process Streams	Ideal Work of Recycle or Process Pump	
Air	Liquid Water	15% SO_2 Vapor in N_2	33.4	7%	1.6 X 10^{-3}%	7%
Oxygen	Liquid Water	Pure SO_2 Vapor	37.5	7%	2.0 X 10^{-3}%	8.6%
Oxygen	Liquid SO_2	Pure SO_2 Vapor	20.5	7%	2.5 X 10^{-3}%	1.6%
Air	Cold Nitrogen/ SO_2 Gas	15% SO_2 Vapor in N_2	35.6	5.9%	0.70%	-
Air	Stack Gas (Once-Through Process Stream)	2% SO_2 Vapor in Stack Gas	41.7	5.2%	1.01%	-
Air	Hot Nitrogen/ SO_2 Gas	15% SO_2 Vapor in N_2	35.6	None	1.19%	-

---

* 6.4 MM BTU of producer gas heating value for each mole of SO_2.

FIGURE 7.1

AIR FEED/STEAM RECYCLE

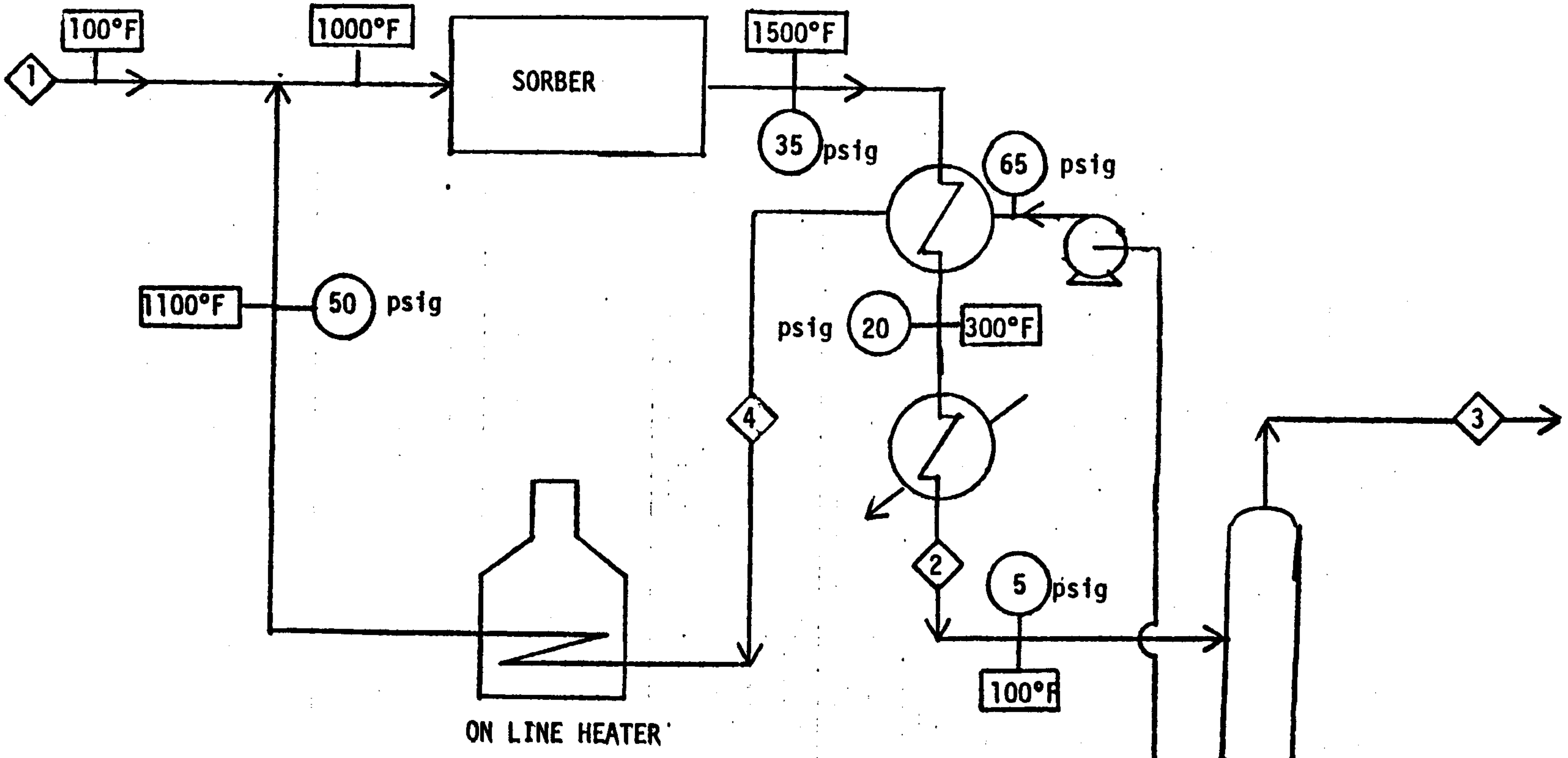

FLOWS (lb.-moles/hr.)	1	2	3	4
O_2	1.00	-	-	-
N_2	3.76	3.76	3.76	-
H_2O	-	22.3	-	22.3
SO	-	0.67	0.67	-

RECYCLE / EFFLUENT EXCHANGER
3×10^5 BTU/Hr.
(300 ft.^{2})

PUMP WORK
0.028 HP

FIGURE 7.2

O_2 FEED/STEAM RECYCLE

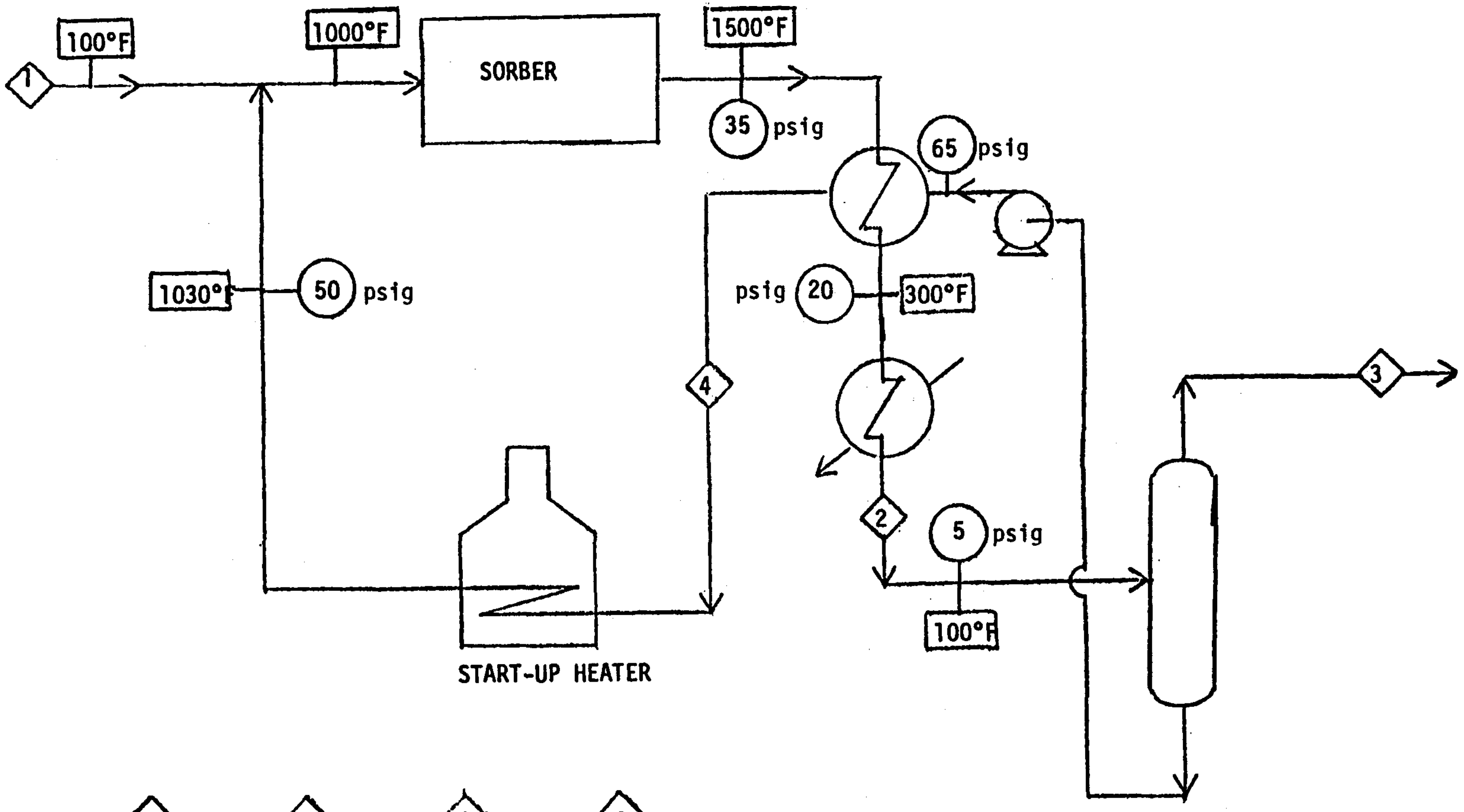

FLOWS (lb.-moles/hr.)	1	2	3	4
O_2	1.0	-	-	-
H_2O	-	25.0	-	25.0
SO_2	-	0.67	0.67	-

RECYCLE/EFFLUENT EXCHANGER
3×10^5 BTU/hr.
(300 ft.^{2})

PUMP WORK
0.031 HP

PCRD-1455
E.L.L.
7-6-76

the recycle water. The steam is removed from the product by a condenser and a knock-out pot. The final product of the regeneration (stream 3 of Figure 7.1) is 15% SO_2 in nitrogen. The water from the knock-out pot is pumped into the recycle/effluent heat exchanger. There it is vaporized and heated to 1100°F by the hot product from the sorber and becomes the steam recycle stream. The heater shown on the flow sheet is for start-up only.

Figures 7.2 through 7.6 show the simplified flow sheets for the other regeneration schemes of Table 7.1. They indicate that all schemes were compared on the following basis:

1. Oxygen source (stream 1) was assumed at ambient temperature (100°F).
2. Flow rate of recycle on process stream added to the oxygen source was such that the regeneration gas entering the sorber had an adiabatic temperature rise of 500°F.
3. The regeneration gas inlet temperature was 1000°F.
4. The pressure drop across each major piece of equipment (sorber, heat exchanger, and start-up heater) was 15 psi.
5. For water recycle schemes, no SO_2 was assumed to be dissolved in the water recycle.

For each scheme, the major energy consumption was considered to be the work of the recycle or process gas pump. Work shown is ideal (frictionless) work for this pump in brake horsepower. The area of the recycle/effluent heat exchanger was estimated, but this estimate of process capital cost was not taken as a criteria to determine the most promising regeneration scheme (see preceding discussion).

7.3 Selection

Based on the cost of recycle pumping, air steam regeneration is promising, but it requires additional heat input. Based on the heat balance alone, air with cold N_2-SO_2 recycle gas is attractive, but it requires somewhat higher recycling costs. In this experimental work the regeneration cycle was examined with steam-air regenerating gas.

FIGURE 7.3

O_2 FEED/SO_2 RECYCLE

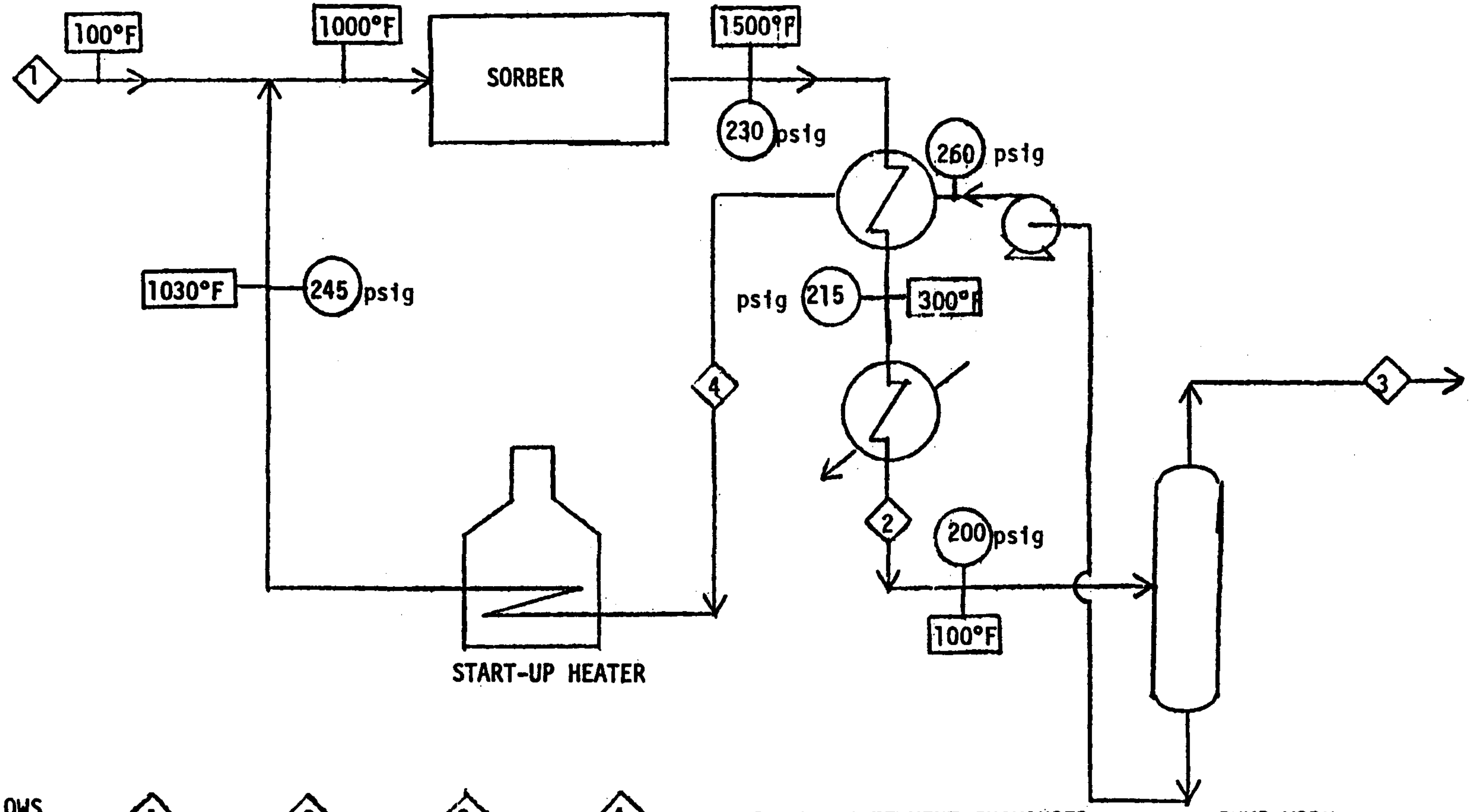

FLOWS (lb.-moles/hr.)	1	2	3	4	RECYCLE/EFFLUENT EXCHANGER	PUMP WORK
O_2	1.0	-	-	-	3 X 10^5 BTU/hr. (300 $ft.^2$)	0.042 HP
SO_2	-	14.4	0.67	13.7		

PCRD-1456
E.L.L.
7-6-76

FIGURE 7.4

AIR FEED/COLD N_2 AND SO_2 RECYCLE

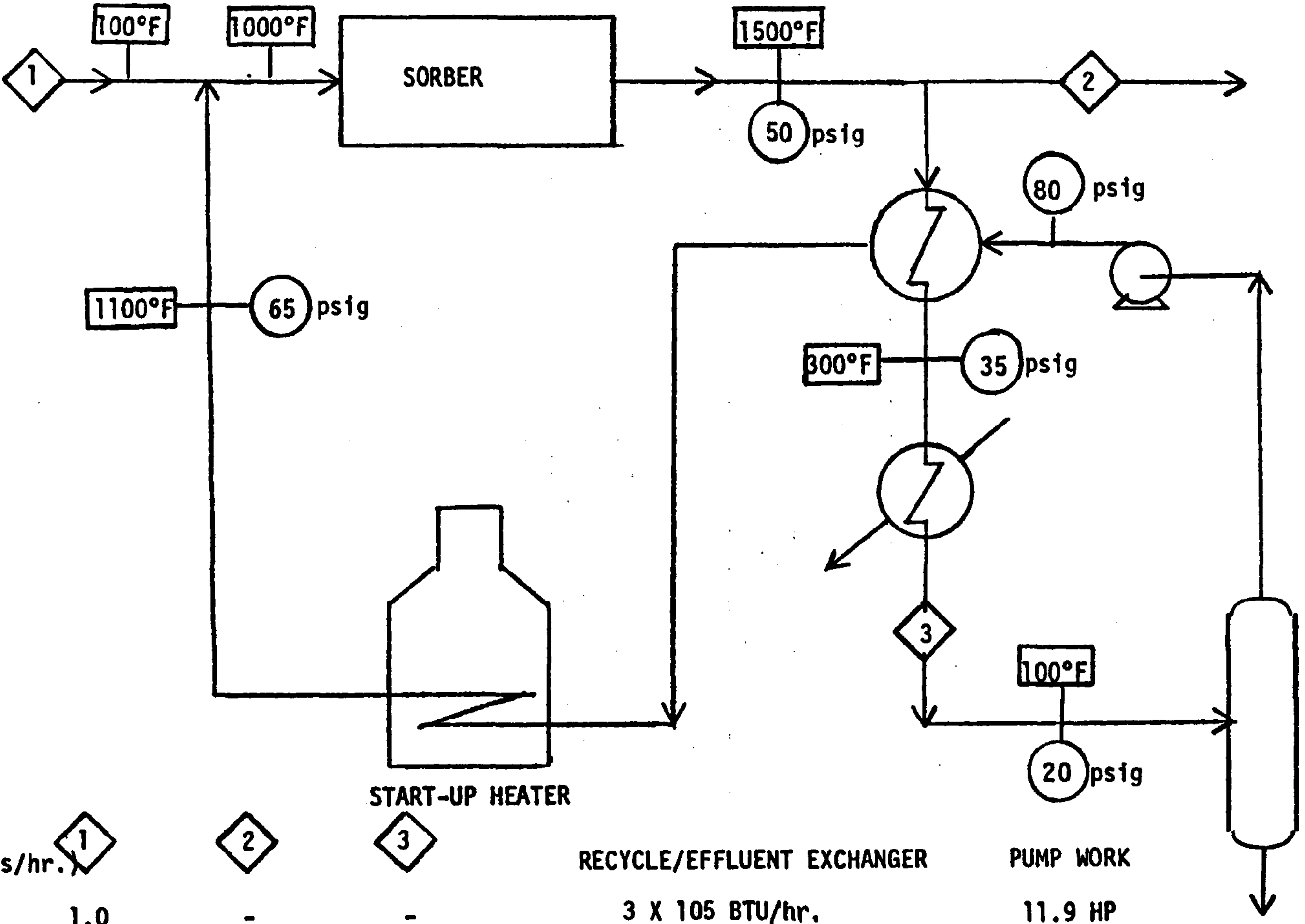

FLOWS (lb.-moles/hr.)	◇1	◇2	◇3
O_2	1.0	-	-
N_2	3.76	3.76	20.2
SO_2	-	0.67	3.58

RECYCLE/EFFLUENT EXCHANGER

3 X 105 BTU/hr.
(300 $ft.^2$)

PUMP WORK

11.9 HP
(3.0×10^4 BTU/hr.)

PCRD-1457
E.L.L.
7-6-76

FIGURE 7.5

AIR FEED/ONCE-THROUGH STACK GAS

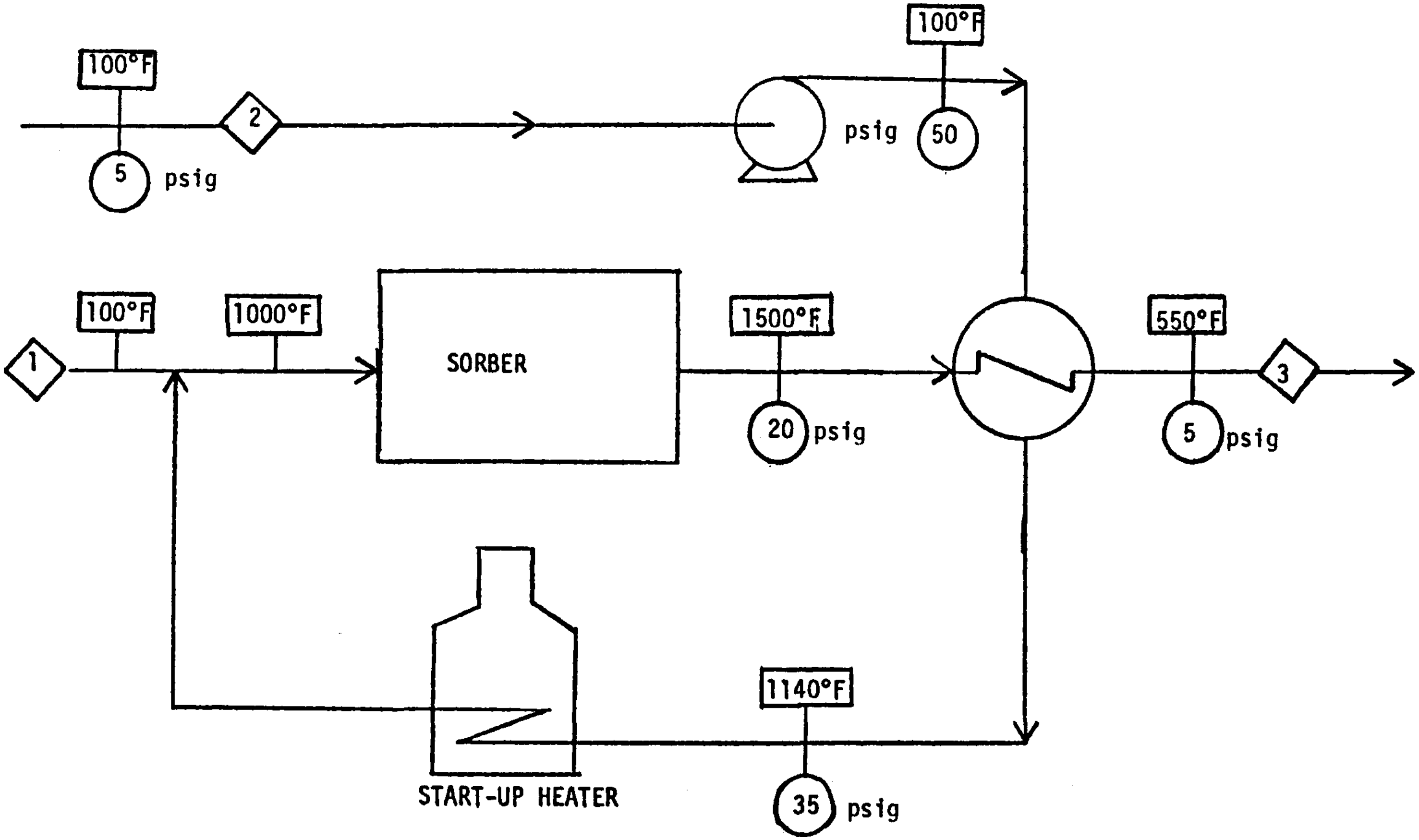

FLOWS (lb.-moles/hr.)	1	2	3
O_2	1	-	-
N_2	3.76	23.6	27.4
CO_2	-	4.2	4.2
SO_2	-	-	0.667

FEED/EFFLUENT EXCHANGER	IDEAL PUMP WORK
2.2×10^5 BTU/hr.	4.3×10^4 BTU/hr.
(55 $ft.^2$)	16.9 HP

PCRD-1458
E.L.L.
7-6-76

FIGURE 7.6

AIR FEED/HOT N_2 AND SO_2 RECYCLE

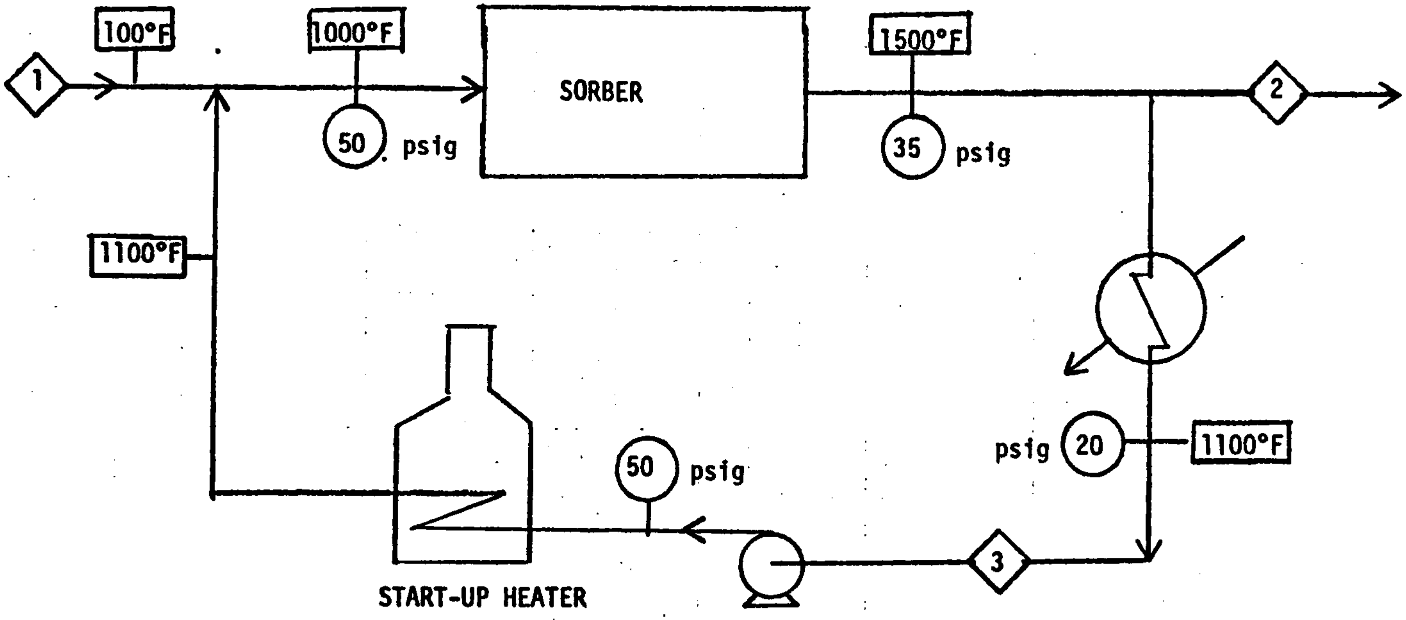

FLOWS (lb.-moles/hr.)	1	2	3	RECYCLE/EFFLUENT EXCHANGER	PUMP WORK
O_2	1.0	-	-	NONE	20 HP
N_2	3.76	3.76	20.2		(5.1 X 10^4 BTU/hr.)
SO_2	-	0.67	3.58		

PCRD-1459
E.L.L.
7-6-76

8.0 EXPERIMENTAL DETAILS

8.1 Experimental Equipment

The unit for dynamic testing of experimental sorbents is described in Appendix A of this report. This unit, herein referred to as the ERDA pressure unit, was used for sorption dynamics studies without excessive modifications. However, several major modifications to the unit were required for regeneration runs using 15% air/85% steam feed gas:

1. Since the regeneration gas was mainly steam, a new higher capacity water feed pump was required. A pump was borrowed from an APCI pilot unit not presently in use.

2. The high water content of the product gas required that all product sample lines be kept above 300°F to prevent water condensation. These lines had to be rewired to increase the heat flux to the pipes. The new circuits required two additional 20 amp Variacs, which were borrowed from an APCI pilot unit.

3. The Applied Automation on-line gas chromatograph was modified to analyze for SO_2 in the regeneration off-gas. An additional precut column was required to keep the other chromatograph columns dry.

4. An APCI-owned Perkin-Elmer gas chromatograph was installed to analyze the oxygen content of the regeneration off-gas.

5. Operating problems caused by the high product gas water content required that the regulator that had been used to control chromatograph pressure be replaced by a pressure control valve.

6. The unit pressure control valve could not maintain pressure because of the large percentage of condensibles in the product gas. A lower range, APCI-owned control valve was installed.

7. As an experimental safeguard against air pollution from SO_2 in the off-gas, the scrubber cupric nitrate was replaced with sodium hydroxide.

The flow scheme for regeneration runs using the modified ERDA pressure unit is diagrammed in Figure 8.1 and outlined below:

FIGURE 8.1 SIMPLIFIED FLOW DIAGRAM FOR REGENERATION RUNS USING THE ERDA PRESSURE UNIT

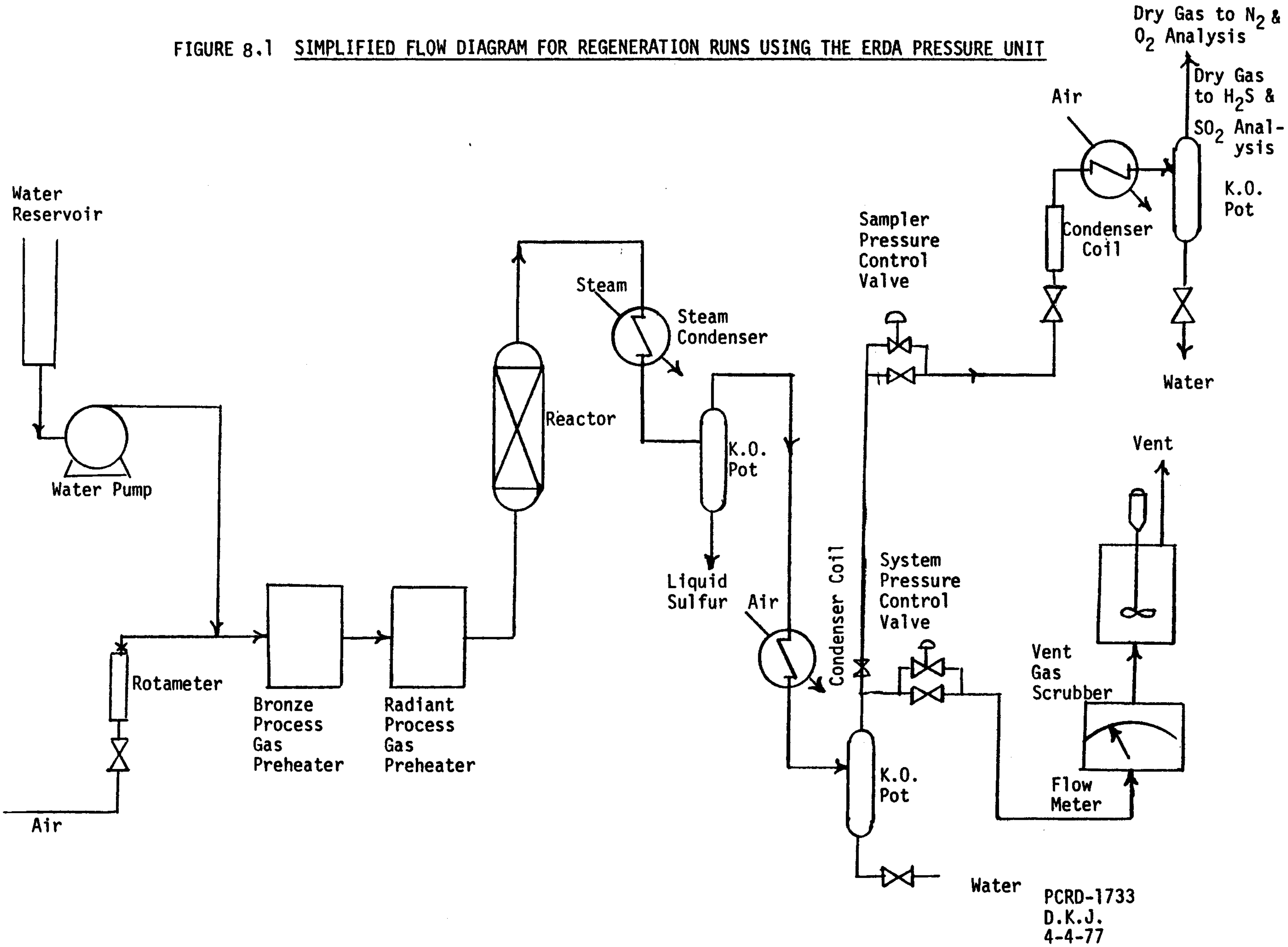

1. Air enters the system through a rotameter, while water is pumped in to join the air flow at the bronze block preheater. The air source is an external bank of compressed air cylinders; the water source is a reservoir of deionized water. Very high steam rates can be achieved by injecting pressurized steam through a rotameter in a separate feed system.

2. The air/steam regeneration gas flows through the bronze block and radiant process gas preheaters and enters the reactor bottom.

3. Inside the reactor, oxygen is consumed to form SO_2 and iron oxide. A side reaction may occur which forms some elemental sulfur vapor. The regeneration off-gas exits through the top of the reactor.

4. From the reactor, the off-gas enters the steam condenser where it is cooled to about 300^oF. Elemental sulfur, if produced, collects in the bottom of the steam condenser knock-out pot.

5. The gas flow passes through a cold condenser and a knock-out pot, to separate gas and liquid.

6. Just after the gas stream leaves the condenser knock-out pot, a side stream of the dry gas is removed and taken over to the on-line chromatographs. A pressure control valve can be used to regulate the sample line pressure. Flows to the chromatographs are controlled at a set of rotameters. SO_2 and H_2S are analyzed by the Applied Automation chromatograph on a dry gas basis. The flow to the Perkin-Elmer chromatograph passes through a knock-out pot, and the off-gas O_2 is analyzed on a dry gas basis.

7. From the cold condenser knock-out pot, the gas stream flows through a pressure control valve, through a gas flow meter, and out through the vent gas scrubber. The scrubber, which consists of a solution of sodium hydroxide in water, acts as an environmental guard to prevent venting of H_2S and SO_2 to the atmosphere.

8.2 Shakedown Runs

Four regeneration shakedown runs were conducted. The objectives of these runs were:

1. Develop operating procedures.
2. Train operating personnel.
3. Identify and correct operating problems.
4. Demonstrate process feasibility.

During the shakedown runs, progress was made in meeting all four objectives.

All operating problems encountered during the shakedown runs were caused by the change in process gas from simulated producer gas (used for sorption studies) to regeneration gas containing 85% steam and 15% air. The major problem encountered was water condensation in the gas chromatographs and their sample lines. The moisture flooded the chromatograph roatmeters and saturated the chromatograph columns during run 1801SG; as a consequence, no product analysis was possible during this run. The problem was alleviated by installing a moisture retaining precut column on the Applied Automation sulfur analysis chromatograph and by installing a water knock-out pot to guard the Perkin-Elmer oxygen analysis chromatograph from water. In addition, gas chromatograph and regeneration off-gas lines were rewired to increase heat flux and eliminate water condensation.

The sampling line from reactor top to the chromatograph was a long line due to the physical space constraints in the pilot plant. To avoid condensation, the entire length was wrapped with heating circuits and insulated. Temperature of the sampling line was measured at two points. The two temperatures were kept around 400°F, and the entire sampling system was purged with dry, hot gas. In spite of this, during the run, the sampling system and rotameter at the inlet to the chromatograph (used to control accurately the sample flow rate which is critical for analysis) were flooded with water. After several unsuccessful attempts, it was decided to analyze the product gas on a dry basis. Sulfur dioxide is very soluble in water as indicated by the vapor-liquid equilibrium for SO_2-H_2O. Hence the breakthrough curves for SO_2 would be substantially modified. In principle, actual dry gas analysis could be calculated by modeling the system. But accurate sulfur balances would still not be obtained due to the side reactions yielding elemental sulfur and SO_3.

Breakthrough curves for oxygen can be obtained with a greater accuracy. Ratio of oxygen to nitrogen in the dry effluents can be measured very accurately by a Perkin-Elmer gas chromatograph using molecular sieve column. Since nitrogen is an inert in the reaction, ratio of oxygen to nitrogen in effluent is a quantitative measure of oxygen utilization throughout the regeneration. Hence it was decided to use the breakthrough curves for oxygen as the basis for analysis.

Small amounts of sulfur formed by side reactions during regeneration also condensed and solidified in the product lines during the first shakedown run. The sulfur condensation was eliminated by heating the line between the reactor and the steam condenser above 600°F. At the condenser, the gas temperature was lowered to 300°F and the sulfur was removed in the knock-out pot.

The steam/SO_2 product gas mixture seemed to increase pipe corrosion. Filters in the chromatograph sample line became clogged with corrosion products. These filters were removed after the steam knock-out pot mentioned above was put in use. This pot collects a large part of the corrosion products and seems to protect the sample lines.

Increased corrosion was probably responsible for the failure of the transfer line between the radiant preheater and the reactor. This line was replaced.

During shakedown, operating problems interrupted the runs and interferred with off-gas analysis. Nevertheless, data showed that regeneration was very efficient in oxygen utilization. Saturation time was close to perfect operation time.

Visual analysis of the regenerated sorbent discharged from these runs indicated that no pellet deterioration had occurred. The pellets appeared to be a brighter red color than the freshly prepared sorbent, which may indicate that the oxidation served to convert any other iron compounds that were originally in the iron oxide source to Fe_2O_3. Sulfur capacity measurements on regenerated sorbent will determine the validity of this hypothesis.

Once sulfided fresh absorbent was used in all regeneration runs.

In summary, all observations made during the shakedown runs indicated that air/steam regeneration is an efficient process that does not cause sorbent deterioration.

8.3 Experimental Program

An experimental program was planned to study the effect of process variables on regeneration dynamics. The variables were: GHSV, velocity, temperature, pressure, sorbent iron sulfide content, oxygen concentration and pellet size.

The experimental conditions and APCI run code numbers for the regeneration experiments are summarized in Table 8.1. Sulfided sorbent from sorption studies was used in most regeneration runs. However, sufficient quantities of the sorbent sulfided in the sorption studies were

TABLE 8.1

REGENERATION DYNAMICS TEST RUNS

APCI Run Code	1807	1813	1809	1808	1810	1806	1805	1811	1814	1815	1817	1818
Run Number	1	2	3	4	5	6	7	8	9	10	11	12
% Air in Steam	15	15	15	20	20	15	15	15	15	15	15	15
Air GHSV	100	100	200	200	200	100	100	100	100	200	1000	1000
Bed Volume, cc.	500	1000	500	500	500	500	500	500	1000	500	500	500
Unit Pressure, psig	30	30	30	30	30	30	150	30	30	30	30	30
Gas Inlet Temp., ^{o}F	1000	1000	1000	1000	1200	1000	1000	1000	1000	1000	1000	1000
% Fe_2O_3 in Unsulf. Sorbent	42	21	42	42	42	21	21	21	42	42	42	42
Sorbent Pellet Diam., in.	1/4	1/4	1/4	1/4	1/4	1/4	1/4	1/8	1/4	1/4	1/4	1/4
Estimated Run Time, hr.*	15.5	7.8	7.8	7.8	7.8	7.0	7.0	7.0	15.0	7.7	1.5	1.5
Variable Studied	Base Run	Bed Depth	GHSV	O_2 Conc.	Inlet Gas Temp.	Fe_2O_3 Content	Unit Press.	Pellet Size	Velocity	GHSV	High GHSV	High GHSV Confirmation

---

*Based on 100% Conversion of O_2.

not available and some fresh sorbent had to be sulfided. Due to the small capacity of the ERDA pressure unit, sulfiding was done in a heat treater at 1000°F and 1 atm pressure using a feed containing 55% nitrogen and 45% hydrogen sulfides. Table 8.1 includes the origin of sulfided sorbent used in each regeneration experiment.

8.4 Sampling Lag

Since analysis was done on a dry gas basis, the sample was taken from the knock-out pot after moisture (85% of the total stream) was removed in a condenser. Due to the large knock-out pot volume and small dry gas flow rate, a composition change in the effluents was modified. The system was modeled as a perfectly mixed stirred tank.

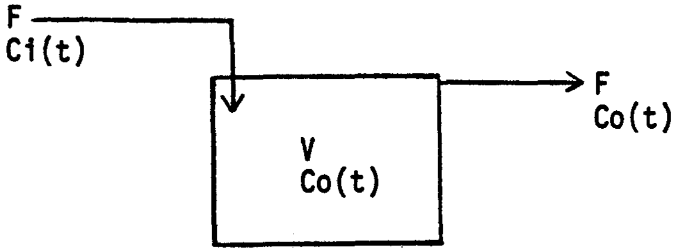

Since volume of water condensed is small compared to the knock-out (K.O.) pot volume, volume of the K.O. pot can be taken as a constant. Co(t) is the time dependent oxygen mole fraction in the outgoing stream and Ci(t) is the time dependent oxygen mole fraction in the incoming stream. F is the flow rate in $ft.^3/sec$. A material balance for oxygen yields:

$$\text{IN} = \text{OUT} + \text{ACCUMULATION}$$

$$F \cdot M \cdot Ci = F \cdot M \cdot Co + V \cdot M \frac{dCo}{dt}$$

where M is a conversion factor to convert $ft.^3$ to moles and is constant at a given temperature and pressure. It is constant in all the three terms as temperatures and pressures do not change.

This reduces to:

$$Ci = Co + \frac{V}{F} \frac{dCo}{dt}$$

Hence, if Co is measured, Ci - the actual composition of the stream coming to the knock-out pot can be calculated.

Before the experimental data are deconvoluted, it was necessary to test the validity of the model. Sample lag studies were carried out in the following manner. Inert nitrogen purged the system for a few hours, then a sudden step change in oxygen concentration was made by replacing it by air. Breakthrough curves for oxygen due to the mixing tank response were obtained. These data were compared with those predicted by the model.

For a step change in concentration, the model results in the following relationship between the incoming and outgoing concentrations.

$$Co = Ci \left(1 - e^{-\frac{t \cdot F}{V}}\right)$$

Figure 8.2 describes a comparison between actual and predicted 'apparent' breakthrough curves. A fairly good agreement is seen.

Figure 8.3 describes how the breakthrough curves for a typical regeneration run are modified after correcting for sample lag on absolute time scale. Breakthrough curves become steeper, representing operation closer to perfect operation. Some gas samples were collected in M.S. bulbs at the reactor outlet. These data points seem to lie on the breakthrough curve corrected for sample lag. This is an additional confirmation of the selected stirred tank model.

It may be noted that time for perfect operation is obtained by dividing total oxygen absorbed during the run by the oxygen flow rate in feed. Hence time for perfect operation will be different for the breakthrough curves uncorrected and corrected for sample lag. Hence though breakthrough curves on an absolute time scale are significantly modified due to sample lag correction, the difference is less significant on an efficiency (actual time / time for perfect operation) scale. Figure 8.4 describes the corrected and uncorrected breakthrough curves on an efficiency scale.

One may ask if such a lag time correction is required to the absorption data. Due to the large dry volumetric flow rates in absorption runs, response of the system is quite fast. Figure 8.5 is a comparison of observed and corrected breakthrough curves for the 400 psig absorption runs - which would have the largest sample lag. It can be seen that even for the worst case, the breakthrough curve is not modified significantly.

Sample lag corrections were applied to all regeneration runs. These corrections do not alter the conclusions drawn from regeneration studies significantly but would be important in selecting a model for regeneration process.

FIGURE 8.2
COMPARISON OF OBSERVED AND PREDICTED (MIXED TANK MODEL) BREAKTHROUGH CURVES FOR A STEP CHANGE IN COMPOSITION

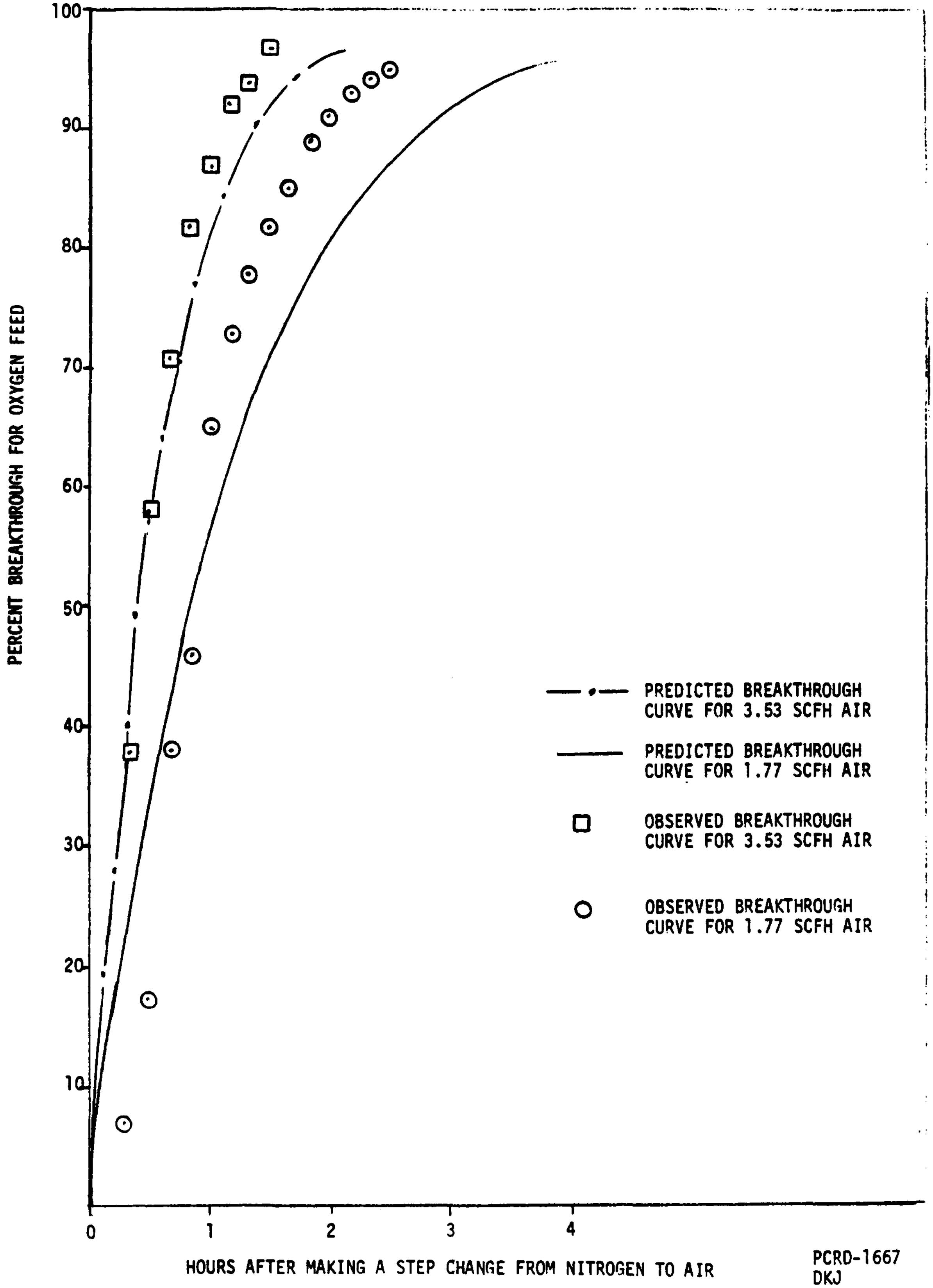

PCRD-1667
DKJ
1-11-77

FIGURE 8.3
ADDITIONAL PROOF OF THE VALIDITY OF STIRRED TANK MODEL
TO CORRECT BREAKTHROUGH CURVES FOR SAMPLE LAG
RUN 1815SG

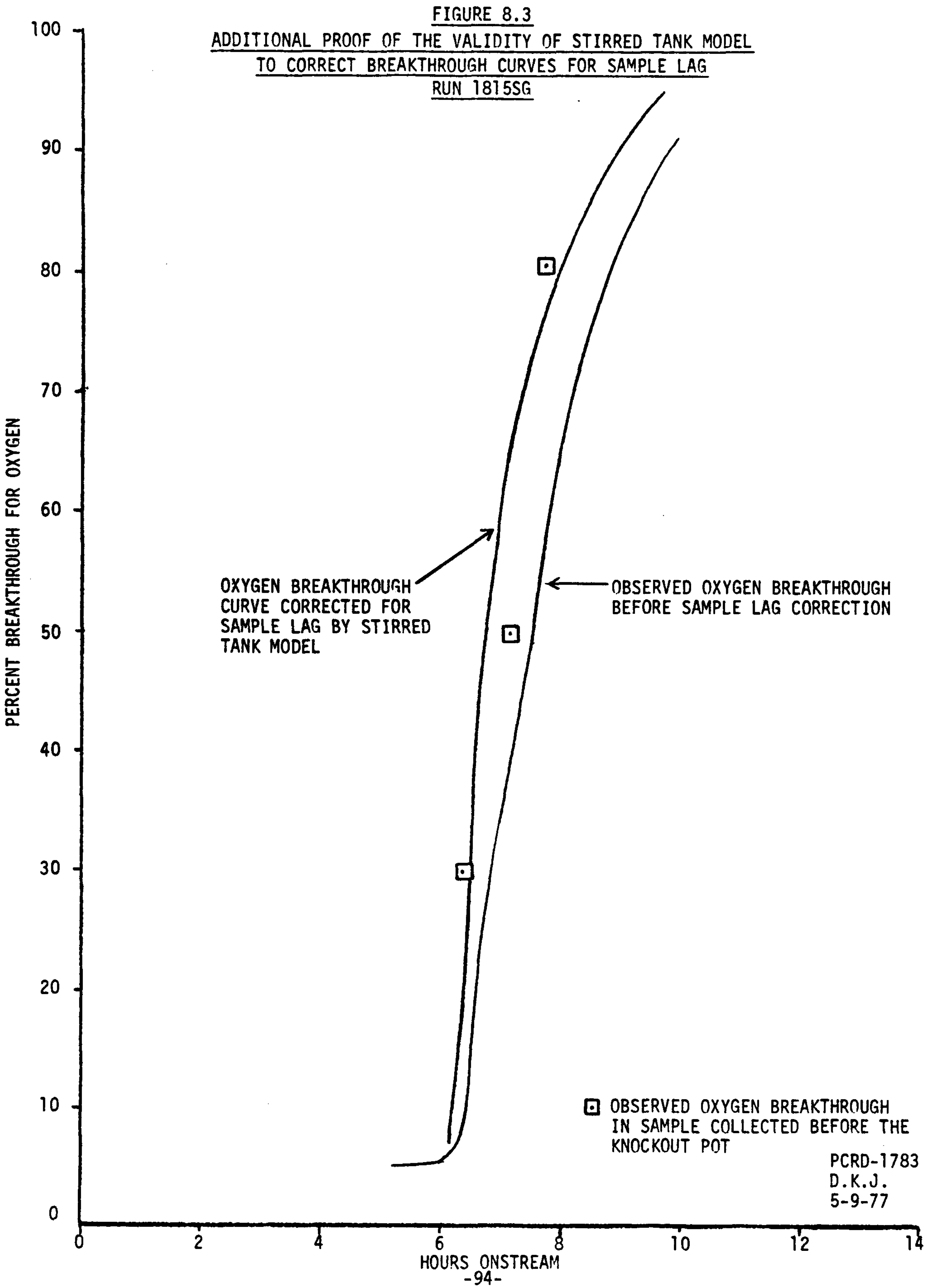

OXYGEN BREAKTHROUGH CURVE CORRECTED FOR SAMPLE LAG BY STIRRED TANK MODEL

OBSERVED OXYGEN BREAKTHROUGH BEFORE SAMPLE LAG CORRECTION

⊡ OBSERVED OXYGEN BREAKTHROUGH IN SAMPLE COLLECTED BEFORE THE KNOCKOUT POT

PCRD-1783
D.K.J.
5-9-77

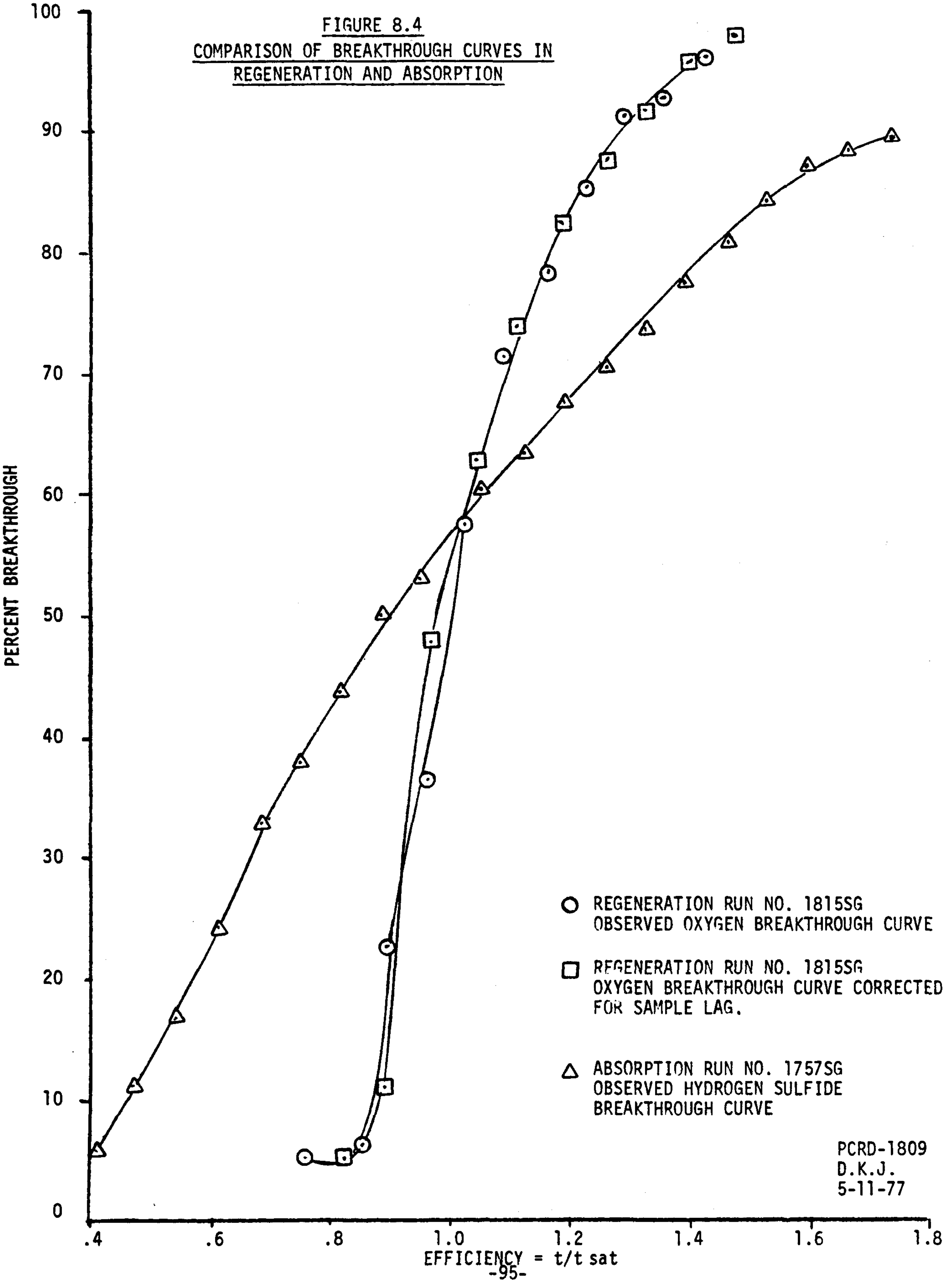
FIGURE 8.4
COMPARISON OF BREAKTHROUGH CURVES IN REGENERATION AND ABSORPTION
PERCENT BREAKTHROUGH
100
90
80
70
60
50
40
30
20
10
0
.4
.6
.8
1.0
1.2
1.4
1.6
1.8
EFFICIENCY = t/t sat
○ REGENERATION RUN NO. 1815SG OBSERVED OXYGEN BREAKTHROUGH CURVE
☐ REGENERATION RUN NO. 1815SG OXYGEN BREAKTHROUGH CURVE CORRECTED FOR SAMPLE LAG.
△ ABSORPTION RUN NO. 1757SG OBSERVED HYDROGEN SULFIDE BREAKTHROUGH CURVE
PCRD-1809
D.K.J.
5-11-77

FIGURE 8.5
COMPARISON OF OBSERVED AND CORRECTED BREAKTHROUGH
CURVE FOR 400 PSIG ABSORPTION RUN

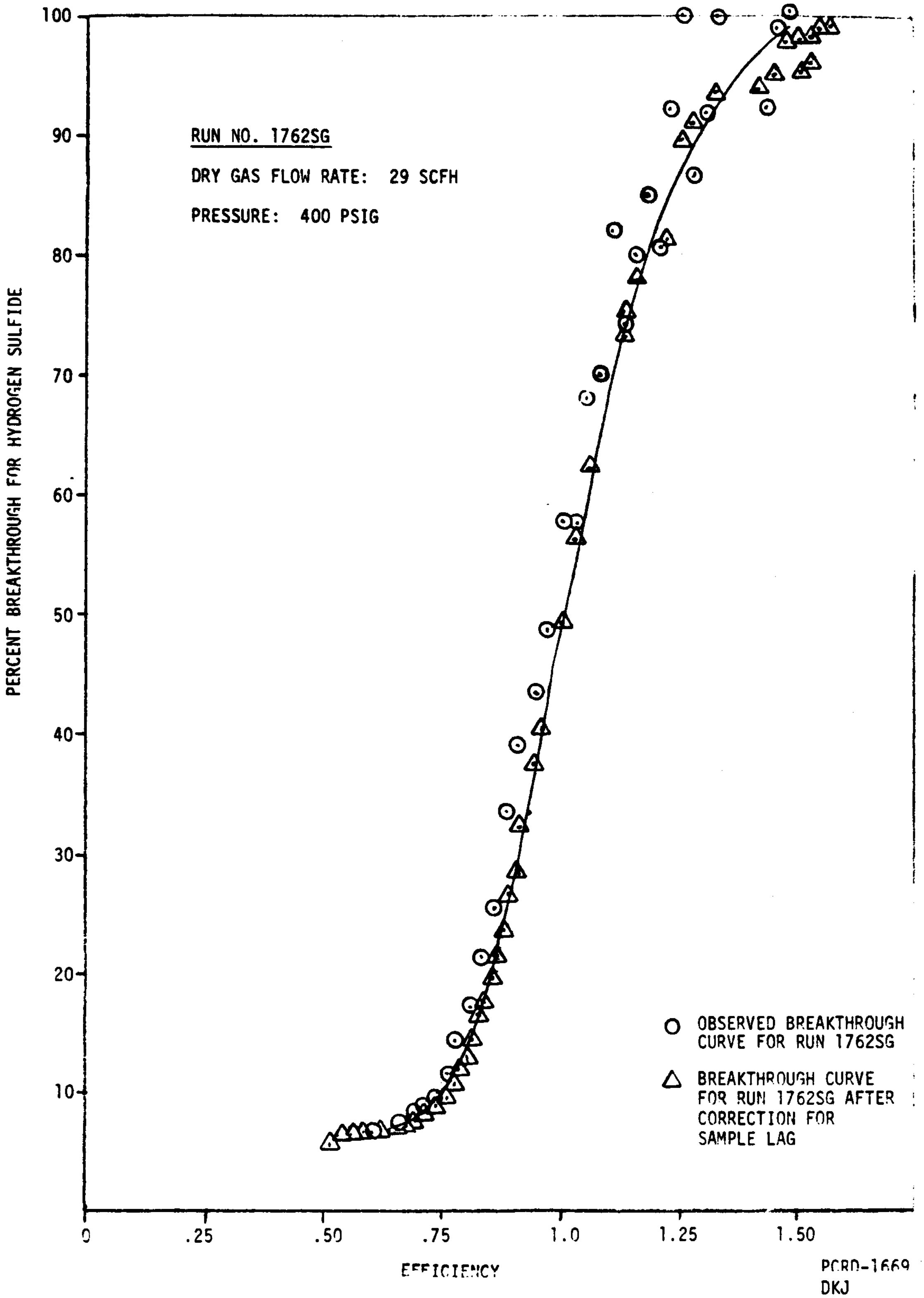

PCRD-1669
DKJ
1-11-77

This analysis could be extended further to include liquid-vapor equilibrium for SO_2-H_2O, mass transfer in the liquid and gas phase to determine SO_2 analysis on a dry basis. However, the utility of the additional information would be low due to side reactions.

8.5 Observed Temperature Exotherms

The extent of regeneration can be very well followed by the temperature profile in the bed. Each section of the bed, from inlet to outlet, goes through a maximum in temperature and returns to the base temperature. Figure 8.6 is a plot of the temperature against time at different depths in the bed. In most runs a temperature rise of 130 to 300°F was observed. This is somewhat lower than the estimated temperature rise based on the heat of reaction.

Due to the uncertainty of oxidation states of iron, several regeneration reactions are postulated:

$$FeS + \frac{3}{2} O_2 \longrightarrow FeO + SO_2 \qquad \Delta H = -75.3 \frac{\text{kcal}}{\text{gmole oxygen}}$$

$$2FeS + \frac{7}{2} O_2 \longrightarrow Fe_2O_3 + 2SO_2 \qquad \Delta H = -84.3 \frac{\text{kcal}}{\text{gmole oxygen}}$$

$$FeS_2 + \frac{5}{2} O_2 \longrightarrow FeO + 2SO_2 \qquad \Delta H = -67.15 \frac{\text{kcal}}{\text{gmole oxygen}}$$

$$2FeS_2 + \frac{11}{2} O_2 \longrightarrow Fe_2O_3 + 4SO_2 \qquad \Delta H = -73.64 \frac{\text{kcal}}{\text{gmole oxygen}}$$

Assuming the typical feed composition of 85% steam and 15% air, this results in a gas adiabatic temperature rise of 400 to 500°F. The actual temperature rise in the bed is lower in all cases. This difference could be due to one or more of the following reasons.

a. The "adiabatic temperature rise" is calculated assuming that all heat of reaction is used to raise temperature of gas. Actually part of that heat is used to raise temperature of solids.

b. Probable inaccuracy in heat of reaction. The heats of reactions are based on heats of formation at 25°C.

FIGURE 8.6

ILLUSTRATION OF THE TEMPERATURE PROFILES IN THE BED DURING REGENERATION

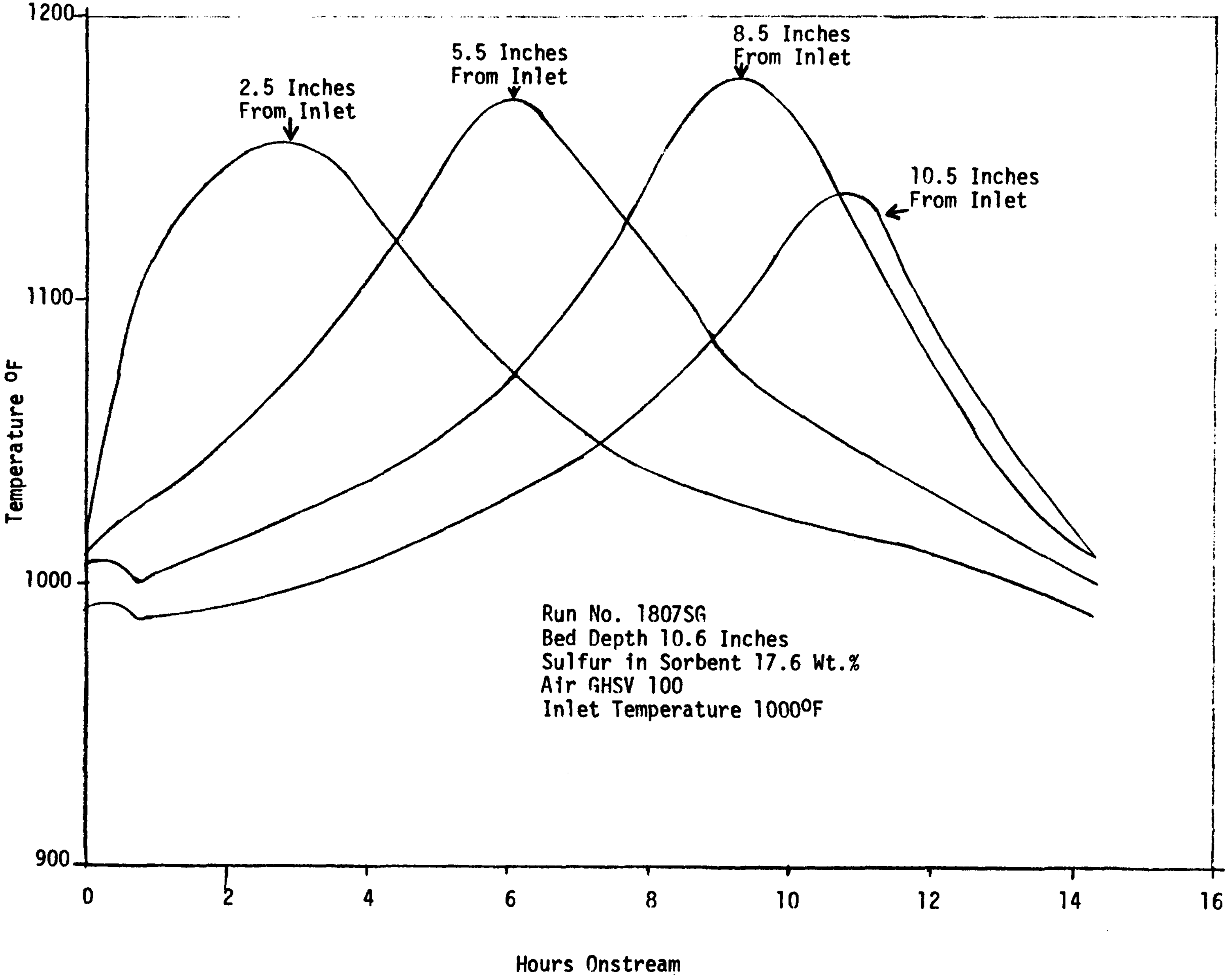

PCRD-1657
DKJ
1/6/77

c. The side reaction

$$FeS + \frac{1}{2} SO_2 \longrightarrow FeO + \frac{3}{2} S$$

may be important, and it is endothermic. It has not been considered.

d. The reactor diameter is 2" and temperatures are measured at the center of the bed. A radial temperature variation caused by heat loss at the reactor wall may exist.

Table 8.2 summarizes the magnitudes and times of occurence of the temperature exotherms observed at different depths in the bed. The complete exotherms can be obtained from the time-temperature data listed in Appendix D.

8.6 Extent of Regeneration

Eighty to ninety-five percent of the absorbed sulfur was removed by regeneration. Table 8.3 summarizes the sulfur content of fresh, sulfided and regenerated sorbents. It can be seen that regeneration is quite uniform throughout the bed. Due to the very fast regeneration reaction, inlet portion of the bed is exposed to oxygen for much longer period (by 8 to 15 hours) than the outlet portion. In spite of this, the residual sulfur content differs by less than .2% by weight.

Wet chemical test on regenerated sorbent showed that the residual sulfur might be present as sulfate or some compound other than sulfide. Possible side reactions resulting in sulfate formation are:

$$FeS + 2O_2 \longrightarrow FeSO_4$$

$$FeS_2 + 3O_2 \longrightarrow FeSO_4 + SO_2$$

$$2FeS_2 + 7O_2 \longrightarrow Fe_2(SO_4)_3 + SO_2$$

$$2FeS + 7O_2 + 2H_2O \longrightarrow 2FeSO_4 + 2H_2SO_4$$

TABLE 8.2

TEMPERATURE EXOTHERMS SEEN IN REGENERATION EXPERIMENTS

Run No.	Maximum Temperature Rise Observed ΔT Max. °F	Peak of Exotherm for Zone 1		Peak of Exotherm for Zone 2		Peak of Exotherm for Zone 3		Peak of Exotherm for Zone 4		Peak of Exotherm for Zone 5	
		Time Hours	ΔT °F	Time Hours	ΔT °F	Time Hours	ΔT °F	Time Hours	ΔT °F	Time Hours	ΔT °F
1805SG	166	.3	125	1.3	156	3.3	155	4.6	166	5.0	72
1806SG	124	.3	43	1.0	124	2.6	117	4.3	109	4.6	36
1807SG	167	.7	36	2.0	149	6.0	160	9.3	167	10.0	165
1808SG	258	.6	82	1.0	258	2.6	242	4.0	258	4.6	205
1809SG	276	4.66	72	0.66	220	2.33	240	4.0	276	4.66	246
1810SG	306	.6	67	1.0	219	2.3	264	3.6	306	4.3	277
1811SG	207	.3	49	1.0	199	2.0	207	3.6	140	3.6	144
1814SG	380	7.0	122	3.0	290	6.5	380	9.5	365	11.5	312
1815SG	320	5.7	320	6.2	210	6.7	140	7.7	75	7.7	28
1817SG	117	.5	103	.5	117	.5	101	.5	81	1.0	68
1818SG	310	.33	310	.5	242	1.0	173	1.5	141	2.0	119

Zone 1	Inlet
Zone 2	24% depth from inlet
Zone 3	52% depth from inlet
Zone 4	80% depth from inlet
Zone 5	99% depth from inlet

TABLE 8.3

EXTENT OF REGENERATION

Run No.	1805	1806	1807	1808	1809	1810	1811	1814	1815	1817	1818
Wt.% Sulfur											
Fresh Sorbent	0.2	0.1	0.1	0.1	0.1	0.1	0.1	0.1	0.1	0.1	0.1
Sulfided Sorbent	10.6	10.1	17.6	18.8	17.7	18.9	10.6	21.9	21.9	21.9	21.9
Regenerated Sorbent											
Top of Bed (Inlet)	2.65	1.46	2.11	2.22	1.30	1.23	1.04	.96	1.38	1.98	2.73
Bottom of Bed	2.48	1.36	1.82	2.14	1.18	1.23	1.04	.96	1.30	1.88	2.80
Wt.% Iron As Total Iron (Added + Fly Ash)											
Fresh Sorbent											
Based on Sulfided Sorbent	20.3	21.9	31.8	33.7	36.3	38.2	21.1				
Based on Regenerated Sorbent	19	20.3	33.7	33.4	34.2	33.9	21.5	30.2	35.1	35.8	34.4

If iron sulfate is formed during regeneration, it will decrease the available capacity of the sorbent to remove H_2S from producer gas. The sulfate formation may or may not increase from cycle to cycle.

X-ray diffraction patterns of the regenerated sorbent did not show any significant sulfate.

8.7 Elemental Sulfur and Sulfur Trioxide Formation

During regeneration a significant amount of elemental sulfur formation was observed. It caused plug-ups in the valves, condenser coils, pipes, pressure controllers, etc. These problems were greatly reduced after introducing a knock-out pot at the reactor outlet where sulfur was solidified and allowed to settle without condensing the steam.

In several experiments, the elemental sulfur content of the product stream was measured at different times during regeneration. The analytical technique used is described below. The results are summarized in Tables 8.4 to 8.8.

Hot effluent gas sample was taken at the reactor outlet and bubbled for 10 minutes at 400 cc/minute through a gas bubbler (maintained at 0^oC with an ice bath) containing a 25 ml. of a 4:1 solution of isopropanol-water. Sulfur trioxide was trapped in the isopropanol solution and elemental sulfur also precipitated in the solution. Remaining gas containing SO_2 was passed through another bubbler having a solution of sodium hydroxide and hydrogen peroxide.

Elemental sulfur precipitated in the first bubbler was dissolved in carbon disulfide after sampling was completed. Carbon disulfide and isopropanol solutions are not miscible and two phases were formed; the bottom carbon disulfide layer trapping sulfur in the gas, while the isopropanol solution trapped SO_3. The two layers were separated carbon disulfide was transferred to a tared beaker and allowed to evaporate at room temperature. The residue after the carbon disulfide had been evaporated was weighed. The sulfur content of the solid was determined by oxidizing the sample in a Schoniger flask and then precipitating the sulfate with $BaCl_2$. The solid residue was found to be 98-100% sulfur.

Only SO_3 is soluble in the cold isopropanol solution and interference by SO_2 is avoided. The isopropanol-water solution was titrated with .0025 M barium perchlorate in four-to-one isopropanol-water using a Thorin indicator end point. Sulfur dioxide was trapped in the sodium hydroxide-hydrogen perioxide solution, and its concentration was determined by back-titration of the base with sulfuric acid to the methyl red end point.

TABLE 8.4

ANALYSIS OF ELEMENTAL SULFUR AND SULFUR TRIOXIDE OF REACTOR OUTLET

RUN 1810SG

	Mole Pct. Elemental S on Wet Gas Basis	PPM SO_3 on Wet Gas Basis
Beginning of Regeneration	0.6	82
Beginning of Breakthrough	0.31	42
End of Breakthrough	0.03	275
End of Regeneration	0.02	36

(1) Calculated mole percent SO_2 in wet gas is 1.8% assuming that all oxygen reacts as

$$2FeS + \frac{7}{2} O_2 \longrightarrow Fe_2O_3 + 2SO_2$$

and there are no side reactions.

TABLE 8.5
RUN NO. 1815SG (1300 WET GHSV)
WET CHEMICAL ANALYSIS FOR ELEMENTAL SULFUR, SULFUR DIOXIDE AND SULFUR TRIOXIDE (ON WET GAS BASIS)

	Results Based on Collected Water Volume			Results Based on Measured Dry Gas Flow		
Hours Onstream	Elemental Sulfur Mole %	Sulfur Dioxide Mole %	Sulfur Trioxide Mole %	Elemental Sulfur Mole %	Sulfur Dioxide Mole %	Sulfur Trioxide Mole %
.5	0.344	1.31	0.0100	0.249	0.95	0.0073
1.25	0.273	1.24	0.0224	0.386	1.76	0.0317
3.0	0.395	1.17	0.0137	0.369	1.09	0.0127
3.75	0.264	1.05	0.0100	0.253	1.01	0.0096
4.4	0.278	1.06	0.0074	0.250	0.96	0.0067
5.25	0.190	1.69	0.0028	0.136	1.21	0.0020
5.83	0.094	1.50	0.0021	0.078	1.25	0.0017
6.40	0.138	0.69	0.0023	0.060	0.30	0.0010
7.25	0.089	0.40	0.0038	0.036	0.17	0.0016
7.75	0.114	0.17	0.0157	0.031	0.05	0.0043
9.25	0.050	0.07	0.0115	0.030	0.04	0.0070
10.25	0.075	0.16	0.0090	0.011	0.02	0.0013

TABLE 8.6
RUN NO. 1817SG (6500 WET GHSV)
WET CHEMICAL ANALYSIS FOR ELEMENTAL SULFUR, SULFUR DIOXIDE AND SULFUR TRIOXIDE (WET GAS BASIS)

	Results Based on Collected Water Volume			Results Based on Measured Dry Gas Flow		
Hours Onstream	Elemental Sulfur Mole %	Sulfur Dioxide Mole %	Sulfur Trioxide Mole %	Elemental Sulfur Mole %	Sulfur Dioxide Mole %	Sulfur Trioxide Mole %
0	0.013	0.350	0.039	0.014	0.360	0.0408
.5	0.032	0.009	0.0524	0.016	0.002	0.0251
1.0	0.023	0.227	0.0011	0.019	0.191	0.0009
1.5	0.030	0.079	0.0131	0.025	0.067	0.0111
2.0	0.019	0.022	0.0032	0.022	0.024	0.0036
2.5	0.013	0.011	0.0015	0.015	0.012	0.0015
3.0	0.046	0.022	0.0035	0.023	0.011	0.0017
	-	-	-	-	-	-
4.0	0.018	0.009	0.0013	0.017	0.008	0.0012

TABLE 8.7
RUN NO. 1818SG (6500 WET GHSV)
WET CHEMICAL ANALYSIS FOR ELEMENTAL SULFUR, SULFUR DIOXIDE AND SULFUR TRIOXIDE (WET GAS BASIS)

	Results Based on Collected Water Volume			Results Based on Measured Dry Gas Flow		
Hours Onstream	Elemental Sulfur Mole %	Sulfur Dioxide Mole %	Sulfur Trioxide Mole %	Elemental Sulfur Mole %	Sulfur Dioxide Mole %	Sulfur Trioxide Mole %
0	0.037	1.221	0.0188	0.041	1.359	0.0210
.5	0.022	0.789	0.0114	0.030	1.122	0.0154
.75	0.038	0.575	0.0227	0.042	0.639	0.0253
1.1	0.017	0.358	0.0287	0.022	0.484	0.0389
1.4	0.037	0.249	0.0247	0.035	0.240	0.0237
1.6	0.015	0.011	0.0170	0.018	0.012	0.0196
1.8	0.023	0.090	0.0085	0.021	0.081	0.0076
2.2	0.032	0.094	0.0207	0.035	0.102	0.0224
2.6	0.014	0.230	0.0083	0.020	0.324	0.0117

TABLE 8.8*
RUN NO. 1814SG (700 WET GHSV)
WET CHEMICAL ANALYSIS FOR ELEMENTAL SULFUR, SULFUR DIOXIDE AND SULFUR TRIOXIDE (WET GAS BASIS)

Hours Onstream	Results Based on Collected Water Volume			Results Based on Measured Dry Gas Flow		
	Elemental Sulfur Mole %	Sulfur Dioxide Mole %	Sulfur Trioxide Mole %	Elemental Sulfur Mole %	Sulfur Dioxide Mole %	Sulfur Trioxide Mole %
0	0.111	0.17	0.0395	0.076	0.12	0.0268
1	0.238	0.69	0.0128	0.052	0.15	0.0028
2	0.167	0.57	0.0069	0.039	0.13	0.0015
2.5	0.121	0.46	0.0169	0.059	0.23	0.0082
3	0.257	0.70	0.0193	0.146	0.40	0.0110
3.5	0.190	0.53	0.0099	0.056	0.16	0.0029
4.0	0.156	0.41	0.0089	0.049	0.13	0.0028
4.5	0.158	0.54	0.0174	0.047	0.16	0.0052
5.0	0.299	0.75	0.0094	0.099	0.25	0.0031
5.5	0.184	0.52	0.0092	0.075	0.22	0.0038
6.0	0.406	0.44	0.0080	0.537	0.58	0.0105
6.5	0.335	0.62	0.0043	0.075	0.14	0.0010
7.0	0.530	1.45	0.0087	0.078	0.21	0.0013
7.5	0.264	0.47	0.0080	0.083	0.15	0.0025
	-	-	-	-	-	-
9.5	0.452	0.78	0.0107	0.129	0.22	0.0030
10.0	0.180	0.87	0.0077	0.111	0.54	0.0048
10.5	0.388	1.08	0.0106	0.319	0.89	0.0087
11.0	0.240	1.60	0.0097	0.058	0.38	0.0023
12.0	0.061	1.24	0.0068	0.022	0.45	0.0024
12.5	0.023	0.47	0.0358	0.017	0.36	0.0269
13.0	0.027	0.26	0.0688	0.019	0.18	0.0479
14.0	0.029	0.13	0.0101	0.014	0.06	0.0049
				0.006	0.03	0.0010
15.0	0.037	0.18	0.0057	0.074	0.05	0.0533
15.5	0.176	0.12	0.1271	0.028	0.04	0.0572
16.5	0.066	0.10	0.1364	0.015	0.03	0.0171
17.0	0.090	0.16	0.1047	0.019	0.05	0.0189
17.5	0.083	0.21	0.0788	0.017	0.04	0.0095
19.0	0.063	0.15	0.0349	-	-	-
	-	-	-			

*Note that there is a discrepancy in the absolute concentrations estimated by the two methods. In this experiment, the heating circuit on the sampling line was not in service. Due to steam condensation in the sampling line, there were wild fluctuations in the sample flow rate. Wet chemical analysis on this run is not reliable and it is given here only for comparison.

There are two possible sources of error in analyses obtained, (a) condensation of elemental sulfur on the pipe surface, and (b) condensation of steam on pipe surface. The gas flow rate was measured on a dry basis after the last flask on the analytical train, and analysis were corrected for wet basis. If elemental sulfur condensed on pipe surfaces (which was kept hot by putting heating circuits over it), the observed elemental sulfur would be lower than actually present. If water condensed, it may cause an error on absolute basis. Hence the S, SO_2, SO_3 analyses were calculated both by measuring dry gas volume and by measuring the volume of water condensed in the cold flask. The agreement between the numbers calculated from both bases was quite good in Run Nos. 1815SG, 1817SG, 1818SG but was poor in Run 1814SG in which the sample valve was cooler than the other three runs.

It should be pointed out that according to the scope of regeneration studies as originally planned and mutually agreed upon, it was not planned to monitor elemental sulfur and SO_3. However, as the experimental work progressed, a great deal of elemental sulfur was observed. Realizing the significant impact it could have on process economics, it was decided to develop analytical techniques to obtain some quantitative information about the sulfur formation.

In the initial period of regeneration elemental sulfur formation was nearly one-third of the anticipated SO_2 formation. Probable reactions are:

$$FeS + \frac{1}{2} SO_2 \longrightarrow FeO + \frac{3}{2} S$$

$$FeS + \frac{1}{2} O_2 \longrightarrow FeO + S$$

$$SO_2 + C \longrightarrow CO_2 + S$$

Experimental observation of high sulfur formation during the initial period of regeneration can be explained by the first reaction. During the initial period of regeneration, residence time of SO_2 in a bed of FeS in longest, increasing the probability for elemental S formation. Preliminary thermodynamics indicate that this reaction may be thermodynamically unfavorable. Since the concentration of oxygen at the reaction zone remains quite constant during the entire regeneration period, the second reaction would predict a uniform, elemental sulfur formation during the entire regeneration. This is not actually the case. The third reaction assumes that sulfur dioxide reacts with carbon deposited on the sorbent to make elemental sulfur and CO_2. This reaction can also explain the observed high elemental sulfur formation in the initial period of regeneration. The regeneration effluents were not analyzed for carbon dioxide. However sulfided sorbent was analyzed for carbon and it contained .7 wt.% carbon while the fresh sorbent contained .5 wt.% carbon. The analyzed carbon may have come from carbonates in fly ash or impure iron oxide or methacel cellulosic additive added to the sorbent as an extrusion aid.

Elemental sulfur formation was observed on sorbents sulfided in the reducing atmosphere of absorption runs as well as sorbents sulfided in the inert atmosphere of heat treater. Hence this phenomenon does not seem to depend on sorbent history.

Since elemental sulfur recovery would improve economics and pollution control from regeneration products this aspect should be studied in further detail. Such studies were beyond the scope of this contract.

Another possible mechanism for sulfur formation involves:

$$FeS + H_2O \longrightarrow FeO + H_2S$$

$$FeS + \frac{3}{2} O_2 \longrightarrow FeO + SO_2$$

$$2H_2S + SO_2 \longrightarrow 2H_2O + 3S$$

Figure 8.7 describes the S, SO_2 and SO_3 concentrations in the wet effluent gas for Run 1815SG at different times during regeneration. It can be seen that in the initial half period of regeneration elemental sulfur formation was very high - as much as 20 to 30% of total sulfur in effluents (SO_2 + SO_3 + S). The amount of elemental sulfur formed decreases significantly at the later stage of regeneration. Amount of sulfur trioxide formed remains nearly constant throughout regeneration and is a very small portion of the total sulfur in effluents.

Figure 8.8 is a plot of S, SO_2 and SO_3 concentrations in the wet effluent gas for Run 1818SG which was a very high GHSV run (6500 on wet basis). The results indicate that elemental sulfur formation was much lower (less than 5% of total sulfur in effluents). In spite of the high oxygen available, sulfur trioxide was fairly low.

FIGURE 8.7

BREAKTHROUGH CURVE FOR ELEMENTAL SULFUR, SULFUR TRIOXIDE AND SULFUR DIOXIDE
RUN 1815SG (1300 GHSV BASED ON WET GAS AT STP)

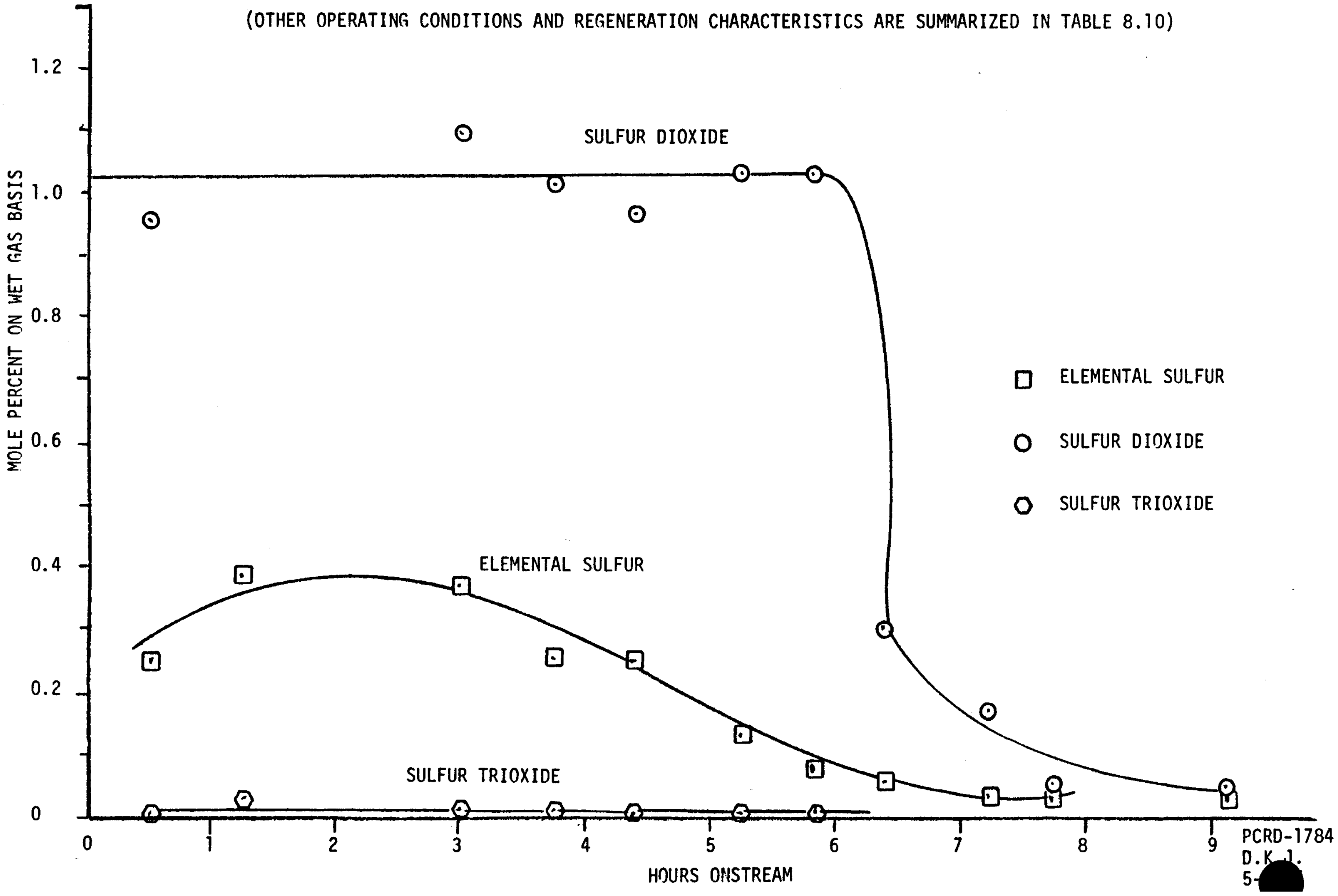

(OTHER OPERATING CONDITIONS AND REGENERATION CHARACTERISTICS ARE SUMMARIZED IN TABLE 8.10)

FIGURE 8.8

BREAKTHROUGH CURVE FOR ELEMENTAL SULFUR, SULFUR TRIOXIDE AND SULFUR DIOXIDE: RUN 1818SG (6500 GHSV BASED ON WET GAS AT STP)

(OTHER OPERATING CONDITIONS AND REGENERATION CHARACTERISTICS ARE SUMMARIZED IN TABLE 8.10)

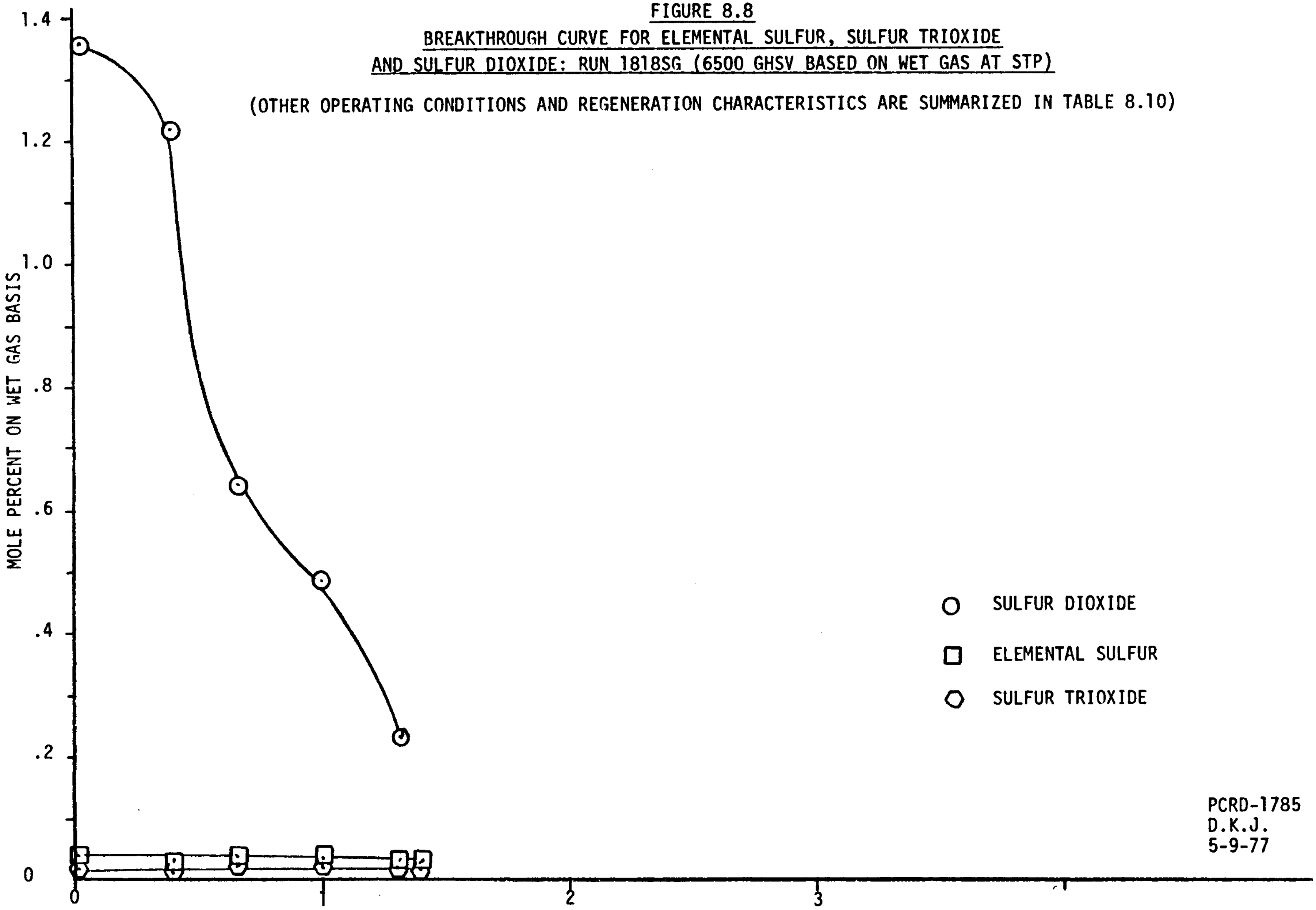

PCRD-1785
D.K.J.
5-9-77

A comparison of Figures 8.7 and 8.8 shows that elemental sulfur formation as a by-product of air-steam regeneration can be maximized by operating at low space rate; but it would require longer downtime for regeneration due to lower air rate.

8.8 Carbon Deposition on Sorbent

The synthetic producer gas used in absorption studies did not contain any tar or particulates reducing the probability of coke formation. Even with clean gas, carbon may be deposited from the following reactions:

$$2\,CO \longrightarrow C + CO_2$$

Another possibility is carbon deposition from methane. The producer gas contains steam and the deposited carbon is immediately removed by water gas reaction:

$$C + H_2O \longrightarrow CO + H_2$$

In one absorption experiment (Run 1751SG), steam was excluded from the producer gas; at the end of the absorption run the inlet portion of the bed which was exposed to highest CO-CH_4 concentration visually appeared to be loaded with carbon while the outlet portion was clean. Analysis indicated that inlet portion contained 11.70 wt.% carbon while the outlet portion of bed contained .29 wt.% carbon. The water gas reaction probably did not take place as steam was absent and carbon depssited on sorbent stayed there. Carbon analysis was done by using a Leco carbon analyzer where a ground sample was combusted in an induction coil (2000°C) the gases were scrubbed using manganese dioxide to remove SO_2, etc. and CO_2 formed was measured in a burette.

The fresh, sulfided and regenerated sorbent from the same batch were analyzed for wt.% carbon. The results are summarized below. The fresh sorbent also contained small amounts of carbon, possibly from CO_2 evolved from carbonates in fly ash or commercial iron oxide or an organic component added to improve extrusion characteristics. There is a small increase in carbon content when the fresh sorbent is sulfided, and the regenerated sorbent has the lowest carbon content of all. The observed trend is explained by assuming coke deposition from CO in producer gas. If CO_2 was evolved from carbonates all samples would show about the same as carbon content. It is necessary to state that in this case wt.% C is very small compared to wt.% S in sulfided sorbent (17% by weight) and the heat effects are not modified significantly by carbon deposition.

Sorbent	Wt.% C
Fresh (814X1-1X7)	0.51
Sulfided (Run 1757SG)	0.70
Regenerated (Run 1807SG)	0.11

It is possible that the high carbon content of fresh sulfided absorbent is what makes possible the recovery of some of the elemental sulfur on regeneration.

It seems that with clean, synthetic producer gas, coking is significant in the absence of steam and insignificant in the presence of steam. In reality, the producer gas will probably contain tar and particulates and in that case we believe that coking will be a serious problem. Carbon deposition is likely to affect adversely full utilization of sorption capacity and modify significantly the regeneration temperatures. due to its high exothermic combustion in commercial operation.

8.9 Incomplete Recovery of Air

In some regeneration experiments, oxygen to nitrogen ratio in the effluents at the end of regeneration did not level out as that in the feed, but to a somewhat lower value (about 70% of the feed) even after a prolonged period. Analysis of the sorbent for sulfur content indicated that regeneration was over. This phenomenon was observed for different sorbents, exposed to different conditions of absorption and regenerations. Air sample injected at the reactor outlet also did not stabilize at the expected value. Hence, it was suspected that some oxygen may be absorbed by some material in the lines. Hence, the entire system after reactor outlet was steamed and plugged valves, controller orifices were cleaned. Then sample lag experiments were carried out by injecting air samples at the reactor outlet. In these experiments oxygen to nitrogen ratio leveled out to that in air. So it is postulated that some oxygen was absorbed by some material in the lines and that material was removed by steaming. The breakthrough curves in all these experiments were very steep.

Regeneration experiments in which this phenomenon was observed are, Run 1809SG, 1810SG, 1811SG. While analyzing the data collected in these experiments, the final oxygen in the effluent was assumed to be 100% oxygen breakthrough - same as in air, and the oxygen breakthrough curve was calculated on this changed scale.

8.10 Process Variables Studies

The objective of these experiments was to study the influence of variables like iron sulfide content, GHSV, velocity, pressure, pellet diameter, oxygen concentration and temperature on the observed characteristics of air-steam regeneration. This was an experimental program in which each variable was studied at two levels. The observed effects are described below. A sample lag correction was required to the oxygen breakthrough curves. Effect of each process variable is described in terms of efficiency, regeneration extent, shapes of breakthrough curves corrected and uncorrected for sample lag. Higher efficiency of regeneration would mean shorter downtime for regeneration. Greater extent of regeneration would mean greater availability of sulfiding capacity for the next absorption cycle, resulting in longer absorption cycle.

8.10.1 Effect of Iron Sulfide Content on Regeneration Dynamics

Two runs at the same operating conditions were carried out with different sorbents, containing 10.1 and 17.6 weight % sulfur. These sulfided sorbents were obtained by sulfiding fresh sorbents containing 21% and 42% added iron oxide. Oxygen breakthrough curves - both observed and after correction for sample lag are illustrated in Figures 8.9 and 8.10. Table 8.9 describes the operating conditions and regeneration characteristics for these runs.

It must be noted that these experiments were done at 30 psig, and with sorbents containing 21% and 42% added iron oxide when fresh. In absorption studies it was seen at 20 psig reactor pressure, the efficiency at 10% oxygen breakthrough increased with an increase in added iron oxide from 8 to 42, however it decreased when iron oxide content was further increased to 63%. Whether similar relationships exist for regeneration or not is now known.

8.10.2 Effect of GHSV on Regeneration Characteristics

GHSV is a variable of significant importance in commercial design. If the efficiency of operation does not reduce at high GHSV, it would be beneficial to operate at higher GHSV. Higher GHSV means higher air rate for a given volume of sorbent. This would reduce the required downtime for regeneration. The effect of GHSV was studied with two sets of experiments.

The first set consisted of a comparison when GHSV was changed from 700 to 1300 (on wet gas basis). This variation in GHSV was achieved by changing the sorbent volume and not by changing flow rate.

FIGURE 8.9

RUN NO. 1806SG: COMPARISON OF REGENERATION DYNAMIC RESPONSE CORRECTED AND UNCORRECTED FOR SAMPLE LAG

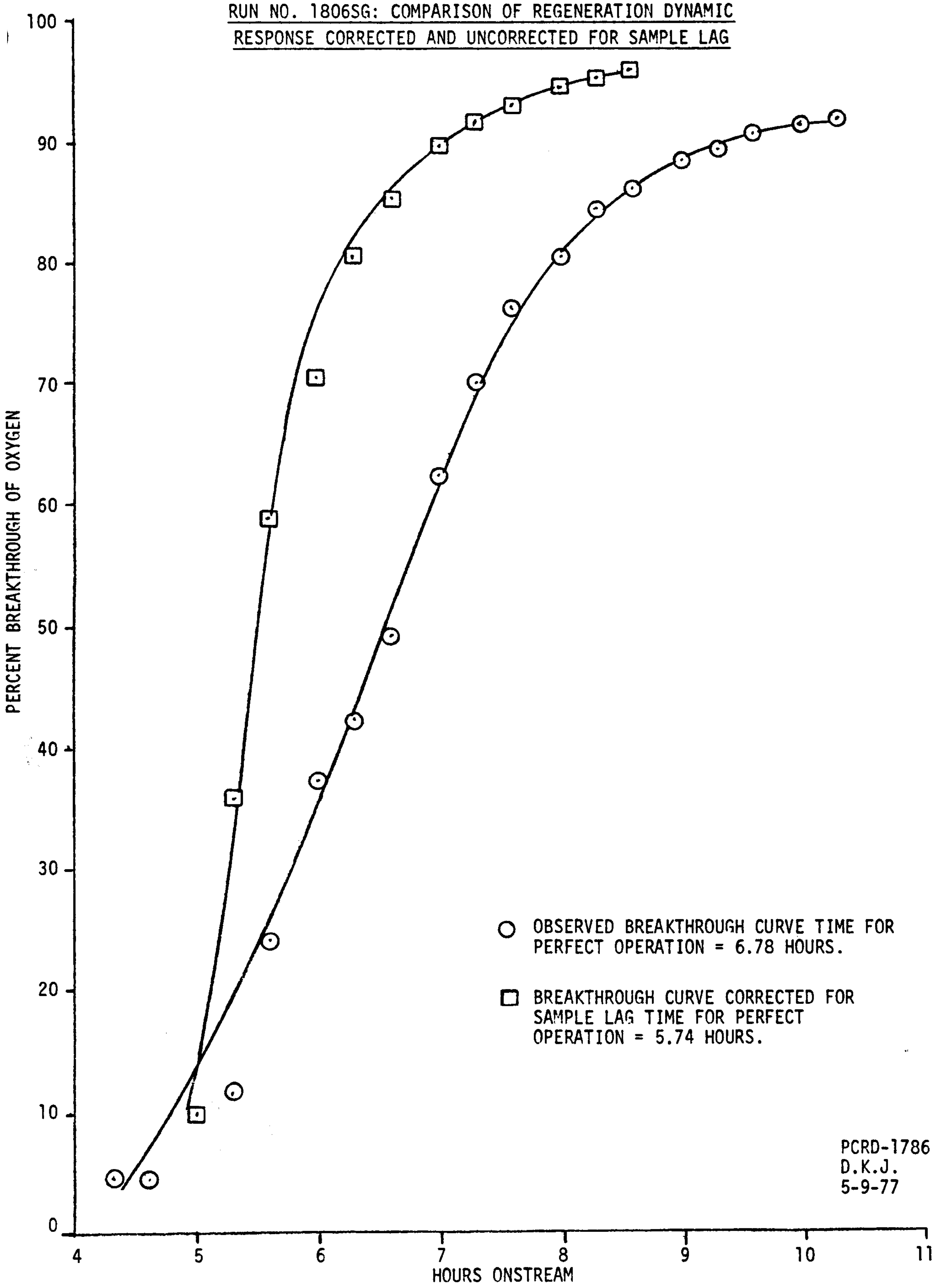

FIGURE 8.10
RUN 1807SG: COMPARISON OF REGENERATION DYNAMIC RESPONSE
CORRECTED AND UNCORRECTED FOR SAMPLE LAG

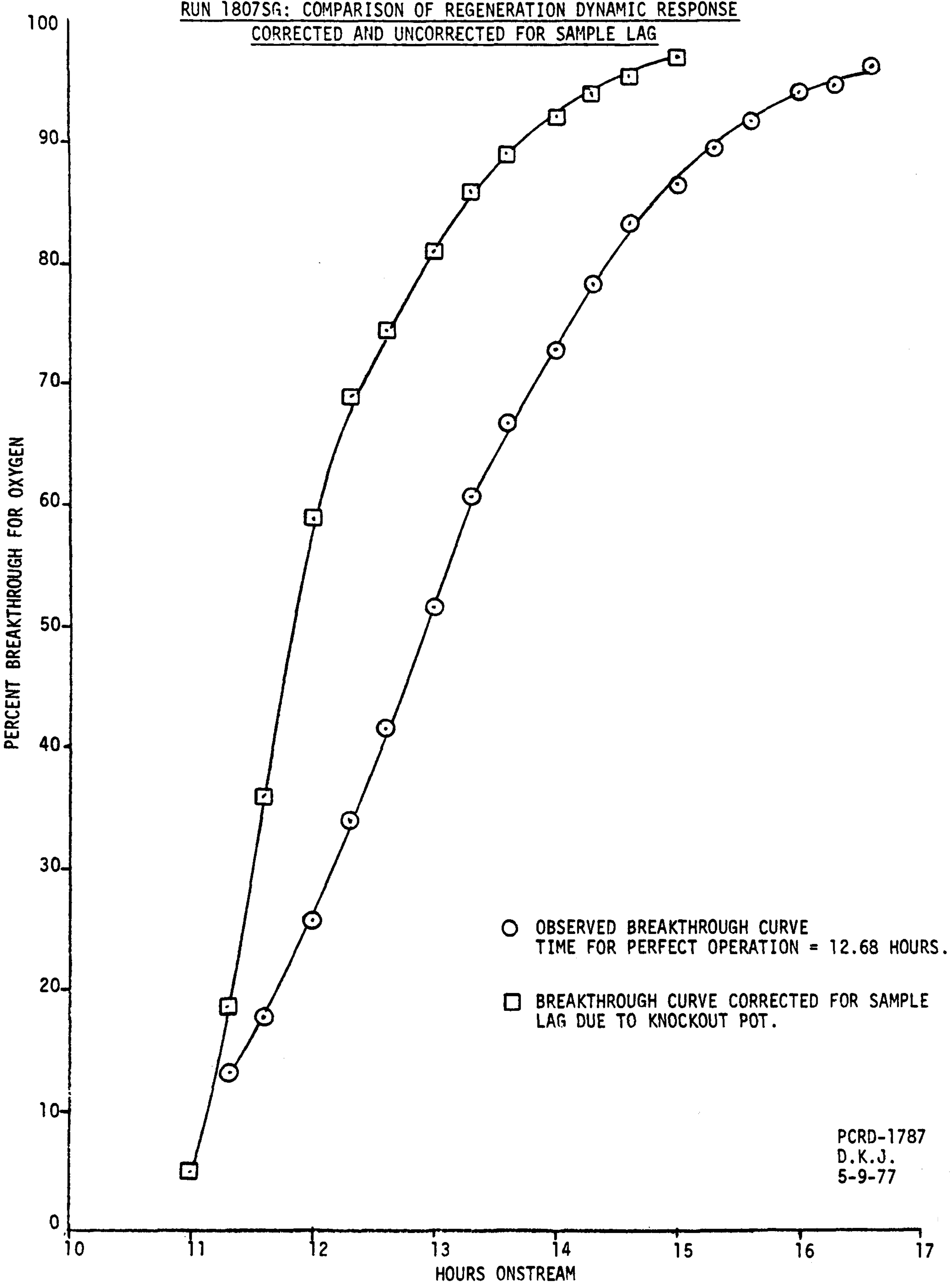

PCRD-1787
D.K.J.
5-9-77

FIGURE 8.11

EFFECT OF IRON OXIDE CONTENT ON REGENERATION DYNAMICS

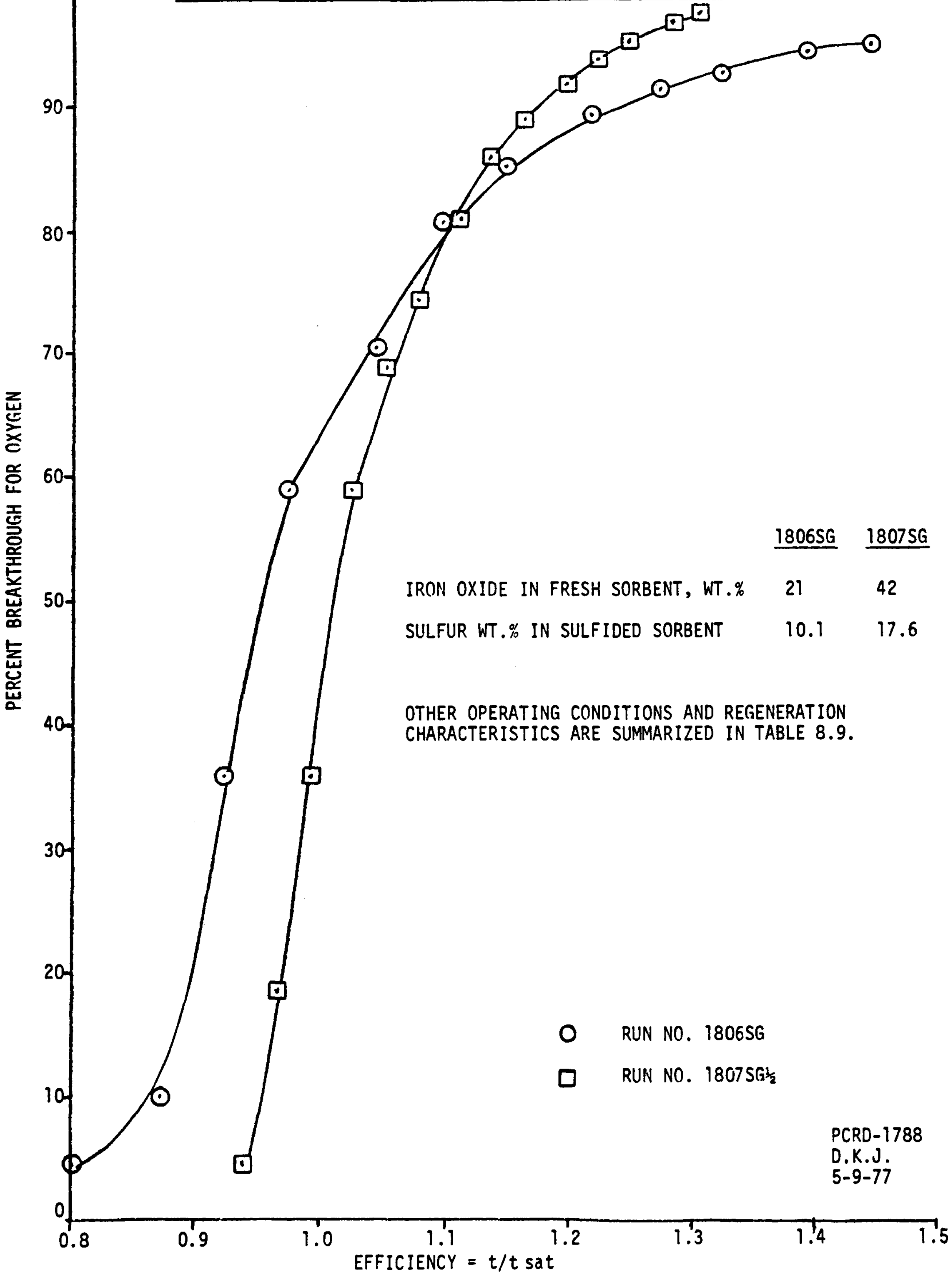

	1806SG	1807SG
IRON OXIDE IN FRESH SORBENT, WT.%	21	42
SULFUR WT.% IN SULFIDED SORBENT	10.1	17.6

OTHER OPERATING CONDITIONS AND REGENERATION CHARACTERISTICS ARE SUMMARIZED IN TABLE 8.9.

PCRD-1788
D.K.J.
5-9-77

TABLE 8.9
INFLUENCE OF IRON SULFIDE CONTENT IN SORBENT ON REGENERATION DYNAMICS

	Run No. 1806SG	Run No. 1807SG
Wt.% Sulfur in Sulfided Sorbent	10.1	17.6
Wt.% Added Iron Oxide in Fresh Sorbent	21	42
Wt.% Sulfur in Fresh Sorbent	.1	.1
GHSV (Air)	97	97
Pellet Diameter, Inches	.25	.25
Inlet Temperature, °F	1028	1011
Pressure, psig	30	30
Mole % Air in Feed	14	14
Sorbent Volume Liters	.5	.5
Velocity, Ft./Sec.	.17	.17
Regeneration Characteristics		
*Efficiency at 10% Oxygen Breakthrough	.87	.95
*Efficiency at 50% Oxygen Breakthrough	.95	1.01
Residual Sulfur Content in Regenerated Sorbent	1.4	2.0
Time for Perfect Operation, Hrs.	5.743	11.69
Observed Maximum Temperature Rise, °F	124	167
Observed Average Mole % SO_2 in Dry Gas	4.0	3.6
% Removal of Absorbed Sulfur	89.7	86.7

* Efficiencies are corrected for sample lag.

Hence, velocity at both GHSV's were the same. The operating conditions and regeneration characteristics for these runs are summarized in Table 8.10. Figures 8.12 and 8.13 describe the oxygen breakthrough curves corrected and uncorrected for sample lag in these experiments (Run 1814SG and 1815SG). Figure 8.14 is a comparison of breakthrough versus efficiency curves for the two runs. It can be seen that an increase in GHSV from 200 to 1300 decreased efficiency at 10% oxygen breakthrough from 1.0 to 0.88. The time required for perfect operation decreased from 11.69 hours to 6.9 hours.

In the other set of experiments GHSV (wet basis) was increased from 1300 to 6500 by keeping the sorbent volume fixed and increasing the flow rate. Hence, velocities in the two cases were also different. Figure 8.15 shows oxygen breakthrough curve corrected and uncorrected for sample lag for Run No. 1818SG. Figure 2.16 shows that efficiency at 10% breakthrough is very poor (.3) at this high GHSV.

Another interesting aspect is the by-product sulfur formation. It was seen that elemental sulfur formation as a by-product is high at low GHSV and decreases greatly at high GHSV. A set of wet chemical analyses were carried out to analyze the elemental sulfur content, SO_3 in the effluent streams of Run No. 1815SG through 1818SG. The results indicated that at low space rate (700 on wet gas at STP), during nearly half the regeneration period, elemental sulfur formation was about 20-30% of the total sulfur output. At high space velocity (6500 based on wet gas at STP), elemental sulfur formation was much lower - about 3 to 5% of the total sulfur output. Hence, elemental sulfur formation as a by-product of air-steam regeneration can be maximized by operating at low space rate; but it would require longer downtime for regeneration due to lower air rate. The experimental work and other analysis on elemental sulfur by-product formation is described in greater detail in Section 8.7.

8.10.3 Effect of Pressure on Regeneration Characteristics

Effect of reactor pressure on regeneration characteristics was studied for 21% iron oxide sorbent. The pressure levels were 30 psig and 150 psig. Absorption characteristics were found to be different functions of iron oxide content at different pressure levels. Whether similar relationships exist for regeneration is not known.

Table 8.11 describes the operating conditions and regeneration characteristics for the runs. Figures 8.17 and 8.10 describe the oxygen breakthrough curves for Run Nos. 1805SG and 1806SG with and without correction for the sample lag due to the knock-out pot. Figure 8.18 is a plot of percent breakthrough versus efficiency for the two runs.

TABLE 8.10

INFLUENCE OF GHSV ON REGENERATION CHARACTERISTICS

Run Number	1814SG	1815SG	1818SG
GHSV (Air)	92	182	909
Wt.% Added Iron Oxide on Fresh Sorbent	42	42	42
Wt.% Sulfur on Fresh Sorbent	.1	.1	.1
Wt.% Sulfur in Sulfided Sorbent	21.9	21.9	21.9
Pellet Diameter, Inches	.25	.25	.25
Inlet Temperature, °F	1000	1000	989
Pressure, psig	30	30	30
Mole % Air in Feed	14	14	14
Sorbent Volume, Liters	1.0	.5	.5
Linear Velocity, Ft./Sec.	.33	.33	1.7
Regeneration Characteristics			
*Efficiency at 10% Oxygen Breakthrough	1.0	.88	.30
*Efficiency at 50% Oxygen Breakthrough	1.04	.99	.68
Residual Sulfur Content in Regenerated Sorbent	.96	1.34	2.8
Time for Perfect Operation, Hrs.	12.13	6.9	1.27
Observed Maximum Temperature Rise, °F	380	320	310
Observed Average Mole % SO_2 in Dry Gas	4.9	5.6	-
% Removal of Absorbed Sulfur	95.6	94.3	87.8

* Efficiencies are corrected for sample lag.

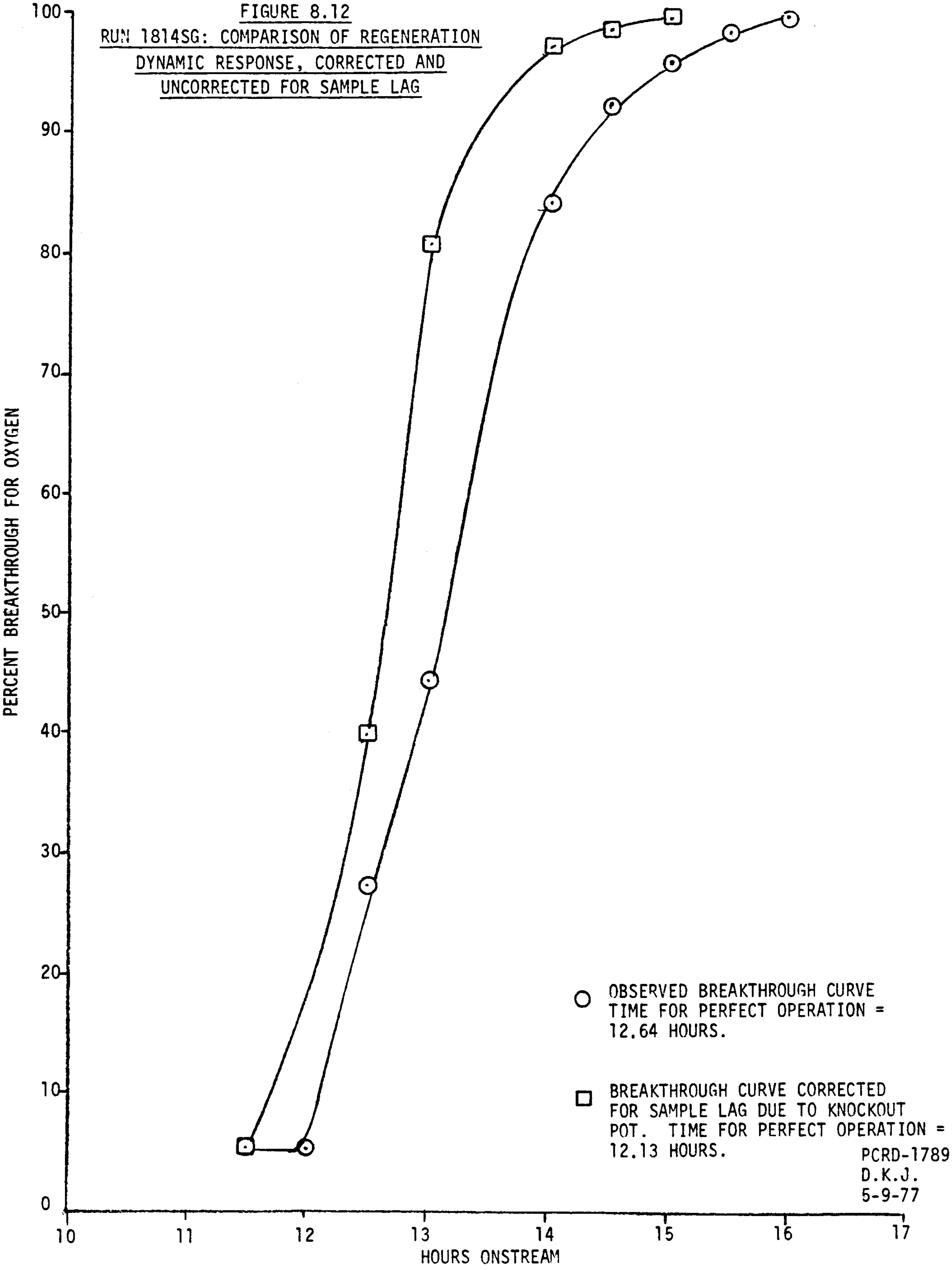

FIGURE 8.12
RUN 1814SG: COMPARISON OF REGENERATION DYNAMIC RESPONSE, CORRECTED AND UNCORRECTED FOR SAMPLE LAG

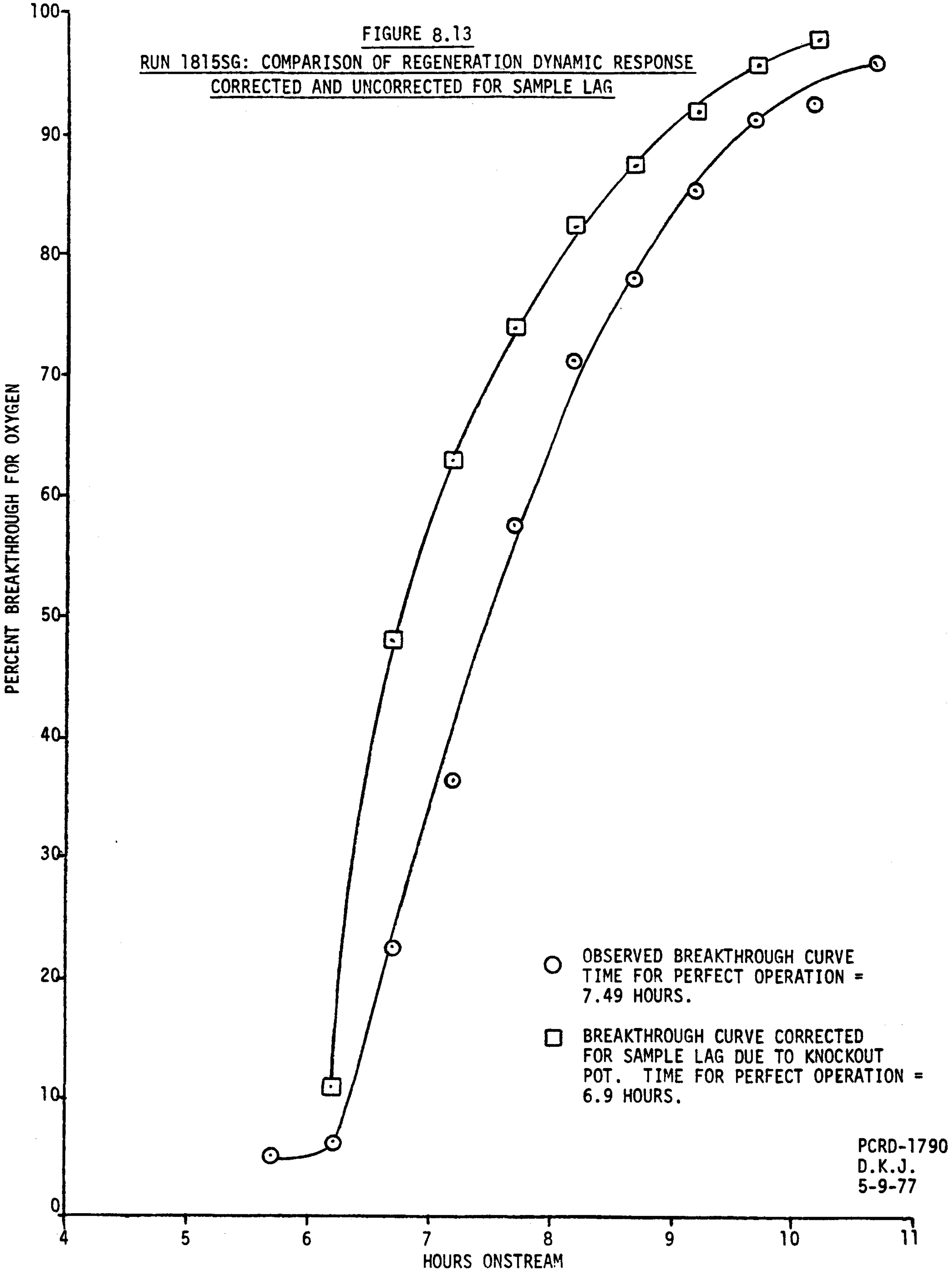

FIGURE 8.13

RUN 1815SG: COMPARISON OF REGENERATION DYNAMIC RESPONSE CORRECTED AND UNCORRECTED FOR SAMPLE LAG

PCRD-1790
D.K.J.
5-9-77

FIGURE 8.14

EFFECT OF GHSV ON REGENERATION DYNAMICS

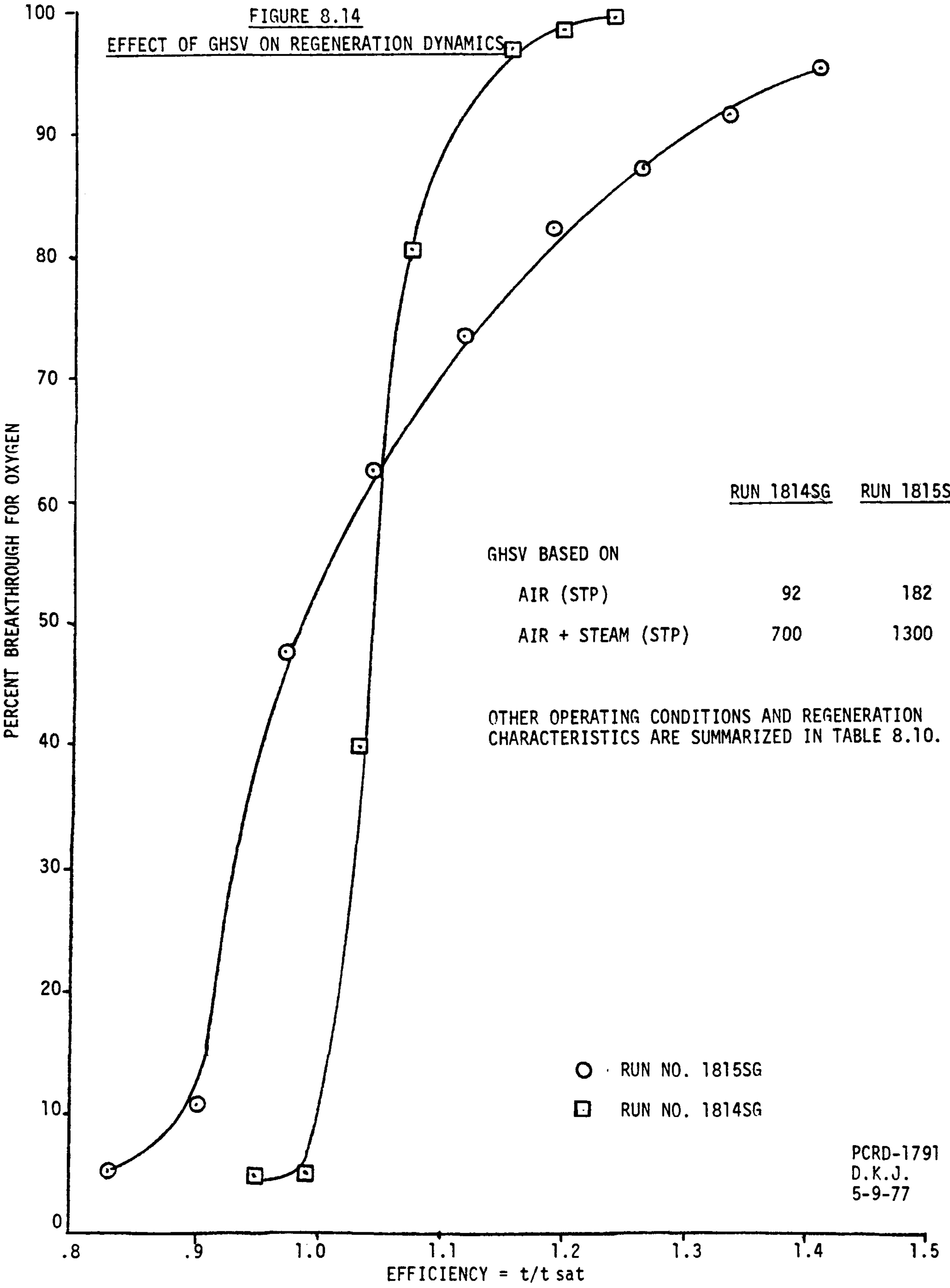

	RUN 1814SG	RUN 1815SG
GHSV BASED ON		
AIR (STP)	92	182
AIR + STEAM (STP)	700	1300

OTHER OPERATING CONDITIONS AND REGENERATION CHARACTERISTICS ARE SUMMARIZED IN TABLE 8.10.

PCRD-1791
D.K.J.
5-9-77

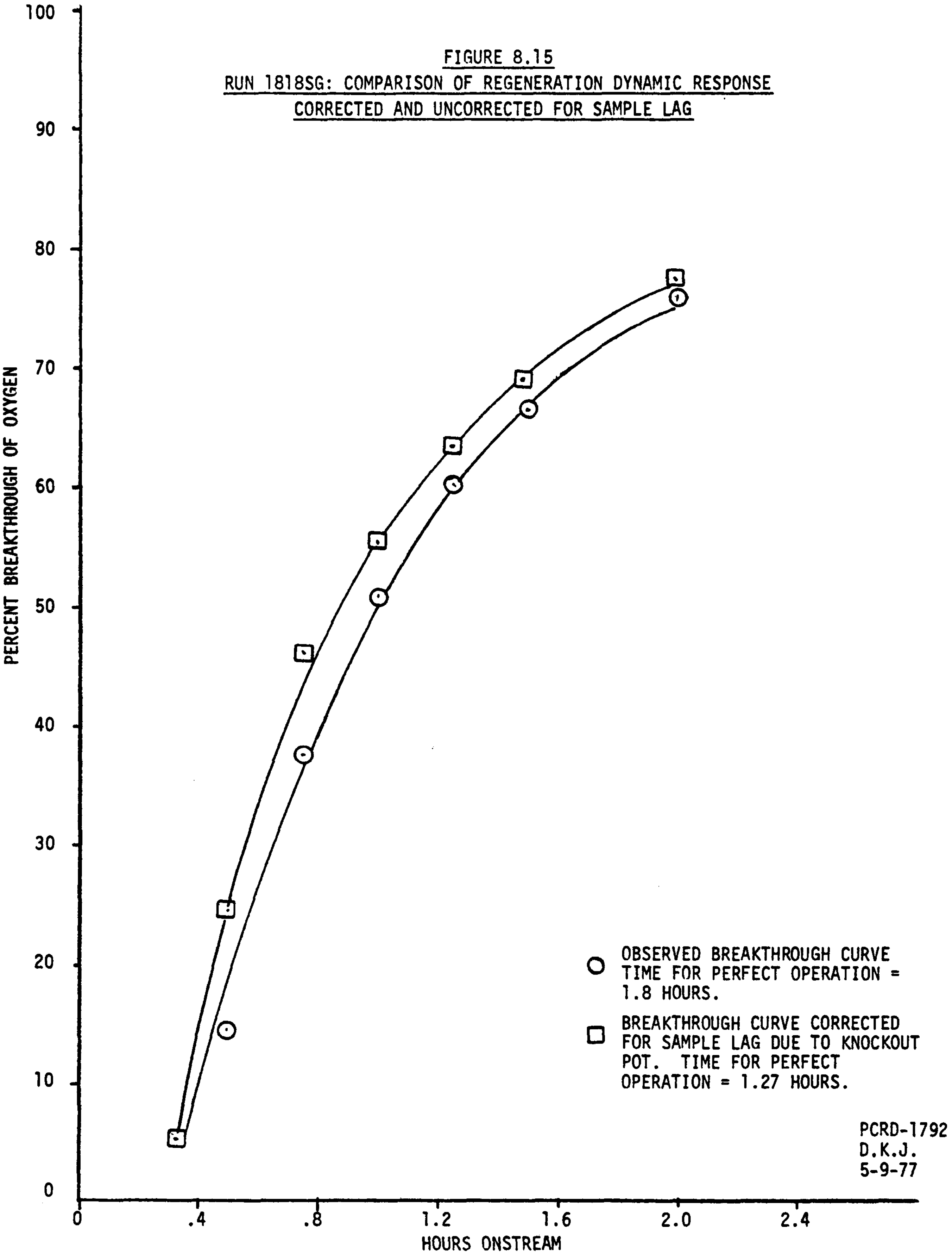

FIGURE 8.15

RUN 1818SG: COMPARISON OF REGENERATION DYNAMIC RESPONSE CORRECTED AND UNCORRECTED FOR SAMPLE LAG

PCRD-1792
D.K.J.
5-9-77

FIGURE 8.16

EFFECT OF VERY HIGH GHSV ON REGENERATION DYNAMICS

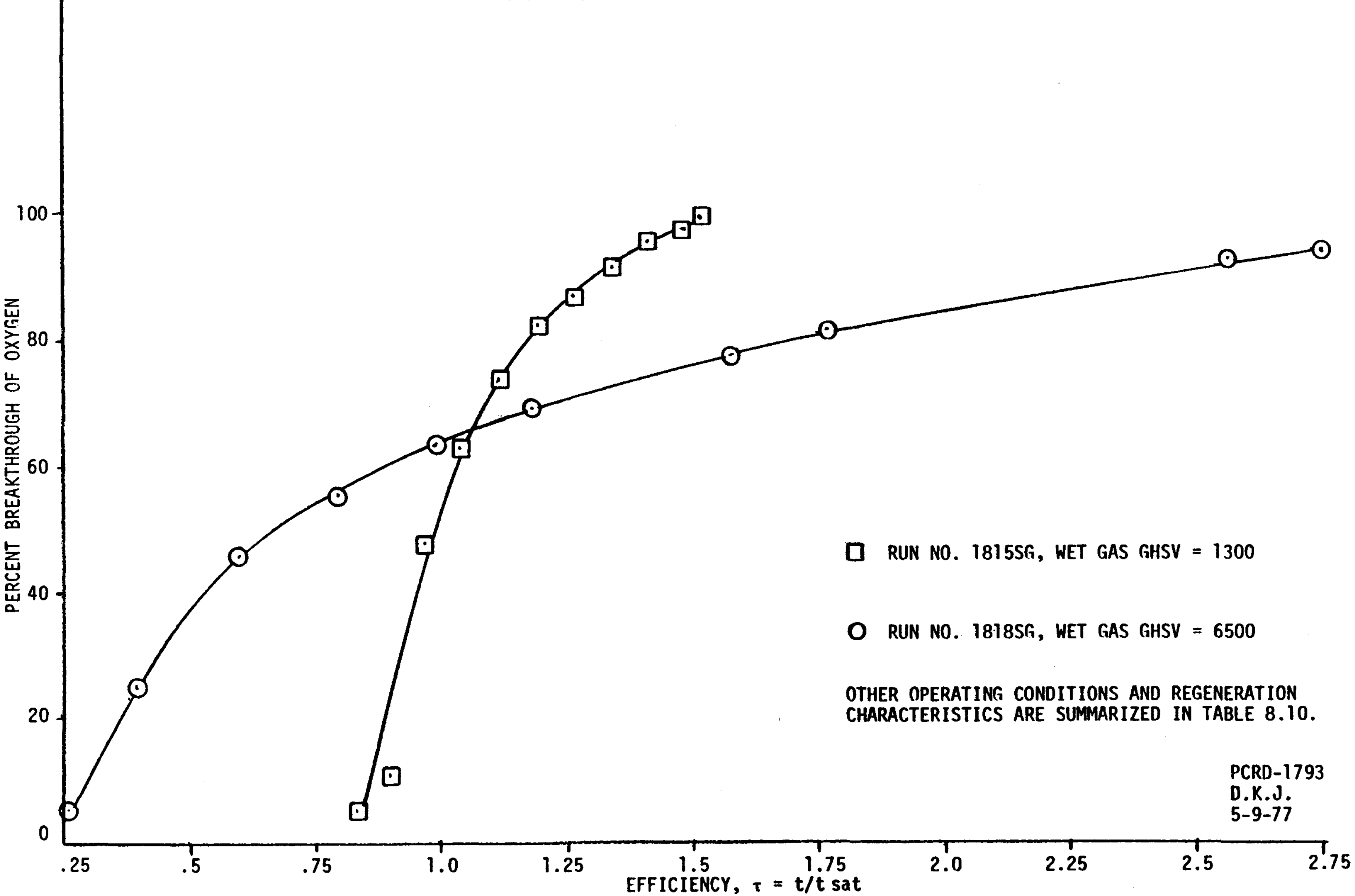

OTHER OPERATING CONDITIONS AND REGENERATION CHARACTERISTICS ARE SUMMARIZED IN TABLE 8.10.

PCRD-1793
D.K.J.
5-9-77

TABLE 8.11

EFFECT OF PRESSURE ON THE REGENERATION CHARACTERISTICS

	Run No. 1805SG	Run No. 1806SG
Pressure, psig	150	30
Wt.% Iron Oxide in Fresh Sorbent	21	21
Wt.% Sulfur in Fresh Sorbent	.1	.1
Wt.% Sulfur in Sulfided Sorbent	10.6	10.1
GHSV (Air)	97	97
Pellet Diameter, Inches	.25	.25
Inlet Temperature, ^{o}F	995	1028
Mole % Air in Feed	14	14
Sorbent Volume, Liters	.5	.5
Linear Velocity, Ft./Sec.	.05	.17
Regeneration Characteristics		
*Efficiency at 10% Oxygen Breakthrough	.89	.87
*Efficiency at 50% Oxygen Breakthrough	.905	.95
Residual Sulfur Wt.% in Regenerated Sorbent	2.6	1.4
Time for Perfect Operation, Hrs.	6.74	5.74
Observed Maximum Temperature Rise, ^{o}F	167	124
Approximate Average Mole % SO_2 in Dry Gas	-	4.0
Percent Removal of Absorbed Sulfur	76.5	89.7

* Efficiencies are corrected for sample lag.

FIGURE 8.17

RUN NO. 1805SG: COMPARISON OF REGENERATION DYNAMIC RESPONSE CORRECTED AND UNCORRECTED FOR SAMPLE LAG

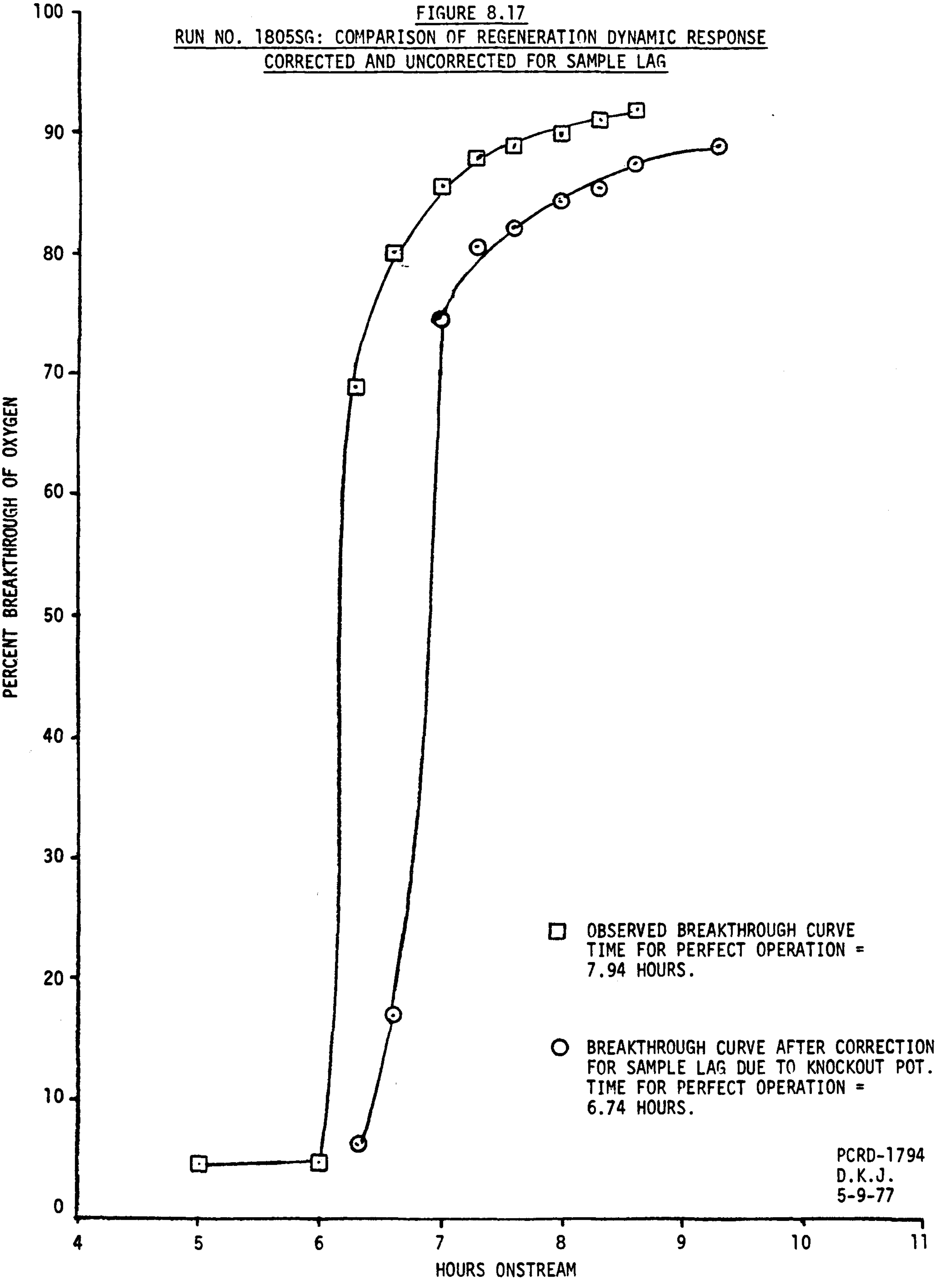

PCRD-1794
D.K.J.
5-9-77

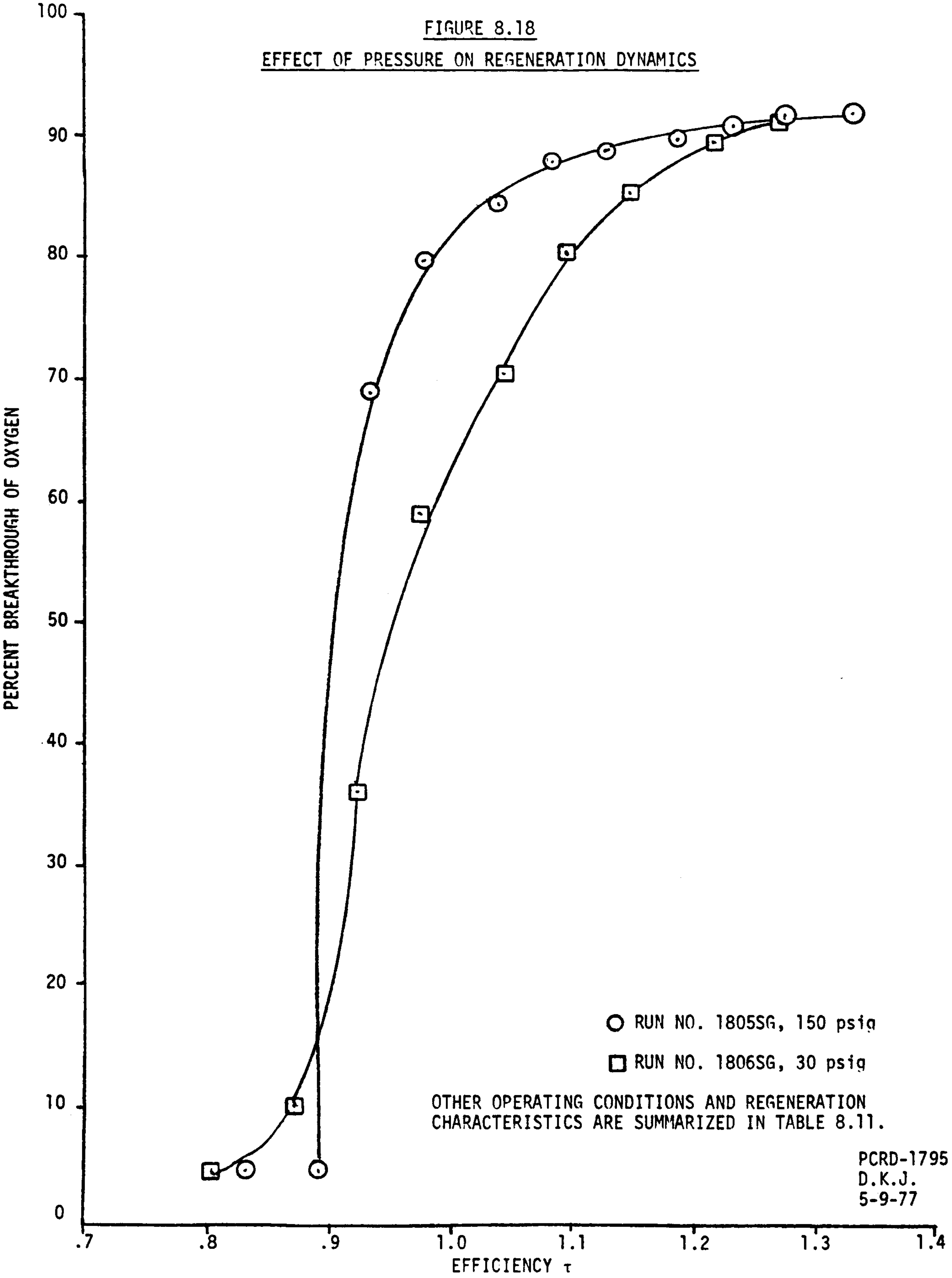

FIGURE 8.18

EFFECT OF PRESSURE ON REGENERATION DYNAMICS

OTHER OPERATING CONDITIONS AND REGENERATION CHARACTERISTICS ARE SUMMARIZED IN TABLE 8.11.

PCRD-1795
D.K.J.
5-9-77

It can be seen that increase in pressure increased the efficiency at 10% breakthrough slightly and made the breakthrough curve steeper. However, the extent of regeneration percent removal of absorbed sulfur decreased significantly.

The ratio of the residual sulfur in these as in other regeneration runs has not been conclusively established.

8.10.4 Effect of Temperature on Regeneration Dynamics

Effect of bed temperature was studied at two levels, 1000°F and 1200°F. Effect of high temperature on regeneration efficiency, regeneration extent and sorbent physical properties were the items of interest. Ideally, one would like to carry out regeneration at the temperature of maximum efficiency to the greatest extent without deterioration in physical properties.

One difficulty arose when the run at 1200°F was carried out. At the end of run, the oxygen breakthrough leveled out at 70% of that in air, instead of 100%. Analysis of the sorbent indicated that it was essentially completely regenerated and the oxygen was not being used for sulfide oxidation. Several possibilities were considered and evaluated.

1. Oxygen may be reacting with support material in the sorbent. This possibility was rejected after carrying out an experiment where air was injected at the reactor outlet. In this experiment, also, oxygen breakthrough was about 70% of that in air.

2. Oxygen may be reacting with some material deposited in pipe lines from reactor to the analytical train. It was seen that these lines were partially plugged with sulfur and corrosion products. It may be possible that some oxygen may be absorbed by these components. After these few runs were completed, the entire pilot unit was cleaned with high pressure steam. In experiments carried out after this, oxygen breakthrough curve leveled out at 100% of that in air.

3. The G.C. calibration may have been off. When air samples were injected at the G.C. it was different. When air samples were injected at the reactor outlet and analyzed at the G.C. the analysis was quite close to observed oxygen breakthrough analysis at the end of the run.

In the following analysis, the final oxygen breakthrough in Run No. 1810SG is assumed to be 100% of that in air and the analysis is done on that basis. Other experiments in which similar phenomenon were observed were Runs 1809SG and 1811SG.

Table 8.12 describes the operating conditions and regeneration characteristics of the two runs. Figures 8.19 and 8.20 are the oxygen breakthrough curves for Run Nos. 1808SG and 1810SG before and after correction for sample lag. Figure 8.21 is the comparison of percent breakthrough versus efficiency plots for the two runs.

It can be seen that an increase in inlet temperature resulted in an increase in the efficiency and steepness of the breakthrough curve. Also the percent removal of absorbed sulfur was slightly greater for the high temperature run. Hence, it is advantageous to carry out regeneration at higher inlet temperature. The disadvantage of high temperature regeneration is that the sorbent is exposed to high temperature and this may result in deterioration in sorbent physical properties. A comparison of the crushing strengths and properties of the sorbents from these two runs indicate that after undergoing one regeneration, the crushing strength of the sorbents was nearly the same for the 1000°F and 1200°F regeneration. Porosity of the sorbent was higher for the 1200°F run (Tables 8.10 and 8.16).

8.10.5 Effect of Velocity on Regeneration Dynamics

The effect of gas velocity in the bed on regeneration character was studied at constant operating conditions. Different velocities were obtained by operating at the same GHSV with two different bed volumes.

At a given GHSV, different velocities can be obtained at different bed cross-sectional areas. Hence, effect of linear velocity can be viewed as the effect of bed geometry. Figures 8.9 and 8.14 describe the uncorrected and corrected oxygen breakthrough curve for Run Nos. 1807SG and 1814SG. The operating conditions and regeneration characteristics for these runs are given in Table 8.13.

The results indicate that increasing velocity at a constant GHSV increased, in this case, the regeneration efficiency slightly (Figure 8.22). It may be possible that reactor geometry is important. However, the differences in efficiencies observed in regeneration studies are so small that they may be within scatter of data. The differences in efficiencies observed in absorption studies are much more significant and absorption should be used as the criteria for reactor geometry decisions.

TABLE 8.12
EFFECT OF INLET TEMPERATURE ON REGENERATION CHARACTERISTICS

	Run No. 1808SG	Run No. 1810SG
Wt.% Iron Oxide in Fresh Sorbent	42	42
Wt.% Sulfur in Fresh Sorbent	0.1	0.1
Wt.% Sulfur in Sulfided Sorbent	18.8	18.9
GHSV (Air)	194	194
Pellet Diameter, Inches	.25	.25
Inlet Temperature, °F	1000	1181
Pressure, psig	30	30
Mole % Air in Feed	19	19
Sorbent Volume, Liters	.5	.5
Linear Velocity, Ft./Sec.	.25	.27
Regeneration Characteristics		
*Efficiency at 10% Oxygen Breakthrough	.85	.95
*Efficiency at 50% Oxygen Breakthrough	.97	1.01
Residual Sulfur Wt.% in Regenerated Sorbent	2.2	1.2
Time for Perfect Operation, Hrs.	5.13	4.87
Observed Maximum Temperature Rise °F	258	306
Approximate Average Mole % SO_2 in Dry Gas	6.0	-
% Removal of Absorbed Sulfur	89.2	94.4

* Efficiencies are corrected for sample lag.

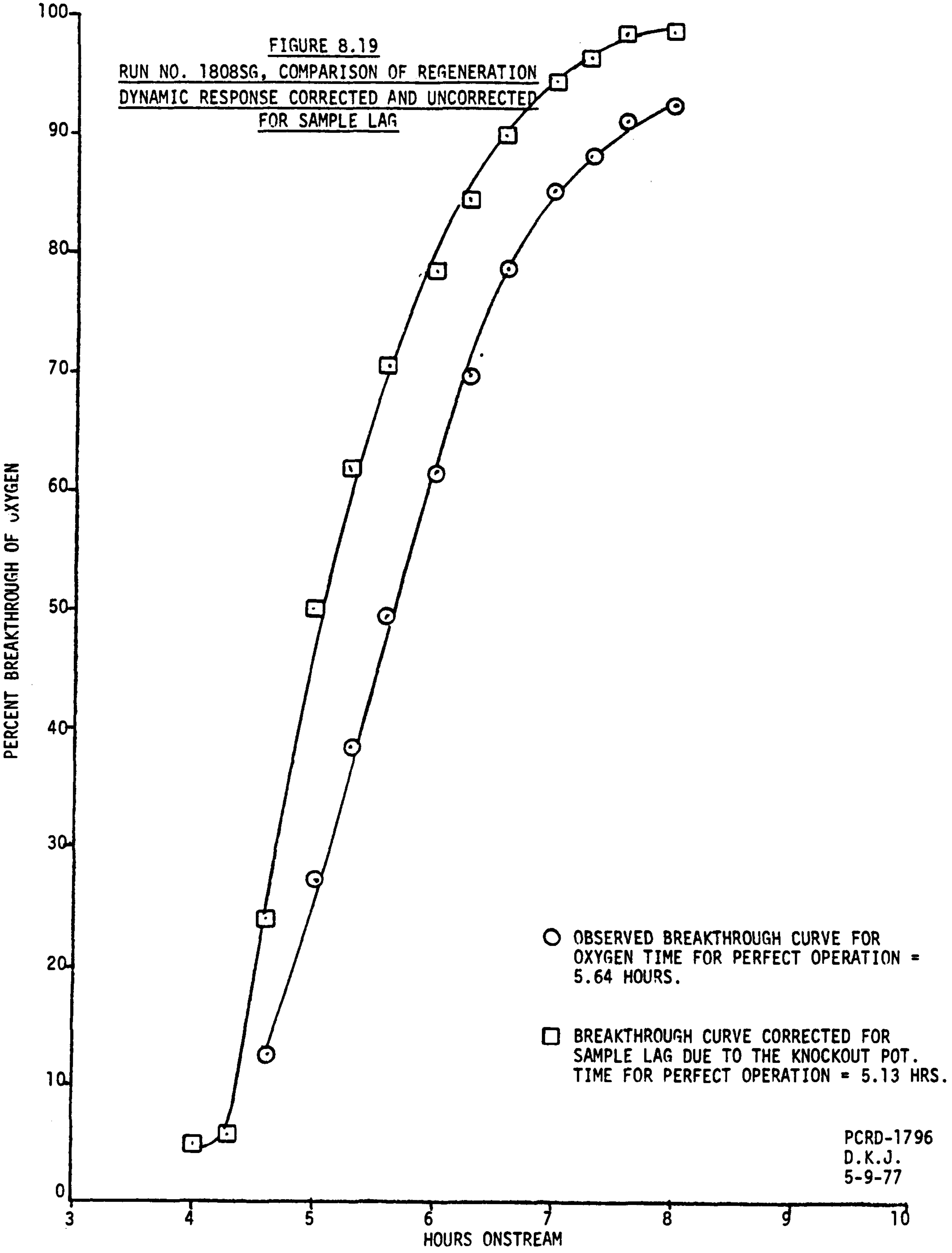

FIGURE 8.19
RUN NO. 1808SG, COMPARISON OF REGENERATION DYNAMIC RESPONSE CORRECTED AND UNCORRECTED FOR SAMPLE LAG

PCRD-1796
D.K.J.
5-9-77

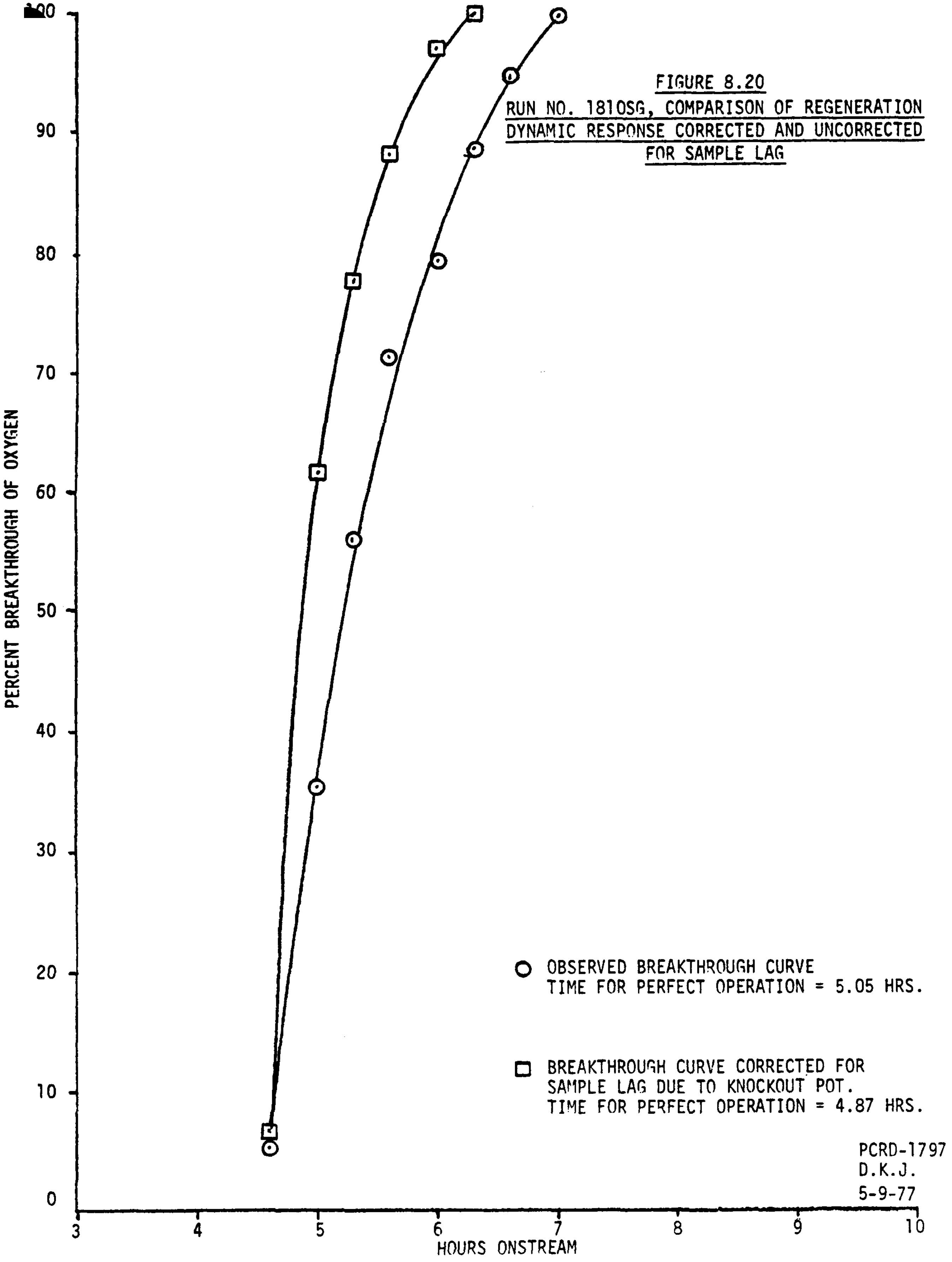

FIGURE 8.20
RUN NO. 1810SG, COMPARISON OF REGENERATION DYNAMIC RESPONSE CORRECTED AND UNCORRECTED FOR SAMPLE LAG

○ OBSERVED BREAKTHROUGH CURVE
TIME FOR PERFECT OPERATION = 5.05 HRS.

☐ BREAKTHROUGH CURVE CORRECTED FOR
SAMPLE LAG DUE TO KNOCKOUT POT.
TIME FOR PERFECT OPERATION = 4.87 HRS.

PCRD-1797
D.K.J.
5-9-77

FIGURE 8.21
EFFECT OF INLET TEMPERATURE ON REGENERATION DYNAMICS

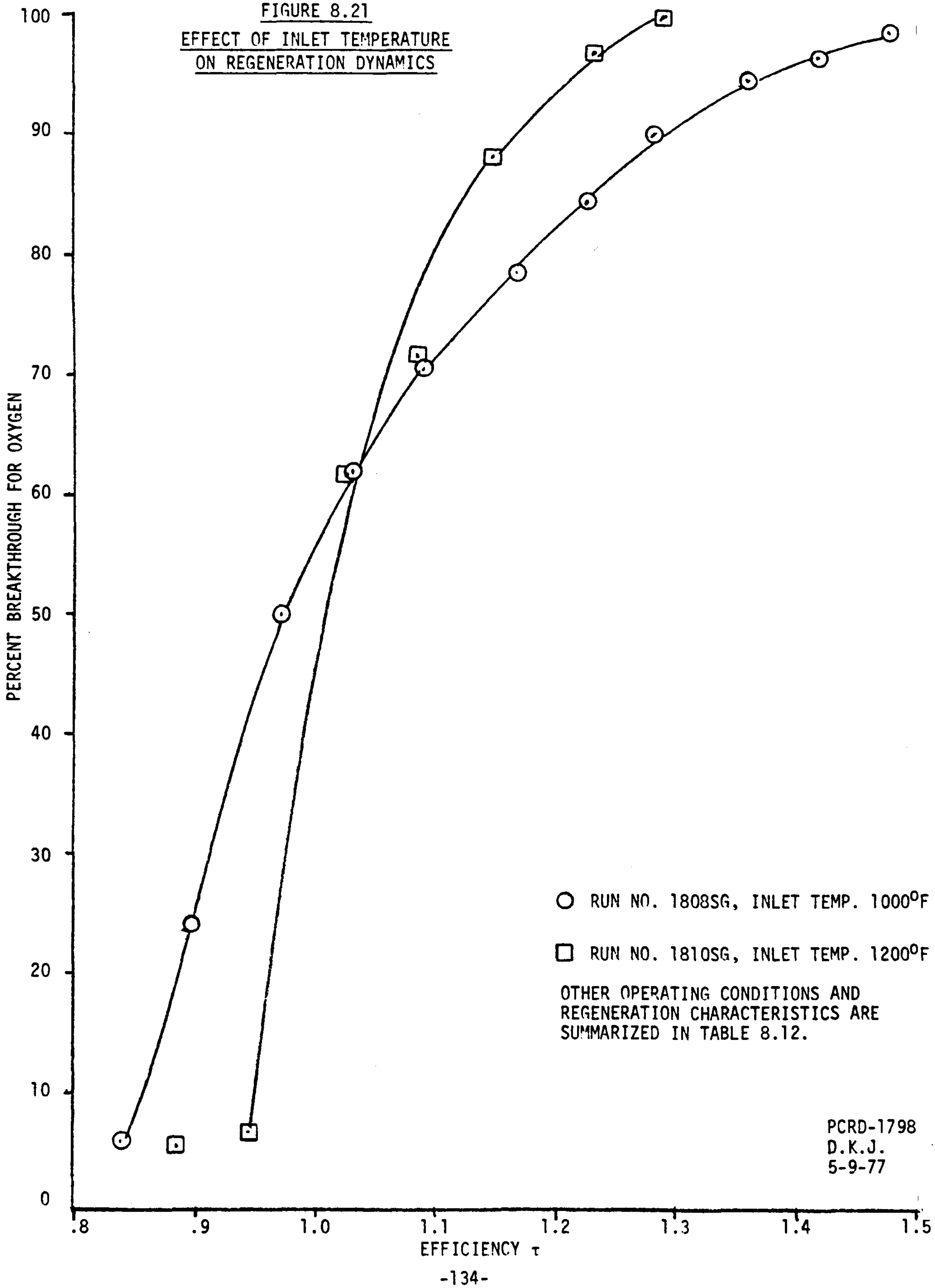

OTHER OPERATING CONDITIONS AND REGENERATION CHARACTERISTICS ARE SUMMARIZED IN TABLE 8.12.

PCRD-1798
D.K.J.
5-9-77

TABLE 8.13

EFFECT OF LINEAR VELOCITY ON REGENERATION DYNAMICS

	Run No. 1807SG	Run No. 1814SG
Linear Velocity, Ft./Sec.	.17	.33
Wt.% Iron Oxide in Fresh Sorbent	42	42
Wt.% Sulfur in Fresh Sorbent	0.1	0.1
Wt.% Sulfur in Sulfided Sorbent	17.6	21.9
GHSV (Air)	97	92
Pellet Diameter, Inches	0.25	0.25
Inlet Temperature, ^{o}F	1011	1000
Pressure, psig	33	30
Mole % Air in Feed	14	14
Sorbent Volume, Liters	.5	1.0
Regeneration Characteristics		
*Efficiency at 10% Oxygen Breakthrough	.95	1.0
*Efficiency at 50% Oxygen Breakthrough	1.01	1.04
Residual Sulfur Content in Regenerated Sorbent, Wt.%	2.0	.096
Time for Perfect Operation, Hrs.	11.69	12.13
Observed Maximum Temperature Rise, ^{o}F	167	380
Approximate Average Mole % SO_2 in Dry Gas	3.6	4.9
% Removal of Absorbed Sulfur	86.7	99.5

* Efficiencies are corrected for sample lag.

FIGURE 8.22
EFFECT OF LINEAR VELOCITY
ON REGENERATION DYNAMICS

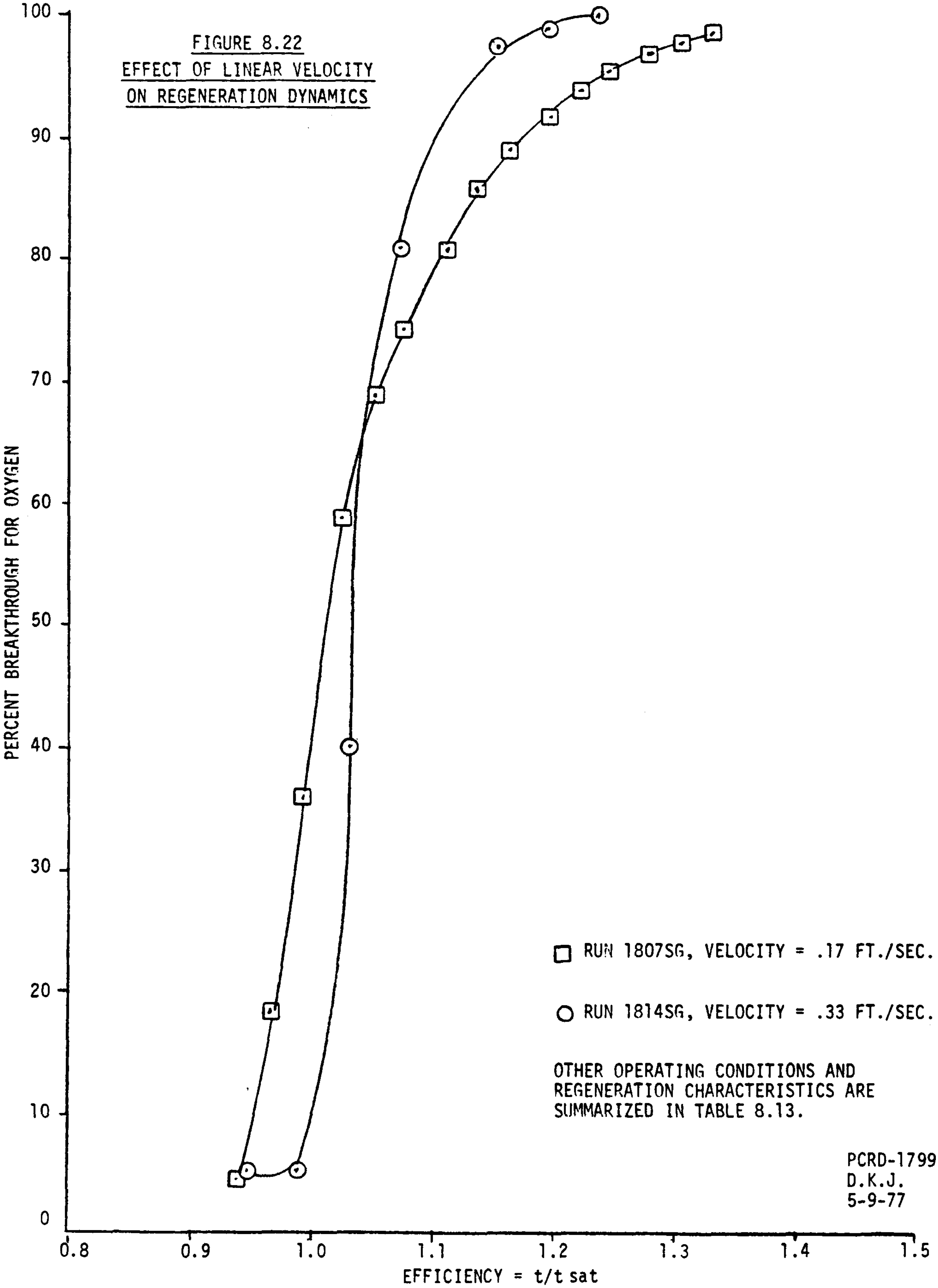

OTHER OPERATING CONDITIONS AND REGENERATION CHARACTERISTICS ARE SUMMARIZED IN TABLE 8.13.

PCRD-1799
D.K.J.
5-9-77

8.10.6 Effect of Pellet Diameter on Regeneration Characteristics

Two regeneration experiments were carried out using 1/8" and 1/4" diameter pellets. Table 8.14 summarizes the operating conditions and regeneration characteristics for the runs. Figures 8.10 and 8.23 are the oxygen breakthrough curves for these runs before and after correction for sample lag. Figure 8.24 is a comparison of the breakthrough versus efficiency curves.

It can be seen that lowering the particle size improved the efficiency of regeneration considerably - by about 10%. This is consistent with the observations in absorption studies.

8.10.7 Effect of Oxygen Concentration on Regeneration Characteristics

The regeneration reaction is very fast and exothermic (heat of reaction is about 78 kcal/gmole oxygen). If the reaction is not controlled, the temperatures will be excessively high and may damage the sorbent and/or the reactor. The adiabatic temperature rise of the gas can be controlled by reducing the oxygen content and increasing the inert gases serving as a heat sink.

Two runs at different oxygen content were carried out - Run 1808SG with 19% air, and Run 1815SG with 14% air. The operating conditions and regeneration characteristics for these runs are described in Table 8.15. Figures 8.13 and 8.19 give the oxygen breakthrough curves - corrected and uncorrected - for sample lag due to the knock-out pot. Figure 8.25 is the comparison of oxygen breakthrough versus efficiency plots for these two runs.

It may be noted that the effect of increased oxygen concentration is a combined effect of the kinetics due to higher oxygen content and different temperature rise. It is seen that the efficiency of regeneration increased slightly with increase in oxygen content. Surprisingly, observed temperature rise decreased slightly (258^{o}F at 3.9% oxygen and 320^{o}F at 2.9% oxygen) with increase in oxygen content. One may remember that the observed heat effects are a combination of the exothermic heat of oxidation of iron sulfide to sulfur dioxide and the endothermic heat of reduction of sulfur trioxide to elemental sulfur. With higher oxygen content in feed, the sulfur dioxide concentration will be higher and this may lead to greater sulfur formation.

TABLE 8.14

INFLUENCE OF PELLET DIAMETER ON REGENERATION CHARACTERISTICS

	Run No. 1806SG	Run No. 1811SG
Pellet Diameter, Inches	.25	.125
Wt.% Added Iron Oxide in Fresh Sorbent	21	21
Wt.% Sulfur in Fresh Sorbent	.1	.1
Wt.% Sulfur in Sulfided Sorbent	10.1	10.6
GHSV (Air)	97	97
Inlet Temperature, ^{o}F	1028	983
Pressure, psig	30	30
Mole % Air in Feed	14	14
Sorbent Volume, Liters	.5	.5
Linear Velocity, Ft./Sec.	.17	.17
Regeneration Characteristics		
*Efficiency at 10% Oxygen Breakthrough	.87	1.0
*Efficiency at 50% Oxygen Breakthrough	.95	1.01
Residual Sulfur Content in Regenerated Sorbent	1.4	1.0
Time for Perfect Operation, Hrs.	5.74	4.01
Observed Maximum Temperature Rise, ^{o}F	124	207
Approximate Average Mole % SO_2 in Dry Gas	4.0	~
% Removal of Absorbed Sulfur	89.7	91.5

* Efficiencies are corrected for sample lag.

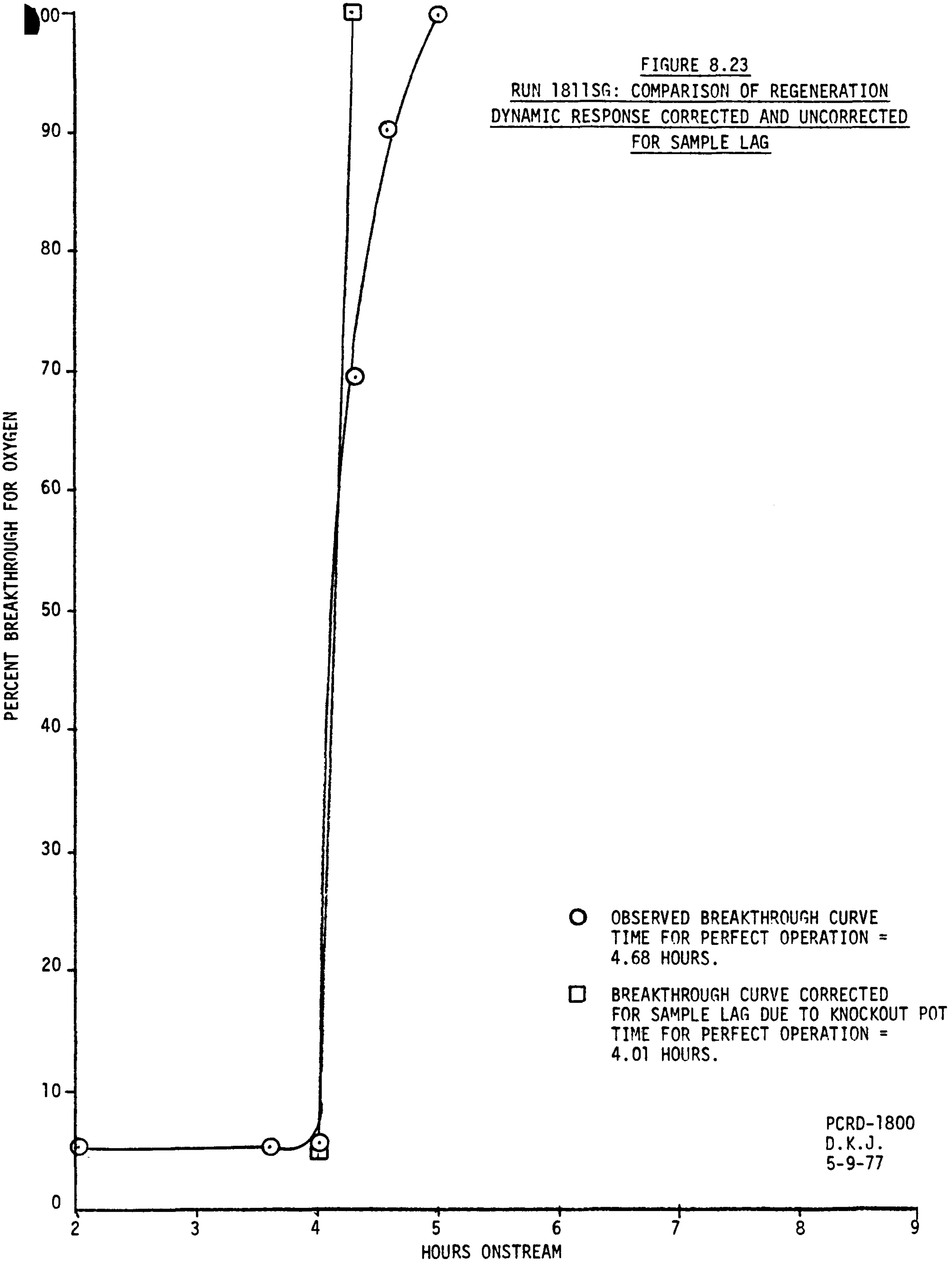

FIGURE 8.23
RUN 1811SG: COMPARISON OF REGENERATION DYNAMIC RESPONSE CORRECTED AND UNCORRECTED FOR SAMPLE LAG

PCRD-1800
D.K.J.
5-9-77

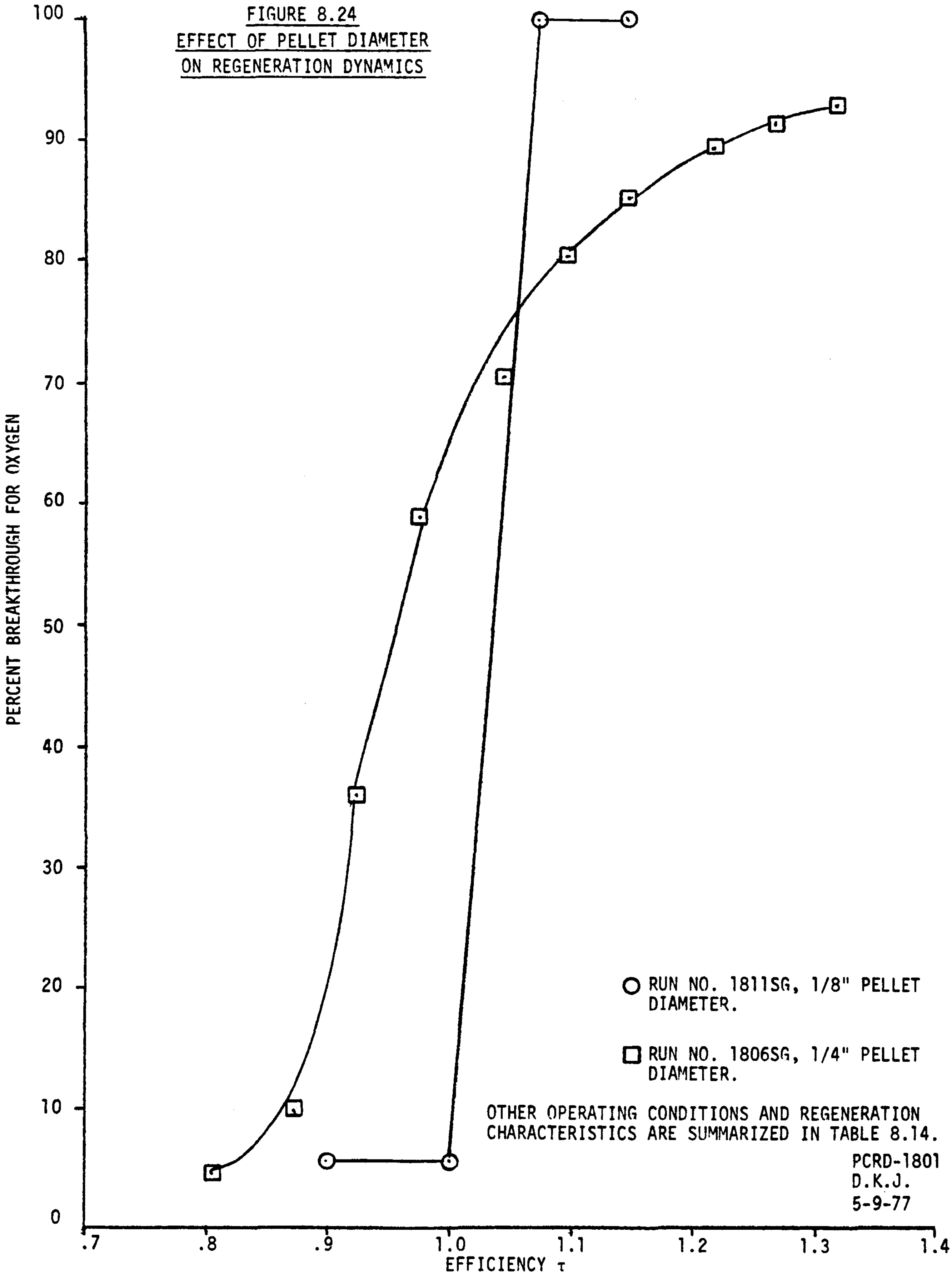

TABLE 8.15

EFFECT OF OXYGEN CONTENT ON REGENERATION CHARACTERISTICS

	Run No. 1808SG	Run No. 1815SG
Mole % Air in Feed	19	14
Wt.% Iron Oxide in Fresh Sorbent	42	42
Wt.% Sulfur in Fresh Sorbent	.1	.1
Wt.% Sulfur in Sulfided Sorbent	18.8	21.9
GHSV (Air)	194	182
Pellet Diameter, Inches	.25	.25
Inlet Temperature, °F	1000	1000
Pressure, psig	30	30
Sorbent Volume, Liters	.5	.5
Linear Velocity, Ft./Sec.	.25	.33
Regeneration Characteristics		
*Efficiency at 10% Oxygen Breakthrough	.85	.88
*Efficiency at 50% Oxygen Breakthrough	.97	.99
Residual Sulfur Wt.% in Regenerated Sorbent	2.2	1.34
Time for Perfect Operation, Hrs.	5.13	6.9
Observed Maximum Temperature Rise, °F	258	320
Approximate Average Mole % SO_2 in Dry Gas	6.0	5.6
% Removal of Absorbed Sulfur	89.2	94.3

* Efficiencies are corrected for sample lag.

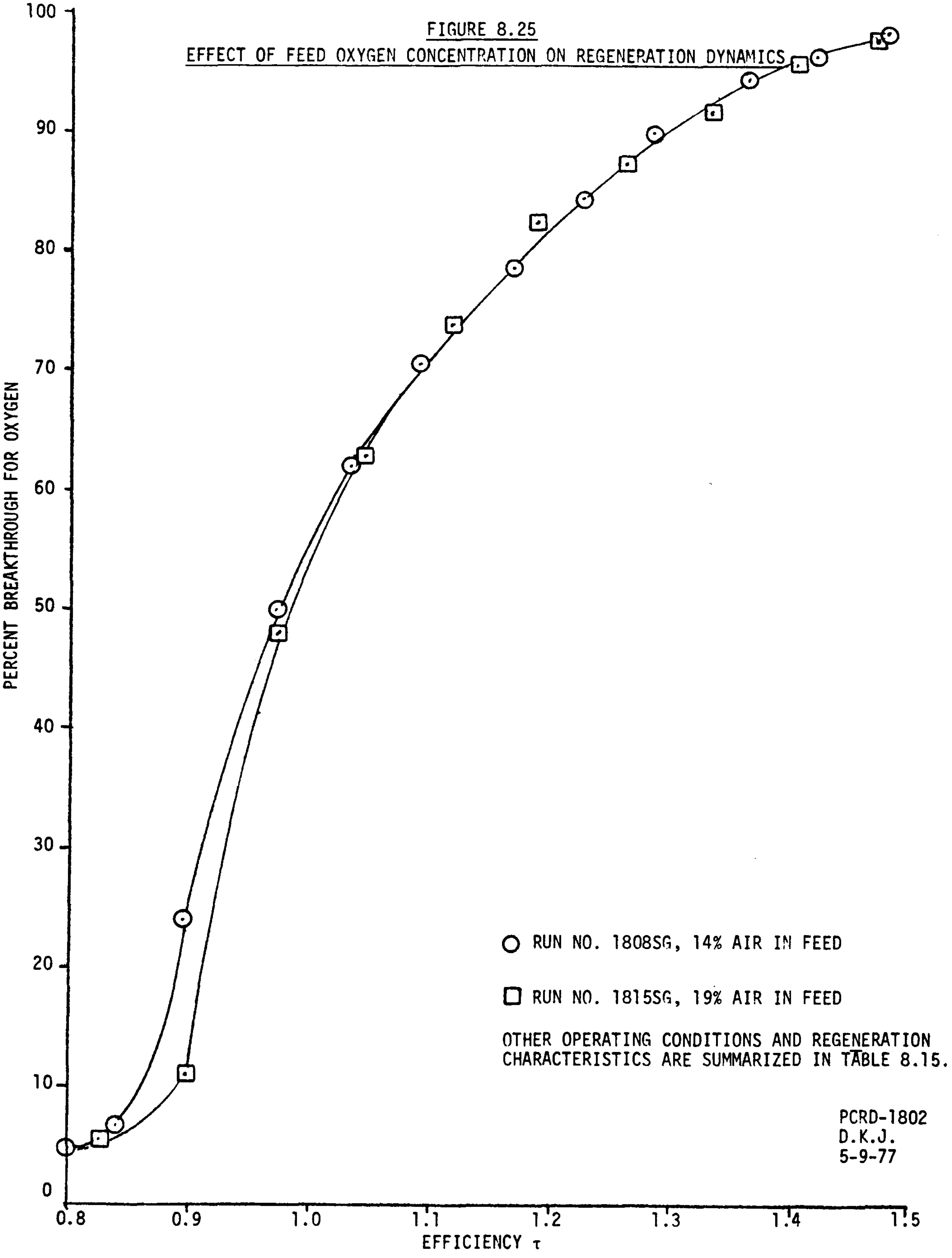

FIGURE 8.25

EFFECT OF FEED OXYGEN CONCENTRATION ON REGENERATION DYNAMICS

OTHER OPERATING CONDITIONS AND REGENERATION CHARACTERISTICS ARE SUMMARIZED IN TABLE 8.15.

PCRD-1802
D.K.J.
5-9-77

8.11 Effect of Operation on Sorbent Characteristics

In this experimental work, the sorbents had undergone one cycle of absorption and regeneration. Several physical properties of fresh, sulfided and regenerated sorbents were measured to see how the physical characteristics of the sorbent are affected by exposure to reducing atmosphere in absorption and high temperature, oxidizing atmosphere during air-steam regeneration. The following properties were measured:

- Porosity
- Pellet Density
- Crushing Strength
- Attrition Resistance
- Surface Area by Micromeratics
- Pore Size Distribution
- Differential Thermal Analysis
- X-ray Diffraction Analysis

Results of the analyses are summarized below.

8.11.1 Porosity of the Sorbent

Porosity of the sorbent was measured by water absorption or kerosene absorption method. The technique involved boiling the sorbent in a liquid of known density to replace all air in the pores with the liquid. Porosity can be calculated based on weight gain. Porosities of all fresh and sulfided sorbents were measured using water as the liquid. When regenerated sorbents were tested by boiling in water, in some cases some material from the sorbent leached into water. This would have given an erroneous value of porosity. Hence, the technique was changed and kerosene was used as the liquid for absorption. To compare results of the two techniques and accuracy of the information, porosity of regenerated sorbent from Run 1810SG was measured by water absorption (33.7%) and kerosene absorption (31.7%). Regenerated sorbent from Run 1810SG had not leached when boiled in water.

Table 8.16 gives the porosities of fresh, sulfided and regenerated sorbents for all regeneration experiments.

8.11.2 True Density of Pellets

True density of pellets was based on weight of the pellet and its volume excluding the open pore volume. Hence, true density of a pellet is a function of both chemical changes (iron sulfide versus iron oxide) and porosity changes. Table 8.17 lists the true densities of the fresh, sulfided and regenerated pellets.

It can be seen that pellet density increases by about 3 to 5% after sulfiding and is decreased after regeneration, and is close to the fresh pellet density.

TABLE 8.16

CHANGES IN THE POROSITY OF THE SORBENT AFTER ABSORPTION AND REGENERATION

Regeneration Run Number	Absorption Run Number	Fresh Sorbent Porosity Volume %	Sulfided Sorbent Porosity Volume %	Regenerated Sorbent Porosity Volume %
1805SG	1735SG	31.7	28.9	23.1*
1806SG	1750SG	28.8	27.5	21.9
1807SG	1756SG	34.2	31.4	27.5*
1808SG	1762SG	33.7	31.4	26.9*
1809SG	1764SG	33.7	30.2	34.0*
1810SG	1762SG	33.7	31.6	33.7 (31.7*)
1811SG	1743SG	33.0	30.9	31.3
1814SG	In Heat Treater	33.7	29.1	32.6*
1815SG	In Heat Treater	33.7	29.1	28.4*
1816SG	In Heat Treater	33.7	29.1	31.5*
1817SG	In Heat Treater	33.7	29.1	26.3*
1818SG	In Heat Treater	33.7	29.1	26.4*

* Porosity measured based on kerosene absorption. All other porosities are measured based on water absorption.

TABLE 8.17

CHANGES IN THE TRUE DENSITY OF THE SORBENT AFTER ABSORPTION AND REGENERATION

Regeneration Run Number	Absorption Run Number	Fresh Sorbent True Density gms/cc	Sulfided Sorbent True Density gms/cc	Regeneration True Density gms/cc
1805SG	1735SG	1.964	1.980	2.036
1806SG	1750SG	1.976	2.042	2.094
1807SG	1756SG	2.138	2.262	2.137
1808SG	1762SG	2.190	2.251	2.161
1809SG	1764SG	2.190	2.229	2.146
1810SG	1762SG	2.190	2.250	2.155
1811SG	1743SG	1.854	1.912	1.893
1814SG	Heat Treater	2.190	2.293	2.139
1815SG	Heat Treater	2.190	2.293	2.209
1817SG	Heat Treater	2.190	2.293	2.203
1818SG	Heat Treater	2.190	2.293	2.255

8.11.3 Crushing Strength of Pellets

The sorbent appeared to maintain its physical integrity after going through one absorption-regeneration cycle. The crushing strengths of all regenerated, fresh and some sulfided sorbents were measured to see the effect of processing on crushing strengths. Crushing strengths were measured using a motorized chatillon crush tester. Total length of ten pellets was measured. The total force required to crush ten pellets was divided by the total length of ten pellets to give a uniform measurement of the sorbent hardness in pounds per millimeter. Results of the analyses are summarized in Table 8.18.

It can be seen that the crushing strength has increased 300 to 400 percent as a result of processing. Crushing strength of the sulfided sorbent is slightly greater than the regenerated sorbent. This difference could be due to the structural differences (iron sulfide against iron oxide) and may not be a deterioration by steam-air.

8.11.4 Attrition Resistance of Sorbents

Fresh, sulfided and regenerated sorbents from the same batch were tested for attrition resistance by measuring weight loss due to attrition by an air jet. A weighed sorbent sample was placed in a metal flask provided with a jet for the introduction of air and a screened outlet to retain large sorbent particles. After one hour subjection to air flow, the sorbent was removed, screened on U.S.S. Sieve No. 10 and the retained portion was weighed.

$$\text{Attrition Loss \%} = \frac{\left(\begin{array}{c}\text{Original Wt. of} \\ \text{Sorbent}\end{array} - \begin{array}{c}\text{Wt. of Sorbent on 10} \\ \text{Mesh After Test}\end{array}\right)}{\text{Original Wt. of Sorbent}} \times 100$$

The results are summarized in Table 8.19. The sulfided sorbent is harder than fresh sorbent and regenerated sorbent is the hardest of all.

Hence, based on the crushing strength and attrition resistance, physical strength of the sorbent has improved significantly after undergoing one absorption-regeneration cycle. Whether this improvement in physical strength is retained in multi-cycle operation or not is not known.

8.11.5 Surface Area of the Sorbent

Surface area of the fresh, sulfided and regenerated sorbents from the same batch were measured using micromeratic technique. Table 8.20 summarized the measured surface areas.

The data indicate that surface area of the sorbent decreased slightly after sulfiding and increased after regeneration. Surface area of the sorbents is much less than that of typical catalysts used in petroleum industry.

TABLE 8.18
EFFECT OF PROCESSING ON MEASURED CRUSHING STRENGTHS

Regeneration Run Number	Crushing Strength of Fresh Sorbent lbs./mm	Crushing Strength of Sulfided Sorbent lbs./mm	Crushing Strength of Regenerated Sorbent lbs./mm
1805SG	7.7		8.1
1806SG	9.33		13.2
1807SG	2.67	12.2	9.4
1808SG	3.35	13.3	12.2
1809SG	3.35		13.7
1810SG	3.35		12.1
1814SG	3.35		10.6
1815SG	3.35		13.7
1817SG	3.35		11.7
1818SG	3.35		10.7

TABLE 8.19

EFFECT OF PROCESSING ON MEASURED ATTRITION RESISTANCE

- ATTRITION BY AN AIR JET - *

Sample(1)	Air Rate SCFM *	Wt.% Loss
Fresh (814X1-1X7)	1.9	5.5
	2.3	8.4
	2.7	50.3
	3.1	72.0
Sulfided (Run 1757SG)	1.9	4.0
	2.3	9.2
	2.7	11.1
	3.1	13.7
Regenerated (Run 1807SG)	1.9	2.2
	2.3	4.1
	2.7	6.8
	3.1	8.5

(1) Sulfided and regenerated sorbents are "harder" than the fresh sorbent.

* Houdry Division Analytical Method No. SG-55.

TABLE 8.20

EFFECT OF PROCESSING ON THE SURFACE AREA OF SORBENT

Sorbent	Surface Area By Micromeratic Technique m^2/gm
Fresh (814X1-1X7)	1.55
Sulfided (Run 1757SG)	0.44
Regenerated (Run 1807SG)	1.26

8.11.6 Pore Size Distribution

Pore size distribution of the fresh, sulfided and regenerated sorbents from the same batch was measured by a mercury porosimeter. The resulting plots of cumulative pore volume versus pore diameter are given in Figure 8.26. It can be seen that the total pore volume of the fresh sorbent decreased by about 34% after sulfiding; and increased slightly after undergoing regeneration. Table 8.21 describes the contribution of each pore size range to the pore volume and surface area. It can be seen that most pore volume is due to pores of .1 to 1 micron diameter. The pore size distribution becomes flatter as a result of processing.

8.11.7 Differential Thermal Analysis

Samples of fresh, sulfided and regenerated iron oxide/fly ash pellets were analyzed for DTA in atmospheres of nitrogen and air. The fresh pellets were exposed to static 1650°F in the oven during preparation. Several qualitative observations about the DTA patterns are made below.

Fresh iron oxide pellets in nitrogen atmosphere show two slightly endothermic transitions - which may be due to αFe_2O_3 (hematite). Fresh pellets in air atmosphere show a very large endothermic transition at 770°C. Origin of this peak is not known. Sulfided pellets in a nitrogen atmosphere showed a fairly flat DTA curve with a small exotherm at 560°C. Sulfided sorbent in air atmosphere showed three significant endothermic transitions at 238°C, 359°C and 743°C. It also showed a large exothermic transition at 580°C. This peak seems to be due to oxidation of iron sulfide to iron oxide. MERC had reported that regeneration did not take place below 900°F (482°C). The sharp exotherm for this peak could explain this fact. The regenerated pellets in air atmosphere showed several small peaks below 200°C, and showed a rather significant exothermic peak at 750°C. This peak was also observed in DTA for regenerated pellets in nitrogen atmosphere. Hence, one may assume that this peak is probably due to phase transformation or chemical decomposition rather than chemical reactions with oxygen. It is interesting to note that this peak was not present in fresh or sulfided sorbents.

One may conclude that there are several structural and chemical changes in the sorbent as a result of processing. A better understanding of these changes may require scientific study by DSC analyses, X-ray diffraction, and chemical and physical analyses of the pellets before and after each transition, as well as the iron oxide powder from which they were made. It should be noted that the sorbents contain fly ash, bentonite, and commercial iron oxide which have several components and the DTA reflects changes occurring in them too.

FIGURE 8.26

VARIATION IN PORE SIZE DISTRIBUTION OF THE SORBENT DUE TO PROCESSING

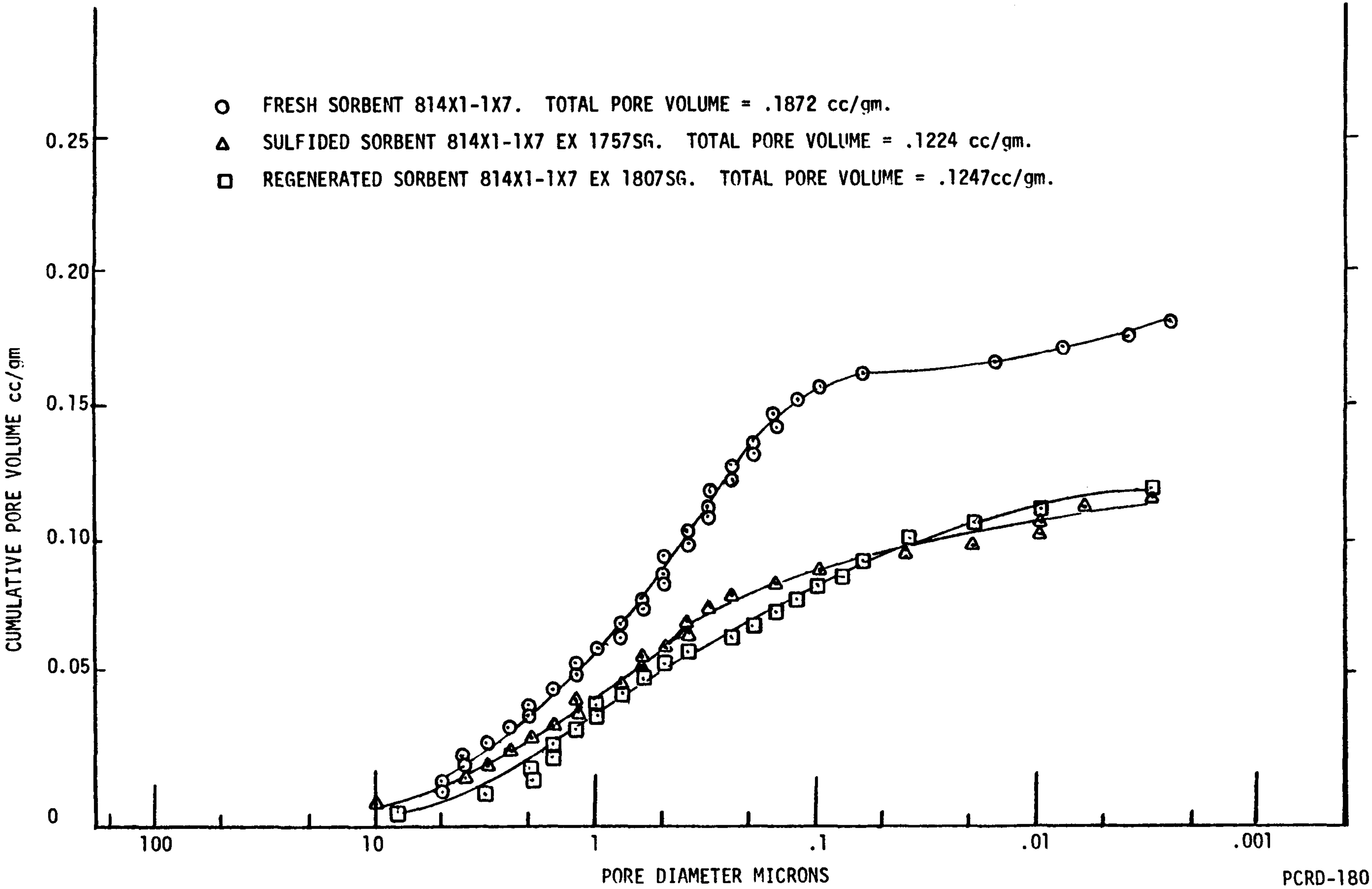

PCRD-180
D.K.J.
5-9-77

TABLE 8.21

EFFECT OF PROCESSING ON PORE SIZE DISTRIBUTION

- PORE SIZE RANGE -

	.001 to .01 Microns	.01 to .1 Microns	.1 to 1.0 Microns	1 to 10 Microns	Total
Absolute Pore Volume, cc/gm					
Fresh Sorbent	.0154	.0282	.0972	.0475	.1883
Sulfided Sorbent	.0179	.0225	.0493	.0335	.1232
Regenerated Sorbent	.0120	.0404	.0486	.0248	.1258
Percent of Total Pore Volume					
Fresh Sorbent	8	15	52	25	100
Sulfided Sorbent	15	18	40	27	100
Regenerated Sorbent	9	32	39	20	100

8.11.8 X-ray Diffraction Patterns

Samples of bentonite, fly ash, U.S. Steel iron oxide, fresh iron oxide pellets, sulfided iron oxide pellets and regenerated iron oxide pellets were analyzed. Comments on the observed crystalline phases are given below:

1. Bentonite - The XRD pattern of this material was used for comparison with the patterns of the other samples. No evidence of bentonite was seen in any of the XRD analyzed samples.

2. Fly Ash - The major crystalline phases identified in this material were SiO_2 (alpha-quartz) and alpha-Fe_2O_3. The pattern contained many unidentified lines, some of which could possibly be assigned to Al_2O_3. A very broad maximum near 3.7 dA° indicated the presence of some amorphous phase.

3. Iron Oxide - The major crystalline phase in this material was identified as alpha-Fe_2O_3. Several intense lines in the XRD pattern of this material were identified as possible epsilon-Fe_2O_3. Fe_3O_4 and $ZnFe_2O_4$, which are isomorphous and indistinguishable by XRD, were also possibly present. Crystalline carbon was identified as a possible constituent as well.

4. Fresh Iron Oxide Pellets (814X1-1X7) - The major crystalline phase present was identified as alpha-Fe_2O_3. Some of the additional lines observed in the pattern for the iron oxide sample were also in this pattern and they were identified as possible Fe_3O_4 and/or $ZnFe_2O_4$. The epsilon-Fe_2O_3 phase identified in the iron oxide pattern was not identified or detected in the fresh pellet sample. SiO_2 (alpha-quartz) was also identified as a possible constituent.

5. Sulfided Iron Oxide (1757SG) - The major crystalline phase present was identified as a sulfur-rich FeS phase and its pattern matched that of both $Fe_{0.91}S$ and $Fe_{0.88}S$ phases listed in the XRD file. SiO_2 (alpha-quartz) was also identified as a possible constituent. Several additional weak lines in the pattern were not identified. No matches for any of the iron sulfides or sulfates in the XRD file were found for these additional lines.

6. Regenerated Pellets (1807SG) - The major crystalline phase present was identified as alpha-Fe_2O_3. A few weak unassigned lines were also present. No matches for any of the iron sulfates or sulfides in the XRD file were found for the additional lines in this pattern. SiO_2 (alpha-quartz) was also identified as a possible constituent. No evidence of any Fe_3O_4 and/or $ZnFe_2O_4$, or epsilon-Fe_2O_3 was detected in this pattern.

FIGURE 8.27

DIFFERENTIAL THERMAL ANALYSIS OF THE FRESH SORBENT (814X1-1X7) IN INERT (N_2) ATMOSPHERE

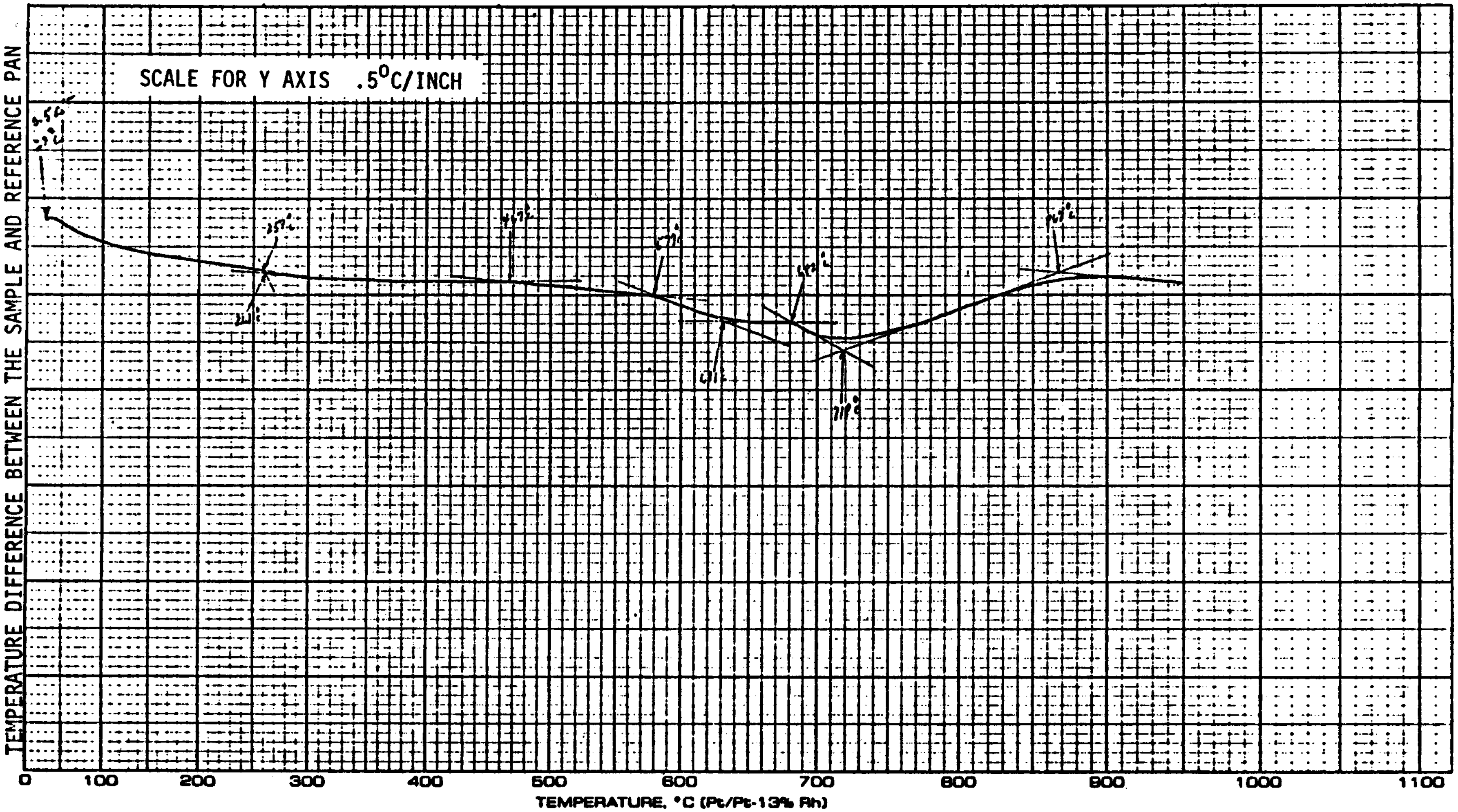

PCRD-1810
D.K.J.
5-11-77

FIGURE 8.28

DIFFERENTIAL THERMAL ANALYSIS OF THE FRESH SORBENT (814X1-1X7) IN AIR

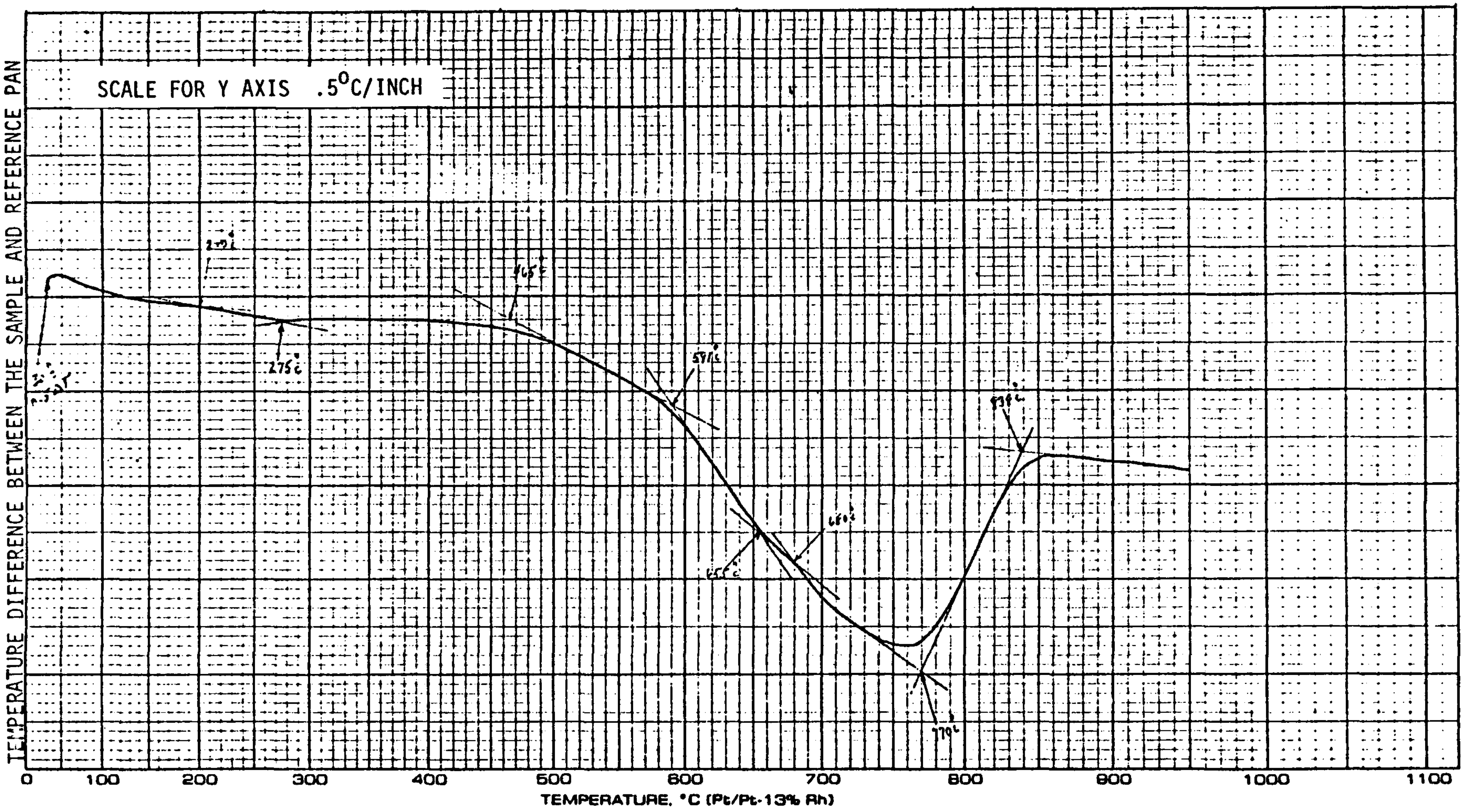

PCRD-1811
D.K.J.
5-11-77

FIGURE 8.29

DIFFERENTIAL THERMAL ANALYSIS OF SULFIDED SORBENT (RUN NO. 1757SG) IN INERT (N_2) ATMOSPHERE

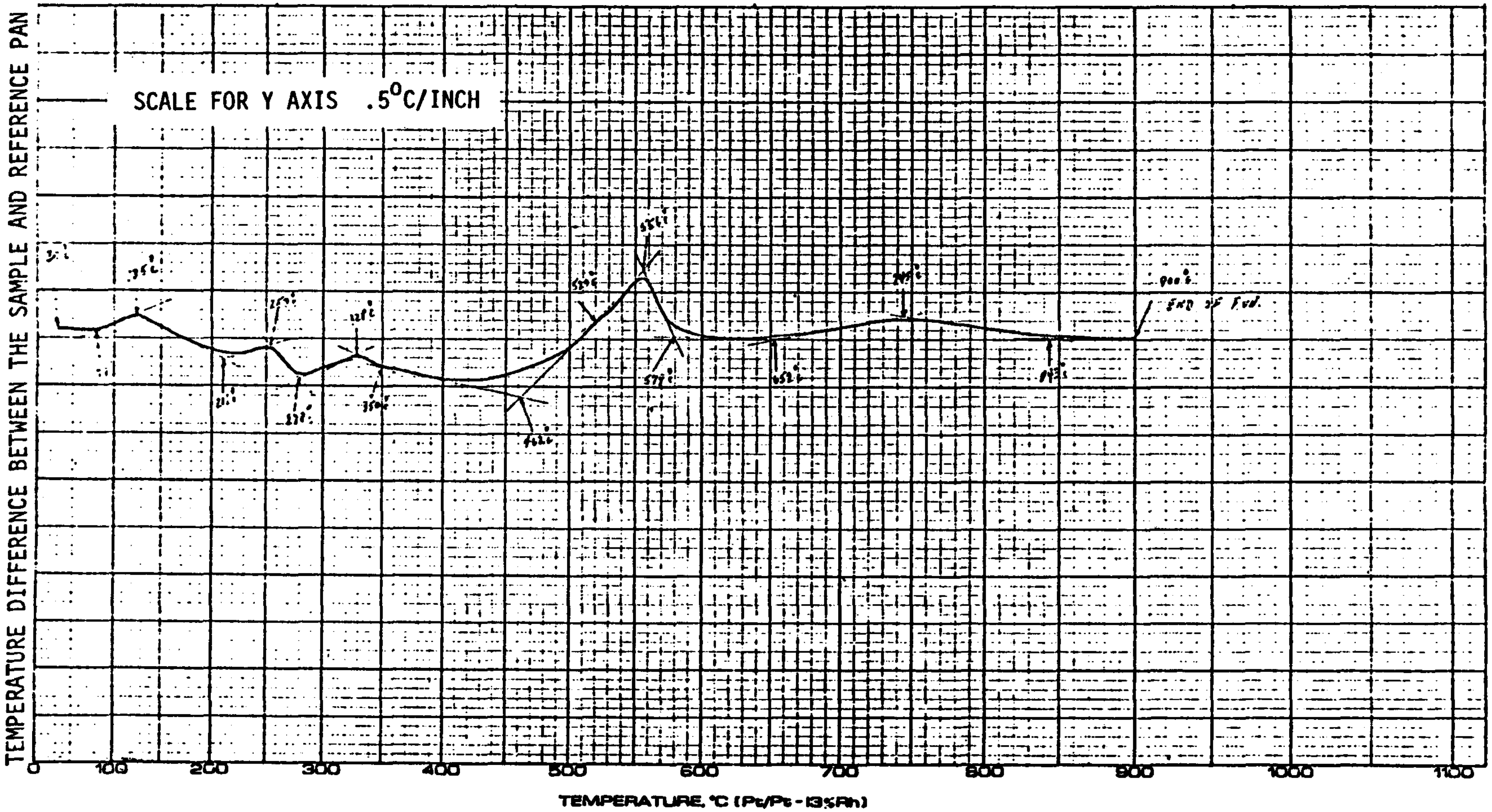

PCRD-1812
D.K.J.
5-11-77

FIGURE 8.30

DIFFERENTIAL THERMAL ANALYSIS OF SULFIDED SORBENT (RUN 1957SG) IN AIR

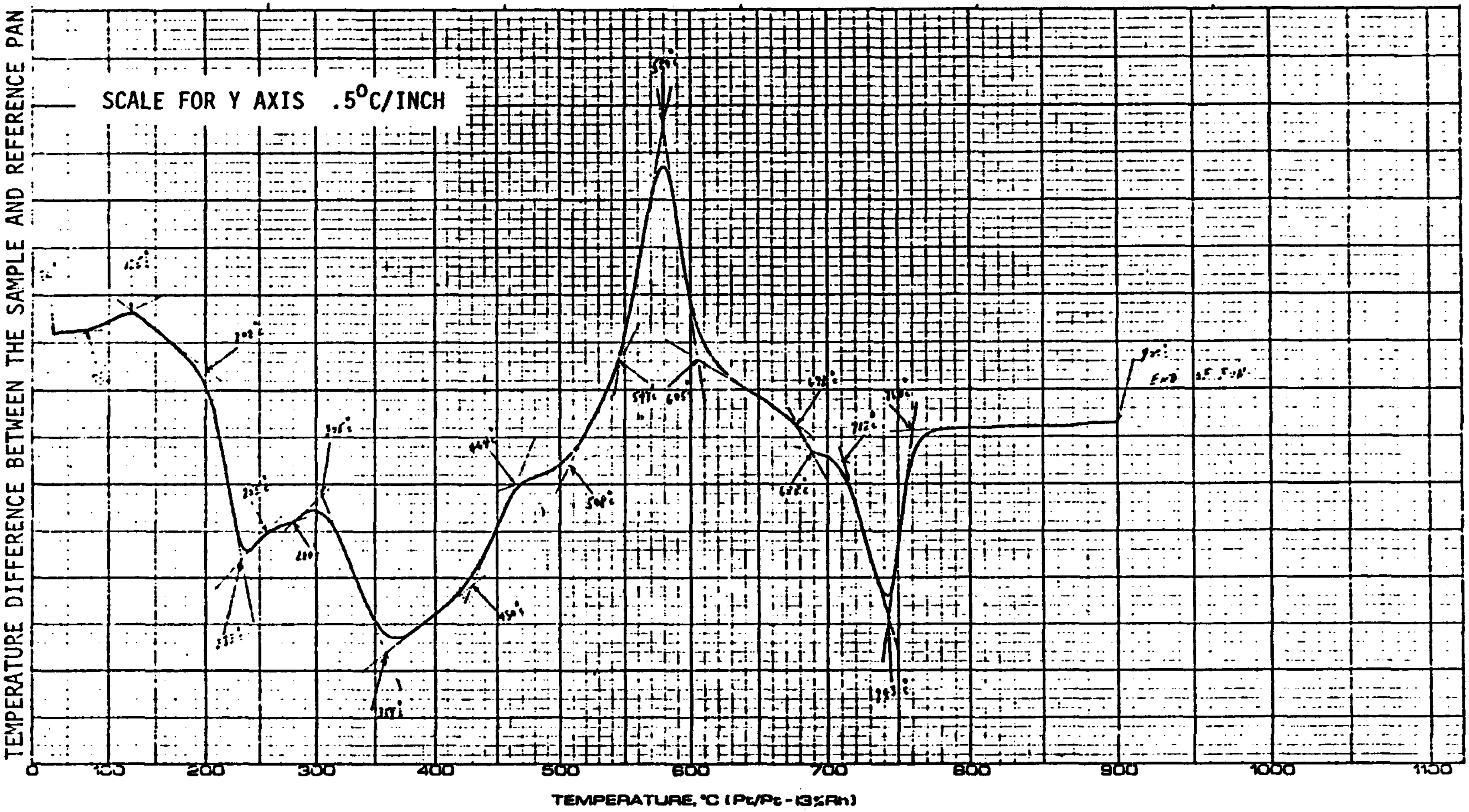

PCRD-1813
D.K.J.
5-11-77

FIGURE 8.31

DIFFERENTIAL THERMAL ANALYSIS OF REGENERATED SORBENT (RUN 1807SG) IN NITROGEN

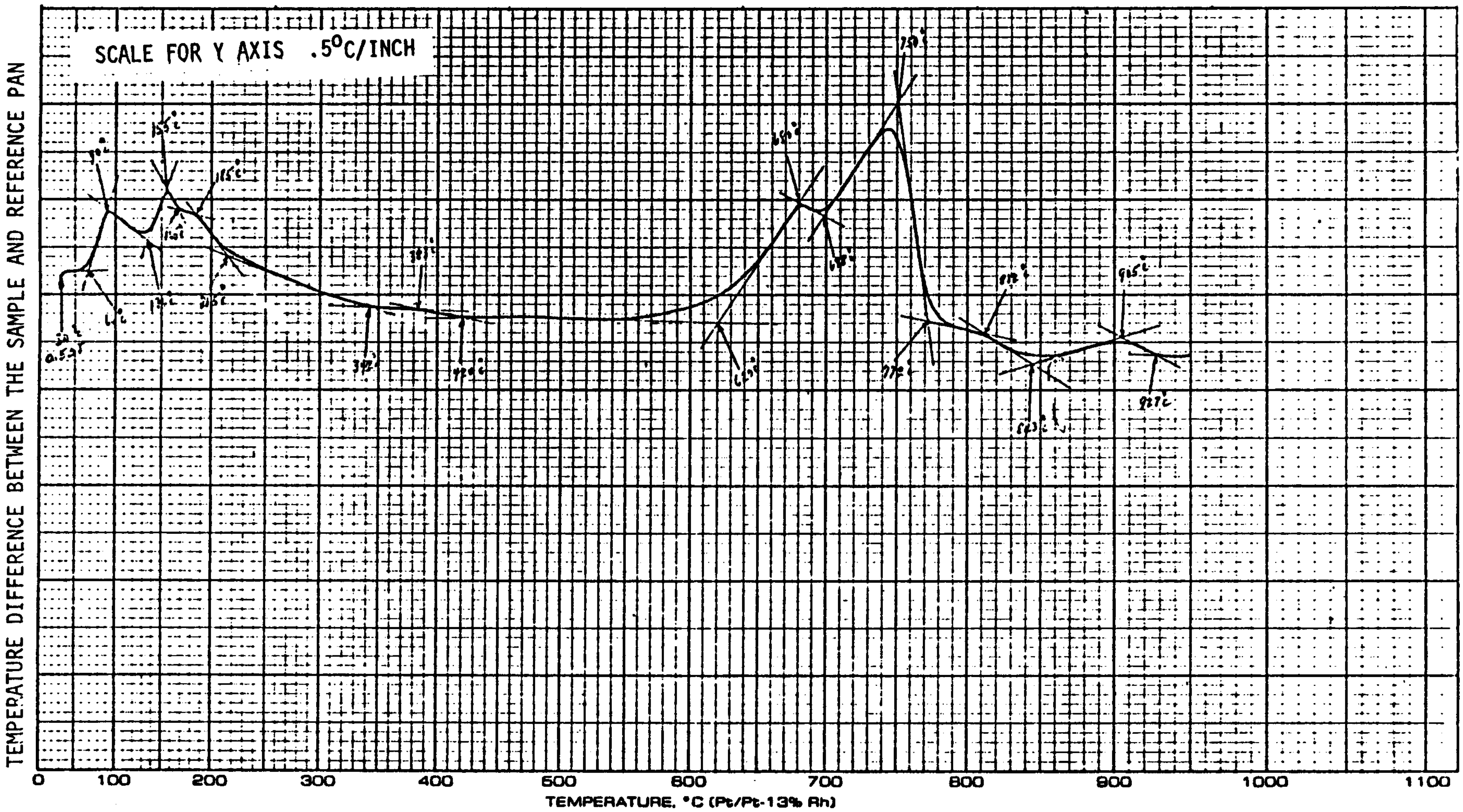

PCRD-1814
D.K.J.
5-11-77

FIGURE 8.32

DIFFERENTIAL THERMAL ANALYSIS OF REGENERATED SORBENT (RUN 1807SG) IN AIR

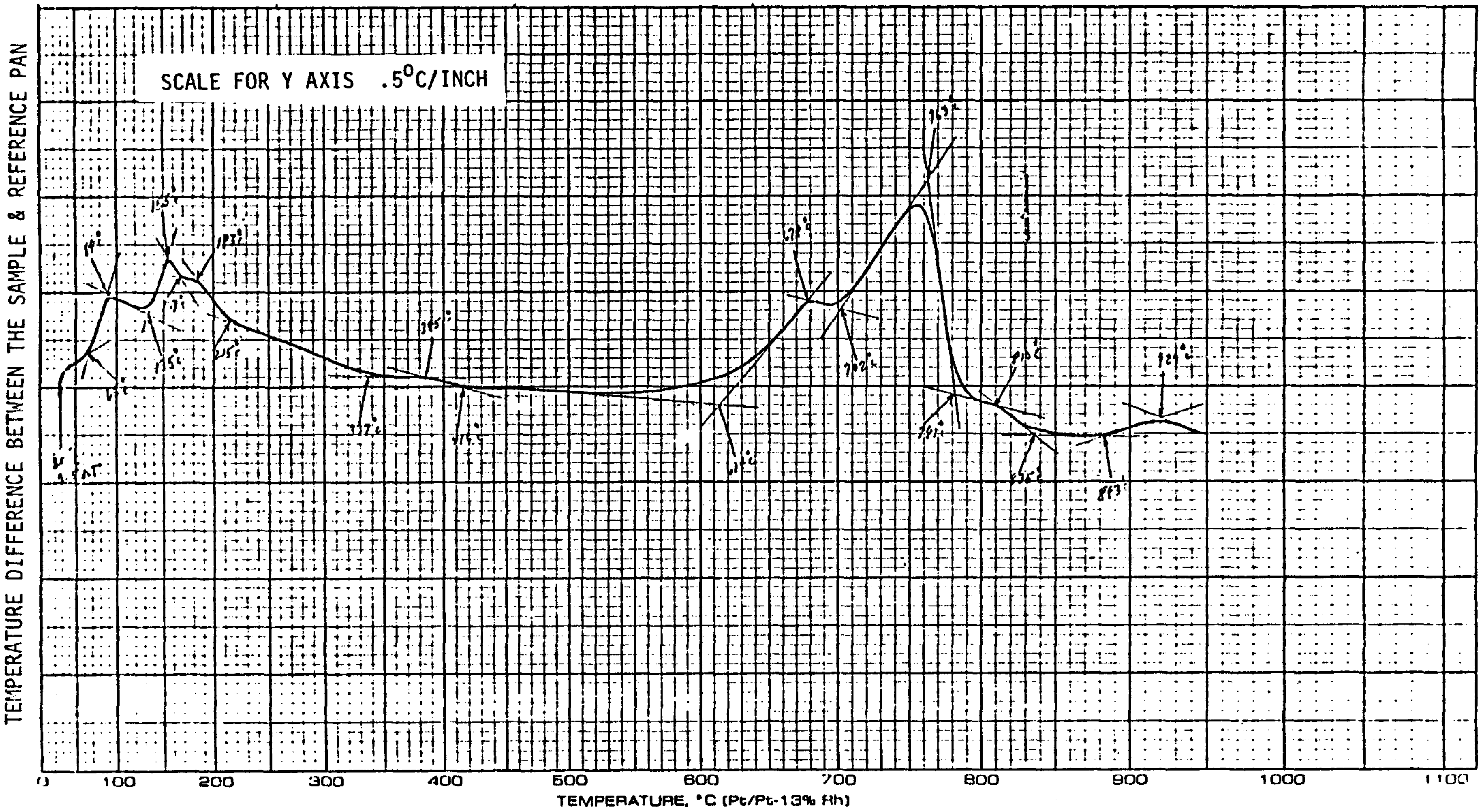

PCRD-1815
D.K.J.
5-11-77

9.0 MODELING REGENERATION PROCESS

9.1 Adiabatic Regeneration Dynamic Models

9.1.1 Differential Equations

The experimental regeneration dynamics runs have demonstrated that the regeneration of sulfided iron oxide/fly ash is an exothermic reaction. Bed temperature rises of 300°F have been observed under the test conditions chosen. Since such temperature effects could affect the regeneration dynamics, it is necessary to include an adiabatic heat balance in the regeneration model. The adiabatic regeneration models presented in this section are applicable to the core of a large diameter reaction vessel or to a well insulated lab scale reactor such as the ERDA pressure unit.

Three isothermal sorption dynamics models have been investigated to simulate desulfurization:

1. The shrinking core model, derived in Appendix B.1.
2. The film-kinetic model, derived in Appendix B.2.
3. The kinetic model, which is a special case of the film-kinetic model with zero film resistance to sorption (zero film sorption number).

Each of these three isothermal models may be coupled with the adiabatic heat balance derived in Appendix B.3. The resulting adiabatic models are described by the differential equations in Table 9.1. Nomenclature for this table can be found in Table C.1 of the appendix.

The first two equations of Table 9.1 describe the dynamic breakthrough curve in terms of the dimensionless rate. Equation (3) of the table describes the bed temperature profile as a function of reaction rate. The temperature effects equations determine the effect of temperature profile on reaction rate. If temperature effects on the rate are small, then the adiabatic breakthrough curves determined by the equations of Table 9.1 are identical to breakthrough curves predicted by the isothermal models. The temperature effect on the shrinking core rate is small even for 300°F bed temperature rises, while temperature effects on the kinetic part of the film-kinetic model may cause the rate to double for each 40°F increase in bed temperature. As a result, the isothermal breakthrough curves presented in Appendix B.1 are adequate to describe the adiabatic shrinking core model, while the adiabatic film-kinetic model predicts different breakthrough curves than does the isothermal model.

TABLE 9.1

ADIABATIC SORPTION DYNAMICS EQUATIONS

1. DEPLETION OF SORBENT IRON SULFIDE WITHIN SPHERICAL PARTICLE:

$$- \frac{\partial W}{\partial \tau} = R_X$$

2. DEPLETION OF SORBATE OXYGEN WITHIN GAS PHASE BETWEEN PARTICLES:

$$- \frac{\partial F}{\partial X} = R_X$$

3. ACCUMULATION OF HEAT WITHIN ADIABATIC SORPTION VESSEL:

$$\frac{\partial T}{\partial X} + N_{cp} \frac{\partial T}{\partial \tau} = T_{Ab} R_X$$

4. TEMPERATURE EFFECTS ON RATES FOR SHRINKING CORE AND FILM KINETIC MODELS:

SHRINKING CORE

$$R_X = \frac{3F \sqrt[3]{W}}{N_{Ab}^{\phi} (1 - \sqrt[3]{W})}$$

$$N_{Ab}^{\phi} = C_0 \text{ GHSV } \frac{a^2 \sqrt{T}}{P}$$

FILM-KINETIC

$$R_X = \frac{FW}{N_{Ab}^{K} + N_{Ab}^{F} W}$$

$$N_{Ab}^{K} = \frac{C_2 \text{ GHSV}}{PI_0} T e^{\beta/T}$$

$$N_{Ab}^{F} = C_1 \sqrt{\frac{\text{GHSV } a^3}{L}} T^{-1/3}$$

The remaining sections of this discussion describe the adiabatic film-kinetic model. The discussion in Section 9.1.5 on temperature profiles can also be qualitatively applied to the temperature profiles predicted by the adiabatic shrinking core model. Both adiabatic models are generated by the computer program of Appendix C.

9.1.2 Computer Model for Adiabatic Kinetically Controlled Sorption

The regeneration dynamics equations of Table 9.1 describe the oxygen breakthrough curve (F vs. τ), the level of bed regeneration (1 - W), and the bed temperature profile. The adiabatic computer model of Appendix C solves the dynamics equations if the following five inputs are supplied:

1. Kinetic sorption number at bed inlet conditions, N_{Ab}^{K}.
2. Film sorption number at bed inlet conditions, N_{Ab}^{F}.
3. Adiabatic heat balance number, N_{cp}.
4. Dimensionless gas adiabatic temperature rise, T_{Ab}.
5. Dimensionless activation energy, β.

The sorption numbers are functions of operating conditions, sorbent properties, and reactor geometry. The heat balance number depends on sorbante concentration, sorbent concentration, and heat capacities. The adiabatic temperature rise and the activation energy are thermodynamic functions of the reaction process. Given these five dimensionless inputs and the necessary boundary conditions, the computer program will predict a unique solution to the sorption dynamics equations.

The computer program developed to solve the adiabatic regeneration dynamics equations of Table 9.1 has the following features that increase program flexibility:

1. Either the dimensionless numbers or the operating conditions and sorbent properties that describe the regeneration may be inputs to the program.
2. Four different output formats for the sorption dynamics are provided. The outputs range in complexity from a single listing of oxygen breakthrough and percent regeneration versus regeneration time to a complete description of bed iron sulfide and temperature profiles at selected regeneration times.

3. The mass balance equations are programmed as separate subroutines. This method of programming allows new sorption mechanisms to be added to the computer model with minimum modification to the program logic. The model listed in Appendix B contains the kinetically controlled mechanism of Table 9.1, the shell progressive mechanism found to be applicable for hydrogen sulfide sorption on iron oxide/fly ash.

4. The energy and mass balance equations can be uncoupled by suppressing the dependence of the sorption numbers on temperature.

Suppressing the dependence of the sorption numbers on the energy balance allows the mass balance solution (oxygen breakthrough curve) to be compared with the analytical solutions for isothermal sorption of Appendix B.2. This procedure,which is an accuracy check on the computer generated solution, is demonstrated in Section 9.3. Other options listed above for the computer generated solution are fully described in Appendix C.

The following assumptions limit the applicability of the computer generated adiabatic solution:

1. Heat transfer between the gas phase and the sorbent pellets is large enough so that gas and pellet temperatures are equal.
2. The ratio of gas phase adiabatic temperature rise to bed adiabatic temperature rise must be less than the ratio of the time finite difference interval to the distance interval.
3. Neither mass nor thermal axial dispersion are significant in the bed. This is a plug flow assumption for both the mass and temperature balances.
4. Neither solid nor gas phase adiabatic temperature rises vary over the range of bed temperatures generated by the computer model.

The preceding assumptions are required by the computer technique used to solve the bed temeprature balance. The first, third, and fourth assumptions are implicit in the heat balance equation of Table 9.1.

9.1.3 Computer Model Accuracy Checks

Two different accuracy checks of the computer generated solution have been made. In the first check, the dependence of the kinetic rate constant on bed temperature was suppressed and the film sorption number (N_{Ab}^F) was set equal to zero. This limiting case of the adiabatic sorption problem has been solved analytically by Johnson et al and is presented in Chemical Reaction Engineering, Advances in Chemistry Series 109, American Chemical Society, (1972), pages 434 to 443. The computer generated test case is compared with the analytical solution in Figure 9.1. No significant difference between analytical and computer solutions for the test case were observed.

The second check is provided by overall mass and energy balances on the computer generated solutions. The overall mass and energy balances are described below:

1. Overall Mass Balance:

   Sorbate that has entered the bed = sorbate accumulated in bed + sorbate that has left the bed. (9.1)

2. Overall Energy Balance:

   Heat released by sorption of H_2S for absorption or O_2 for regeneration + heat that has entered bed = heat accumulated in bed + heat that left the bed. (9.2)

The computer program determines the values of the left and right hand sides of each of the above overall mass and energy balance equations. The overall mass balance error is one minus the ratio of the left to the right side of Equation 9.1 above. The energy balance error is similarly determined from Equation 9.2. For the sample cases presented in Section 3.1.4, which use a finite difference grid of 100 distance intervals by 150 time intervals, the mass balance errors are less than 3% and the energy balance errors less than 1%. Using a larger finite difference grid reduces the overall mass and heat balance errors; the computer program has space for a grid of 1000 to 1000.

9.1.4 Effects of Model Parameters on the Computer Generated Breakthrough Curves

The computer generated solution to the dynamic equations for adiabatic sorption of oxygen on iron sulfide determined percent regeneration versus time information from five dimensionless numbers that characterize the regeneration:

1. N_{Ab}^K Kinetic Sorption Number at Gas Inlet Temperature.
2. N_{Ab}^F External Film Sorption Number at Gas Inlet Temperature.

FIGURE 9.1

ANALYTICAL AND COMPUTER GENERATED SOLUTIONS FOR TEST PROBLEM

MODEL PARAMETERS:

N_{Ab}^{K} = KINETIC SORPTION NO. = 0.1
N_{Ab}^{F} = FILM SORPTION NO. = 0.0
N_{cp} = HEAT BALANCE NO. = 0.1

ANALYTICAL SOLUTION: (REPRESENTED BY SOLID LINES)

MASS BALANCE $\tau = 1 + N_{Ab}^{K} \ln \left(\frac{F}{1 - F}\right)$

HEAT BALANCE $\Theta = \frac{1}{2\,(1 - N_{cp})} \left[\tanh\left(\frac{1 - \tau}{2\, N_{Ab}^{K}}\right) - \tanh\left(\frac{N_{cp} - \tau}{2\, N_{Ab}^{K}}\right) \right]$

COMPUTER SOLUTION:

MASS BALANCE = ⊙
HEAT BALANCE = ▽

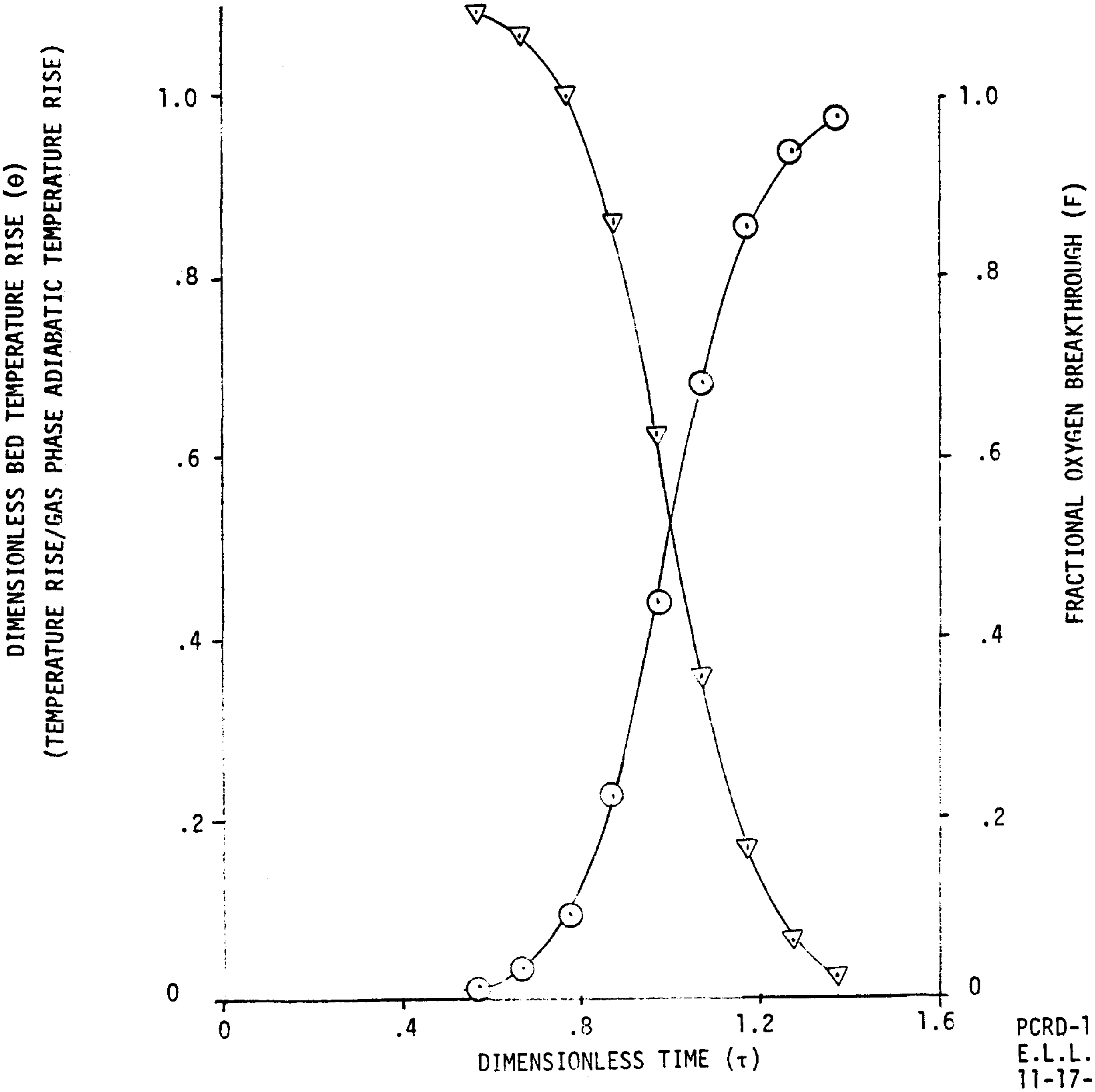

PCRD-1577
E.L.L.
11-17-76

3. N_{cp} Heat Balance Number.

4. T_{Ab} Gas Phase Adiabatic Temperature Rise.

5. β Kinetic Activation Energy

The five dimensionless numbers are functions of sorbent properties, bed geometry, and operating conditions. The two sorption numbers are functions of bed temperature, while the heat balance number is temperature independent. The adiabatic temperature rise and the activation energy determine the effect of temperature on the sorption numbers. The percent regeneration used in the program is the average iron oxide concentration of freshly prepared sorbent times 100%.

A series of eight test cases were run using the adiabatic computer model to demonstrate the effect of the five dimensionless numbers on regeneration dynamics. The base case dimensionless heat balance number adiabatic activation energy, and adiabatic temperature rise are appropriate numbers for adiabatic regeneration of sulfided 42% added iron oxide on fly ash. Gas inlet temperatures were assumed to be 1000°F; inlet gas composition was 20% air in steam. The heat balance number for the base case is characteristic of regeneration where the vessel wall heat capacity is small compared to the capacity of the sorbent bed. This assumption is valid for the core of a large diameter vessel. For a small lab scale regeneration vessel, wall effects will increase the heat balance number. Further information on the effect of vessel heat capacity on the heat balance number can be found in the heat balance derivation of Appendix B.3.

The base case sorption numbers may be appropriate for regeneration at 2000 GHSV where space rate is based on the wet regeneration gas.

Figure 9.2 is a plot of percent regeneration versus onstream time for the base case and for two other runs which demonstrate activation energy and adiabatic temperature rise effects. The solid line on the figure is the curve for perfect regeneration, a process in which 100% of the regeneration gas oxygen is consumed by the regeneration reaction at all onstream times. Figure 9.2 illustrates little change in bed regeneration was caused by a significant increase in activation energy or in adiabatic temperature rise. For all three cases plotted regeneration is efficient below a dimensionless time of 0.8 (i.e., the ratio of percent regeneration to perfect percent regeneration at times less than 0.8 is more than .95 for the test cases).

Figure 9.3 shows the oxygen breakthrough curves for the same three computer test cases. When Figure 9.3 is compared with the percent regeneration versus time plots of Figure 9.2. It is apparent that the performance curves of Figure 9.3 are more sensitive to the adiabatic model parameters than the percent regeneration plots. For example, at dimensionless time of 0.7, the base case is 67% regenerated and the other two test cases are 69% regenerated. However, at the same time of 0.7, base case oxygen breakthrough is 15% while the

FIGURE 9.2
EFFECT OF ACTIVATION ENERGY AND ADIABATIC TEMPERATURE RISE ON PERCENT REGENERATION

BASE CASE PARAMETERS

KINETIC SORPTION NO. .375
FILM SORPTION NO. .025
HEAT BALANCE NO. .12

ACTIVATION ENERGY, $\beta = 10$
ADIABATIC TEMPERATURE RISE, $T_{Ab} = 0.2$

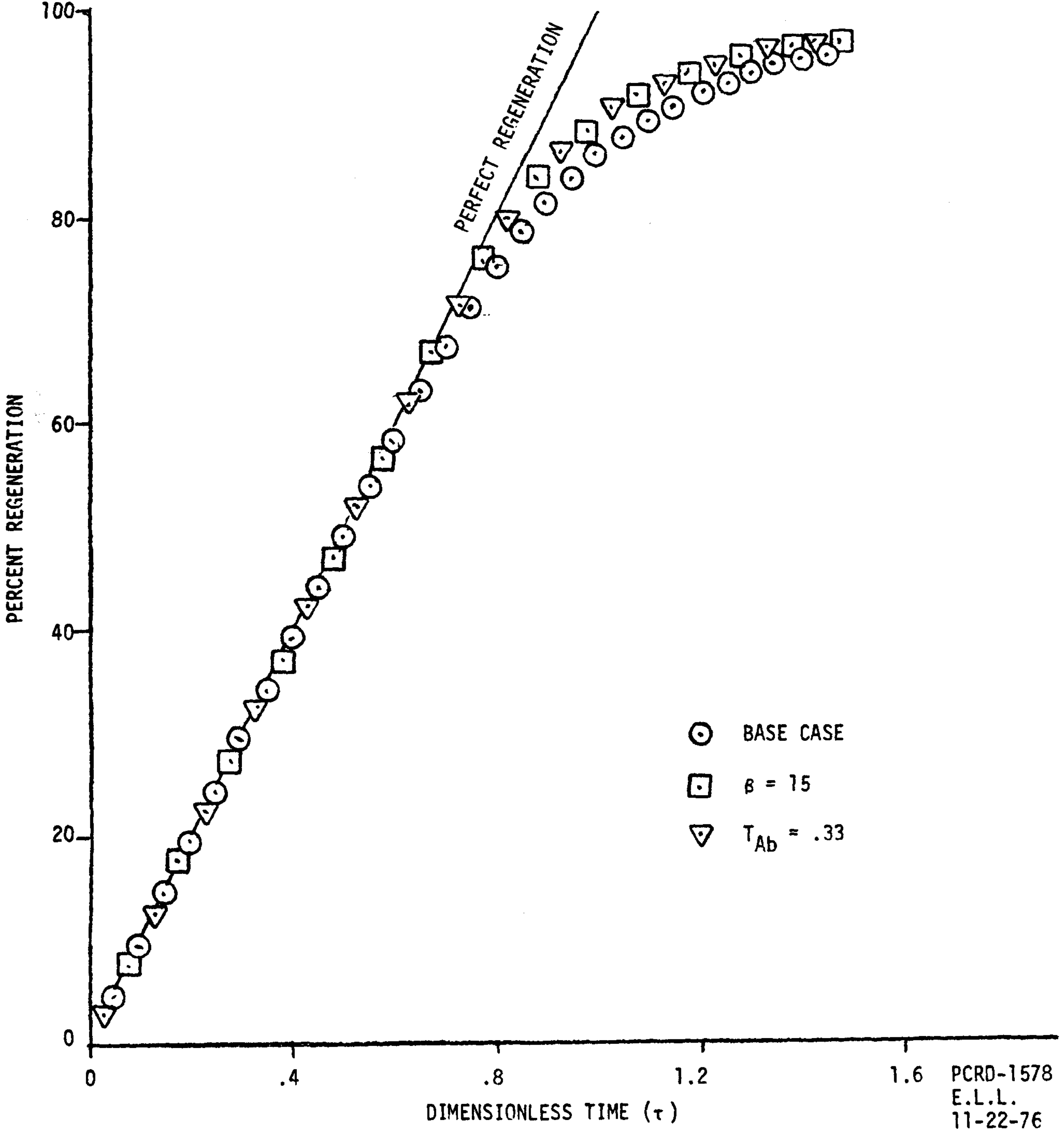

PCRD-1578
E.L.L.
11-22-76

FIGURE 9.3
EFFECT OF ACTIVATION ENERGY AND ADIABATIC TEMPERATURE RISE ON REGENERATION DYNAMICS

BASE CASE PARAMETERS

KINETIC SORPTION NO. = .375
FILM SORPTION NO. = .025
HEAT BALANCE NO. = .12

ACTIVATION ENERGY, $\beta = 10$
ADIABATIC TEMPERATURE RISE, $T_{Ab} = .2$

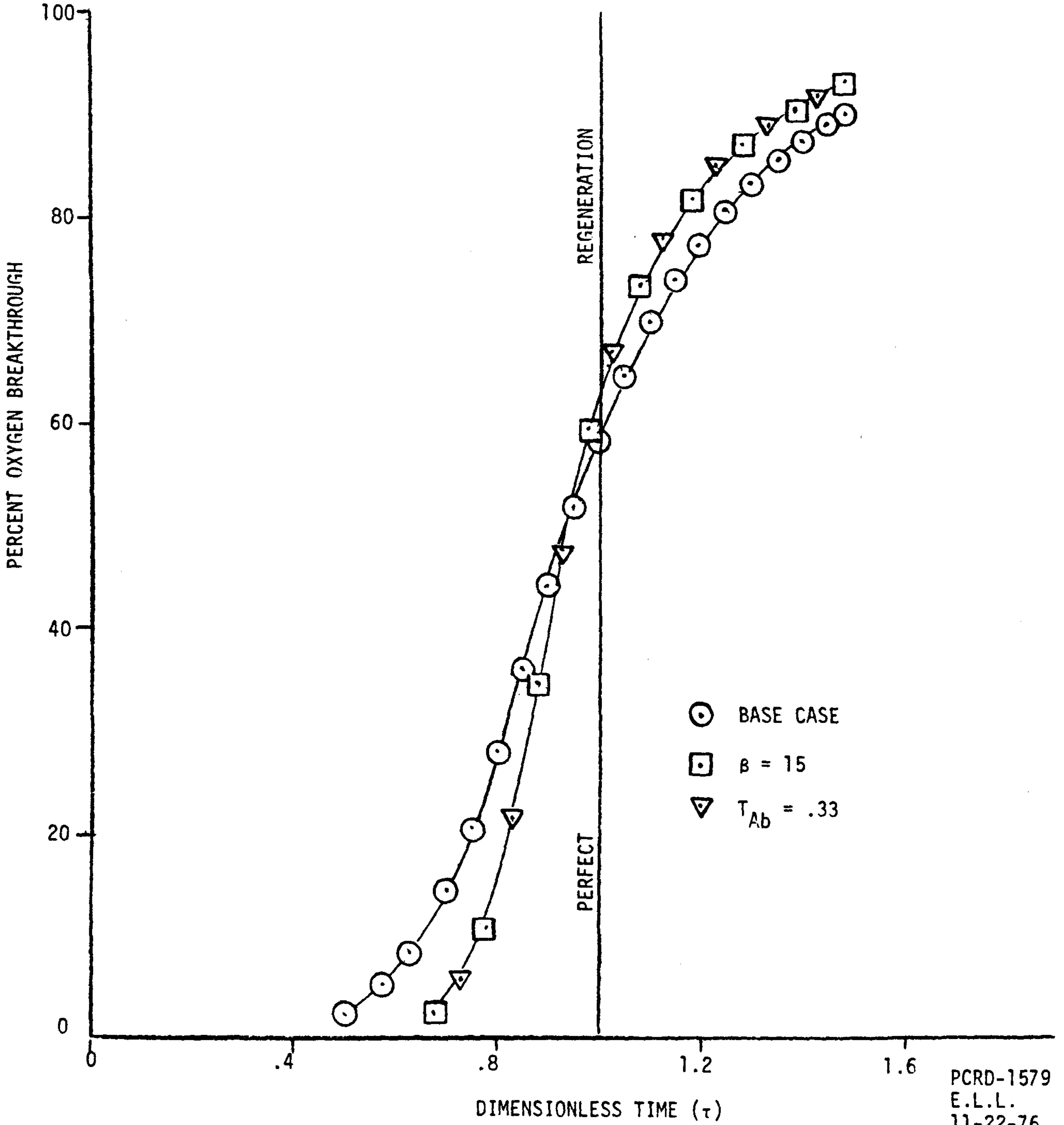

PCRD-1579
E.L.L.
11-22-76

the other test cases have 4% breakthroughs. The indicated conclusion is that oxygen breakthrough curves are both easier to measure and more sensitive to model parameters than percent regeneration curves. For these reasons, future discussion on regeneration performance will be limited to oxygen breakthrough curves throughout Section 9 of the report.

Figure 9.3 also illustrates that the performance curves for the increase in dimensionless activation energy from the base case value of 10 to 15 has the same effect on performance as an increase in dimensionless adiabatic temperature rise from a base case value of .2 to .33. The reason these two performance curves are identical is that both changes have nearly the same effect on the relationship between kinetic sorption number and bed temperature. At inlet conditions both runs have kinetic numbers of .375. At a bed temperature equal to the adiabatic temperature rise plus the inlet temperature, the run with higher activation energy has a kinetic sorption number of .037 and the run with higher adiabatic temperature rise has a kinetic number of .042. Similar agreement is found using other dimensionless bed temperature rises, where dimensionless temperature rise is defined as the temperature rise divided by the gas phase adiabatic temperature rise. Note that equal bed temperature rises are not necessarily equal dimensionless temperature rises. Figure 9.3 thus indicates that oxygen breakthrough curves are equivalent if the film number, heat balance number, and kinetic number are equal at zero and one dimensionless temperature rises.

Figure 9.4 is another indication of the effect of kinetic sorption number temperature dependence on regeneration performance curves. The performance curve represented by circles on the plot is the base case of Figure 9.4. The triangles on the plot define the breakthrough curve for isothermal sorption at the inlet temperature, while the squares are the curve for isothermal sorption at maximum bed temperature. Note that the adiabatic performance curve below 50% breakthrough has approximately the same shape as the isothermal curve at maximum bed temperature. The shape of the adiabatic curve above 50% breakthrough is roughly approximated by the isothermal curve for inlet bed temperature. The performance curve of Figure 9.4 thus indicates that sorption dynamics at small breakthroughs are determined by the model parameters at maximum bed temperature, while dynamics at large breakthroughs are determined by model parameters at inlet bed temperature.

A method of analyzing regeneration performance curves is suggested by Figure 9.4. If the isothermal sorption numbers at low and high fractional breakthroughs were estimated for an experimental run, then these estimates would indicate the sorption numbers at maximum and inlet bed temperatures, respectively. Figure 9.5 illustrates the estimation of these isothermal sorption numbers using a plot of ln F/(1 - F) versus dimensionless time, where F is fractional oxygen breakthrough. The reciprocal of the slope of the plot is an estimate of the kinetic sorption number. Figure 9.5 is a linearized plot of three computer test runs, all with the same kinetic sorption number at inlet temperature (0.175). The reciprocals of the slopes of the plots above 50% breakthrough vary between 0.15 and 0.16, thus providing an estimate of the kinetic sorption number at inlet conditions. As expected, each of the three plots is discontinuous near 50% breakthrough. Reciprocal slopes at low oxygen breakthroughs appear to be approximately equal to the sum of the film and kinetic sorption numbers at the maximum bed temperature. Table 9.2 demonstrates the validity of

FIGURE 9.4

COMPARISON OF ADIABATIC REGENERATION DYNAMICS WITH ISOTHERMAL REGENERATION DYNAMICS

ADIABATIC REGENERATION PARAMETERS

KINETIC SORPTION NO. AT INLET T = .375, AT MAXIMUM BED T = .072
FILM SORPTION NO. AT INLET T = .025, AT MAX. BED T = .023
HEAT BALANCE NO. = .12

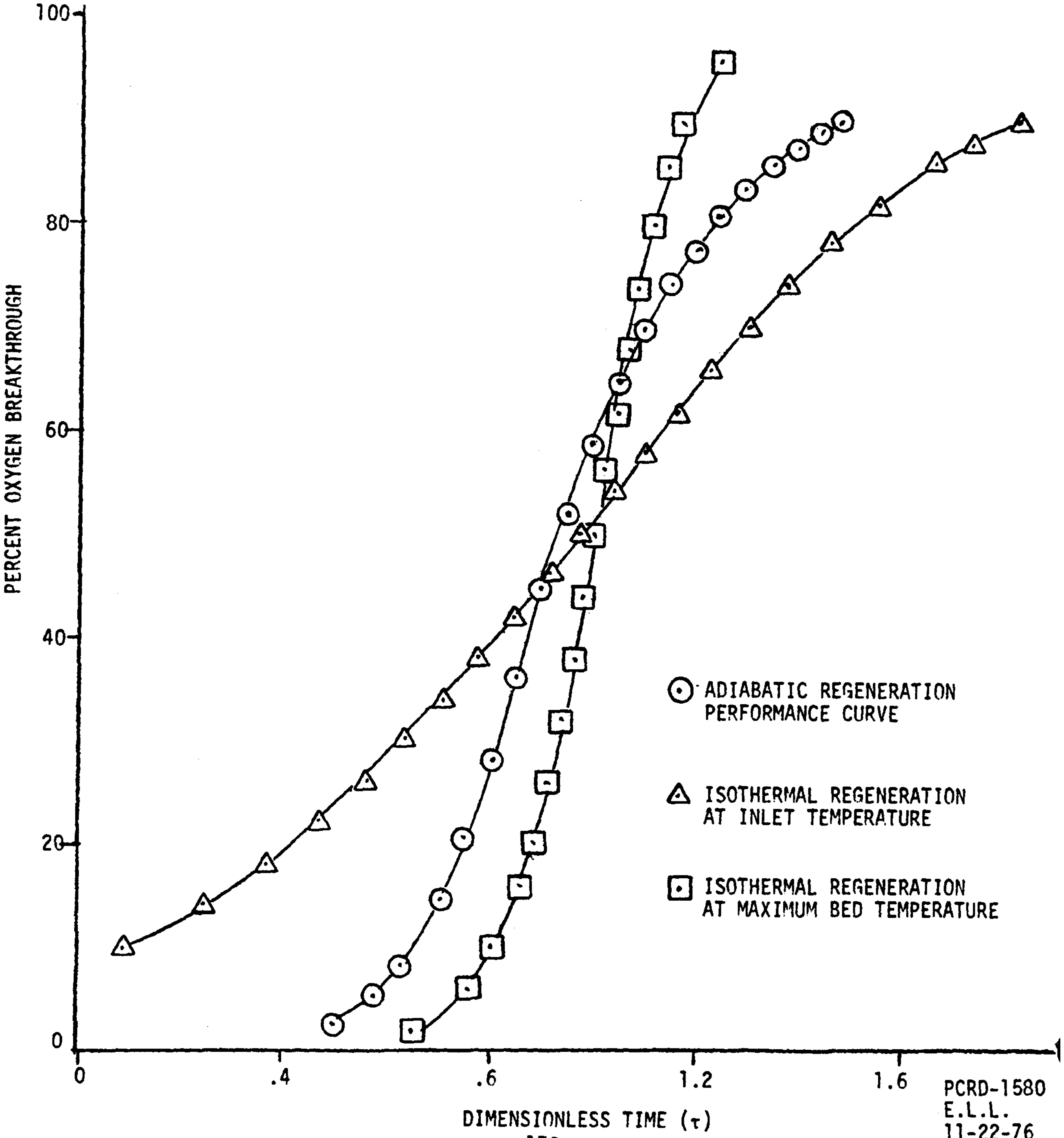

PCRD-1580
E.L.L.
11-22-76

FIGURE 9.5

LINEARIZED REGENERATION PERFORMANCE CURVES FOR THREE ADIABATIC COMPUTER TEST RUNS

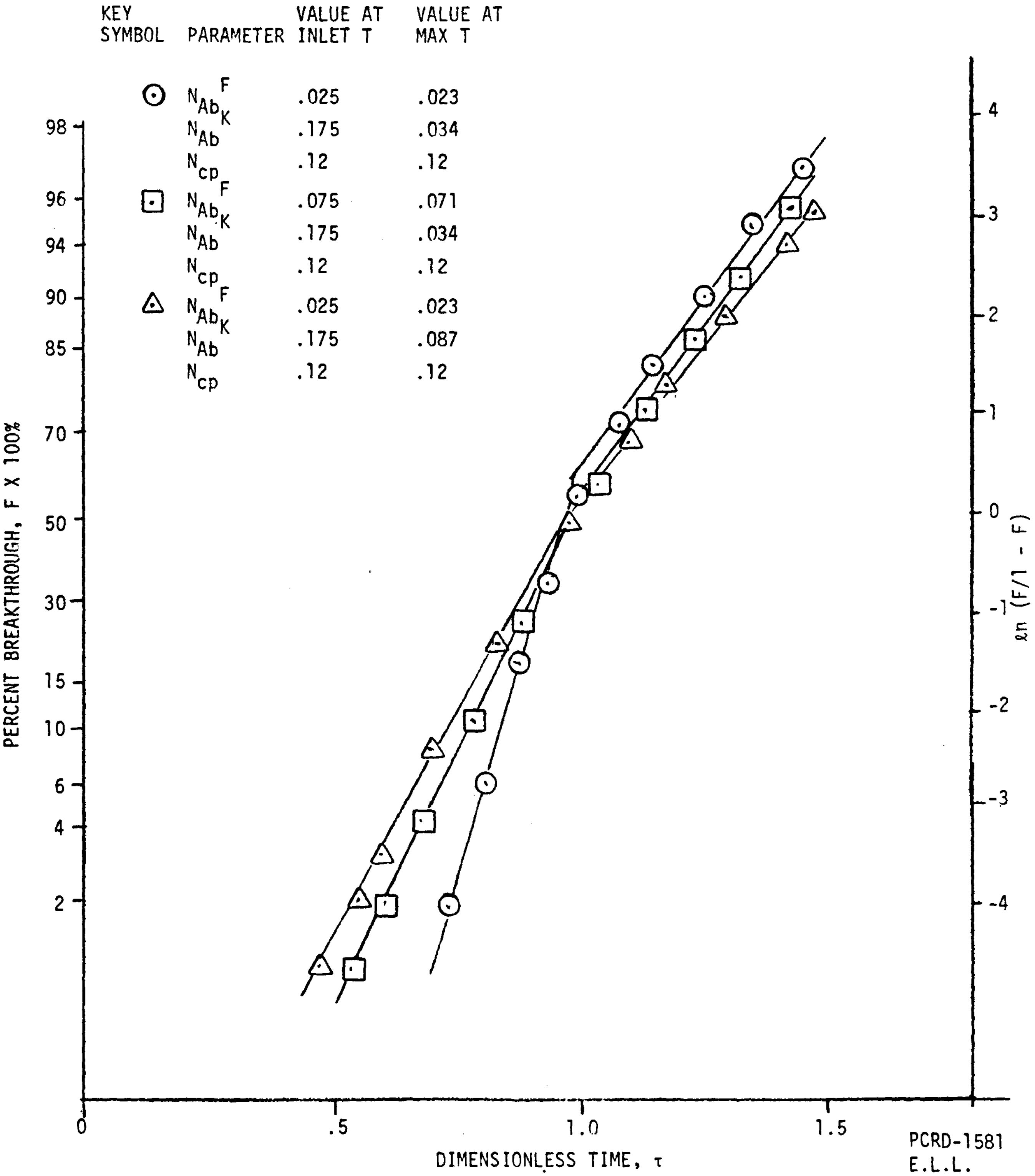

PCRD-1581
E.L.L.
11-22-76

of these conclusions using the results of eight computer test runs. The slopes of the eight linearized oxygen breakthroughs were obtained from plots of the computer generated solution, such as Figure 9.5. Bed temperature profiles were also obtained from the computer model and used to evaluate the sorption numbers at maximum bed temperature. It was found that the sum of film and kinetic sorption numbers at maximum bed temperature could be accurately estimated from the reciprocal slopes of the linearized plots at low breakthroughs. Estimates of the kinetic sorption number at the gas inlet temprature obtained at high breakthroughs were less accurate. It is expected that linearized breakthrough curves, between 95 and 99+ percent breakthrough would provide better estimates of the kinetic number at the gas inlet temperature. Estimates using the slope between 50 and 95 percent breakthrough, used in Figure 9.5 and Table 9.2 provide systematically low estimates of this variable.

The rule of thumb parameter estimation demonstrated in Table 9.2 provides a simple method of fitting experimental oxygen breakthrough curves using the kinetically controlled adiabatic model.

9.1.5 Effects of Model Parameters on the Computer Generated Temperature Profiles

The three major variables that affect bed temperature profiles are the heat balance number, the gas adiabatic temperature rise, and the regeneration efficiency. The regeneration efficiency is, in turn, determined by the dimensionless sorption numbers as described in Section 9.1.4. This section discussed the effects of these variables on temperature profiles.

The dimensionless adiabatic temperature rise , T_{Ab}, is a scale factor on the bed temperature rise. In other words, if the other parameters are unchanged and the adiabatic temperature rise is doubled, then the bed temperature rise at each time and each position in the bed is boubled. As a consequence, the dimensionless adiabatic temperature rise need not be considered in future discussions in this section if a dimensionless temperature rise is defined according to the equation below:

$$\text{Dimensionless Temperature Rise} = \frac{\text{Dimensionless Temperature - Dimensionless Inlet Temperature}}{\text{Dimensionless Adiabatic Temperature Rise}}$$

Or, using the notation of Table 9.1 (with dimensionless temperature rise Θ):

$$\Theta = \frac{T - T_o}{T_{Ab}} \qquad (9.4)$$

Figure 9.6 demonstrates the effect of regeneration efficiency on bed temperature profile. A total of six temperature profiles are plotted on the figure for three levels of efficiency; at each efficiency level the profiles at dimensionless time of .4 and .8 are presented. The profiles at 1.00 efficiency are from the asymptotic solution to the heat balance of Table 9.1, while those at lower efficiencies are computer generated solutions.

TABLE 9.2
COMPARISON OF COMPUTER GENERATED ADIABATIC REGENERATION DYNAMICS WITH "RULE OF THUMB" MODEL EMPIRICAL PREDICTIONS

A. "Rule of Thumb" Model:

1. Regeneration dynamics below 50% breakthrough are characterized by the kinetic sorption number at inlet temperature.
2. Regeneration dynamics above 50% breakthrough are characterized by the kinetic + film numbers at maximum bed temperature.

Run Number	1	2	3	4	5	6	7	8
Film No. at Inlet T (N_{Ab}^F)	.025	.025	.025	.025	.025	.075	.025	.025
Kinetic No. at Inlet T (N_{Ab}^K)	.375	.375	.375	.375	.175	.175	.175	.175
Heat Balance Number (N_{cp})	.12	.12	.12	.80	.12	.12	.12	.25
Activation Energy (β)	10	15	10	10	10	10	5	10
Dimensionless Adiabatic Temperature Rise (T_{Ab})	.2	.2	.33	.2	.2	.2	.2	.4
Maximum Bed Temperature Rise Divided by T_{Ab} From Computer Model (Θ_m)	1.09	1.12	1.12	2.33	1.13	1.11	1.10	1.32
Kinetic Number at Θ_m $K_m = N_{Ab}^K \left(1 + T_{Ab}\,\Theta_m\right) \exp\left(\frac{-\beta\, T_{Ab}\,\Theta_m}{1 + T_{Ab}\,\Theta_m}\right)$	.0763	.0295	.0346	.0229	.0340	.0348	.0867	.0084
Film Number at Θ_m $F_m = N_{Ab}^F \left(1 + T_{Ab}\,\Theta_m\right)^{-1/3}$	.0234	.0234	.0225	.0220	.0234	.0701	.0234	.0217
Reciprocal Slope of Linearized Performance Curve Above 50% Breakthrough Computer Prediction Rule of Thumb (N_{Ab}^K)	 .25 .375	 .22 .375	 .22 .375	 .24 .375	 .15 .175	 .15 .175	 .16 .175	 .15 .175
Reciprocal Slope of Linearized Performance Curve Below 50% Breakthrough Computer Prediction Rule of Thumb ($K_m + F_m$)	 .12 .10	 .05 .05	 .06 .06	 .05 .045	 .06 .06	 .10 .105	 .11 .11	 .05 .03

FIGURE 9.6
EFFECT OF REGENERATION EFFICIENCY
ON TEMPERATURE PROFILES

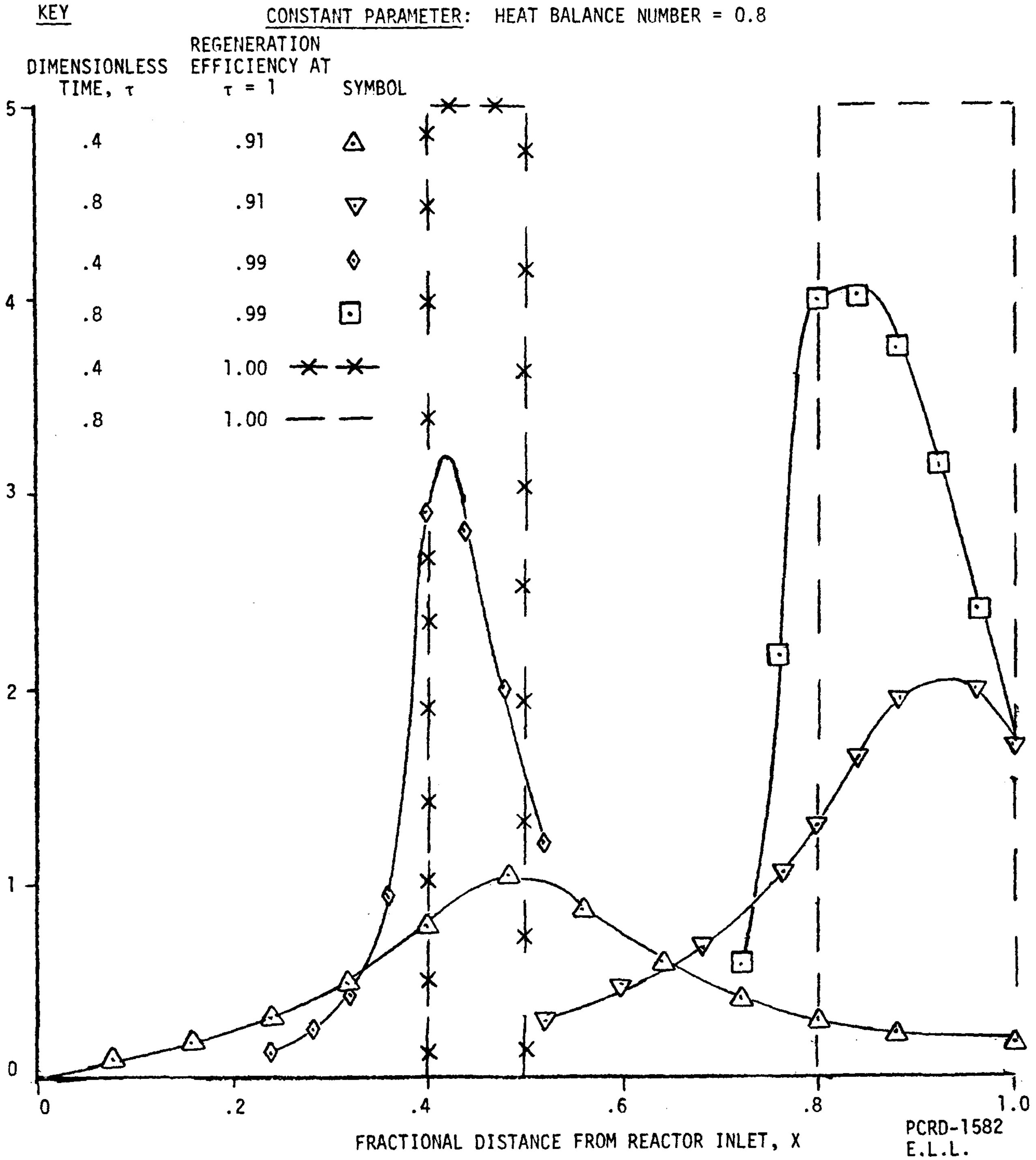

PCRD-1582
E.L.L.
11-22-76

FIGURE 9.7

EFFECT OF HEAT BALANCE NUMBER ON BED TEMPERATURE PROFILES

CONSTANT PARAMETERS: DIMENSIONLESS TIME (τ) = 0.6
REGENERATION EFFICIENCY = .99+

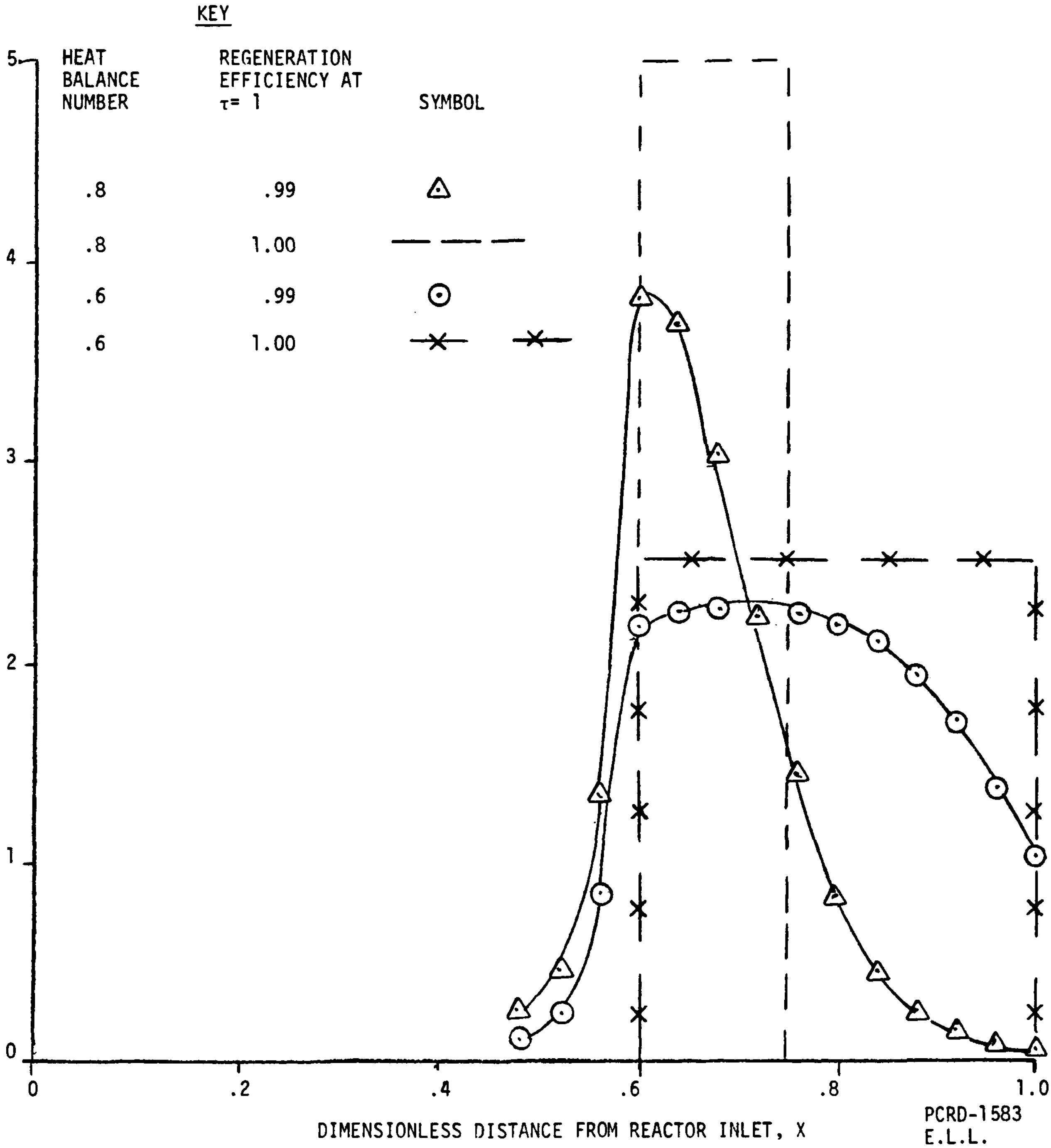

PCRD-1583
E.L.L.
11-22-76

The bed temperature profiles of Figure 9.6 demonstrate that, at constant heat balance number, the maximum temperature rise occurs when regeneration efficiency is 1.00 (i.e., perfect regeneration). When this temperature rise is expressed as dimensionless temperature rise Θ, its value is the reciprocal of one minus the heat balance number:

$$\Theta \text{ Max.} = \frac{1}{1 - N_{cp}} \qquad (9.4)$$

As efficiency is decreased, the maximum bed temperature decreases. This decrease in temperature is accompanied by a more even distribution of temperature throughout the bed. At the high levels of efficiency plotted on Figure 9.5, the position of the maximum bed temperature rise is still well defined. At lower efficiencies, the temperature rise may be nearly uniform throughout the bed. For cases where the maximum temperature rise is discernable, it is located at a dimensionless position larger than the dimensionless time and less than the dimensionless time divided by the heat balance number:

$$\tau < X_{\text{Max.}} < \frac{\tau}{N_{cp}} \qquad (9.5)$$

Note that the range of positions defined by Equation (9.5) describes the location of the maximum temperature for perfect regeneration (dashed lines on Figure 9.6).

The temperature profiles also illustrate that maximum bed temperature increases as the temperature wave passes through the sorbent bed. Thus, if the bed is adiabatic and the assumptions involved in the heat balance derivation hold (see Appendix B.3), a plot of maximum bed temperature versus bed position will show a uniform increase from bed inlet to bed outlet. Figure 9.6 illustrates that the increase in maximum temperature rise with bed position is minimized at high regeneration efficiencies.

Equations (9.4) and (9.5) above define the effect of heat balance number at constant regeneration efficiency. These effects are further demonstrated in Figure 9.7. This figure shows computer generated profiles for .99 regeneration efficiency and asymptotic profiles for perfect regeneration at two different heat balance numbers. All temperature profiles are at dimensionless time of 0.6. Figure 9.7 illustrates that at the heat balance number is increased, the maximum bed temperature increases and the location of the maximum bed temperature is more sharply defined. These effects are qualitatively the same as those of increased regeneration efficiency. The change in maximum bed temperature with bed position is not significantly effected by the heat balance number. For all computer test runs made, the maximum temperature was less than that of Equation (9.2) and its location was defined by Equation (9.3).

9.1.6 A Summary of the Effects of Model Parameters on Computer Generated Adiabatic Regeneration Dynamics

Computer generated test cases have demonstrated the following effects of model parameters on adiabatic regeneration dynamics:

1. Regeneration efficiency is determined by two parameters: the kinetic sorption number at regeneration gas inlet temperature and the sum of kinetic and film sorption numbers at maximum bed temperature. The sorption number at gas inlet temperature defines the performance curve above 50% oxygen breakthrough; regeneration performance below 50% oxygen breakthrough is defined by the sorption number at maximum bed temperature.

2. Bed temperature profiles are influenced by three model variables: the heat balance number, the dimensionless adiabatic temperature rise, and the efficiency of the regeneration process. Bed temperature rise is directly proportional to the adiabatic temperature rise. Increased regeneration efficiency and increased heat balance number both have the same qualitative effects: increased maximum bed temperature and a more sharply defined bed hot spot.

The regeneration efficiency dynamic curve and the bed temperature profiles are coupled by temperature effects on regeneration efficiency. Maximum bed temperature determines the regeneration efficiency; regeneration efficiency, in turn, affects the maximum bed temperature. This coupling was observed in the model differential equations; it is represented in Table 9.1 as the effect of temperature on kinetic rate of regeneration. Due to the difficulty of uncoupling the mass and heat balances, the adiabatic regeneration model was solved using computer techniques.

9.1.7 Computer Program to Simulate Commercial Hot Stage Desulfurization of Producer Gas

The computer program described in Appendix C has the capability to simulate multiple cycles of desulfurization followed by sorbent regeneration as well as the capability to simulate single sorption processes. The sample problem presented in Section C.3.3 of the appendix illustrates this option of the process simulation computer program. Model parameters used in the sample problem represent the most current estimates obtained from experimental test runs in the ERDA pressure unit. In using the program, it should be noted that experimental vertification of multiple cycle absorptions was not within the scope of this program and was not done.

The process simulation model will compute onstream time for each cycle of sorption or regeneration from sorbent properties, operating conditions, thermodynamic properties, and model parameters supplied by the program user. The sample problems presented in Appendix C assume bed geometry and bed heat capacity that are appropriate to a commercial scale process. Sorbent heat capacity includes the effect of the wall as a bed heat sink and is thus an empirical parameter for lab scale reactors and a thermodynamic property for commercial scale reactors.

The process simulation model can be used during optimization studies to predict the effects of bed geometry and operating conditions on sorber onstream times.

9.2 Correlation of a Regeneration Process Model Using Dynamic Data

9.2.1 Methodology for Model Selection

The performance curves presented in Section 8.10 illustrate the effects of process variables on regeneration efficiency. The dynamic data can be correlated using an adiabatic regeneration model over the following range of operating conditions:

Inlet temperature	1000°F and 1200°F
Pressure	30 psig and 150 psig
GHSV (air)	100, 200 and 1000
Superficial velocity	.05 to .33 ft/sec
Air concentration	15% and 20% by volume
Sorbent pellet diameter	1/8 inch and 1/4 inch
Fresh sorbent iron oxide content	21 and 42 added wt.%

The dynamic data are correlated with the adiabatic models developed for regeneration. The regeneration process is treated as absorption of oxygen. It should be noted that this model does not provide for the high elemental sulfur levels observed in the effluents. Both, oxygen utilization and heat effects are significantly modified by this side reaction. How the side reaction is affected by process variables is not known. Hence while comparing results of process variables and model predictions, this fact must be kept in mind. Elemental sulfur formation was found, unexpectedly, to be very significant after the experimental program was underway. Then an analytical technique was developed to analyze elemental sulfur formation; and elemental sulfur and sulfur-trioxide in the effluent stream were monitored in the remaining experiments. Hence there is not sufficient information to develop a complete model.

The details of the derivations of mathematical models developed for adiabatic regeneration are given in Section 9.1.

A successful regeneration model must meet three levels of model confirmation criteria:

Level 1 - The model must be able to predict the shape of the experimentally observed breakthrough curves.

Level 2 - The model must predict the experimentally observed effects of design variables on regeneration efficiency.

Level 3 - The model must be able to predict the observed temperature exotherms.

This section examines the adiabatic regeneration models in terms of the first two levels of model confirmation. An appropriate model satisfying both levels will be selected

9.2.2 Level 1 Confirmation: Prediction of the Shape of the Breakthrough Curve

Section 9.1 describes how the shapes of the breakthrough curves for the shrinking core, film and kinetic models change when heat effects are incorporated in the model. Shapes of breakthrough curves for shrinking core and film model are the same for isothermal and adiabatic model, for the 300°F bed temperature rise in the regeneration experiments. Hence for the adiabatic shrinking core model, plot of $\ln (1 - F)$ vs τ would be a straight line and for the adiabatic film model, plot of $\ln F$ vs τ would be a straight line. For the kinetic model, the rate is a very strong function of the temperature; and shape of the breakthrough curve is significantly modified by inclusion of the heat effects. For the isothermal kinetic model, a plot of $\ln (\frac{F}{1-F})$ vs τ is a straight line, while for the adiabatic kinetic model a similar plot consits of two straight lines, one represnting data at low oxygen breakthrough and the other representing data at high oxygen breakthrough.

It is necessary to ascertain these results on at least two runs. Level 1 confirmation is obtained for run no. 1807 SG at 700 GHSV and run no. 1815 at 1300 GHSV. Plots of lf F vs τ, $\ln (1-F)$ vs τ and $\ln \frac{F}{(1-F)}$ vs τ for both the runs are drawn. It can be seen that for both runs, the film model predicts the shape of breakthrough curve very poorly while the shrinking core model and the kinetic model both explain the shapes of breakthrough curves very well.

FIGURE 9.8

LEVEL 1 CONFIRMATION OF THE SHRINKING CORE AND FILM KINETIC MODEL FOR REGENERATION

RUN 1807SG

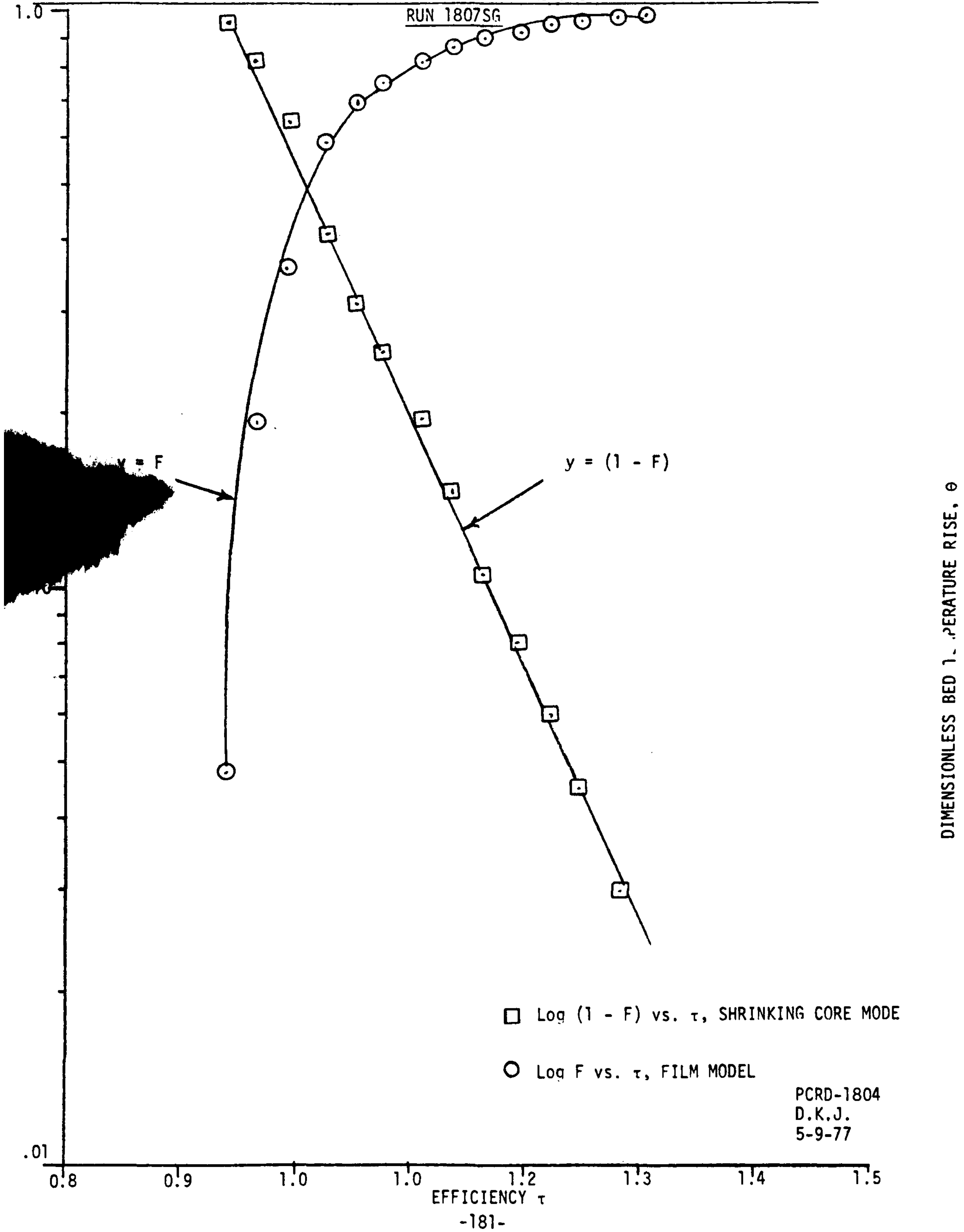

PCRD-1804
D.K.J.
5-9-77

FIGURE 9.9

LEVEL 1 CONFIRMATION OF THE KINETIC AND EMPIRICAL MODEL FOR REGENERATION

RUN NO. 1807SG

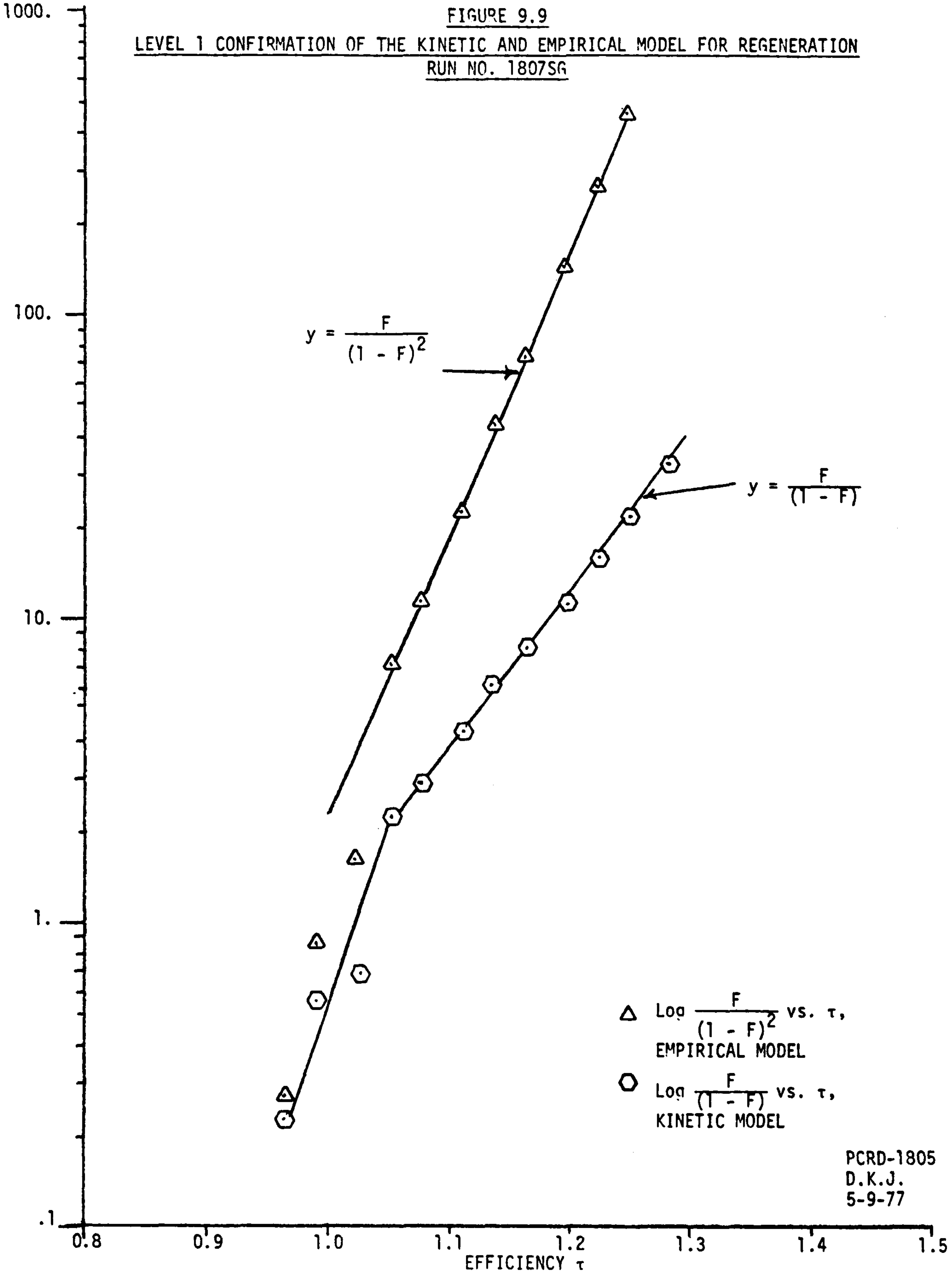

PCRD-1805
D.K.J.
5-9-77

FIGURE 9.10

LEVEL 1 CONFIRMATION OF THE SHRINKING CORE AND FILM MODEL FOR REGENERATION

RUN NO. 1815SG

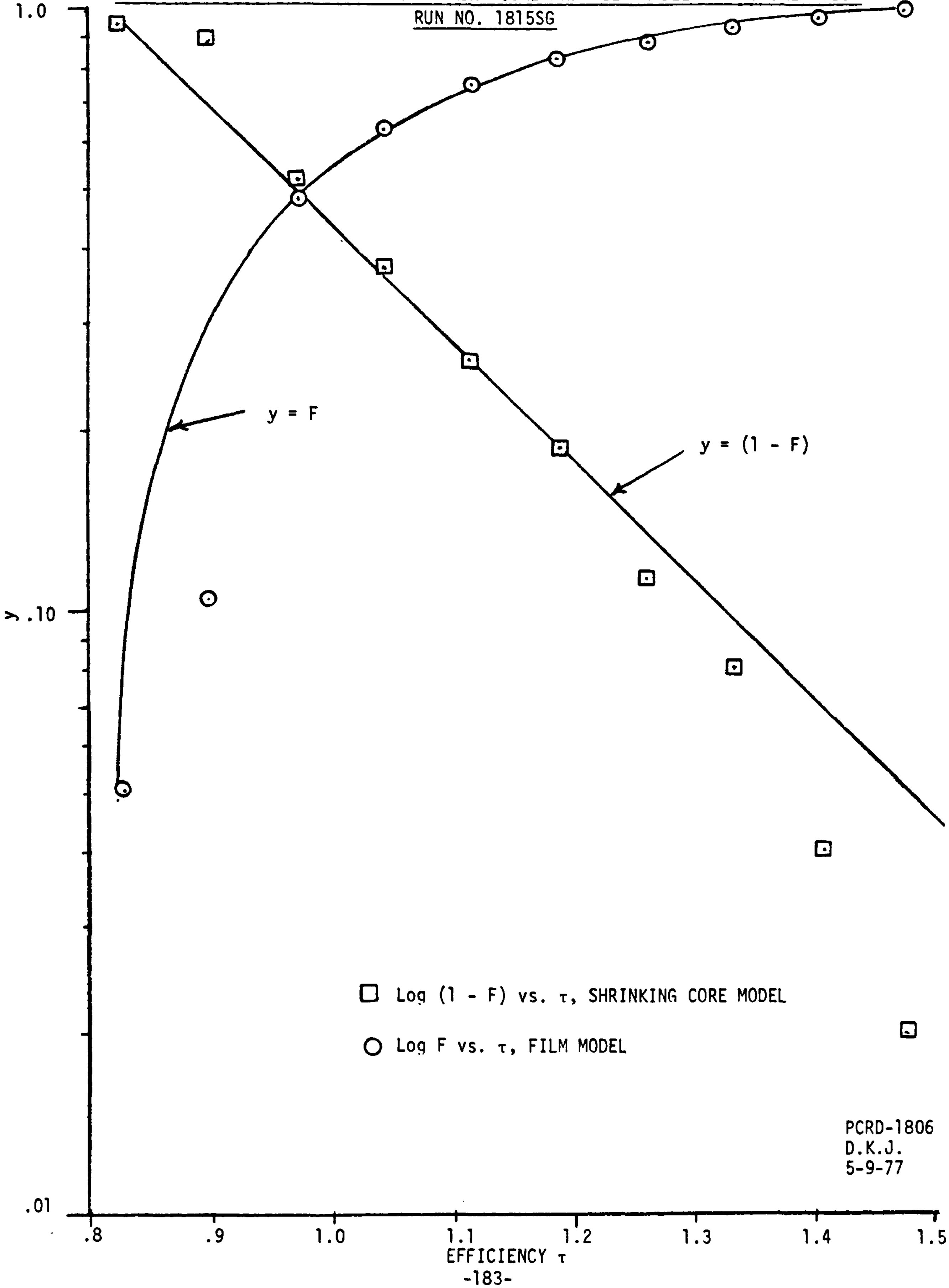

PCRD-1806
D.K.J.
5-9-77

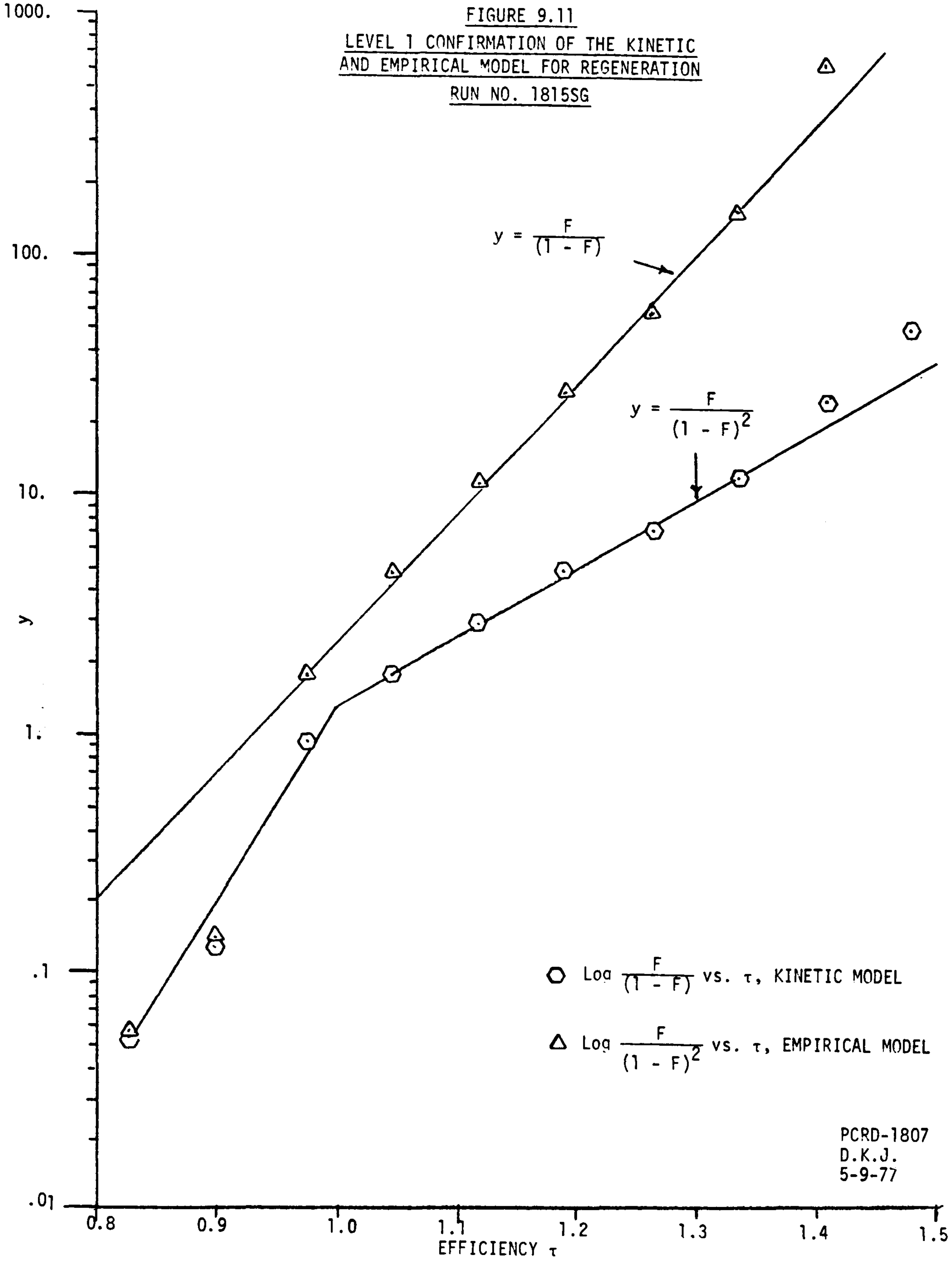

FIGURE 9.11

LEVEL 1 CONFIRMATION OF THE KINETIC AND EMPIRICAL MODEL FOR REGENERATION

RUN NO. 1815SG

PCRD-1807
D.K.J.
5-9-77

9.2.3 Level 2 Confirmation: Prediction of the Effects of Process Variables on the Breakthrough Curves

The criteria used for level 2 confirmation is very similar to that in the absorption study (Section 6.1.3). The absorption numbers used are the numbers at the inlet bed temperature. Table 9.3 describes the results of comparison of the three fundamental models. Expressions for the constant pattern solutions were obtained using run 1807 SG as a base run. The sorption numbers used are functions of design variables, iron sulfide content, GHSV, velocity, pellet size and unit pressure as described in Table 9.1. The empirical constants are combined in the proportionally constant K. All efficiencies of Table 9.3 are at 10% oxygen breakthrough.

A study of Table 9.3 and Table 9.4 reveals two facts:

1. Regeneration is a very efficient process; i.e., the efficiency at 10% is much higher than absorption and the difference between efficiency at 10% and 50% was much lower than absorption.

2. Variations in the efficiency due to changes in process variables are very small -- within 20%.

Table 9.3 illustrates that shrinking core model can explain effects of GHSV and pressure, but cannot correlate the observed effects of iron sulfide content, velocity, temperature and pellet diameter. Film transfer model is the worst and it can explain the effects of GHSV only; and fails to correlate the effects of iron sulfide content, velocity, pressure, temperature and pellet diameter. The kinetic model gives the best correlation for the observed effects of iron sulfide content, GHSV, velocity and temperature. It somewhat overpredicts the effect of pressure and fails to predict the effect of pellet diameter.

The level 1 confirmation indicated that shape of the oxygen breakthrough curve is predicted well by the kinetic model and the shrinking core model while the film model cannot predict the shape of breakthrough.

Hence the kinetic model best explains the effects of process variables at 1/4 inch particle size adequately.

TABLE 9.3

OBSERVED EFFECTS OF EXPERIMENTAL VARIABLES ON REGENERATION EFFICIENCY VERSUS EFFECTS PREDICTED BY SHRINKING CORE, KINETIC AND FILM TRANSFER MODELS

Run No.	1807 SG	1806 SG	1815 SG	1814 SG	1807 SG	1814 SG	1806 SG	1805 SG
Variable Changed	Iron Sulfide Content		GHSV(Air)		Velocity (ft/sec)		Pressure (atm)	
Level	17.6	10.1	182	92	.15	.31	3.04	11.2
Observed Efficiency (at 10% breakthrough)	.95	.87	.88	1.0	.95	1.0	.87	.89
Predicted Efficiency								
A. Shrinking Core	.95	.95	.88	.94	.95	.95	.95	.986
B. Kinetic	.95	.91	.88	.94	.95	.99	.91	.977
C. Film	.95	.95	.88	.94	.95	.93	.95	.95
Observed Change in Efficiency	-.08		+ .12		+ .05		+ .02	
Predicted Change in Efficiency								
A. Shrinking Core	0		+ .06		0.		+ .016	
B. Kinetic	-.04		+ .06		+ .04		+ .067	
C. Film	0		+ .06		- .02		0	

TABLE 9.3 - continued

OBSERVED EFFECTS OF EXPERIMENTAL VARIABLES ON REGENERATION EFFICIENCY VERSUS EFFECTS PREDICTED BY SHRINKING CORE, KINETIC AND FILM TRANSFER MODELS

Run No.	1808 SG	1810 SG	1808 SG	1815 SG	1806 SG	1811 SG
Variable Changed	Inlet Temperature		Oxygen Concentration		Pellet Diameter Inch	
Level	1000°F	1200°F	3.9%	2.9%	.25	.125
Observed Efficiency (at 10% breakthrough)	.85	.95	.89	.88	.87	1.0
Predicted Efficiency						
A. Shrinking Core	.85	.84	.85		.95	.99
B. Kinetic	.85	.95*	.85		.81	.88
C. Film	.85	.853	.85		.95	.98
Observed Change in Efficiency	+ .100		+ .03		+ .13	
Predicted Change in Efficiency						
A. Shrinking Core	- .010				+ .04	
B. Kinetic	+ .100				- .03	
C. Film	+ .003				+ .03	

* If $\beta = \Delta E = 17.6 \frac{\text{Kcal}}{\text{g mole}}$

TABLE 9.4

OBSERVED EFFECTS OF EXPERIMENTAL VARIABLES ON DIFFERENCE BETWEEN REGENERATION EFFICIENCY AT 10% AND 50% OXYGEN BREAKTHROUGH VS. DIFFERENCE PREDICTED BY SHRINKING CORE, KINETIC AND FILM TRANSFER MODEL

Run Number	1807SG	1806SG	1815SG	1814SG	1807SG	1814SG	1806SG	1805SG
Variable Changed	Iron Sulfide Content		GHSV (Air)		Velocity		Pressure (atm)	
Level	17.6	10.1	182	92	.15	.31	3.04	11.2
Observed Efficiency at 10% Breakthrough	.95	.87	.88	1.0	.95	1.0	.87	.89
Observed Efficiency at 50% Breakthrough	1.01	.95	.99	1.04	1.01	1.04	.95	.905
Observed Difference Between Efficiency at 10% and 50% Breakthrough	.06	.080	.11	.04	.06	.04	.08	.015
Predicted Difference Between Efficiency at 10% and 50% Breakthrough								
Shrinking Core Model	.06	.06	.11	.055	.06	.06	.06	.016
Kinetic Model	.06	.106	.11	.055	.06	.046	.106	.027
Film Model	.06	.06	.11	.055	.06	.08	.06	.06

TABLE 9.4

OBSERVED EFFECTS OF EXPERIMENTAL VARIABLES ON DIFFERENCE BETWEEN REGENERATION EFFICIENCY AT 10% AND 50% OXYGEN BREAKTHROUGH VS. DIFFERENCE PREDICTED BY SHRINKING CORE, KINETIC AND FILM TRANSFER MODEL

(CONTINUED)

Run Number	1808SG	1810SG	1808SG	1815SG	1806SG	1811SG
Variable Changed	Inlet Temperature, ^{o}F		Oxygen Concentration		Pellet Diameter Inches	
Level	1000	1200	3.9%	2.9%	.25	.125
Observed Efficiency at 10% Breakthrough	.85	.95	.85	.88	.87	1.0
Observed Efficiency at 50% Breakthrough	.97	1.01	.97	.99	.95	1.01
Observed Difference Between Efficiency at 10% and 50% Breakthrough	.12	.06	.12	.11	.08	.01
Predicted Difference Between Efficiency at 10% and 50% Breakthrough						
Shrinking Core Model	.12	.12	.12	-	.06	.015
Kinetic Model	.12	.04	.12	-	.106	.14
Film Model	.12	.12	.12	-	.06	.02

☆U.S. GOVERNMENT PRINTING OFFICE: 1977-744-007/4360 REGION NO. 4